



**BACTERIAL CELL DIVISION; A NOVEL
TARGET FOR NEW ANTIBACTERIALS**

Kennardy Dewanto Kusuma

January 2019

A thesis submitted in fulfilment of the requirements for the degree of
Doctor of Philosophy

Certificate of originality

I certify that the work in this thesis has not previously been submitted for a degree nor has it been submitted as part of requirements for a degree except as fully acknowledged within the text.

I also certify that the thesis has been written by me. Any help that I have received in my research work and the preparation of the thesis itself has been acknowledged. In addition, I certify that all information sources and literature used are indicated in the thesis.

I also verify that the research conducted for this thesis is supported by the Australian Government Research Training Program.

Production Note:
Signature removed prior to publication.

Kennardy D. Kusuma

August 2018

Acknowledgements

This PhD project has been a very long and exciting journey for me and I have many people to thank for that. First and foremost, I have to thank God for His grace and mercy in keeping my health and giving me the time to undertake this journey and see it through to completion. I would also like to thank my principal supervisor, Professor Liz Harry, as well as my secondary supervisors, Associate Professor Alison Ung and Dr Amy Bottomley. They have all constantly inspired me with their enthusiasm and passion for science. They have not only taught me how to be a better scientist but have also shaped me into the person that I am today. Their constant encouragement and advice on all things related to science and otherwise are words that have kept me going throughout this PhD project and I know that this PhD would not have been possible without their help. The three of them have been fantastic mentors throughout my research journey and I couldn't have asked for better supervisors. I would also like to thank the three of them in helping read and re-reading this thesis. Without their proof-reading efforts, I fear that this thesis would have been incomprehensible.

I would also like to thank the people of the Harry lab (past and present) for their friendship and assistance both in and outside the lab; Hajime, Sam, Leigh, Jaye, Mike S, Mike L, Andrew, Cath, Amy, Nural, Cindy, Isa, Shirin, Beth, Daniel, Riti and Liz P. You guys have made the lab such an amazing place to work! Your knowledge and passion for science is infectious and inspiring.

A special thanks to Iain Duggin and Amy for being great mentors in the early years of my PhD during protein purifications. Also, Nick Dixon, Aaron Oakley, Nan and Faye with all protein chemistry knowledge and the tricks of the trade. I would also like to thank Joel Mackay and Lorna White for their help and insights into the world of NMR and both David Jacques and Kate Michie for mentoring me in the art of protein

crystallization. I would also like to thank the university and the i3 institute for providing equipment and lab space for conducting experiments. I would also like to thank our collaborators overseas for providing strains and assistance. In particular, I would like to thank Professor Frederico José Gueiros Filho from the Universidade de São Paulo for providing the *B. subtilis* FtsZ mutant protein that allowed me to complete my PhD and submit this thesis.

On a personal note, I would like to thank my family; dad, mum, Fabian and Quentina for their continuous love and support, as well as reminders which constantly drives me to be the best that I can be. I owe a big thanks to my extended family of uncles, aunties and friends from Galilee Best Unity Church Inc. which have supported me and encouraged me along the way. I wouldn't even be here without your support.

Lastly, I would like to thank the Australian government for providing me with an Australian postgraduate award. Without this financial assistance, I would not have a roof over my head and meals would be limited to drinking water.

Table of Contents

Certificate of originality	I
Acknowledgements	II
Table of Contents	IV
List of Figures and Tables	X
Abbreviations	XVI
Publications	XIX
Abstract.....	XXI
 CHAPTER 1 - INTRODUCTION.....	 1
 1.1 THE IDEAL ANTIBIOTIC	 1
1.2 TARGETS OF CURRENTLY APPROVED ANTIBIOTICS	5
1.3 MECHANISMS OF RESISTANCE TO CURRENTLY APPROVED ANTIBACTERIAL AGENTS.....	10
<i>1.3.1 Modification of the target.....</i>	<i>10</i>
<i>1.3.2 Enzymatic inactivation</i>	<i>12</i>
<i>1.3.3 Efflux pumps</i>	<i>13</i>
<i>1.3.4 Reduced permeability</i>	<i>15</i>
<i>1.3.5 Possible solutions to antibiotic resistance.....</i>	<i>15</i>
1.4 CELL DIVISION AND DIVISION PROTEINS	18
1.6 FTSZ: THE PROKARYOTIC HOMOLOGUE OF TUBULIN	21
1.7 FTSA: AN ACTIN-LIKE FTSZ-INTERACTING PROTEIN	23
1.8 INTERACTION BETWEEN FTSZ AND FTSA.....	25
1.9 IS FTSZ A GOOD ANTIBACTERIAL TARGET?.....	27
1.10 INHIBITORS OF FTSZ: THE BENZAMIDE DERIVATIVES	31
1.10 THESIS AIMS	33

CHAPTER 2 - MATERIALS AND METHODS	43
2.1 MATERIALS	43
2.1.1 Chemicals	43
2.1.2 Solutions	44
2.1.3 Bacterial strains and plasmids	47
2.2 METHODS	56
2.2.1 DNA manipulation.....	56
2.2.1.1 Plasmid extraction.....	56
2.2.1.2 Preparation and transformation of electro-competent <i>E. coli</i>	56
2.2.1.3 PCR amplification of wild-type <i>B. subtilis</i> <i>ftsZ</i> ¹²⁻³¹⁵ gene	57
2.2.1.4 Restriction digest of the PCR product and plasmid	58
2.2.1.5 Ligation of the PCR product and plasmid.....	58
2.2.1.6 Colony PCR	59
2.2.2 Protein purification	59
2.2.2.1 Overproduction trial of <i>Acinetobacter</i> FtsZ and FtsA	59
2.2.2.2 Analysis of the <i>Acinetobacter</i> FtsZ and FtsA protein overproduction and solubility.....	60
2.2.2.4 Ammonium sulphate precipitation trial	61
2.2.2.5 Sodium chloride dialysis trial	62
2.2.2.6 Optimized purification protocol.....	62
2.2.3 Functional assays	68
2.2.3.1 GTPase assay using wild-type <i>B. subtilis</i> FtsZ ¹²⁻³¹⁵	68
2.2.4 Nuclear Magnetic Resonance.....	70
2.2.4.1 Competition experiment using HSQC	70
2.2.5 Crystallography.....	70

2.2.5.1 Setting up crystal trays.....	70
2.2.6 <i>Molecular modelling</i>	71
2.2.6.1 Creating a protein homology model of <i>Staphylococcus aureus</i> FtsZ and <i>Acinetobacter</i> FtsA	71
2.2.6.2 Assessing the validity of the homology models	72
2.2.6.3 Protein-protein interaction using docking.....	73
2.2.6.4 Superimposition of multiple crystal structures	74
2.2.6.5 Identification of Accessible Binding Spheres.....	75
2.2.6.6 Molecular Dynamics Simulations.....	75
 CHAPTER 3 - UNDERSTANDING THE INTERACTION OF <i>ACINETOBACTER</i> FTSZ AND FTSA USING <i>IN SILICO</i> METHODS	 77
3.1 INTRODUCTION	77
3.1.1 <i>Interaction between FtsZ and FtsA</i>	79
3.2 RESULTS: <i>IN SILICO</i> INVESTIGATION OF THE INTERACTION BETWEEN FTSZ AND FTSA IN <i>ACINETOBACTER</i>	 82
3.2.1 <i>Analysis of full-length FtsZ amino acid sequence alignment to identify the conserved C-terminal peptide in Acinetobacter FtsZ</i>	82
3.2.2 <i>Accuracy validation of the 3D modelling program through the re-construction of the published Staphylococcus aureus FtsZ structure</i>	87
3.2.3 <i>In silico reconstruction of Acinetobacter spp. FtsA tertiary structure</i>	92
3.2.4 <i>In silico model of Acinetobacter spp. FtsZ and FtsA interaction</i>	97
3.3 DISCUSSION	103
 CHAPTER 4 – PROTEIN PURIFICATION OF FULL-LENGTH <i>ACINETOBACTER</i> FTSZ AND FTSA FOR <i>IN VITRO</i> INTERACTION STUDY	 108

4.1 INTRODUCTION	108
4.2 RESULTS: OVERPRODUCTION AND PURIFICATION OF THE FULL-LENGTH ACINETOBACTER FtsZ AND FtsA PROTEINS	110
4.2.1 <i>Overproduction and solubility analysis of Acinetobacter baumannii and Acinetobacter baylyi full-length FtsZ.....</i>	110
4.2.2 <i>Ammonium sulphate precipitation trial of untagged Acinetobacter full- length FtsZ.....</i>	114
4.2.3 <i>Purification trial of full-length Acinetobacter untagged FtsZ.....</i>	117
4.2.4 <i>Analysis and prevention of proteolysis of full-length A. baylyi untagged FtsZ during purification</i>	119
4.2.5 <i>Purification of full-length A. baylyi untagged FtsZ leading to X-ray crystallography trials</i>	122
4.2.6 <i>Crystallography trials using full-length A. baylyi untagged FtsZ.....</i>	123
4.2.7 <i>Overproduction analysis of full-length A. baylyi N-terminus and C- terminus hexa-histidine-tagged FtsA.....</i>	125
4.2.8 <i>Purification trial of full-length A. baylyi C-terminal hexa-histidine-tagged FtsA using nickel affinity chromatography</i>	129
4.2.9 <i>Concentrating full-length A. baylyi C-terminal hexa-histidine-tagged FtsA using various methods</i>	130
4.2.10 <i>Confirming full-length A. baylyi C-terminal hexahistidine-tagged FtsA polymeric state via size exclusion chromatography.....</i>	132
4.3 DISCUSSION	134
CHAPTER 5 - IN SILICO ANALYSIS OF FtsZ CRYSTAL STRUCTURES TO BETTER UNDERSTAND ITS POTENTIAL AS A DRUG TARGET	138
PREFACE	138

5.1 INTRODUCTION	138
5.2 RESULTS AND DISCUSSION: <i>IN SILICO</i> ANALYSIS OF FtsZ STRUCTURES FROM DIFFERENT BACTERIAL SPECIES	141
5.2.1 <i>Comparison of GDP-bound FtsZ structures from different bacterial species</i>	141
5.2.1.1 Superimposition of published FtsZ X-ray crystal structures	141
5.2.1.3 Comparison of accessible binding sites between GDP-bound FtsZs from various bacterial species.....	149
5.2.2 <i>Comparing GTP and GDP-bound FtsZ of various bacterial species</i>	154
5.2.2.1 Comparison of GTP- and GDP-bound FtsZ structures.....	154
5.2.2.2 Accessible binding site comparison of GTP- and GDP-bound non- staphylococcal FtsZ structures.....	157
5.2.3 <i>Molecular dynamics simulation.....</i>	161
5.3 CONCLUSION	167
CHAPTER 6 - FRAGMENT-BASED DRUG DISCOVERY USING FtsZ AS A TARGET.....	168
6.1 INTRODUCTION	168
6.1.1 <i>Inhibitors of FtsZ.....</i>	168
6.1.2 <i>Fragment-based drug discovery.....</i>	169
6.1.3 <i>Requirements for a successful FBDD project</i>	170
6.1.4 <i>Fragment-based drug screening using NMR.....</i>	171
6.1.5 <i>Producing compounds by fragment-linking and -growing.....</i>	173
6.2 RESULTS: FRAGMENT-BASED DRUG DISCOVERY USING <i>B. SUBTILIS</i> FtsZ AS THE TARGET	176

6.2.1 Bioinformatically identifying the mutation A182E on <i>B. subtilis</i> FtsZ structure.....	176
6.2.2 Initial fragment-based drug screening	177
6.2.3 TROSY-HSQC screen with ^{15}N labelled <i>B. subtilis</i> FtsZ ^{I-315} A182E	182
6.2.4 HSQC-NMR competition experiment using <i>B. subtilis</i> FtsZ ^{I-315} A182E...	184
6.2.5 Overproduction and purification of wild-type <i>B. subtilis</i> FtsZ ^{I2-315}	188
6.2.6 Functional assay using a GTPase kit with the wild-type <i>B. subtilis</i> FtsZ ^{I2-315}	192
6.2.7 Triple-ligand detect experiment using wild-type <i>B. subtilis</i> FtsZ ^{I2-315} to confirm the binding of the fragment 1, 3 and 14 to the wild-type protein.....	195
6.2.8 Crystallization of wild-type <i>B. subtilis</i> FtsZ ^{I2-315}	197
6.3 DISCUSSION	208
CHAPTER 7 - GENERAL DISCUSSION	214
CHAPTER 8 - REFERENCES	223

List of Figures and Tables

Figure 1.1: Pathways targeted by antibiotics	3
Figure 1.2: Timeline of antibiotic discovery	4
Figure 1.3: Mechanisms of lateral gene transfer	9
Figure 1.4: Vancomycin resistance mechanism of action	11
Figure 1.5: The working of the efflux pump complex TolC-AcrAB in <i>E. coli</i>	14
Figure 1.6: Schematic of <i>E. coli</i> and <i>B. subtilis</i> cell division	19
Figure 1.7: The <i>E. coli</i> cell division proteins and their partners that form the divisome	20
Figure 1.8: Crystal structure of <i>M. jannaschii</i> FtsZ and its ability to polymerise	23
Figure 1.9: The crystal structures of FtsA from <i>T. maritima</i> and actin..	25
Figure 1.10: Structural comparison of <i>S. aureus</i> FtsZ and human α -tubulin	29
Figure 2.1: Standard curve of known phosphate concentration vs absorbance at 650 nm	68
Figure 2.2: An example of a well set up in the 96-welled MRC plate for crystallography	71
Figure 3.1: Crystal structure of FtsA from <i>T. maritima</i> bound to FtsZ C-terminal peptide	80
Figure 3.2: Full-length FtsZ amino acid sequence alignment using Clustal Omega	83
Figure 3.3: Peptide location affects linker length	86

Figure 3.4: Superimposition of <i>S. aureus</i> FtsZ homology model to that of the <i>S. aureus</i> FtsZ X-ray crystal structure using Discovery Studio 4.5	91
Figure 3.5: Homology modeling workflow in Discovery Studio 4.5	92
Figure 3.6: 3D-Profile Verification of the <i>Acinetobacter</i> spp. homology FtsA model using Discovery Studio 4.5	96
Figure 4.1: <i>A. baylyi/baumannii</i> untagged FtsZ purification workflow	113
Figure 4.2: Ammonium sulphate precipitation trials of untagged <i>A. baumannii</i> and <i>A. baylyi</i> FtsZ	115
Figure 4.3: Testing of untagged <i>A. baumannii</i> and <i>A. baylyi</i> FtsZ stability in a range of sodium chloride concentrations	116
Figure 4.4: Testing gel filtration method using <i>A. baylyi</i> and <i>A. baumannii</i> untagged FtsZ revealed a double band	117
Figure 4.5: <i>A. baylyi</i> untagged FtsZ purification	120
Figure 4.6: Test to see if proteolysis happens during cell lysis for <i>A. baylyi</i> FtsZ	121
Figure 4.7: Successful <i>A. baylyi</i> untagged FtsZ purification	123
Figure 4.8: Microcrystal formation of <i>A. baylyi</i> untagged full-length FtsZ	125
Figure 4.9: Overproduction screening of full-length <i>A. baylyi</i> N-terminus and C-terminus hexa-histidine-tagged FtsA	127
Figure 4.10: <i>A. baylyi/baumannii</i> N- and C-hexahistidine tagged FtsA purification workflow	128
Figure 4.11: Inclusion bodies purification trial of N-terminus and C-terminus his-tagged <i>A. baylyi</i> full-length FtsA from 1L culture ...	128

Figure 4.12: Purification trial of <i>A. baylyi</i> C-terminal hexahistidine-tagged full-length FtsA	130
Figure 4.13: Concentrating full-length <i>A. baylyi</i> C-terminal hexahistidine-tagged FtsA via dialyzing against PEG 20,000	132
Figure 5.1: Druggable regions of FtsZ	140
Figure 5.2: Superimposition of FtsZ from various organisms and of FtsZ structures with human α- and β-tubulin	143
Figure 5.3: Comparison of druggable pocket sizes between FtsZ from different organisms	147
Figure 5.4: Comparison of the accessible binding sites of various GDP-bounded FtsZ structures	152
Figure 5.5: Amino acid sequence alignment of the T6-loop from multiple bacterial species using Clustal Omega	153
Figure 5.6: Analysis of the accessible binding sphere of <i>S. aureus</i> FtsZ when bound to different nucleotides and the FtsZ inhibitor PC190723	157
Figure 5.7: A model of structural changes in monomeric FtsZ upon binding to GDP and GTP	160
Figure 5.8: Conformational change of <i>B. subtilis</i> FtsZ	162
Figure 5.9: Conformational change of <i>S. aureus</i> FtsZ when bound to nucleotides and an inhibitor	165
Figure 5.10: Conformational change of <i>S. aureus</i> FtsZ	166
Figure 6.1: Chemical structure of Vemurafenib and Venetoclax	171
Figure 6.2: Examples of antibacterials that were developed from fragment-based drug discovery	171

Figure 6.3: Typical schematic of fragment-based drug discovery	173
Figure 6.4: The process of fragment linking	174
Figure 6.5: The process of fragment growth	174
Figure 6.6: Indication of the A182E mutation position in the <i>B. subtilis</i> FtsZ	177
Figure 6.7: Cut-off value for determining “hit” fragments in the triple- ligand detect experiments	180
Figure 6.8: Mapping the binding location of the four hit fragments on the <i>B. subtilis</i> FtsZ crystal structure	183
Figure 6.9: An example spectrum showing fragment binding to <i>B.</i> <i>subtilis</i> FtsZ ¹⁻³¹⁵ A182E	186
Figure 6.10: The preferred binding site of fragment 1, 3 and 14 on the <i>B. subtilis</i> FtsZ ¹⁻³¹⁵ A182E	187
Figure 6.11: Overproduction of wild-type <i>B. subtilis</i> FtsZ ¹²⁻³¹⁵	189
Figure 6.12: Chromatogram and SDS-PAGE of size exclusion chromatography during the purification of wild-type <i>B. subtilis</i> FtsZ ¹²⁻³¹⁵	191
Figure 6.13: Concentrated protein sample of wild-type <i>B. subtilis</i> FtsZ ^{12- 315} from peak 1 and peak 2	192
Figure 6.14: Testing the protein sample for phosphate contamination using malachite green	193
Figure 6.15: Calculated GTPase specific activity of wild-type <i>B. subtilis</i> FtsZ ¹²⁻³¹⁵ at different protein concentrations	195
Figure 6.16: Diffraction pattern produced by wild-type <i>B. subtilis</i> FtsZ ¹²⁻³¹⁵ crystal	203

Figure 6.17: Optimization of crystallization condition of wild-type <i>B. subtilis</i> FtsZ¹²⁻³¹⁵ protein resulted in the increase of crystal size	204
Figure 6.18: The effect of using 20% glycerol as a cryoprotectant to the crystal diffraction pattern	207
Table 1.1: Current reported inhibitors of FtsZ and experimental evidence provided	35
Table 2.1: Antibiotic sources and their working concentration for <i>E. coli</i>	43
Table 2.2: Media used in this study	43
Table 2.3: Solutions used in this study	44
Table 2.4: Bacterial strains used in this study	47
Table 2.5: Plasmids used and constructed in this study	53
Table 2.6: Primers used for the PCR amplification of <i>B. subtilis</i> FtsZ¹²⁻³¹⁵	57
Table 2.7: The molecular weight, pI and extinction coefficient of proteins used in this study	67
Table 3.1: <i>S. aureus</i> FtsZ homology model analysis	90
Table 3.2: <i>Acinetobacter</i> spp. FtsA homology model analysis	95
Table 3.3: Simulated interactions of <i>T. maritima</i> FtsZ to <i>A. baumannii</i>/<i>baylyi</i> FtsA	99
Table 4.1: Examination of strains and induction temperatures to overproduce soluble <i>A. baumannii</i> and <i>A. baylyi</i> FtsZ	112
Table 5.1: RMSD values obtained from the superimposition of FtsZ and tubulin structures	144
Table 5.3: FtsZ structural differences between the GDP- and GTP-bound states	155

Table 6.1: Mutant <i>B. subtilis</i> FtsZ amino acid residues which changed upon fragment binding during the TROSY-HSQC experiment.....	182
Table 6.2: Amino acid of mutant <i>B. subtilis</i> FtsZ which experienced a change in their signals upon the addition of fragments and GDP.....	185
Table 6.3: Comparison of triple-ligand detect experimental data between mutant and wild-type <i>B. subtilis</i> FtsZ protein.....	197
Table 6.4: Conditions which were identified to produce <i>B. subtilis</i> FtsZ¹²⁻³¹⁵ crystal with sharp edges.....	199
Table 6.5: Cell dimension of the crystal form pursued in this study	205

Abbreviations

°C	Degrees Celcius
μ	Micro (10 ⁻⁶)
¹⁵ N	Nitrogen 15
Å	Angstrom
ADP	Adenosine 5'-diphosphate
Amp ^r	Ampicillin resistance
APS	Ammonium per sulfate
ATP	Adenosine 5'-triphosphate
bp	Base pair(s)
cm	centimeter
Cα	alpha carbon
Da	Dalton(s)
DNA	Deoxyribose nucleic acid
dNTPs	deoxyribonucleotide triphosphate
DTT	Dithiothreitol
FD	Faraday constant
<i>fts</i>	Filamentous temperature sensitive
g	Gram(s)
GDP	Guanosine 5'-diphosphate
GTP	Guanosine 5'-triphosphate
h	Hour(s)
HEPES	(4-(2-hydroxyethyl)-1-piperazineethanesulfonic acid)
IPTG	Isopropyl-1-thio-β-D-galactopyranoside
K	Kelvin

Kan ^r	Kanamycin resistance
kb	Kilobase(s)
K _d	Dissociation constant
kDa	Kilo (10 ³)
L	Liter
LB both	Luria-Bertani broth
m	Milli (10 ⁻³)
M	Moles per Liter (Molar)
min	Minute(s)
MTS	Membrane targeting sequence
MWCO	Molecular weight cut off
n	Nano (10 ⁻⁹)
NBD	nucleotide-binding domain
OD _(x)	Optical density measured at x nanometer wavelength
p	Probability
PCR	Polymerase chain reaction
PEG	Poly-ethylene glycol
PMSF	Phenylmethylsulfonyl fluoride
ps	Picosecond
R	resolution
RMSD	root mean square deviation
RNA	Ribonucleic acid
rpm	Revolution per minute
rRNA	Ribosomal ribonucleic acid
SDS	Sodium dodecyl sulphate

SDS-PAGE	Sodium dodecyl sulfate-polyacrylamide gel electrophoresis
sec	Second(s)
STD-NMR	Saturated transfer difference nuclear magnetic resonance
TEMED	Tetramethylethylenediamine
Tet ^r	Tetracycline resistance
Tris	Tris(hydroxymethyl)methylamine
TROSY-HSQC	Transverse relaxation optimized spectroscopy-heteronuclear single quantum coherence
U	Units (enzyme activity)
V	Volts
v/v	Volume per volume
w/v	Weight per volume
X _g	Times gravity
Ω	Ohms

Publications

Journal articles

Bottomley AL, Liew ATF, **Kusuma KD**, Peterson E, Seidel L, Foster SJ, et al. Coordination of Chromosome Segregation and Cell Division in *Staphylococcus aureus*. Frontiers in Microbiology. 2017;8(1575).

Kusuma KD, Griffith R, Harry EJ, Bottomley AL, Ung AT. *In silico* Analysis of FtsZ Crystal Structures Towards a New Target for Antibiotics. Australian Journal of Chemistry. 2018

Conference proceedings

Kusuma KD, Amy Bottomley, Alison Ung, Aaron Oakley, Nick Dixon, Nan Li, Elizabeth Harry (**2015**) Cell division as a new target for the development of antibiotics against *Acinetobacter*, **East Coast Protein Meeting, Brisbane, Poster presentation.**

Kusuma KD, Amy Bottomley, Elizabeth Harry, Renate Griffith, Alison Ung (**2017**) Understanding FtsZ as an antibacterial target, **Solution for Drug-Resistant Infections Conference, Brisbane, Poster presentation.**

Abstract

The problem of antibiotic resistance is a complex issue and one that urgently needs addressing from multiple sectors, including agriculture, medicine, science/research, government, social science, businesses and the community. Although many strategies are being implemented around the world to address these different aspects that contribute to the rise and spread of antibiotic resistance, one further possibility to help alleviate this problem is through the design of novel antibiotics. The essential process of bacterial cell division, is yet to be targeted by any of the FDA-approved antibiotics and represents an untapped area of potential drug targets. In this thesis, the overall strategy of inhibiting the bacterial cell division process is to target the essential and conserved protein FtsZ in two ways: Firstly, to understand the essential interaction of FtsZ with another division protein, FtsA as a starting point to design inhibitors of division complex formation and, secondly, to develop compounds that inhibit FtsZ function.

Characterizing the protein-protein interaction of FtsZ and its partner FtsA used the proteins from the organism *Acinetobacter* spp.. This is because *A. baumannii* is now classified by the World Health Organization as a priority 1 pathogen that urgently needs an antibiotic against due to its high multidrug resistance profile, as well as causing high mortality rates. Two of the most highly conserved bacterial cell division proteins, FtsZ and FtsA, have been recognised as promising drug targets in *Acinetobacter* spp. and other bacteria. The interaction of these two proteins has been known for over a decade with mutational studies indicating that the conserved aspartate and proline at the extreme C-terminal peptide of FtsZ being the important amino acid residues for the interaction of FtsZ and FtsA in *Escherichia coli* and other bacterial species. Co-crystallography of *Thermotoga maritima* FtsZ C-terminal peptide and FtsA identified

an additional amino acid; arginine, to be important in the interaction of FtsZ and FtsA. In the *Acinetobacter* spp. the aspartate, proline and arginine have been changed to a serine, glutamine and lysine, respectively. Understanding this could potentially be used to develop new narrow-spectrum antimicrobials to specifically treat *Acinetobacter* infections. The work in this thesis attempted to understand the implication of these amino acid differences by initially conducting an *in silico* study. The data obtained suggests that the serine, glutamine and lysine are important for the FtsZ/FtsA interaction of *Acinetobacter* spp. Further follow up co-crystallographic studies were planned using full-length *Acinetobacter* FtsZ and FtsA. Both of these full-length *Acinetobacter* proteins were successfully purified in this study but, the purified FtsZ protein was unable to form crystals of acceptable size for structure determination, while the purified FtsA were found to be aggregated. Therefore, in the interest of time and for gaining positive results, the focus of the project was shifted towards solely understanding and targeting FtsZ.

Thus far, many published FtsZ inhibitors have been shown to target FtsZ in one of the three druggable regions on the protein: nucleotide-binding domain, interdomain cleft and T7-loop. A missing piece of information is an in-depth understanding of FtsZ structure at the molecular level across diverse bacterial species to ensure inhibitors have high affinity for the FtsZ target in a variety of clinically relevant pathogens. To address this, an *in silico* investigation was conducted by analysing multiple FtsZ structures, which revealed that FtsZ groups into two distinct classes based on structural differences. The outcome of this analysis lead to the suggestion of several binding pockets on FtsZ which can potentially be used as a broad- and narrow-spectrum target. The use of fragment-based drug discovery approach, allowed the confirmation of one of the suggested pockets, which is located towards the front of the nucleotide-binding domain.

This pocket is yet to be reported in the literature, therefore, allowing the possibility of novel drug design to contribute in tackling the global issue of antimicrobial resistance.

Chapter 1 - Introduction

Ever since the discovery of penicillin in 1928, antibiotics have revolutionized medicine by allowing various types of medical therapies and surgeries, such as bowel surgery, hip replacements and treatment of leukaemia, to be routinely conducted (1, 2). It has also been estimated that the widespread availability of antibiotics in developed countries has added 30 years to human life expectancy (3). This, however, is changing due to the rise of antimicrobial resistance which is shifting society into a post-antibiotic era where common and minor infections will once again be lethal and will cause many of the routinely conducted medical procedures to be too risky due to the high-risk of attaining complications associated with untreatable infections (2, 4). One measure to help alleviate the antibiotic resistance crisis is to develop new antimicrobials which have a novel mechanism of action. However, prior to discussing new antimicrobials with a novel mechanism of action, it is imperative that we ask, “What is an ideal antibiotic?” and also understand how resistance occurs.

1.1 The ideal antibiotic

Since the discovery of penicillin, many highly effective antibiotics have been identified and their chemical variants developed for clinical use in the treatment of bacterial infections (1, 5). With this comes the question, “What is an ideal antibiotic?” Philosophically, an ideal antibiotic is an antibacterial agent that kills or inhibit the growth of harmful bacteria in a host regardless of the site of infection without affecting beneficial microbes (gut/skin flora) or causing undue toxicity to the host, and with low potential for resistance (6). To achieve this, the antibacterial agent has to exhibit broad-spectrum ability towards the harmful bacteria, while at the same time demonstrate

exceptional blood/fluid circulation as well as, absorption, distribution, metabolism and excretion (ADME) properties (6). These properties of an ideal antibiotic will allow the use of these drugs in low dosage and at the same time create a large therapeutic window. Unfortunately, no such antibiotics have ever existed as most clinically used antibiotics today do not have a broad enough spectrum to treat infections caused by all Gram-positive and –negative bacteria (6). For that reason, most clinically used antibiotics today are grouped as Gram-positive agents, Gram-negative agents and a few others with partial broad-spectrum activity (7). Antibiotics, without a doubt, have revolutionized modern medicine but many of these drugs are failing to treat infections effectively due to the rapid increase in the number of bacteria resistant to these drugs. Today, the majority of modern antibiotics target either cell wall synthesis, protein biosynthesis, DNA repair and replication, RNA polymerase or bacterial cellular metabolism, such as folic acid metabolism (Figure 1.1) (8). These types of antibiotics are the last novel class developed during the 1940s to 1980's and, in the 21st century, only a handful have been approved by the FDA. These antibiotics have, thus far, proven to be successful in treating infections. However, recently, bacteria resistant to these antibiotics have increased in numbers which have caused these drugs to be ineffective for use in treating infections. Figure 1.2 shows a timeline of antibiotic approved by the FDA from the discovery of penicillin up to the year 2000 onwards.

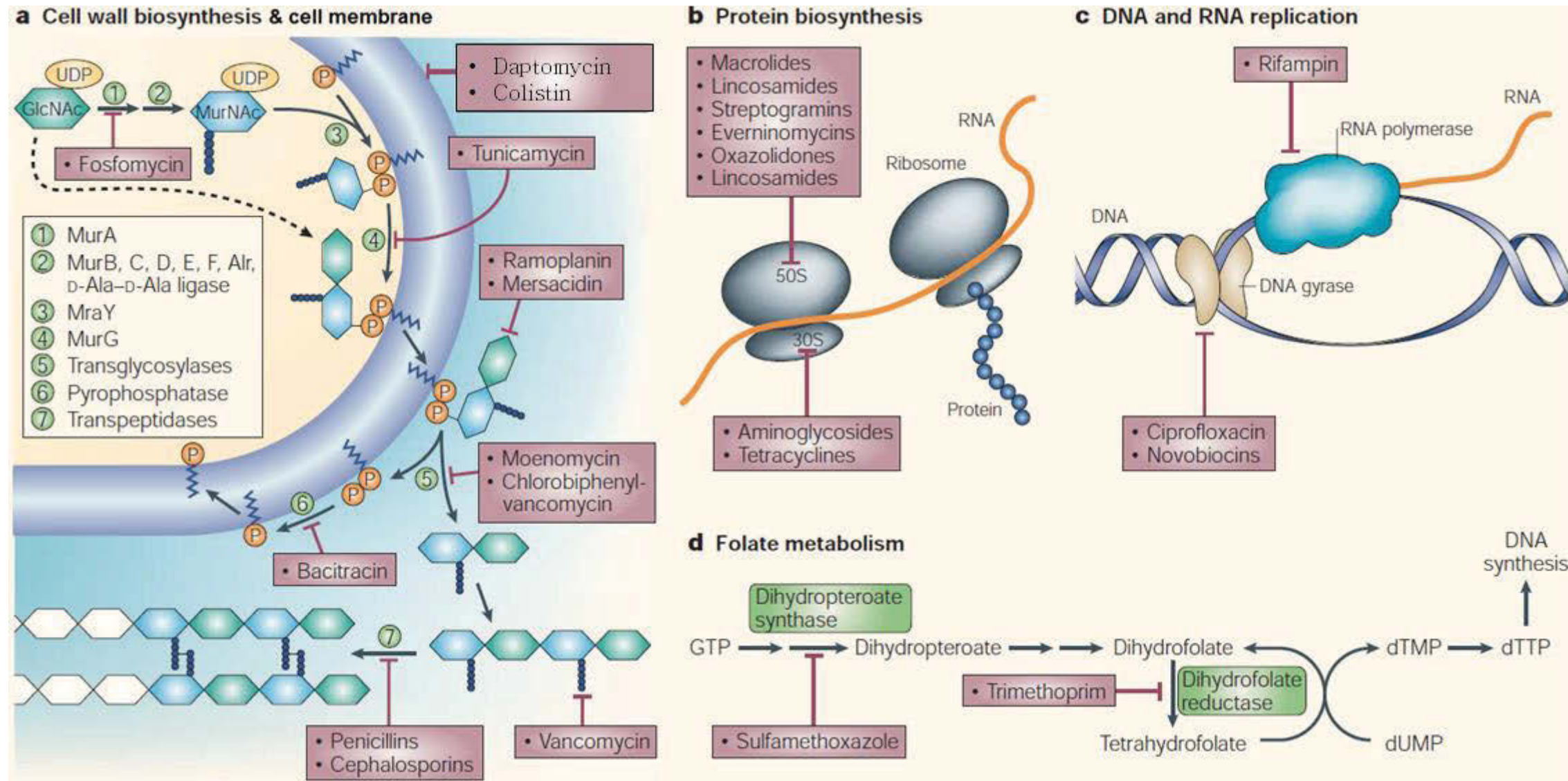


Figure 1.1: Pathways targeted by antibiotics. a–e depicts metabolic pathways in the cell that have been, or are proposed to be, targets for antibiotic action. **a** | Cell-wall biosynthesis & cell membrane: the intracellular steps of murein (peptidoglycan) biosynthesis are catalysed by the enzymes MurA–F and MurG (steps 1–4). Peptidoglycan is a polymer of two hexoses (filled hexagons) — N-acetylglucosamine (GlcNAc) and N-acetyl-muramic acid (MurNAc). Peptidoglycan units are transferred to a carrier lipid — bactoprenol-phosphate (orange circles) — which transports precursor molecules across the cell membrane, generating Lipids I and II. Sugars and phosphates are added by transglycosylation and pyrophosphorylation (steps 5 and 6), and finally, a peptide bond between the peptide chains is formed (step 7). Antibiotics that inhibit cell-wall synthesis are indicated. Antibiotics such as deptomycin and colistin interferes with the cell membrane by affecting the cell membrane potential **b** | Protein biosynthesis: bacterial ribosomes comprise two subunits (30S and 50S) of rRNA and protein. Structural studies have identified the sites at which antibiotics bind. **c** | DNA and RNA replication: rifampin binds to RNA polymerase and prevents attachment of the polymerase to DNA, thereby inhibiting transcription. Ciprofloxacin and novobiocin bind to DNA gyrase, thereby preventing the introduction of supercoils in DNA. **d** | Folate metabolism: folate is necessary for the synthesis of thymine, which, in turn, is an essential component of DNA. The figure shows antibiotics that block steps in folate metabolism and therefore block the synthesis of thymine. Adapted from (9).

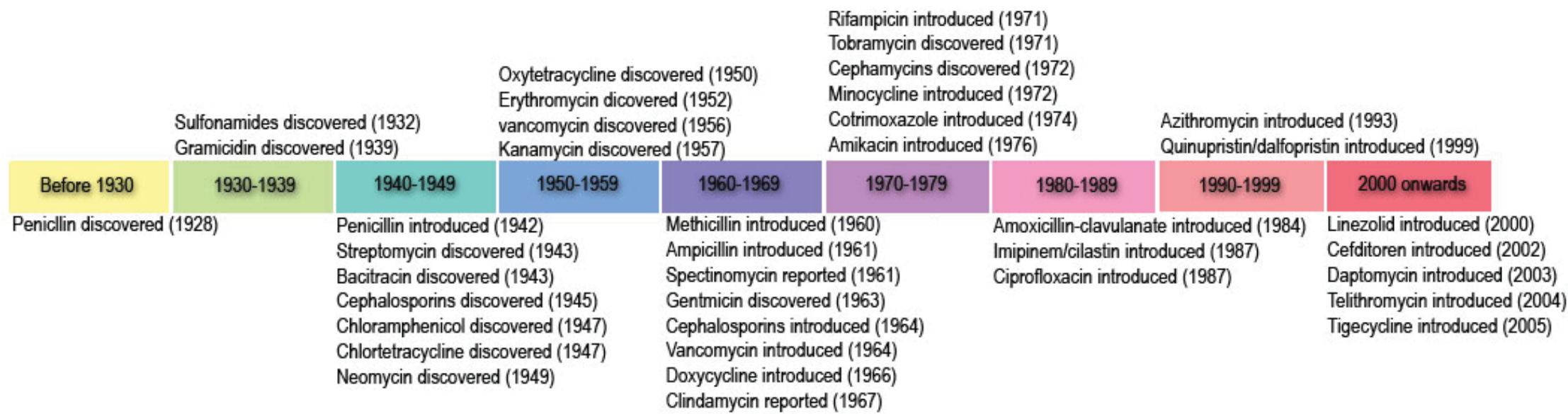


Figure 1.2: Timeline of antibiotic discovery. Antibiotic discovery peaked in the mid- towards the late-1900s and these are still use clinically today. These, however, are increasingly becoming inadequate to treat infections as bacteria resistant to these antibiotics are increasing in numbers. Numbers of discovered antibiotics have since dwindled in the 21st century. Adapted from (10).

1.2 Targets of currently approved antibiotics

Bacterial cell wall is made up of a key component known as peptidoglycan, which function in maintaining cell shape and protects the cell from bursting by its internal turgor (11). Peptidoglycan itself consists of glycan strands connected by short peptides which form a continuous, mesh-like structure around the cytoplasmic membrane (12). The glycan strands are made up of alternating *N*-acetylglucosamine (GlcNAc) and *N*-acetylmuramic acid (MurNAc) residues linked by β -1,4 glycosidic bonds and the peptide is made out of L- and D-amino acids which are linked to MurNAc residues (12). The peptide group in Gram-negative bacteria is typically comprised of L-alanine- γ -D-glutamate-diaminopimelate(*meso*-DAP)-D-alanine-D-alanine (13). The peptide group in some Gram-positive bacteria like *Bacillus subtilis* is the same as that of the Gram-negative peptide group, while the peptide group in other Gram-positive bacteria will be a variation of this. For example, the peptide group of *Staphylococcus aureus* is typically comprised of L-alanine- γ -D-glutamate-L-lysine-D-alanine-D-alanine with a pentaglycine branch protruding from the L-lysine residue (13). Protruding peptides from adjacent glycan strands may then be connected through the carboxyl group of D-alanine at position 4 of one peptide to the ϵ -amino group of the *meso*-DAP residue at position 3 of another peptide, creating an amide bond (12). During cell growth and division, peptidoglycan synthesis starts with the production of precursors to the glycan strands and the peptide in the cytoplasm of the cell (Figure 1.1a). These precursors are then phosphorylated in the cytoplasm to finally produce lipid II, which is then brought to the vicinity of the inner membrane and then translocated to the outside of the cell by a lipid II flippase (Figure 1.1a). For the duration of cell growth and division, the surface area of the cell membrane increases and through the aforementioned process, new peptidoglycan is incorporated into the new site by class A penicillin-binding proteins

(PBPa's), through the polymerization of peptidoglycan by cross-linking the peptide chains (12). For a more detailed explanation of peptidoglycan synthesis, the reader is directed to reference (14). As shown in Figure 1.1a, a number of highly effective antibiotics have been developed to target the various enzymes and/or proteins involved in the peptidoglycan synthesis pathway(15).

The first antibiotic discovered, penicillin, is part of the β -lactam class of antibiotics and is known to target the PBPs that assemble and cross-link the peptidoglycan of the bacterial cell wall (16). Penicillin compounds (e.g. penicillin G, methicillin, aminopenicillin) bind strongly to class A PBPs, resulting in the prevention of cell wall synthesis and causing cell death (17). Since then, more β -lactams have been developed, including cephalosporins, carbapenems and monobactams (13). Unfortunately, there now exists bacterial strains, especially those of the *Enterobacteriaceae* family, that are resistant to even third generation β -lactams like cephalosporins, due to the production of extended-spectrum β -lactamases (ESBLs) (18). There are also other antibiotic classes that are non- β -lactam antibiotics which are known to inhibit cell wall synthesis by targeting molecules other than the PBPs and these include glycopeptide (e.g. vancomycin), lipopeptide (e.g. friulimicin B) and lipodepsipeptide (e.g. daptomycin (A)) antibiotics (15). Similarly, there also exist bacterial strains that are resistant to the glycopeptide, lipopeptide and lipodepsipeptide classes of antibiotics.

Protein synthesis is essential for all life and in bacterial cells, the process is carried out by a 70S rRNA which is made up of 50S and 30S ribosomal subunits, while eukaryotic cells use an 80S rRNA which comprise of the 60S and 40S ribosomal subunit. Antibiotics such as aminoglycosides (e.g. streptomycin), tetracycline and macrolides (e.g. erythromycin) selectively bind to the 30S or 50S subunit of the bacterial ribosome, which inhibits protein biosynthesis in bacteria. One such example is erythromycin,

which binds to the 23S rRNA of the 50S subunit causing a blockage at the exit of the growing peptide chains, thus inhibiting translocation of the growing peptide chain (19, 20). However, the effective use of erythromycin in clinical settings has been hindered due to the rise of erythromycin-resistant strains such as erythromycin-resistant *Streptococcus pneumoniae* (6).

Transcription has also been successfully targeted by antibiotics. Rifampicin specifically targets bacterial RNA polymerase by binding to the β -subunit. This inhibition sterically blocks the growth of the RNA chain during the transcription process (21). DNA replication can also be targeted safely without affecting the eukaryotic host. The DNA gyrase enzyme, also known as DNA topoisomerase type II, controls the topological state of DNA by relieving strain as DNA is unwound by helicase enzymes during DNA synthesis. Antibiotics such as fluoroquinolones (e.g. ciprofloxacin) successfully target DNA gyrase without inhibiting eukaryotic topoisomerase by binding to the N-terminal domain of the enzyme and preventing the DNA from binding, hence inhibiting DNA replication (22). Similar to erythromycin, the use of fluoroquinolones in clinical settings is also being affected due to the rise of resistant strains to this class of antibiotics; for example *Escherichia coli* (23) and *Neisseria gonorrhoeae* (24).

Lastly, the synthesis of folic acid is another target for antibiotics. Sulfonamides (e.g. prontosil) and trimethoprim are known to inhibit dihydropteroate synthase (DHPS), an enzyme that acts as an intermediate in folate biosynthesis. Antibiotic drugs such as sulfonamides and DHPP (6-hydroxymethyl-7,8-dihydropterin monophosphate) bind the DHPS binding pocket and act as competitive inhibitors of the enzyme (25), which will eventually lead to the inhibition of DNA synthesis (7). Again resistance to these

class of antibiotics is already being seen; not just in hospital settings but also in the environment (26, 27).

Additionally, genes giving rise to resistance are able to be transferred across bacterial species in the environment through lateral gene transfer (26-28) and this has been shown to accelerate the spread of resistance, particularly with respect to multidrug resistance genes (29). Exacerbating this is that, the whole process of lateral gene transfer is not dependant on cell division and so enrichment of these resistant genes happens very rapidly and without the need for multiplication. Mechanisms of lateral gene transfer are depicted in Figure 1.3. The acquisition of these genes by bacteria have caused bacterial cells to become resistant in several ways and these are discussed further below.

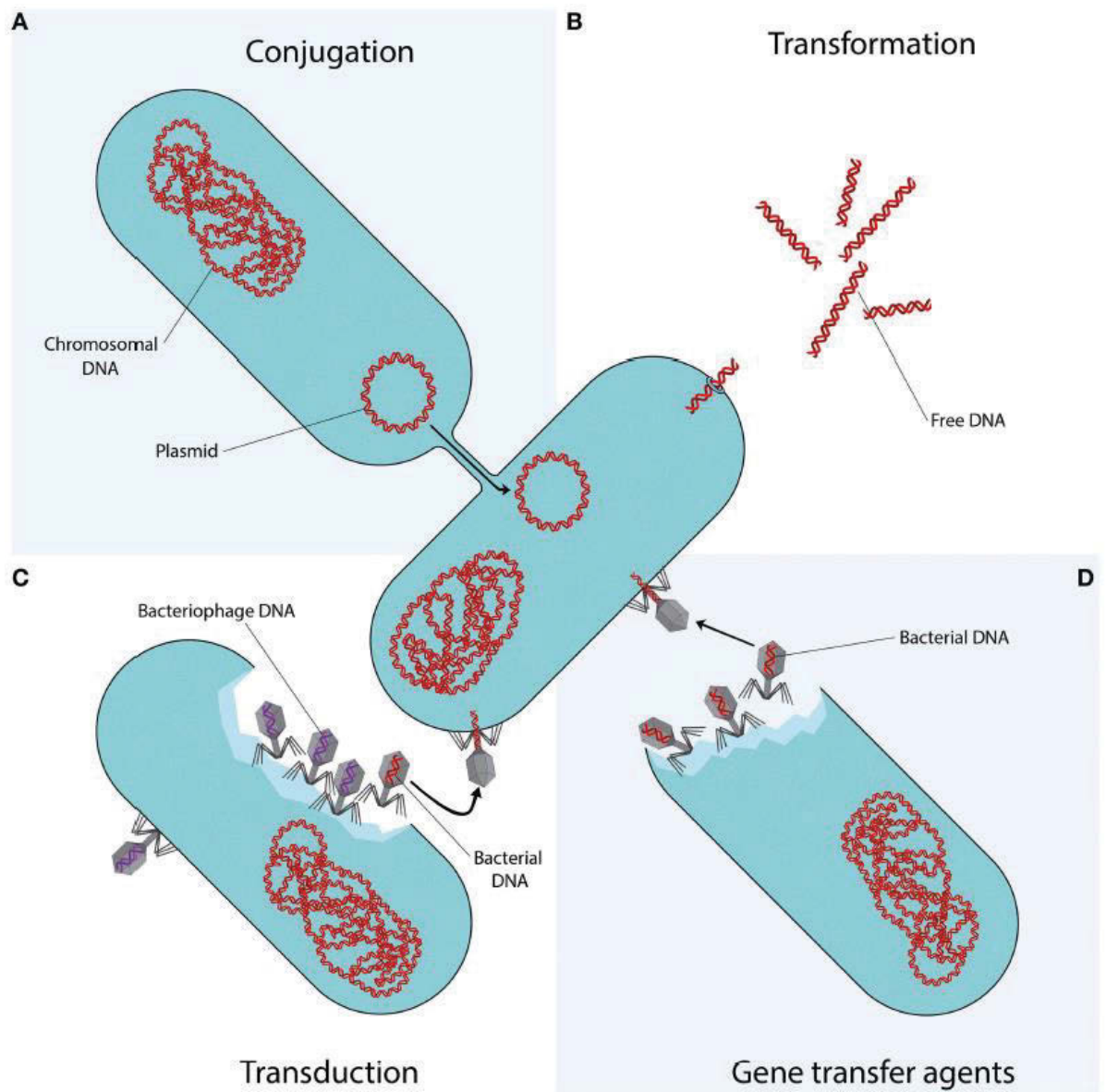


Figure 1.3: Mechanisms of lateral gene transfer. Each quadrant represents one different method of lateral gene transfer. **(A)** Conjugation is a process requiring cell to cell contact via cell surface pili or adhesins, through which DNA is transferred from the donor cell to the recipient cell. **(B)** Transformation is the uptake, integration, and functional expression of naked fragments of extracellular DNA. **(C)** Through specialized or generalized transduction, bacteriophages may transfer bacterial DNA from a previously infected donor cell to the recipient cell. During generalized transduction, bacterial DNA may be accidentally loaded into the phage head (shown as a phage with a red DNA strand). During specialized transduction, genomic DNA neighbouring the prophage DNA is co-excised and loaded into a new phage (not shown). **(D)** Gene transfer agents (GTAs) are bacteriophage-like particles that carry random pieces of the producing cell's genome. GTA particles may be released through cell lysis and spread to a recipient cell. Adapted from (29).

1.3 Mechanisms of resistance to currently approved antibacterial agents

Bacterial cells become resistant to our currently available antimicrobials *via* numerous biological factors including mutation or modification of the drug target site, enzymatic inactivation or modification of the antibiotic, resistance through decreased permeability of the antibiotic to get inside the cell, acquisition of alternative metabolic pathways and finally through efflux pump proteins (30-32).

1.3.1 Modification of the target

Most antibiotics specifically bind to their target in order to disrupt the normal function of the target. Mutation or modification of the target drug site has contributed to antibiotic resistance and this is responsible for the resistance to aminoglycosides, β -lactams, quinolones, rifamycins, lipopeptides, tetracyclines and macrolides. For example, the most common mechanism of resistance to macrolides is by target modification, which is through methylating the adenine residue in domain V of the 23S rRNA of the 50S ribosomal unit and hence blocking macrolides to bind that site (30).

Target modification has also been linked to vancomycin resistance in *Enterococci* species through the modification of its peptidoglycan. Vancomycin is known to bind D-alanine-D-alanine found in the peptide portion of peptidoglycan, thereby inhibiting the cross-linking of this peptide and causing cell death (33). Resistance to vancomycin has been attributed to the modification of the target by replacing the amide link in an alanine residue with a ketone group, which converts a D-alanine residue to a D-lactate, giving rise to a D-alanine-D-lactate sequence instead of D-alanine-D-alanine (33) (Figure 1.4). This effectively eliminates the crucial hydrogen bond through the amide

group on the peptide and instead introduces lone pair repulsion by replacing the amide group with oxygen on the peptide (33) (Figure 1.4). By doing this, the affinity of vancomycin for peptidoglycan is reduced almost 1000-fold.

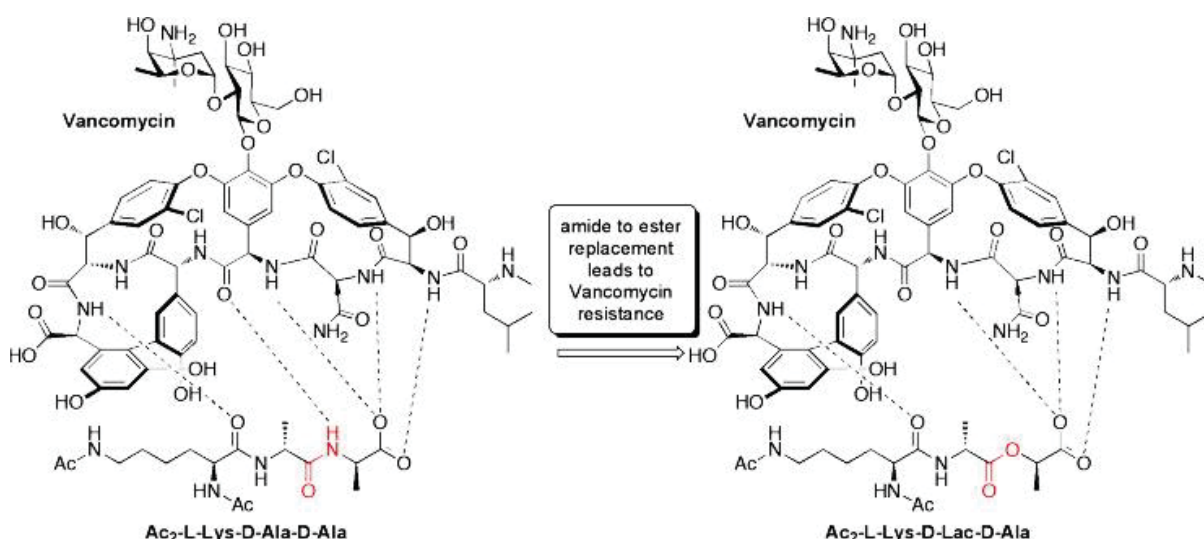


Figure 1.4: Vancomycin resistance mechanism of action. Vancomycin is known to bind to D-alanine-D-alanine (D-Ala-D-Ala) residue in the peptide portion of peptidoglycan. Resistance to vancomycin is caused by the conversion of D-Ala-D-Ala to D-Lactate-D-Alanine (D-Lac-D-Ala). The normal D-Ala-D-Ala structure allow for a crucial hydrogen bond through the interaction of the nitrogen of the amide group in the peptide (coloured red on the left) but the conversion of D-alanine to D-lactate changes the amide group to an oxygen (coloured red on the right), which results in the abolishment of the crucial hydrogen bond between the oxygen of vancomycin and the amide group on the peptide. Adapted from (33).

Resistance arising from the mutation of the target site has also been identified for several other antibiotic classes such as oxazolidinone and β -lactam (34). Most often than not, this mechanism of resistance is usually through the acquisition of a gene encoding a protein homologous to the original target but the acquired gene contains a mutation at the encoded antibiotic target site, giving resistance to the bacterial cell (34). For example, methicillin-resistant *Staphylococcus aureus* (MRSA) have acquired the staphylococcal chromosome cassette *mec* (SCC*mec*) element (35). The element carries the *mecA* gene which encodes the β -lactam insensitive protein PBP2a. Methicillin,

being a derivative of penicillin, will also target the PBP and in this case PBP2a (35). *S. aureus* sensitive cells will only have one copy of this gene encoding the wild-type protein, which will be targeted by methicillin, causing the cells to die. However, MRSA, have two copies of this gene, one coding for the wild-type protein in its chromosome and the mutated version encoded on the *SCCmec* element (35). Cells which have the *SCCmec* element will use the wild-type PBP2a as a decoy for the target of methicillin while at the same time using the methicillin-insensitive PBP2a to carry out normal peptidoglycan synthesis.

1.3.2 Enzymatic inactivation

Enzymatic modification and degradation of an antibiotic is another cause of resistance that has limited the use of several antibiotics, including chloramphenicol and β -lactams. The increase in resistance against chloramphenicol and β -lactams has been partly due to the ability of bacteria to easily and readily transfer genes encoding resistance *via* lateral gene transfer. Enzymes such as chloramphenicol acetyltransferase, which inactivates chloramphenicol by acetylating the hydroxyl group on the carbon at position 3 (36), and β -lactamases, which hydrolyse the amide bond of a β -lactam ring, has rendered chloramphenicol and penicillin derivatives inactive and therefore ineffective in the clinic (30, 37, 38). A study conducted in 2010 by Karthikeyan *et al.* analysed a number of ESBL isolates of Gram-negative *Enterobacteriaceae* such as *E. coli* and *Klebsiella pneumoniae* and found an increase in prevalence of a novel gene dubbed New Delhi metallo- β -lactamase 1 (*NDM-1*) (18). The presence of this gene in a bacterial cell confers resistance to all β -lactams, fluoroquinolones and aminoglycosides (18). This is of major concern, as these three families of antibiotics are the frontline treatment for Gram-negative infections.

1.3.3 Efflux pumps

Another major mechanism of resistance is the efflux pumps. Efflux pumps are a complex of proteins located across the cell membrane, with some spanning from the inner- to the outer-membrane in Gram-negative bacteria and some spanning from the inner-membrane to the peptidoglycan layer in Gram-positive bacteria (39). Antibiotics are firstly brought in from the extracellular matrix and into the vicinity of the inner-membrane through porin proteins *via* passive diffusion. While being in the vicinity of the inner-membrane, the antibiotics are then detected by transporter efflux proteins (TEPs), and subsequently pumped back out into the extracellular matrix *via* active transport (39). Thus, the antibiotic is unable to reach its target inside the cell.

Efflux pumps have contributed to resistance to β -lactams, rifampicin, chloramphenicol, aminoglycosides, tetracycline, quinolones and glycopeptides as well as the derivatives of each drug (28, 39, 40). An example of a well-studied efflux pump is the TolC-AcrAB complex found in *E. coli* (and numerous homologues found in other Gram-negative species) which is responsible for resistance to linezolid (oxazolidinone class) (Figure 1.5). This complex creates a tunnel across the cell membrane (spanning from the inner- to the outer-membrane) that allows antibiotics to be transported out into the extracellular space with the assistance of a number of other proteins. The pump contains the outer-membrane TolC channel, which is connected to the inner-membrane transporter AcrB *via* the periplasmic AcrA. This complex is assisted by a number of other proteins which are known as the resistome (31, 39).

A notable example of efflux pumps in Gram-positive bacteria is the NorA protein which was the first chromosomally-encoded efflux pump identified and it was in *S. aureus* (41). Based on its nucleotide sequence, this protein was predicted to have 12 trans-

membrane segments and overexpression of this efflux protein in both *E. coli* and *S. aureus* resulted in the resistance to fluoroquinolones such as norfloxacin (41).

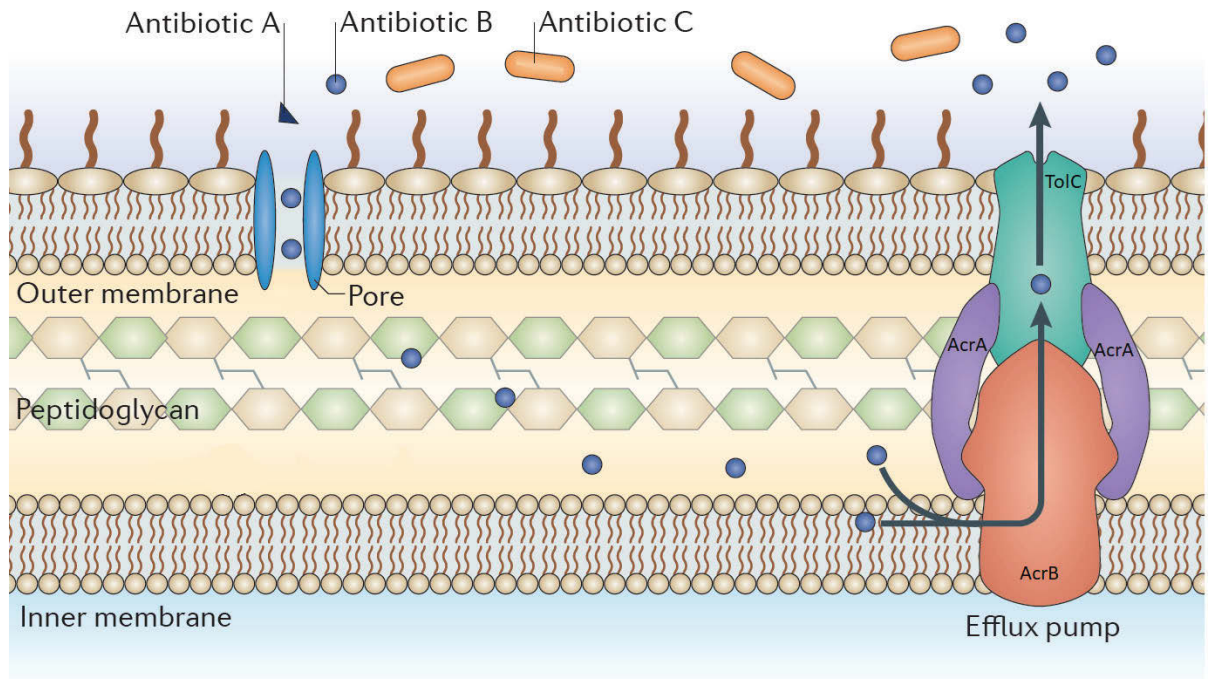


Figure 1.5: The working of the efflux pump complex TolC-AcrAB in *E. coli*. Three types of antibiotics were presented to the cell and only one (Antibiotic B) were taken up inside the cell via an outer-membrane pore (pore), but as soon as it comes into the vicinity of the inner-membrane, it is taken up by TolC-AcrAB complex and is pumped out. Figure was adapted from (34).

1.3.4 Reduced permeability

In general, membrane permeability is different between Gram-positive and Gram-negative bacteria, with Gram-negative bacteria being intrinsically less permeable to many antibiotics due to the presence of its outer-membrane which acts a permeability barrier (42, 43). Antibiotics enter bacterial cells by diffusing through the outer-membrane porin proteins (Figure 1.5). In most *Enterobacteriaceae*, such as *E. coli*, the major porin proteins are OmpF and OmpC, which function as non-specific channels (34). Multiple studies have shown that *Pseudomonas* spp. and *Acinetobacter* spp. are able to reduce the expression of these proteins, causing resistance to newer β -lactam class drugs such as carbapenems and cephalosporins, which are usually inactivated through enzymatic degradation in other resistant bacterial species (44-48).

1.3.5 Possible solutions to antibiotic resistance

With all the knowledge and understanding about how antibiotic resistance works and how it is transferred between bacterial species, it is still realistic to ask the question, “what can we do about it?” There are a number of approaches that have been suggested in the literature and this falls into the term coined as “antibiotic stewardship”. The Transatlantic Taskforce on Antimicrobial Resistance (TATFAR) outlined the most pressing needs that should be addressed immediately to tackle antibiotic resistance (49). These include (1) appropriate therapeutic use in human and veterinary medicine, (2) prevention of drug-resistant infections, and (3) strategies for improving the pipeline of new antimicrobial drugs (50).

The fight for appropriate use of antibiotics involves increasing public knowledge about antibiotics as well as understanding antibiotics usage in relation to animal farming (51).

Investigation carried out by the World Health Organization across 12 countries found that two-thirds of the population believed that antibiotics could cure viral infections such as flu and colds (52). Such misconceptions will drive antibiotics consumption (51). A systematic review of public-targeted communication interventions to improve antibiotic use conducted by Cross *et al.*, which included 74 – 75 million participants across America and Europe, found that multi-faceted communication interventions that target both the general public, as well as clinicians can reduce incorrect antibiotic prescribing in developed countries (53).

In both the developed and the developing world, the usage of antibiotics in animal feed have primarily been for the purpose of growth supplement in livestock (54). Animals that are fed with antibiotic-supplemented feed are known to have a 1-10% increase in their daily growth rate, compared to animals fed with feed without antibiotics (54). The basis of growth-promoting effect of antibiotics is not clearly known (54). However, it is hypothesized that antibiotics in the animal feed function by suppressing harmful bacteria which affects animal growth, for example by consuming nutrients in the feed and by producing toxins in the gut of the animal (54). Multiple studies have provided evidence for the selection of multidrug resistant bacteria from the use of antibiotics in animal feeds (55-58) but it is argued by farmers which practice such methods that the doses of antibiotics used for this purpose are small compared to their therapeutic dose and it is not definitely known whether such low doses really select for resistance or not (54). For this reason, policy makers around the world are in a quandary to formulate a guideline for the addition of antibiotics to the animal feed (54). Denmark is currently the only country that has now completely stopped the use of antibiotics as a growth promoter in animal farming (59, 60), and Netherland is in the process of eliminating the use of antibiotics as growth promoters in animal farming (59).

Prevention of drug-resistant infections is mainly focused towards good hygiene practices in health care settings. Hand washing is acknowledged to be the single most important activity for reducing transmission of infectious agents by both contact and fecal-oral routes (61). However, compliance to protocol by health care workers remains inadequate (62). A review of global hand hygiene studies by the World Health Organization found that, on average only 38.7% of health care workers around the world comply with the standard of hand hygiene (63). A systematic review on the effectiveness of interventions to improve hand hygiene compliance conducted by Dornina *et al.* found that interventions consisting of strategies which promote hand washing in the hospital setting were able to improve hand hygiene practices among nurses (64).

With the concerted effort to bring about public knowledge about antibiotics and also improvement to hygiene compliance in health care settings, new antibiotics with a novel mechanism of actions are without a doubt still needed as an arsenal in the fight against multidrug resistant pathogens. There are multiple areas that scientists are researching into for the purpose of creating new antibiotics with a novel mechanism of action. For the purpose of this thesis, only cell division (65, 66) and the inhibitors of this process will be covered further, as the main focus of this thesis is targeting the bacterial cell division process.

The process of bacterial cell division involves many protein-protein interactions to form the division machinery, termed the divisome, so that it can carry out its function (67). The inhibition of these interactions will no doubt be detrimental to the cell. Additionally, since the division proteins are known to be essential and that their roles appear to be structural (stabilizing the divisome), rather than enzymatic; targeting the interacting sites is likely to be highly effective (68). This approach will also arguably have a lower

rate of resistance since the cell will need to accommodate and balance the change in amino acids between multiple proteins to maintain its interactions. For example, since one of the well-known cell division protein called FtsZ is understood to bind multiple proteins, a single inhibiting molecule may simultaneously disrupt many essential interactions and lower the chance of resistance (69).

1.4 Cell division and division proteins

Cell division, a process whereby one cell divides to form two identical daughter cells, is fundamental for the propagation of all living organisms. The bacterial cell cycle (Figure 1.6) involves chromosome replication, followed by chromosome segregation, and then cell division between the two newly replicated chromosomes. After chromosome replication and segregation into nucleoids, FtsZ, the first protein to be recruited to midcell, forms a structure known as the Z-ring *via* self-polymerisation. The formation of the Z-ring serves as a scaffold for the assembly of the division machinery, a complex macromolecular structure composed of over 20 known proteins in the Gram-negative model organism *E. coli* and a similar number in the Gram-positive model organism *B. subtilis* (although not all are conserved. See Figure 1.7) (70). In *E. coli*, ten of these (FtsA, -B, -I, -K, -L, -N, -Q, -W, -Z and ZipA) are considered to form the core of the divisome and are essential for the process of cell division (67). These proteins are distributed between the cytoplasm, cytoplasmic membrane and periplasmic space (68, 71-75). This study focuses on two of these divisome proteins: FtsZ and FtsA

There are two different modes of division based on the model organism Gram-negative *E. coli* and Gram-positive *B. subtilis* (76, 77) (Figure 1.6). In *E. coli*, synthesis of the division septum is accompanied by constriction of the outer-membrane, while in *B.*

subtilis, a cross-wall of peptidoglycan initially divides the cell before it is degraded and remodelled to form the new, hemi-spherical cell poles (65). Following this, the septum is then cleaved to form two new daughter cells containing the same genetic material as the parent cell.

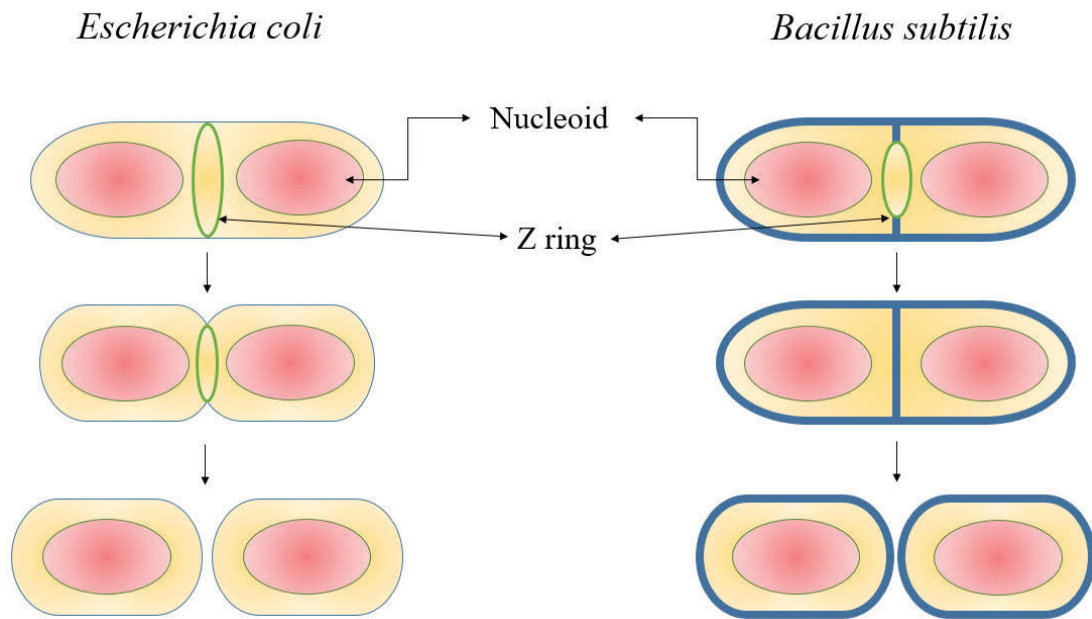


Figure 1.6: Schematic of *E. coli* and *B. subtilis* cell division. Different modes of division occur in different bacterial species. After chromosome replication and segregation into nucleoids, the Z-ring assembles at mid-cell. The ring then constricts to bring about division. Cell wall synthesis follows the ring inwards. In *E. coli*, synthesis of the division septum is accompanied by constriction of the outer membrane. In *B. subtilis*, a cross wall of peptidoglycan initially divides the cell before it is degraded and remodelled to form the new, hemi-spherical cell poles.

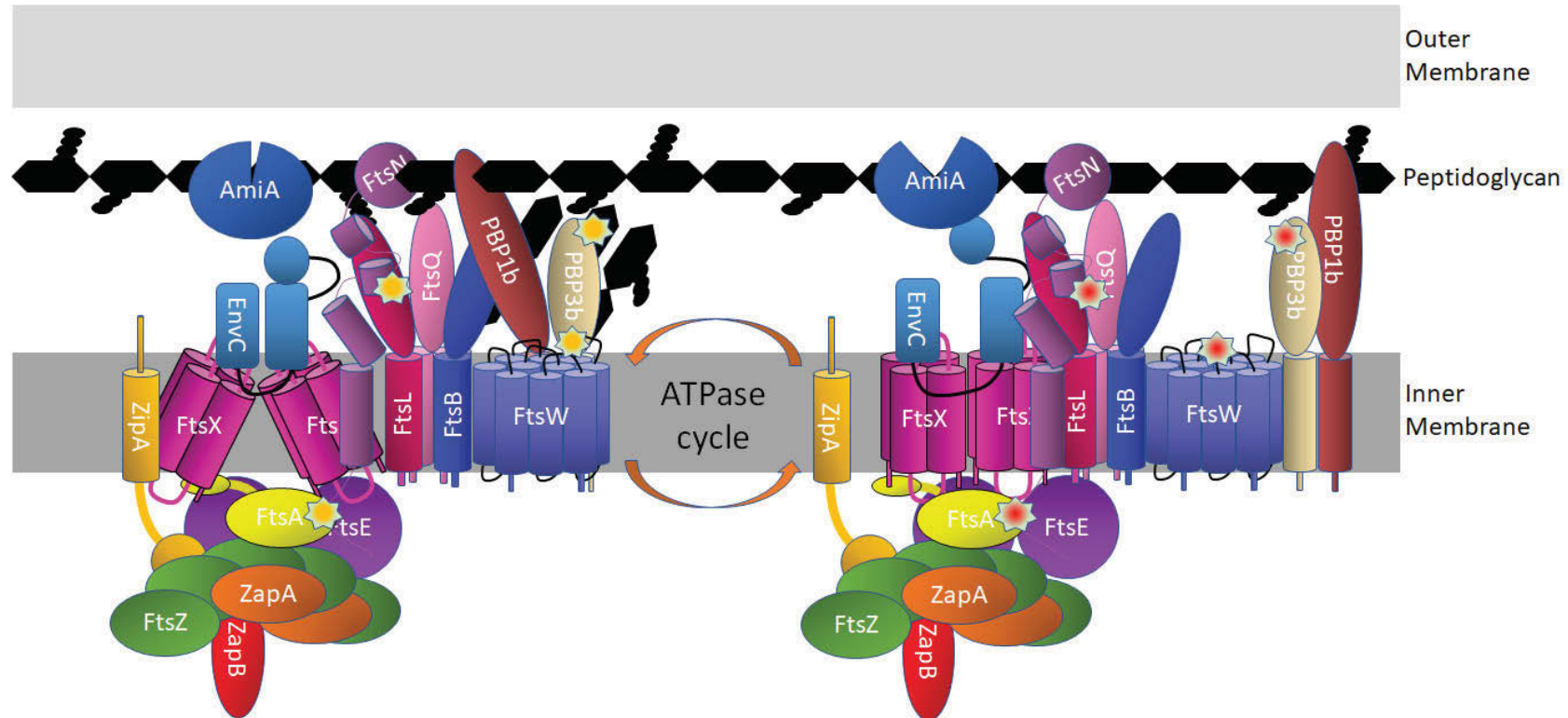


Figure 1.7: The *E. coli* cell division proteins and their partners that form the divisome. The *E. coli* divisome comprises of two sets of factors: the early proteins which forms the protoring (FtsZ, FtsA, ZipA, and ZapB in this figure) and the late proteins, whose recruitment is subsequent to and dependent upon the early proteins. FtsN connects the early and late proteins by interacting with FtsA to stabilize the FtsQLB complex in the periplasm and with FtsI/PBP3 and FtsW to stimulate cell wall synthesis (the latter interaction is not shown). Green and orange starbursts indicate pre-activation state of FtsA, FtsN, FtsW and FtsI/PBP3 while green and red starburst indicates activated state. Moreover, FtsEX mediated ATP hydrolysis stimulates amidase activity (AmiA in this figure), consequently coordinating cell wall synthesis with hydrolysis to facilitate daughter cell separation. The model is not meant to reflect actual interaction stoichiometries, because they have yet to be determined. In addition, it is not yet clear if the amidases remain in complex with EnvC as drawn or if this interaction is also regulated. Figure was adapted from (70).

1.6 FtsZ: the prokaryotic homologue of tubulin

FtsZ is highly conserved amongst bacteria (78). In *E. coli*, FtsZ is a soluble protein of 389 amino acids in length (79) and has a molecular mass of ~40 kDa (80). The FtsZ crystal structure was first solved using an archaean protein from *Methanocaldococcus jannaschii* (81), which showed structural similarity to the eukaryotic cytoskeletal tubulin (80). Structural similarities and differences between multiple FtsZ species and tubulin will be examined further in Chapter 4.

The X-ray crystal structure shows that FtsZ consists of an N-terminal and C-terminal domain that are separated by a central core helix called the H7-helix (Figure 1.8) (82). The nucleotide-binding domain is located within the N-terminal domain and is bound to the guanosine triphosphate (GTP) molecule, which is a substrate for its GTPase activity (83). The C-terminal globular domain is followed by a disordered region (known as the linker) and ends at a conserved extreme C-terminal peptide. The length of the linker varies between FtsZ from different species, with experimental data from *E. coli* (84) and *B. subtilis* (85) suggesting that the linker plays a major role in acting as a flexible tether. This tether binds FtsZ to membrane anchoring proteins, FtsA and ZipA, through the conserved extreme C-terminal peptide while simultaneously interacts with itself and other modulatory proteins in the cytoplasm (84, 85). A study using *Caulobacter crescentus* further indicates that this linker has a role in regulating peptidoglycan metabolism (86). Another study using *C. crescentus* FtsZ also identified the FtsZ linker to have a role in regulating the structural integrity of polymerized FtsZ and dynamics through intrinsic effects on lateral interactions and turnover of polymerized FtsZ, while at the same time influencing the extrinsic regulation of FtsZ by binding partners (87). In *E. coli* and other bacterial species, the conserved extreme

C-terminal peptide is essential for interacting with other cell-division proteins such as FtsA and ZipA (88-90).

FtsZ polymerizes in a head-to-tail fashion; a process that requires the presence of GTP (91, 92). Polymerization is initiated when the catalytic synergy T7-loop of one FtsZ subunit inserts into the nucleotide-binding domain of another FtsZ subunit (Figure 1.8) (93, 94). The polymerization process results in the hydrolysis of GTP to guanosine diphosphate (GDP) and the repetition of such events gives rise to the formation of the Z-ring at the cell centre (73, 95-97). In the earlier years, it was thought that the Z-ring was the sole contributor for the generation of constrictive force to direct septum formation during division (89). This, however, raises a number of questions (89): Is FtsZ really the only protein to generate constrictive force and if so, how? How is assembly and constriction of the Z-ring coordinated with peptidoglycan synthesis? These questions were recently addressed by both Bisson-Filho *et al.* and Yang *et al.* (98, 99). Bisson-Filho *et al.* showed that the Z-ring in *B. subtilis* performs a treadmilling action *via* the FtsZ and FtsA complex, while Yang *et al.* showed the same FtsZ action in *E. coli* *via* the FtsZ and FtsI complex. Both groups showed that the process is driven by the hydrolysis ability of FtsZ and is coupled to peptidoglycan synthesis (98, 99). Thus, giving an overall picture of the function of FtsZ in the generation of force to bend membranes (100, 101) and as a scaffold for peptidoglycan synthesis during cell division (102, 103).

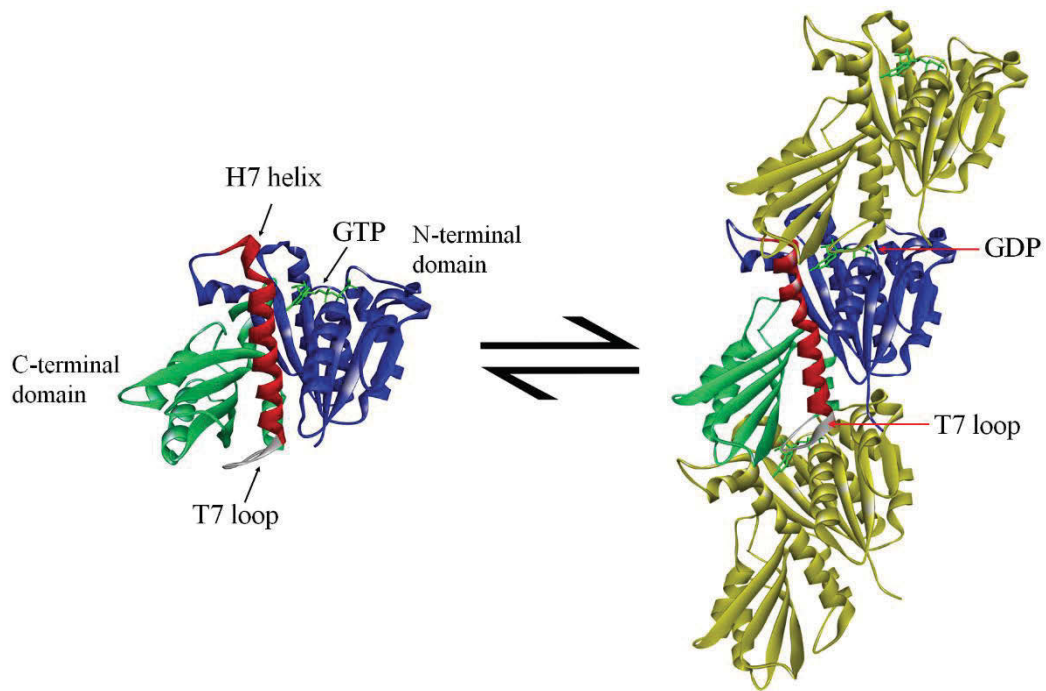


Figure 1.8: Crystal structure of *M. jannaschii* FtsZ and its ability to polymerise. Protein Data Bank Entry 1W5B. The monomer unit of *M. jannaschii* FtsZ is shown on the left with GTP occupying the nucleotide-binding pocket. Polymerisation involves the insertion of T7-loop of one subunit into the nucleotide-binding pocket of another subunit forming FtsZ filaments. In the process, GTP is hydrolysed to GDP, which in-turn causes the de-polymerization of the FtsZ filaments back into FtsZ monomer units.

1.7 FtsA: an actin-like FtsZ-interacting protein

FtsA in *E. coli* is a protein with 420 amino acids (79) and a molecular mass of 50 kDa. After FtsZ, FtsA is the second highly conserved cell division protein in bacteria (78). *E. coli* studies have shown that FtsA plays two critical roles in cytokinesis (77). First, together with ZipA, it tethers FtsZ filaments to the membrane to stabilize the Z-ring (104). Second, also together with ZipA, it is required for the recruitment of the other division proteins to the Z-ring (105). FtsA belongs to the actin/HSP70/sugar kinase ATPase superfamily (106) and this homology was confirmed through the analysis of the crystal structure of FtsA from *Thermotoga maritima* (107) and *S. aureus* (108). The

FtsA crystal structures indicated that it is comprised of four domains (Figure 1.9); 1C, which interacts with division proteins FtsI and FtsN (109), and domains 1A, 2A, and 2B, which together form the nucleotide-binding domain that binds to ATP (107). It is now understood that the FtsA 2B domain plays a role in the interaction between FtsA and FtsZ (110), and this is discussed below. Analysis of the amino acid sequence of FtsA from several Gram-positive and Gram-negative bacteria has revealed that this protein localizes to the cell membrane *via* its C-terminal amphipathic helix, which is a membrane-targeting sequence (MTS) (111). Mutants with the MTS removed show a loss in the ability to adhere to the membrane and instead form rods of FtsA in the cytoplasm of the cell, while FtsZ was still observed to form a Z-ring at midcell but is non-functional for division (88, 111). This suggests that the function of FtsZ relies on the correct localization of FtsA.

The 3D structure of FtsA and actin resemble each other in three of the four domains and in containing a nucleotide-binding domain (107). The difference between FtsA and actin is that FtsA does not have a 1B domain but instead has a 1C (divisome-interacting) domain, which is absent in actin (Figure 1.9) (107). Szwedziak *et al.* (110) and Fujita *et al.* (108) showed that in *T. maritima* and *S. aureus*, FtsA can polymerize and form actin-like protofilaments *in vitro*, which further supports the notion that FtsA and actin are homologues. In addition to that, bacterial cells also have another actin-like protein, known as MreB, which has the same domains as actin. Its function, however, is different to that of FtsA with MreB having more of a role in the determination and maintenance of rod cell shape in bacteria (112). For further information on this protein, the reader is directed to a review article on MreB (112).

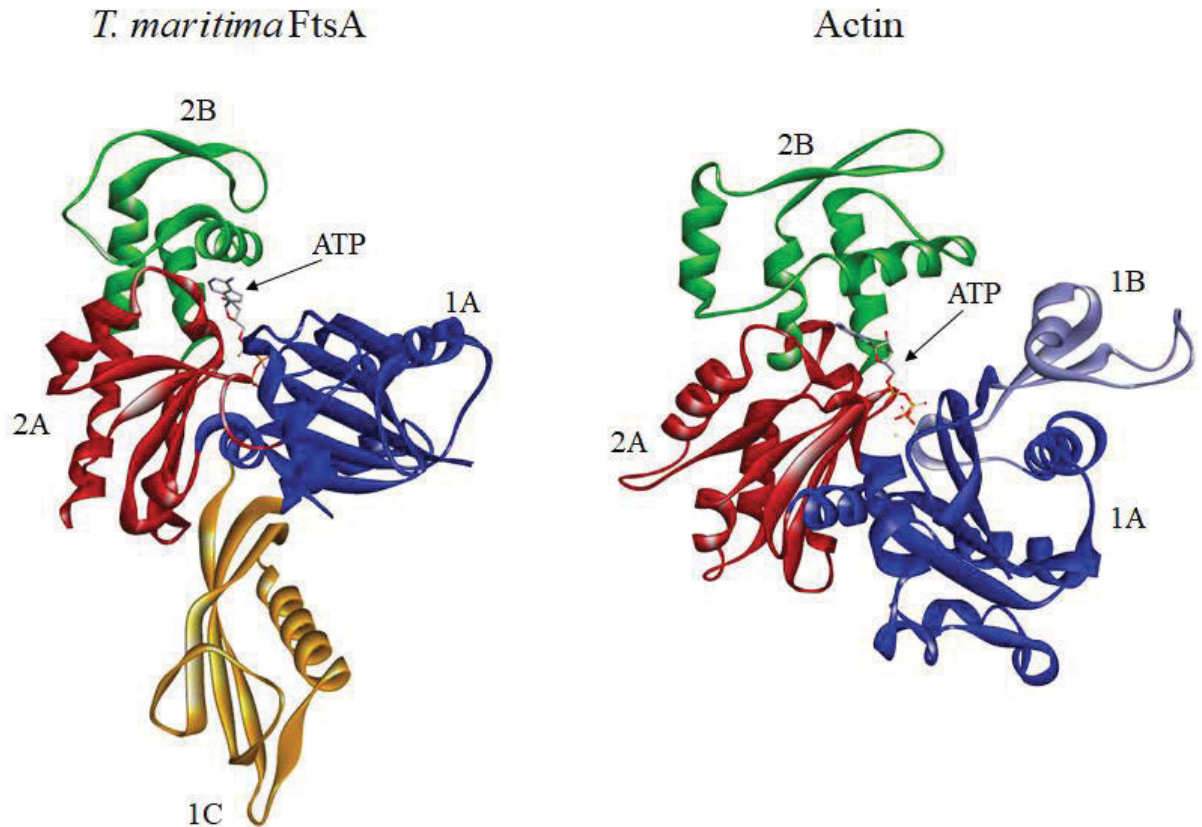


Figure 1.9: The crystal structures of FtsA from *T. maritima* and actin. *T. maritima* FtsA structure is 1E4G (107) and actin structure is 4JHD (113). (A) The FtsA structure is divided into four domains: 1A (blue), the FtsA-specific 1C domain (orange), 2A (red) and 2B (green). Secondary structure elements are labelled according to their order of appearance in the primary sequence of FtsA. (B) Actin structure is divided into four domains: 2B (green), the actin specific domain 1B (purple), 2A (red) and 1A (blue). ATP in both structures is depicted in a stick form.

1.8 Interaction between FtsZ and FtsA

The interaction between FtsZ and FtsA has been known for over a decade (114). Studies involving yeast two-hybrid assays (115, 116) and systematic deletion mutagenesis (116, 117) in several organisms have shown that the C-terminal FtsZ interacts with FtsA via conserved amino acid residues on the very extreme of the C-terminal region of FtsZ. The mechanism of interaction between the FtsZ peptide and FtsA was discovered by Szwedziak *et al.* through the co-crystallization of *T. maritima* FtsA and the *T. maritima* FtsZ peptide (110). Further details will be covered in Chapter 3.

In this study, the FtsZ and FtsA interaction from the organism *Acinetobacter baumannii* was pursued for several reasons. Firstly, *A. baumannii* is now classified by the World Health Organization as a bacterium that the world urgently needs an antibiotic against due to its high multidrug resistance profile, as well as causing high mortality (118). Secondly, the FtsZ C-terminal peptide, which is conserved in other bacterial species is different in *A. baumannii*, especially at the residues that are known to be important for the binding of FtsZ with its protein partner FtsA. This in-itself is of interest to further understand the interaction of FtsZ and FtsA and its mechanisms in *A. baumannii*, as well as having the potential which can lead to the development of an *A. baumannii* specific antibiotic, which is needed at once. This thesis also examined targeting cell division from another angle; that is by focusing solely on the FtsZ protein. Below the suitability of FtsZ as a target and its current well-studied inhibitors are discussed.

1.9 Is FtsZ a good antibacterial target?

To date, many potential FtsZ inhibitors have been reported in the literature. Table 1.1 below displays the most active compounds from a large number of derivatives in each referenced publication, including evidence that suggests FtsZ is the target. Currently, not a single inhibitor has made it to phase I clinical trials, with the inhibitor **TXA709** currently undergoing some pre-clinical assessments in preparation for phase I (119). This is due to many of the published FtsZ inhibitors not meeting the required specifications and also showing worrying resistance frequencies (120).

Traditional antibacterial targets of known antibiotics generally share a number of parameters which make them effective for the treatment of bacterial infections (121). A target should ideally be essential for bacterial growth or viability, be highly conserved amongst different species, contain minimal eukaryotic homology (and therefore minimal toxicity), be druggable and finally, be situated in an accessible location within the bacterial cell. Future novel targets should meet this criterion, with an added focus of a low natural tendency for resistance. So, does FtsZ fit the criterion of a good target?

The essential nature of FtsZ in bacterial cell division was confirmed in *E. coli* by Dai and Lutkenhaus in 1991 (122). It was found that when the function of FtsZ was inhibited, it gives rise to a phenotype where the bacterial cell would form long “spaghetti-like” cells, known as filaments, which eventually lyse, causing cell death. Coccus-shaped bacteria, like *S. aureus*, do not filament but instead increase to about eight times their normal size. Cell wall synthesis occurs at the division site in *S. aureus*, however when division is inhibited, cell wall synthesis occurs in a non-regulated manner dispersed over the entire cell surface. Eventually this results in the ballooning of the cell, leading to lysis and cell death (123, 124).

FtsZ is also highly conserved amongst most bacterial species, with some exceptions such as the *Chlamydiaceae* family and *Ureaplasma Urealyticum* (122, 125, 126). Interestingly, the bacterium *Streptomyces coelicolor* carries the *ftsZ* gene, although when deleted, growth was not impaired. This is due to the mycelial growth habit of the bacterium, which allows for growth in the absence of cell division (127). It was identified that the FtsZ protein was essential for sporulation as spores requires cell division to enter its vegetative state but not essential for non-sporulating cells, a feature common in all *Streptomyces* species (128, 129). The essential nature of FtsZ in all but one species, and its high conservation creates an opportunity to develop broad-spectrum FtsZ inhibitors (130).

Druggability and the lack of eukaryotic homology of FtsZ needs to be evaluated to determine FtsZ as a potential target. Currently, there appear to be three druggable protein pockets; the nucleotide-binding domain (131), the synergistic T7-loop (Figure 1.10) (132) and the interdomain cleft (133). The nucleotide-binding domain has been successfully targeted by a C8-substituted GTP analogue that could selectively inhibit the GTPase activity of FtsZ, while having no effect on tubulin (131). The second druggable protein cleft, the T7-loop, has also been shown to bind small molecules, as predicted by the *in silico* modelling and STD-NMR studies for the binding of non-toxic cinnamaldehyde to FtsZ (132). The final druggable region, the interdomain cleft between the central core helix (H7-helix) and the C-terminal domain (Figure 1.10), is structurally different to tubulin, and can be successfully inhibited (80). **PC190723** has been shown to directly bind the interdomain cleft of *S. aureus* FtsZ through the use of X-ray crystallography. The interdomain cleft, however, is not well conserved across species, evident as **PC190723** only inhibits Gram-positive *S. aureus* and *B. subtilis* FtsZ, but not Gram-positive *E. faecium* and *S. pyogenes* FtsZ, suggesting variations in this

pocket between species (134). This was further shown computationally by Miguel *et al.*, who discovered that the **PC190723** binding region of FtsZ is significantly different in various bacteria (135). Whilst not highly conserved, this pocket can be successfully targeted with minimal toxicity, evident by the ability of **PC190723** to efficaciously clear *S. aureus* infections in a septicemia mouse model. **PC190723** and its derivatives are shown to be non-toxic, which is evident by the inability of the compound to affect the growth of yeast and human hepatocytes cells *in vitro* (133). The evidence thus far shows the feasibility of selectively targeting one of the three druggable pockets in FtsZ.

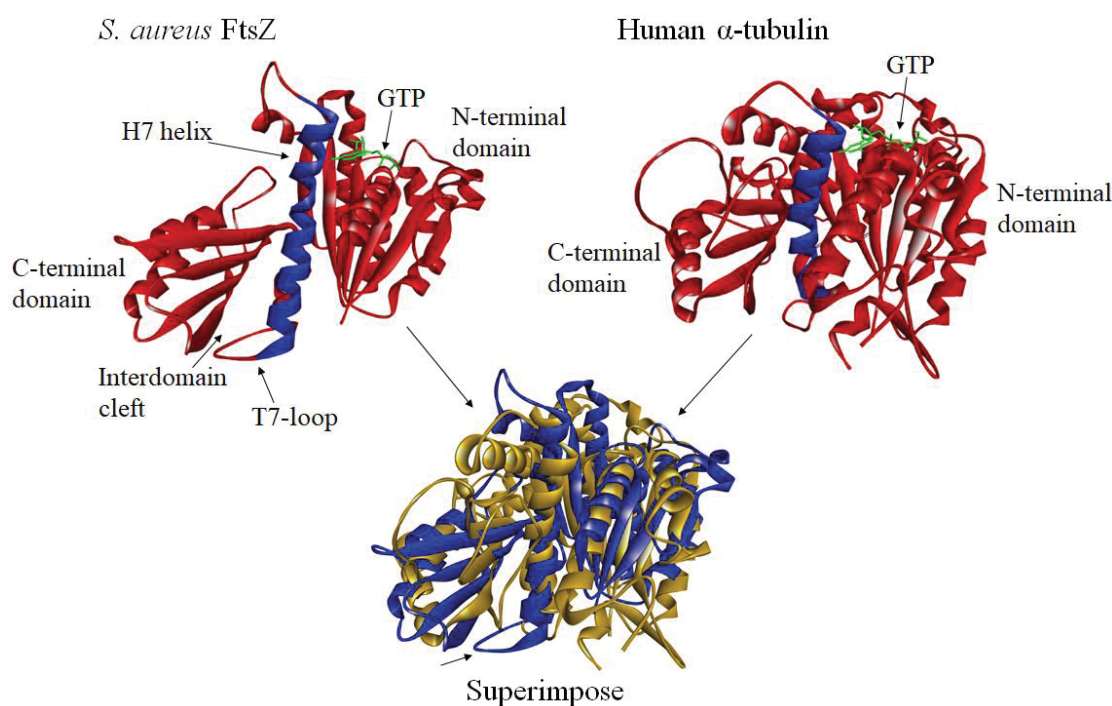


Figure 1.10: Structural comparison of *S. aureus* FtsZ and human α -tubulin. Protein structure for *S. aureus* FtsZ is 3VOB (93) and the human α -tubulin is 5ITZ (136). Cartoon representation showing the structural homology of GTP-bound FtsZ and GTP-bound human α -tubulin. Most of the molecules are coloured red. The FtsZ H7-helix (residues 179–202) and the helix in α -tubulin, which corresponds to the FtsZ H7-helix is shown in blue. GTP is represented as green sticks. FtsZ in blue and α -tubulin in gold, shows that there are structural differences such as the existence of the T7-loop and interdomain cleft in FtsZ and its absence in α -tubulin (denoted by the bottom arrow). This is further supported by the obtained C α atom root-mean-square deviation (RMSD) value of 10.75 Å (unpublished data).

The suitability of a target for antibacterial development must consider the cellular location of the protein within the cell. FtsZ resides in the cytoplasm of the cell (137). When treating a Gram-negative bacterial infection, an inhibitor must circumvent the porin β -barrels proteins and the transporter efflux pump proteins, generally absent in Gram-positive species (138, 139). However for broad-spectrum activity, the inhibitor must still be able to permeate both Gram-negative and Gram-positive bacteria, a very difficult undertaking (140). One method to address this is by using combination compound treatment. A previous study showed the FtsZ inhibitor **TXA436**, a derivative of **PC190723** (Table 1.1), which is only active against Gram-positive species, inhibited *E. coli* cell growth when treated in combination with an efflux pump inhibitor such as phenylalanine-arginine β -naphthylamide (*Pa β N*) (141). The dual treatment gave a phenotype characteristic of cell division inhibition in *E. coli*, and **TXA436** also inhibited the polymerization of *E. coli* FtsZ *in vitro*. Furthermore, the use of an *E. coli* strain that expressed mYFP (yellow fluorescent protein)-tagged FtsZ suggested that the co-treatment disrupted the ability of the *E. coli* cells to form Z-rings (141). This co-treatment supports the potential of a combination of FtsZ inhibitors and efflux pumps inhibitors in inducing activity in Gram-negative species. Furthermore, the limitation of a cytoplasmic location of a target can be overcome, as there are current commercialised compounds such as fluoroquinolones and macrolides that inhibit cytoplasmic targets (22, 142).

Resistance is the major issue that all current commercial antibiotics face, regardless of the target. Only a small number of publications conduct a frequency of resistance (FOR) assay for FtsZ inhibitors. This absence of rigorous evaluation of resistance means that the likelihood of bacteria developing resistance to FtsZ inhibitors cannot be quantified. In the small number of publications that do assess the FOR, it was found that *S. aureus*

and *B. subtilis* successfully develop resistance to the benzamide derivatives, such as **PC190723**, that arose during single exposure to a high concentration of the inhibitor (143-145). The sequencing of a *B. subtilis* resistant isolates by Stokes *et al.* identified several single-point mutations in *ftsZ* per isolate, generally at one of six residues: R191, G193, G196, V214, N263 and G266, all located in the interdomain cleft discussed previously (143). This spontaneous resistance is a caveat, much like that of the current antibiotics available. However, this has only thus far been shown for **PC190723** and its derivatives. Inhibitors that bind other pockets are yet to be tested. Interestingly, a synergistic study showed that treatment with the FtsZ inhibitor **TXA709** (**PC190723** derivative) and a β -lactam can greatly reduce the frequency of resistance in both compounds below detectable levels (145). This is a potential indicator that an FtsZ inhibitor could be utilised in combination therapy. Using a combination treatment with an already-marketed antibiotic is obviously much more commercially attractive than using two uncharacterized, undeveloped compounds.

1.10 Inhibitors of FtsZ: The Benzamide Derivatives

Currently as it stands, only the benzamide derivatives have been studied extensively and provided the most conclusive evidence to suggest that FtsZ is the target. The work done on these derivatives could be considered a gold standard in FtsZ drug discovery. The benzamide derivative, **PC190723** is the most studied scaffold of any inhibitor of FtsZ and has presented the most informative and direct evidence for FtsZ specificity. The history of benzamide inhibitors started in 1999 when Ohashi *et al.* showed that 3-methoxybenzamide (3-MBA) induced filamentation in *B. subtilis* and that FtsZ mutations also allowed cell growth in the presence of 3-MBA, indicating that the target was FtsZ (146). Some years later, Haydon *et al.* reported a potent and selective anti-

staphylococcal benzamide derivative named **PC190723** that contained the 3-MBA moiety and demonstrated FtsZ inhibition (143). Since the discovery of **PC190723**, a number of derivatives were developed to increase potency and bioavailability while trying to overcome any resistance. However, later derivatives still developed spontaneous resistant mutants at a similar rate (147-151). Evidence that shows FtsZ is the target of **PC190723** and its derivatives includes: a GTPase light scattering assay, cell filamentation in *B. subtilis* and ballooning in *S. aureus*, the disruption of Z-ring formation as seen using FtsZ-GFP constructs in *B. subtilis* and, lastly, sequencing of the *ftsZ* gene in spontaneous mutants to identify if resistance was due to mutations in *ftsZ*. Matsui *et al.* also successfully co-crystallised *S. aureus* FtsZ with **PC190723** (93) and very recently, Fujita *et al.* also successfully co-crystallised the compounds **TXA707** and **TXA6101**, which are derivatives of **PC190723**, with *S. aureus* FtsZ (152). These benzamide derivatives are the only inhibitors to ever been co-crystallised with FtsZ. This evidence of, if and how an inhibitor binds, is what are missing in many studies in the field.

As previously mentioned in Section 1.1, there is yet to exist an ideal antibiotic since many antibiotics do not have a large enough broad-spectrum activity. The field of FtsZ inhibitors is also shadowed by this in that the majority of the reported inhibitors only target either Gram-positive or Gram-negative species, exclusively. A key question can be raised from this, which is, is it possible to create a broad-spectrum FtsZ inhibitor? The work conducted by Chan *et al.* with **Compound 12** (153, 154) and the work by Lian *et al.* with **Compound 5c** (155) suggests that it might be possible, but more work is still needed to support this idea. As part of this thesis, this question is examined by conducting an *in silico* analysis of published FtsZ crystal structures from various bacterial species to identify druggable regions on the protein for developing broad- and

narrow-spectrum FtsZ inhibitors and also to understand the FtsZ structure as a drug target.

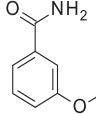
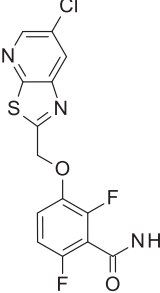
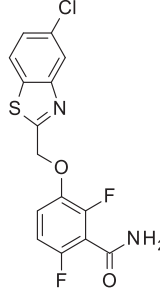
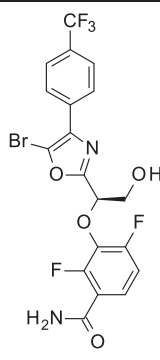
1.10 Thesis aims

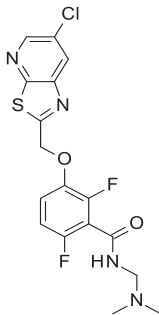
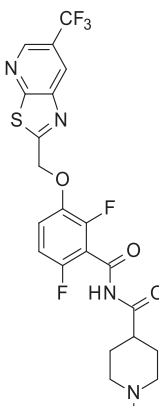
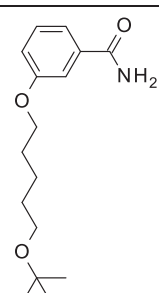
The long-term objective of the project this thesis is a part of, is to address the rising problem of antibiotic resistance and to provide a solution by targeting the bacterial cell division proteins for the purpose of creating new antimicrobials with a novel mechanism of action. The work in this thesis attempted to target the bacterial cell division protein FtsZ in two ways. Firstly, to inhibit FtsZ function by blocking its interaction with another division protein, FtsA and, secondly, to inhibit FtsZ function by targeting just this protein.

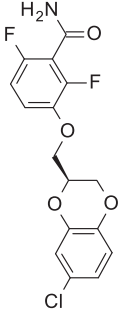
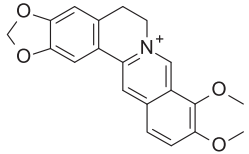
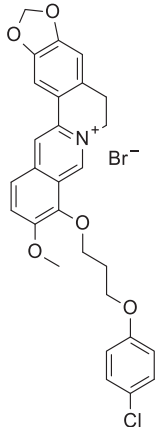
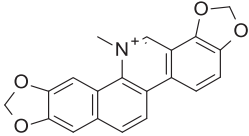
Chapter 3 reports the use of an *in silico* approach to understand the differences and similarities of the FtsZ and FtsA interaction in the Gram-negative pathogen, *A. baumannii*, and compares the data obtained to the current knowledge of the FtsZ-FtsA interaction from the organism *T. maritima*. The information gained could then be used for the development of an antibiotic which targets the FtsZ and FtsA interaction in *A. baumannii*. Chapter 4 builds upon the *in silico* work carried out in Chapter 3 by investigating the FtsZ-FtsA interaction in *Acinetobacter* spp. *in vitro*; the aim being to purify both FtsZ and FtsA, co-crytallize them, and determine the structure of the complex. However, there were several challenges that were not all solved. In the interest of time, the project focus was shifted to providing structural insight into FtsZ as a drug target. This is dealt with in Chapter 5 by carrying out an *in silico* analysis of FtsZ crystal structures and identifying differences and similarities of multiple FtsZ structures from a range of bacterial species, with the aim of identifying other possible

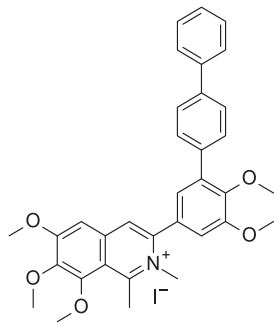
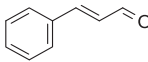
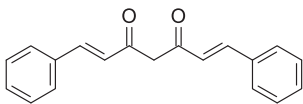
pockets within the protein which can be targeted with small molecules to create broad- and narrow-spectrum antibiotics, which target this protein. Chapter 6 continues on from Chapter 5 with confirming other possible binding pockets in FtsZ using a fragment-based drug discovery approach and at the same time identify fragment leads which will be used in creating new antibacterials with a novel mechanism of action.

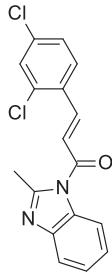
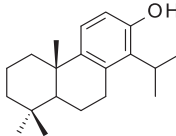
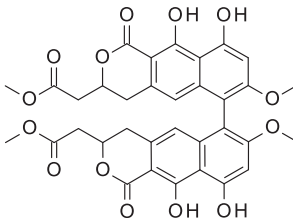
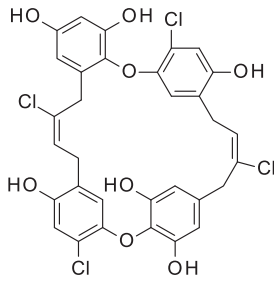
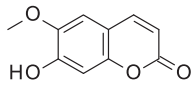
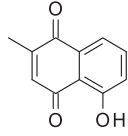
Table 1.1: Current reported inhibitors of FtsZ and experimental evidence provided.

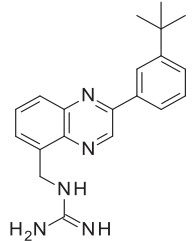
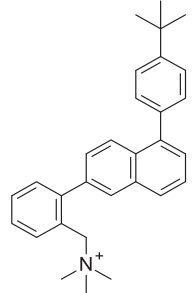
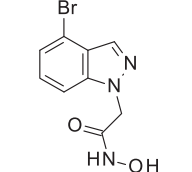
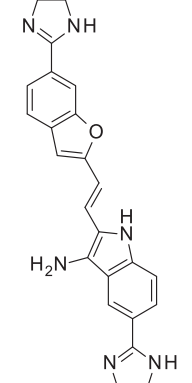
Compounds structure/ Name	Minimum Inhibitory Concentration ^a	Evidence for FtsZ inhibition ^b				Ref
		Phenotype	Protein Inhibition assay	Direct Protein binding	Other	
 3-methoxybenzamide (3-MBA)	<i>B. subtilis</i> (5 mM)	Phase contrast microscopy showed filamentous phenotype in <i>B. subtilis</i>	-	-	FtsZ mutations allows cell growth in the presence of 3-MBA	(146)
 PC190723	<i>B. subtilis</i> (1.0 µg/ml) <i>S. aureus</i> (1.0 µg/ml) MRSA (1.0 µg/ml) MDRSA (1.0 µg/ml) <i>S. epidermidis</i> (1.0 µg/ml) <i>S. haemolyticus</i> (0.5 µg/ml) <i>S. hominis</i> (1.0 µg/ml) <i>S. lugdunensis</i> (1.0 µg/ml) <i>S. saprophyticus</i> (1.0 µg/ml) <i>S. warneri</i> (1.0 µg/ml)	Phase contrast microscopy showed ballooning phenotype in <i>S. aureus</i> . Fluorescence microscopy found GFP-tagged FtsZ showed the FtsZ monomers as discrete foci throughout the filamentous <i>B. subtilis</i> cells	GTPase assay Polymerisation assay	<i>In silico</i> molecular modelling X-ray crystallography	The <i>ftsZ</i> gene of resistant mutants was sequenced.	(93, 143, 147, 156, 157)
 8j	<i>S. aureus</i> (0.25 µg/ml)	-	-	<i>In silico</i> molecular modelling	-	(147)
 Compound 1	<i>B. subtilis</i> (0.03 µg/ml) <i>S. aureus</i> (0.12 µg/ml) MRSA (0.12 µg/ml) MDRSA (0.12 µg/ml) <i>S. epidermidis</i> (0.12 µg/ml) <i>S. haemolyticus</i> (0.12 µg/ml) <i>S. hominis</i> (0.12 µg/ml) <i>S. lugdunensis</i> (0.25 µg/ml) <i>S. saprophyticus</i> (0.06 µg/ml) <i>S. warneri</i> (0.25 µg/ml)	-	-	-	The <i>ftsZ</i> gene of resistant mutants was sequenced.	(144, 148)

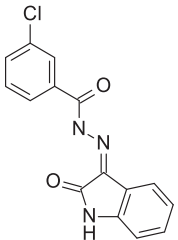
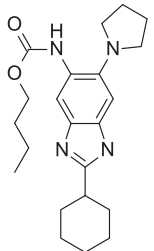
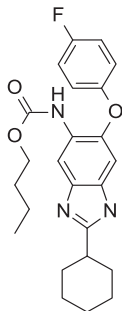
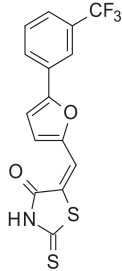
 <p>TXY436</p>	MSSA (0.5 µg/ml) MRSA (0.5 µg/ml)	<p>Phase contrast microscopy showed ballooning phenotype in <i>S. aureus</i>.</p> <p>Fluorescence microscopy found GFP-tagged FtsZ showed the FtsZ monomers as discrete foci throughout the filamentous <i>B. subtilis</i> cells</p>	Polymerisation assay	-	-	(150)
 <p>TXA709</p>	MRSA (2-4 µg/ml) VRSA (2 µg/ml) MSSA (2-4 µg/ml)	<p>Fluorescence microscopy found GFP-tagged FtsZ showed the FtsZ monomers as discrete foci throughout the filamentous <i>B. subtilis</i> cells</p> <p>TEM imaging showed that no septa are observed in <i>S. aureus</i> cells. The peptidoglycan synthesis shifted to discrete locations at the cell periphery.</p> <p>TEM showed ballooning (approximately 3-fold) which eventually led to lysis.</p>	Polymerisation assay	-	The <i>ftsZ</i> gene of resistant mutants was sequenced.	(151)
 <p>Compound 7</p>	<i>S. aureus</i> (8 µg/ml) <i>B. subtilis</i> (8 µg/ml)	Phase contrast microscopy showed ballooning phenotype in <i>S. aureus</i> and filamentation in <i>B. subtilis</i> .	-	-	-	(158)

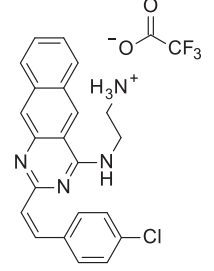
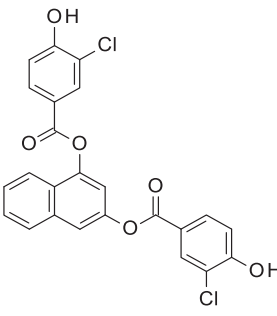
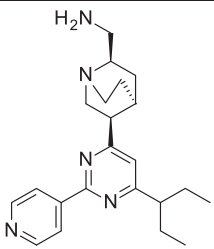
 <p>Compound (S)-13</p>	<i>S. aureus</i> (0.25 µg/ml)	Phase contrast microscopy showed ballooning phenotype in <i>S. aureus</i>	-	-	-	(159)
 <p>Berberine</p>	<i>S. aureus</i> (128 µg/ml) <i>B. subtilis</i> (128 µg/ml) <i>E. faecium</i> (>196 µg/ml) <i>S. epidermidis</i> (128 µg/ml) <i>E. coli</i> (>500 µg/ml) <i>K. pneumoniae</i> (>500 µg/ml)	TEM showed reduction of <i>E. coli</i> FtsZ bundles when treated with berberine Fluorescence microscopy found that GFP-tagged FtsZ in <i>E. coli</i> was dispersed as discrete foci throughout filamentous cells.	GTPase assay Polymerisation assay	<i>In silico</i> molecular modelling STD NMR binding studies Isothermal calorimetry to determine K_d	-	(160)
 <p>Compound 2</p>	<i>B. subtilis</i> (4 µg/ml) <i>S. aureus</i> (2 µg/ml) <i>E. faecium</i> (8 µg/ml) <i>S. epidermidis</i> (4 µg/ml) <i>E. coli</i> (96 µg/ml) <i>K. pneumoniae</i> (128 µg/ml)	TEM showed <i>S. aureus</i> FtsZ polymers drastically reduced in size and thickness, as well as the binding of FtsZ protofilaments. Phase contrast microscopy showed filamentous phenotype in <i>B. subtilis</i> Fluorescence microscopy found that GFP-tagged FtsZ in <i>E. coli</i> was disorganized and the filamentous phenotype was seen.	GTPase assay Polymerisation assay	<i>In silico</i> molecular modelling	-	(160)
 <p>Sanguinarine</p>	<i>S. aureus</i> (1 µM) VRE (8 µM) <i>B. subtilis</i> (1 µM) MRSA (2 µM) <i>E. coli</i> (8 µM) <i>K. pneumoniae</i> (16 µM) <i>A. baumannii</i> (16 µM) <i>P. aeruginosa</i> (128 µM)	Phase contrast microscopy showed filamentous phenotype in <i>B. subtilis</i> Fluorescence microscopy found that GFP-tagged FtsZ in <i>E. coli</i> was disorganized and the filamentous phenotype was seen.	GTPase assay Polymerisation assay	-	-	(161)

		TEM showed reduction of <i>E. coli</i> FtsZ bundles when treated with berberine and gave rise to aggregates				
 <p>Compound 6b</p>	<i>S. aureus</i> (1 µg/ml) <i>E. faecalis</i> (4 µg/ml)	-	GTPase assay Polymerisation assay	-	FtsZ binding assay developed that involved monitoring protein induced changes in the intrinsic fluorescence of the compound.	(162)
 <p>Cinnamaldehyde</p>	<i>B. subtilis</i> (500 µg/ml) <i>E. coli</i> (1000 µg/ml)	Fluorescence microscopy using a GFP-tagged FtsZ in <i>E. coli</i> gave a filamentous phenotype with dissipated Z-ring morphology. EM shows a loss of polymerized FtsZ bundles when treated.	GTPase assay Polymerisation assay	<i>In silico</i> molecular modelling STD NMR binding studies Isothermal calorimetry to determine K_d	-	(132)
 <p>Curcumin</p>	<i>B. subtilis</i> (100 µM) <i>E. coli</i> (80% inhibition at 100 µM)	Phase contrast microscopy showed filamentous phenotype in <i>B. subtilis</i> . TEM showed the size and thickness of FtsZ polymers reduced extensively, and FtsZ polymers were considerably when exposed to curcumin Immunofluorescence microscopy showed curcumin strongly inhibited the Z-ring formation.	GTPase assay	-	-	(163)

 <p>Compound 10</p>	<p><i>S. aureus</i> (4 µg/ml) <i>B. subtilis</i> (128 µg/ml) <i>E. coli</i> (128 µg/ml) <i>P. aeruginosa</i> (128 µg/ml)</p>	<p>Cell division phenotype seen in <i>S. aureus</i>, <i>B. subtilis</i>, <i>E. coli</i> and <i>P. aeruginosa</i></p>	<p>GTPase assay Polymerisation assay</p>	-	-	(164)
 <p>Totarol</p>	<p><i>B. subtilis</i> (2 µM)</p>	<p>Phase contrast microscopy showed filamentous phenotype in <i>B. subtilis</i>.</p>	<p>GTPase assay Polymerisation assay</p>	-	-	(165)
 <p>Viriditoxin</p>	<p><i>S. aureus</i> (4-8 µg/ml) <i>E. faecium</i> (8-16 µg/ml) <i>S. pneumoniae</i> (16-32 µg/ml) <i>E. coli</i> (>64 µg/ml)</p>	<p>Phase contrast microscopy showed filamentous phenotype in <i>E. coli</i>.</p>	<p>GTPase assay</p>	-	-	(166)
 <p>Chrysophaentin A</p>	<p><i>S. aureus</i> (2 µg/ml) MRSA (1.5 µg/ml) <i>E. faecium</i> (4 µg/ml) VRE (3 µg/ml)</p>	<p>Fluorescence microscopy</p>	<p>GTPase assay Polymerisation assay</p>	STD NMR binding studies	-	(167-169)
 <p>Scopoletin (Coumarins)</p>	<p><i>M. tuberculosis</i> (42 µg/ml)</p>	<p>Phase contrast microscopy showed filamentous phenotype in <i>B. subtilis</i>.</p> <p>TEM shows that scopoletin at 100 µM concentrations perturb the FtsZ polymerization</p>	<p>Polymerisation assay</p>	-	-	(170)
 <p>Plumbagin</p>	<p><i>M. smegmatis</i> (31 µM) <i>B. subtilis</i> (29 µM)</p>	<p>Phase contrast microscopy showed filamentous phenotype in <i>B. subtilis</i>.</p> <p>Immunofluorescence microscopy showed Plumbagin inhibited Z-ring</p>	<p>GTPase assay Polymerisation assay</p>	<i>In silico</i> molecular modelling	-	(171)

		<p>formation and considerable reduced the number of mid-cell Z-rings.</p> <p>TEM found Plumbagin inhibited <i>B. subtilis</i> FtsZ assembly and induced aggregation of <i>B. subtilis</i> FtsZ monomers at high concentrations</p>				
 <p>Compound 11a</p>	<p><i>S. aureus</i> (4.0 µg/ml) MRSA (4.0 µg/ml) <i>E. faecalis</i> (8.0 µg/ml) VRE (16 µg/ml)</p>	-	Polymerisation assay	-	-	(172)
 <p>Compound 9</p>	<p><i>S. aureus</i> (0.5 µg/ml) MRSA (1.0 µg/ml) <i>E. faecalis</i> (2 µg/ml) VRE (2 µg/ml)</p>	-	Polymerisation assay	-	-	(173)
 <p>Compound 18</p>	<p><i>S. aureus</i> (128 µg/ml) <i>B. subtilis</i> (128 µg/ml) <i>E. coli</i> (128 µg/ml) <i>P. aeruginosa</i> (128 µg/ml) <i>S. epidermidis</i> (>128 µg/ml)</p>	Cell division phenotype seen in <i>S. aureus</i> , <i>B. subtilis</i> , <i>E. coli</i> and <i>P. aeruginosa</i>	-	-	-	(174)
 <p>Zanterin 5</p>	<i>EcFtsZ</i> IC ₅₀ (30 µM)	<p><i>E. coli</i> gave filamentous phenotype prior to lysis.</p> <p>Fluorescence microscopy shows Z5 perturbs Z-ring assembly, without effecting chromosome segregation.</p>	<p>GTPase assay</p> <p>Sedimentation assay</p>	-	Identified through high-throughput screen using pure <i>E. coli</i> FtsZ	(138)

 <p>Compound 5c</p>	<p><i>S. aureus</i> IC₅₀ (0.030 mM) <i>E. coli</i> IC₅₀ (1.112 mM) <i>P. aeruginosa</i> IC₅₀ (13.25mM)</p>	-	-	<i>In silico</i> molecular modelling	-	(155)
 <p>Compound 1b-G1</p>	<i>M. tuberculosis</i> (1.0 μM)	<p>TEM showed significant reduction in the extent of <i>M. tuberculosis</i> FtsZ protofilaments formation. Density of protofilaments was reduced.</p> <p>SEM of <i>M. tuberculosis</i> cells revealed altered cell lengths and aberrant division.</p>	<p>GTPase assay</p> <p>Polymerisation assay</p>	-	-	(175)
 <p>Compound 5a</p>	<i>M. tuberculosis</i> (0.63 μg/ml)	TEM showed <i>M. tuberculosis</i> FtsZ polymers drastically reduced in length and density.	Polymerisation assay	-	Fluorescence anisotropy of compound was measured to determine <i>K_d</i>	(176)
 <p>CCR-11</p>	<i>B. subtilis</i> IC ₅₀ : 1.2 ± 0.2 μM	<p>Phase contrast microscopy showed filamentous phenotype in <i>B. subtilis</i>.</p> <p>Fluorescence microscopy shows CCR-11 exposure resulted in no Z-rings at Midcell in <i>B. subtilis</i>, rather FtsZ was present as helices and spots throughout elongated cell.</p>	<p>GTPase assay</p> <p>Polymerisation assay</p>	<i>In silico</i> molecular modelling	-	(177)

 <p>Compound 13L</p>	<i>E. coli</i> FtsZ IC ₅₀ (9 μM)	-	GTPase assay Polymerisation assay	-	GTP competition experiment	(178)
 <p>UCM53</p>	4-128 μg/ml across species. Selectively against Gram-positive.	Phase contrast microscopy showed filamentous phenotype in <i>B. subtilis</i> . Fluorescence microscopy found that GFP-tagged FtsZ in <i>B. subtilis</i> is delocalized with the formation of numerous punctuate foci and distorted ring structures.	GTPase assay Polymerisation assay	<i>In silico</i> molecular modelling	-	(179)
 <p>Compound 12</p>	<i>S. aureus</i> (24.6 μM) <i>E. coli</i> (49.2 μM)	-	GTPase assay	<i>In silico</i> molecular modelling	-	(153)

^a MIC is recorded as either μg/ml or μM as presented in publications. If the IC₅₀ is given instead, the antibacterial activity was not determined.

^b Evidence encompasses any data presented in the publication that indicates FtsZ inhibition. Any other work not directly related to FtsZ was omitted.

Chapter 2 - Materials and Methods

2.1 Materials

2.1.1 Chemicals

Antibiotic sources and their working concentration are listed in Table 2.1. Media used in this study are listed in Table 2.2.

Table 2.1: Antibiotic sources and their working concentration for *E. coli*.

Antibiotic	Working concentration	Source
Ampicillin	100 µg/mL	Sigma-Aldrich, Australia
Kanamycin	50 µg/mL	Sigma-Aldrich, Australia
Tetracycline	5 µg/mL	Sigma-Aldrich, Australia

Table 2.2: Media used in this study.

Luria-Bertani broth (LB)	1% (w/v) sodium chloride, 1% (w/v) Tryptone, 0.5% (w/v) yeast extract
Minimal media (M9)	1X M9 salts, 2 mM MgSO ₄ , 0.1 mM CaCl ₂ and 0.2% (w/v) glucose

2.1.2 Solutions

Solutions used in this work are described in Table 2.3.

Table 2.3: Solutions used in this study.

Solution	Ingredients
Coomassie Blue Stain	50% Ethanol (v/v), 10% Glacial Acetic acid \geq 99.85% (v/v), 0.5% Coomassie R-250 (w/v)
Destaining buffer	20% Ethanol (v/v), 10% Glacial Acetic acid \geq 99.85% (v/v)
SDS-PAGE loading buffer (2X)	0.62 M Tris-HCl pH 6.8, 10% SDS (w/v), 20% Glycerol (v/v), 0.1% Bromophenol blue (w/v)
SDS-PAGE loading buffer (1X)	SDS-PAGE loading buffer (2X) with 10% of 2-Mercaptoethanol (v/v)
SDS-PAGE running buffer (10X)	14.42% (w/v) Glycine, 3% (w/v) Tris, 1% (w/v) SDS
Resolving gel buffer	For a 10% gel = 25% (v/v) N,N' -methylenebisacrylamide stock (40%), 25% (v/v) 4x Tris/SDS buffer, 1% (v/v) APS (10%), 0.1% (v/v) TEMED (pure)-catalyst For a 12% gel, change to 30% (v/v) acrylamide stock (40%)
Stacking gel (4%) buffer	10% (v/v) N,N' -methylenebisacrylamide stock (40%), 25% (v/v) 4x Tris/SDS buffer, 1% (v/v) APS (10%), 0.1% (v/v) TEMED (pure)-catalyst
4x resolving Tris/SDS buffer	1.5 M Tris-HCl pH 8.8, 0.4% SDS
4x stacking Tris/SDS buffer	500 mM Tris-HCl pH 6.8, 0.4% SDS

10X M9 salts	6% (w/v) Na ₂ HPO ₄ , 3% (w/v) KH ₂ PO ₄ , 0.5% (w/v) NaCl, 1% (w/v) NH ₄ Cl pH 7.4 ¹⁵ N-NH ₄ Cl is added to media just before use, as it degrades over time if mixed in solutions
<i>A. baylyi</i> untagged FtsZ and FtsA-6xhis purification lysis buffer	25 mM Tris-HCl (pH 7.6), 2 mM DTT, 1 mg/mL lysozyme, 50 µg/mL DNase (Sigma), 1 complete protease inhibitor tablet (Roche), 2 mM 1,10-phenanthroline, 1 mM PMSF
<i>A. baylyi</i> untagged FtsZ purification anion exchange buffer A	20 mM Tris-HCl pH 7.74
<i>A. baylyi</i> untagged FtsZ purification anion exchange buffer B	20 mM Tris-HCl, 1M NaCl pH 7.74
<i>A. baylyi</i> untagged FtsZ purification size exclusion buffer	20 mM Tris-HCl, 200 mM NaCl pH 7.74
<i>B. subtilis</i> 6xhis-FtsZ purification lysis buffer	50 mM Tris-HCl pH 8.0, 50 mM KCl, 5% glycerol (v/v), 100 µg/mL lysozyme, 1 mM PMSF
<i>B. subtilis</i> 6xhis-FtsZ purification his trap and anion exchange buffer A	50 mM Tris-HCl pH 8.0, 50 mM KCl, 5% glycerol (v/v)
<i>B. subtilis</i> 6xhis-FtsZ purification his trap buffer B	50 mM Tris-HCl pH 8.0, 50 mM KCl, 5% glycerol (v/v), 1 M imidazole
<i>B. subtilis</i> 6xhis-FtsZ purification anion exchange buffer B	50 mM Tris-HCl pH 8.0, 5% glycerol (v/v), 1 M KCl
<i>B. subtilis</i> 6xhis-FtsZ purification gel filtration buffer	50 mM NaH ₂ PO ₄ ·2H ₂ O pH 7.4, 200 mM NaCl

<i>A. baylyi</i> FtsA-6xhis purification inclusion bodies wash buffer	25 mM Tris-HCl pH 7.6, 2 mM DTT
<i>A. baylyi</i> FtsA-6xhis purification his trap wash buffer	20 mM Tris-HCl, 500 mM NaCl, 20 mM imidazole, 6 M Urea, 1 mM DTT pH 7.7
<i>A. baylyi</i> FtsA-6xhis purification refolding buffer	20 mM Tris-HCl, 500 mM NaCl, 20 mM imidazole, 1 mM DTT pH 7.7
<i>A. baylyi</i> FtsA-6xhis purification his trap elution buffer	20 mM Tris-HCl, 500 mM NaCl, 1 M imidazole, 1 mM DTT pH 7.7
<i>A. baylyi</i> FtsA-6xhis purification concentrating buffer	20% PEG 20 000 (w/v), 20% glycerol (v/v)
<i>A. baylyi</i> FtsA-6xhis purification storage buffer	20 mM Tris-HCl pH 7.76, 300 mM NaCl, 20% glycerol (v/v)
Tris-Salt (TS) buffer	200 mM Tris-HCl pH 7.74, 100 mM NaCl

2.1.3 Bacterial strains and plasmids

The bacterial strains and plasmids used in this study are described in Table 2.4 and 2.5, respectively.

Table 2.4: Bacterial strains used in this study.

Strains	Description ^a	Sources
<i>Escherichia coli</i>		
B834 (DE3)	<i>F⁻ hsdS metE gal ompT</i>	Gift from Iain Duggin (University of Technology Sydney)
BLR (DE3)	<i>F⁻ ompT hsdS_B(r_B⁻ m_B⁻) gal lac ile dcm Δ(srl-recA)306::Tn10 (tet^R)(DE3)</i>	Novagen [®]
BL21 codonplus (DE3) RIPL	<i>B F⁻ ompT hsdS (rB⁻ mB⁻) dcm⁺ Tetr gal λ(DE3) endA Hte [argU proL Camr] [argU ileY leuW Strep/Spe^r]</i>	Gift from Iain Duggin (University of Technology Sydney)
BL21-AI	<i>B F⁻ ompT gal dcm lon hsdSB (rB⁻ mB⁻) araB::T7RNAP-tetA</i>	Gift from Iain Duggin (University of Technology Sydney)

C41 (DE3)	<i>B F⁻ ompT gal dcm hsdSB (rB- mB-)(DE3)</i>	Gift from Iain Duggin (University of Technology Sydney)
DH5α	<i>F' proA+B+ lacIq Δ(lacZ)M15 / fhuA2 Δ(lac-proAB) glnV gal R(zgb-210::Tn10) (TetS) endA1 thi-1 Δ(hsdS-mcrB)5</i>	Laboratory stock
BL21 (DE3)	<i>fhuA2 [lon] ompT gal (λ DE3) [dcm] ΔhsdS. λ DE3 = λ sBamHI ΔEcoRI-B int::(lacI::PlacUV5::T7 gene1) i21 Δnin5</i>	Laboratory stock
DH5α pETMCSI <i>A. baylyi</i> untagged FtsZ	DH5α containing pETMCSI <i>A. baylyi</i> untagged FtsZ; Amp ^r	Dr Amy Bottomley
DH5α pETMCSI <i>A. baylyi</i> FtsZ-6xhis	DH5α containing pETMCSI <i>A. baylyi</i> FtsZ-6xhis; Amp ^r	Dr Amy Bottomley
DH5α pETMCSI <i>A. baumannii</i> untagged FtsZ	DH5α containing pETMCSI <i>A. baumannii</i> untagged FtsZ; Amp ^r	Dr Amy Bottomley
DH5α pETMCSI <i>A. baumannii</i> FtsZ-6xhis	DH5α containing pETMCSI <i>A. baumannii</i> FtsZ-6xhis; Amp ^r	Dr Amy Bottomley

B834 (DE3) pETMCSI <i>A. baylyi</i> untagged FtsZ	B834 (DE3) containing pETMCSI <i>A. baylyi</i> untagged FtsZ; Amp ^r	This study
B834 (DE3) pETMCSI <i>A. baylyi</i> FtsZ-6xhis	B834 (DE3) containing pETMCSI <i>A. baylyi</i> FtsZ-6xhis; Amp ^r	This study
B834 (DE3) pETMCSI <i>A. baumannii</i> untagged FtsZ	B834 (DE3) containing pETMCSI <i>A. baumannii</i> untagged FtsZ; Amp ^r	This study
B834 (DE3) pETMCSI <i>A. baumannii</i> FtsZ-6xhis	B834 (DE3) containing pETMCSI <i>A. baumannii</i> FtsZ-6xhis; Amp ^r	This study
BLR (DE3) pETMCSI <i>A. baylyi</i> untagged FtsZ	BLR (DE3) containing pETMCSI <i>A. baylyi</i> untagged FtsZ; Amp ^r ; Tet ^r	This study
BLR (DE3) pETMCSI <i>A. baylyi</i> FtsZ-6xhis	BLR(DE3) containing pETMCSI <i>A. baylyi</i> FtsZ-6xhis; Amp ^r ; Tet ^r	This study
BLR (DE3) pETMCSI <i>A. baumannii</i> untagged FtsZ	BLR (DE3) containing pETMCSI <i>A. baumannii</i> untagged FtsZ; Amp ^r ; Tet ^r	This study
BLR (DE3) pETMCSI <i>A. baumannii</i> FtsZ-6xhis	BLR (DE3) containing pETMCSI <i>A. baumannii</i> FtsZ-6xhis; Amp ^r ; Tet ^r	This study
BL21 codonplus (DE3) RIPL pETMCSI <i>A. baylyi</i> untagged FtsZ	BL21 codonplus (DE3) RIPL containing pETMCSI <i>A. baylyi</i> untagged FtsZ; Amp ^r	This study

BL21 codonplus (DE3) RIPL pETMCSI <i>A. baylyi</i> FtsZ-6xhis	BL21 codonplus (DE3) RIPL containing pETMCSI <i>A. baylyi</i> FtsZ-6xhis; Amp ^r	This study
BL21 codonplus (DE3) RIPL pETMCSI <i>A. baumannii</i> untagged FtsZ	BL21 codonplus (DE3) RIPL containing pETMCSI <i>A. baumannii</i> untagged FtsZ; Amp ^r	This study
BL21 codonplus (DE3) RIPL pETMCSI <i>A. baumannii</i> FtsZ-6xhis	BL21 codonplus (DE3) RIPL containing pETMCSI <i>A. baumannii</i> FtsZ-6xhis; Amp ^r	This study
BL21-AI pETMCSI <i>A. baylyi</i> untagged FtsZ	BL21-AI containing pETMCSI <i>A. baylyi</i> untagged FtsZ; Amp ^r	This study
BL21-AI pETMCSI <i>A. baylyi</i> FtsZ-6xhis	BL21-AI containing pETMCSI <i>A. baylyi</i> FtsZ-6xhis; Amp ^r	This study
BL21-AI pETMCSI <i>A. baumannii</i> untagged FtsZ	BL21-AI containing pETMCSI <i>A. baumannii</i> untagged FtsZ; Amp ^r	This study
BL21-AI pETMCSI <i>A. baumannii</i> FtsZ-6xhis	BL21-AI containing pETMCSI <i>A. baumannii</i> FtsZ-6xhis; Amp ^r	This study
C41 (DE3) pETMCSI <i>A. baylyi</i> untagged FtsZ	C41 (DE3) containing pETMCSI <i>A. baylyi</i> untagged FtsZ; Amp ^r	This study
C41 (DE3) pETMCSI <i>A. baylyi</i> FtsZ-6xhis	C41 (DE3) containing pETMCSI <i>A. baylyi</i> FtsZ-6xhis; Amp ^r	This study

C41 (DE3) pETMCSI <i>A. baumannii</i> untagged FtsZ	C41 (DE3) containing pETMCSI <i>A. baumannii</i> untagged FtsZ; Amp ^r	This study
C41 (DE3) pETMCSI <i>A. baumannii</i> FtsZ-6xhis	C41 (DE3) containing pETMCSI <i>A. baumannii</i> FtsZ-6xhis; Amp ^r	This study
DH5α pETMCSI <i>A. baylyi</i> FtsA-6xhis	DH5α containing pETMCSI <i>A. baylyi</i> FtsA-6xhis; Amp ^r	Dr Amy Bottomley
DH5α pETMCSIII <i>A. baylyi</i> 6xhis-FtsA	DH5α containing pETMCSIII <i>A. baylyi</i> 6xhis-FtsA; Amp ^r	Dr Amy Bottomley
BL21-AI pETMCSI <i>A. baylyi</i> FtsA-6xhis	BL21-AI containing pETMCSI <i>A. baylyi</i> FtsA-6xhis; Amp ^r	This study
BL21-AI pETMCSIII <i>A. baylyi</i> 6xhis-FtsA	BL21-AI containing pETMCSIII <i>A. baylyi</i> 6xhis-FtsA; Amp ^r	This study
C41 (DE3) pETMCSI <i>A. baylyi</i> FtsA-6xhis	C41 (DE3) containing pETMCSI <i>A. baylyi</i> FtsA-6xhis; Amp ^r	This study
C41 (DE3) pETMCSIII <i>A. baylyi</i> 6xhis-FtsA	C41 (DE3) containing pETMCSIII <i>A. baylyi</i> 6xhis-FtsA; Amp ^r	This study
DH5α pAT20 <i>B. subtilis</i> FtsZ ¹⁻³¹⁵ A182E	DH5α containing pAT20 <i>B. subtilis</i> FtsZ ¹⁻³¹⁵ A182E; Kan ^r	Gift from Frederico José Gueiros Filho (University of São Paulo)

BL21 (DE3) pAT20 <i>B. subtilis</i> FtsZ ¹⁻³¹⁵ A182E	BL21 (DE3) containing pAT20 <i>B. subtilis</i> FtsZ ¹⁻³¹⁵ A182E; Kan ^r	This study
DH5α pETMCSI WT <i>B. subtilis</i> FtsZ ¹²⁻³¹⁵	DH5α containing pETMCSI wild-type <i>B. subtilis</i> FtsZ ¹²⁻³¹⁵ ; Amp ^r	This study
BL21-AI pETMCSI WT <i>B. subtilis</i> FtsZ ¹²⁻³¹⁵	BL21-AI containing pETMCSI wild-type <i>B. subtilis</i> FtsZ ¹²⁻³¹⁵ ; Amp ^r	This study

^aAntibiotic resistance markers are expressed as follows: Amp^r = ampicillin resistance; Kan^r = kanamycin resistance; Tet^r = tetracycline resistance.

Table 2.5: Plasmids used and constructed in this study.

Plasmid	Description ^a	Sources
pETMCSI	Stable high-copy number plasmid which contains a modified bacteriophage T7 promoter for overexpression of genes that have a <i>NdeI</i> site at their start codon. The multi-cloning site is located downstream the T7 promoter and ribosome binding site. This plasmid allows the creation of untagged and C-terminus hexa-histidine tagged protein for overproduction. The histidine tag is incorporated during PCR; Amp ^r	Gift from Nick Dixon (University of Wollongong) (180)
pETMCSIII	Stable high-copy number plasmid which contains a modified bacteriophage T7 promoter. <i>Met-His6</i> was inserted upstream the multi-cloning site, allowing the creation of N-terminus hexa-histidine tagged protein for overproduction; Amp ^r	Gift from Nick Dixon (University of Wollongong) (180)
pETMCSI <i>A. baylyi</i> untagged FtsZ	pETMCSI plasmid encoding full length <i>A. baylyi</i> untagged FtsZ downstream of T7 promoter; Amp ^r Restriction sites used were for <i>EcoRI</i> and <i>NdeI</i>	Dr Amy Bottomley
pETMCSI <i>A. baylyi</i> FtsZ-6xhis	pETMCSI plasmid encoding full length <i>A. baylyi</i> C-terminus hexa-histidine tagged FtsZ downstream of T7 promoter; Amp ^r Restriction sites used were for <i>EcoRI</i> and <i>NdeI</i>	Dr Amy Bottomley

pETMCSI <i>A. baumannii</i> untagged FtsZ	pETMCSI plasmid encoding full length <i>A. baumannii</i> untagged FtsZ downstream of T7 promoter; Amp ^r Restriction sites used were for <i>EcoRI</i> and <i>NdeI</i>	Dr Amy Bottomley
pETMCSI <i>A. baumannii</i> FtsZ-6xhis	pETMCSI plasmid encoding full length <i>A. baumannii</i> C-terminus hexa-histidine tagged FtsZ downstream of T7 promoter; Amp ^r Restriction sites used were for <i>EcoRI</i> and <i>NdeI</i>	Dr Amy Bottomley
pETMCSI <i>A. baylyi</i> FtsA-6xhis	pETMCSI plasmid encoding full length <i>A. baylyi</i> C-terminus hexa-histidine tagged FtsA downstream of T7 promoter; Amp ^r Restriction sites used were for <i>EcoRI</i> and <i>NdeI</i>	Dr Amy Bottomley
pETMCSIII <i>A. baylyi</i> 6xhis-FtsA	pETMCSI plasmid encoding full length <i>A. baylyi</i> N-terminus hexa-histidine tagged FtsA downstream of T7 promoter; Amp ^r Restriction sites used were for <i>EcoRI</i> and <i>NdeI</i>	Dr Amy Bottomley
pAT20 <i>B. subtilis</i> FtsZ ¹⁻³¹⁵ A182E	Stable high-copy number plasmid containing a bacteriophage T7 promoter. <i>B. subtilis ftsZ</i> gene coding for amino acid 1-315 was inserted downstream of T7 promoter. Sequence encodes for A182E mutation within <i>B. subtilis ftsZ</i> . The resulting protein is unable to polymerize; Kan ^r	Gift from Frederico José Gueiros Filho (University of São Paulo)

pETMCSI wild-type <i>B. subtilis</i> FtsZ ¹²⁻³¹⁵	<p>pETMCSI plasmid encoding wild-type <i>B. subtilis</i> FtsZ downstream of T7 promoter.</p> <p>The protein produce will have truncations at both the N- and C-terminus and will only produce the globular domain, which is amino acid residue 12-315; Amp^r</p> <p>Restriction sites used were for <i>EcoRI</i> and <i>NdeI</i></p>	This study
---	--	------------

^aAntibiotic resistance markers are expressed as follows: Amp^r = ampicillin resistance; Kan^r = kanamycin resistance.

2.2 Methods

2.2.1 DNA manipulation

2.2.1.1 Plasmid extraction

Plasmids used were extracted from *E. coli* strains containing the plasmid of interest by using GenElute™ Plasmid Miniprep kit (Sigma-Aldrich, Australia). Protocol followed was in accordance to the manufacturer's instructions and the quantity and quality of the plasmid was measured using the nanodrop "NanoDrop One" (Thermo Scientific).

2.2.1.2 Preparation and transformation of electro-competent *E. coli*

Electro-competent *E. coli* were prepared in the following way. An overnight culture of *E. coli* was diluted to OD₆₀₀ of 0.05 in 500 mL of LB broth and incubated at 37°C with vigorous shaking to an OD₆₀₀ of 0.5. The samples were then put on ice-slurry for 20 min and the cells were harvested by centrifugation at 3,761 xg for 10 min. Following harvest, the cells were resuspended and washed with 30 mL of ice cold MilliQ water three times, with centrifugation at 3,761 xg for 10 min at 4°C between each washing. After the last washing, the supernatant was removed and ice cold 50% (w/v) glycerol was added to a final concentration of 10%. The cells were then distributed in 50 µL aliquots, froze in liquid nitrogen and stored at -80°C.

Transformation of electro-competent *E. coli* is as follows. The entire procedure was carried out on ice. 1 µL of purified plasmid (~100 ng/µL) was mixed with 50 µL aliquot of electro-competent *E. coli* cells and transferred to 0.2 cm "Gene Pulser® Cuvette" (BioRad, USA). Electroporation conditions were 25 µFD, 200 Ω, 2.0 kV for 5 sec. Following electroporation, cells were resuspended in 500 µL of LB broth and incubated

for 1 h at 37°C with shaking at 145 rpm before being spread on LB plates containing appropriate antibiotics and incubated overnight at 37°C until colonies appeared.

2.2.1.3 PCR amplification of wild-type *B. subtilis* *ftsZ*¹²⁻³¹⁵ gene

PCR was used to amplify a truncated portion of the *ftsZ* gene from *B. subtilis* 168 genomic DNA which encodes amino acid 12 to 315. This was set up with the following components: 1X Phusion HF buffer, 200 µM 10 mM dNTPs, 0.5 µM forward primer and reverse primer (refer to table 2.6), 1 µL of genomic DNA, 1 unit of Phusion DNA Polymerase and MilliQ water was used to make the reaction into 50 µL.

Table 2.6: Primers used for the PCR amplification of *B. subtilis* *FtsZ*¹²⁻³¹⁵.

	Forward primer sequence (KDK30)	Reverse primer sequence (KDK31)
Sequence*	tttttcat <u>ATGT</u> CAATTAA AGTAATCGGAGTAGG AGG	ataataga <u>aattc</u> AACTAAAA GCCGGTTGCAATCAC
Melting point	54.1°C	54.1°C
Restriction enzyme site	<i>NdeI</i>	<i>EcoRI</i>

* lower case letters on the sequence are the sequence overhangs. The restriction enzyme cutting site is underlined, while the upper-case letters are the sequence which directly binds to the genomic DNA.

Amplification was started with initial denaturation at 98°C for 30 sec and followed by 35 cycles of denaturation at 98°C for 10 sec, annealing at 54°C for 25 sec and extension at 72°C for 30 sec. The process was concluded by a final extension at 72°C for 10 min.

The truncated *ftsZ* PCR fragment should be 909 bp. The amplified sample was cleaned with a PCR purification kit from Sigma and stored at 4°C until further use.

2.2.1.4 Restriction digest of the PCR product and plasmid

The *ftsZ* PCR product (Section 2.2.1.3) and plasmid pETMCSI were digested using the restriction enzymes *NdeI* and *EcoRI*. All restriction digests were performed with 1 µg of PCR product or plasmid with 40 U of restriction enzymes at 37°C for 4 h. Appropriate buffers were added to the restriction digest reaction in a total reaction volume of 50 µL in accordance to the manufacturer's instructions. Following digestion, the digested PCR product and plasmid were purified using GenElute™ PCR clean-up kit (Sigma-Aldrich, Australia). To confirm the plasmid digestion efficiency with the restriction enzymes, the digested plasmids were analysed on a 1% agarose gel in which a single band of 909 bp and 4676 bp should be observed for the insert and plasmid, respectively.

2.2.1.5 Ligation of the PCR product and plasmid

Ligation reactions were carried out by mixing 1:3, 1:5 and 1:7, plasmid to PCR product ratio, together with 400 U of T4 DNA ligase and ligase buffer (New England Biolab, United Kingdom) in a total reaction volume of 20 µL. The ligation reaction was incubated overnight at 16°C and 10 µL of the reaction was used for transformation into electro-competent *E. coli* DH5α to make DH5α pETMCSI WT *B. subtilis* FtsZ¹²⁻³¹⁵.

2.2.1.6 Colony PCR

Colony PCR was carried out in a 20 μ L reaction volume. The reaction mixture contained 0.25 μ L 10 mM dNTPs, 2.5 μ L 10X ThermoPol® Reaction Buffer (New England Biolab, United Kingdom), 0.5 μ L 10 pM of both forward and reverse primers (Table 2.6), 0.25 μ L *Taq* DNA Polymerase (New England Biolab, United Kingdom), and 16 μ L MilliQ to make up to 20 μ L volume. In colony PCR, one bacterial colony was used as a template instead of purified DNA. PCR conditions were as follow. Initial denaturation at 95°C for 2 min and followed by 30 cycles of denaturation at 95°C for 15 sec, annealing at 54°C for 30 sec and extension at 72°C for 1 min. The process was concluded by a final extension at 72°C for 5 min. The amplified sample was stored at 4°C until further use.

2.2.2 Protein purification

2.2.2.1 Overproduction trial of *Acinetobacter FtsZ* and *FtsA*

Overnight culture of the protein overproduction *E. coli* strain which contains the necessary plasmid was firstly inoculated to a fresh 5 mL (small scale trial) or 1 L (large scale production) LB broth containing the necessary antibiotics to OD₆₀₀ of 0.05 and grown at 37°C with shaking at 200 rpm. Once the cells reached OD₆₀₀ of ~0.5, protein production induced with 0.5 mM IPTG. The *E. coli* strain BL21-AI was induced with 0.2% (w/v) arabinose. Following induction, the cells were moved to several induction temperatures to determine optimum conditions for protein yield and solubility (37 °C, 30 °C, 25 °C and 10°C) and left to grow overnight in the separate temperatures with shaking at 200 rpm. The following day, the cells were harvested by centrifugation at 12,600 xg for 15 min at 4°C.

2.2.2.2 Analysis of the Acinetobacter FtsZ and FtsA protein overproduction and solubility

During the preparation of cells in Section 2.2.2.1, 1 mL of culture was removed before the addition of inducer (uninduced sample), and 2x 1 mL of culture were removed after the overnight incubation following the addition of inducer (induced sample). The cultures were centrifuged at 12,600 xg for 15 min at 4°C and the supernatant was discarded. The samples were then resuspended and washed twice with 250 µL TS buffer (refer to Section 2.1.2), snap frozen with liquid nitrogen and stored at -20°C. Upon thawing, the samples were normalized to OD₆₀₀ = 10 by resuspension in TS buffer. Equal volumes of SDS loading buffer (1X) were added to the normalized uninduced and one induced sample. The samples were vortexed and heated for 10 min at 95°C. 10 µL of each sample was analysed by SDS-PAGE and stained with Coomassie blue stain and destained to confirm overproduction of the protein.

To determine the solubility of protein, 15 µL of 5 mg/mL lysozyme was added to the second normalized induced sample. The sample was incubated at room temperature for 1 h with frequent mixing *via* vortexing, followed by sonication for 5 x 10 sec bursts using a Selby-Biolab sonicator. The sample was centrifuged at 16,100 xg for 15 min at 4°C to separate the soluble and insoluble materials. The supernatant containing soluble proteins was removed into a fresh microcentrifuge tube and equal volume of SDS loading buffer was added. The pellet containing the insoluble material was resuspended in an equal volume of TS buffer and equal volume of SDS loading buffer (1X) was also added. The two samples were subsequently vortexed and heated at 95°C for 10 min. 10 µL of each sample was analysed by SDS-PAGE and stained with Coomassie blue stain and destained for visualisation.

SDS-PAGE gels used in the overproduction and solubility studies were made with recipe outlined in Section 2.1.2. The SDS-PAGE running buffer used is also outlined in Section 2.1.2. All SDS-PAGE running conditions were 175 V for 50 min.

2.2.2.4 Ammonium sulphate precipitation trial

Ammonium sulphate trials were conducted at 4°C as a first step of purification for the full-length *Acinetobacter* untagged FtsZ protein. 50 mL of *E. coli* cells harbouring plasmid encoding for this protein were firstly grown and induced for protein overproduction under the conditions determined optimal for protein yield and solubility. The cells were subsequently lysed in *A. baylyi* FtsZ lysis buffer (refer to Section 2.1.2). The amount of lysis buffer used was 15 mL of lysis buffer for 1 g of cell pellet. Once lysed, the cell lysate was centrifuged at 39,856 xg for 30 min to separate the soluble and insoluble material. The soluble material was then filtered using a 0.2 µm filter to remove any remaining debris and divided into six aliquots. The six aliquots were used to determine the optimum concentration of ammonium sulphate resulting in protein precipitation (0.15 g/mL, 0.20 g/mL, 0.25 g/mL, 0.30 g/mL, 0.35 g/mL, and 0.40 g/mL). The solution was stirred gently during the addition of the solid ammonium sulphate in their respective concentrations to avoid protein denaturation, as evidenced by foaming. The solid ammonium sulphate was added slowly to the solution over the duration of 30 min. Once all the ammonium sulphate had been added, the solution was left to continue stirring for a further 20 min, after which 1 mL aliquots were taken and centrifuged at 9,300 xg for 20 min at 4°C to separate the supernatant and precipitate. To determine the location of the protein, the supernatant was transferred to a new tube (soluble fraction) and the precipitate (insoluble fraction) resuspended in 1 mL TS buffer (refer to Section 2.1.2). Optimum ammonium sulphate concentration is determined by the highest

protein yield with minimal contaminants residing in the insoluble fraction. For visualization, equivalent amount of SDS-PAGE loading buffer (1X) was added to both samples and analysed on an SDS-PAGE gel.

2.2.2.5 Sodium chloride dialysis trial

To determine the stability of the protein in no-salt buffer for subsequent experiments, the ammonium sulphate-precipitated pellet, which gave high yield and minimal contamination, was re-dissolved in 30 mL buffer (25 mM Tris-HCl pH 7.6). The supernatant was then divided into four aliquots, placed in a dialysis tube (Sigma) with 10,000 Da MWCO and dialysed overnight at 4°C with gentle stirring against 500 mL buffer (25 mM Tris-HCl pH 7.6) containing 0 M, 0.1 M, 0.2 M or 0.3 M of sodium chloride. After 16 h, a 200 µL sample was taken from each of the four dialysis conditions and centrifuged at 16,100 xg for 20 min to separate the soluble and any insoluble material formed during the dialysis. To determine the location of the protein, the supernatant was transferred to a new tube (soluble fraction) and the precipitate (insoluble fraction) resuspended in 1 mL TS buffer (refer to Section 2.1.2). Optimum sodium chloride concentration is determined by the target protein residing in the soluble fraction. For visualization, an equivalent amount of SDS-PAGE loading buffer (1X) was added to both samples and analysed on an SDS-PAGE gel.

2.2.2.6 Optimized purification protocol

Electro-competent *E. coli* strain BL21-AI was transformed with pMCSI containing full length *A. baylyi* untagged FtsZ (refer to Section 2.2.1.2) and grown at 37°C overnight in 50 mL of LB broth (refer to Table 2.3 in Section 2.1.1) containing 100 µg/mL of Ampicillin with shaking. The following morning, the cells were diluted to OD₆₀₀ = 0.05

in 1 L of LB with the same concentration of antibiotic. Cells were grown at 37°C until mid-exponential phase ($OD_{600} = 0.5$) and 0.2% arabinose was added to induce the cells for protein overproduction. The induced cells were grown at 25°C for 24 h with shaking at 200 rpm. Subsequently, the cells were harvested by centrifugation at 12,600 xg for 15 min at 4°C. The cell pellet was collected and resuspended in 15 mL of lysis buffer per 1 g of cell pellet (refer to *A. baylyi* untagged FtsZ and FtsA-6xhis purification Lysis buffer in Section 2.1.2). The lysate was then incubated at 25°C for 1 h and subsequently freeze-thawed four times to ensure complete cell lysis. The freezing process used liquid nitrogen, while the thawing was conducted in a shaking water bath at 25°C. After freeze-thawing, the lysate was centrifuged at 39,856 xg for 30 min to separate the soluble and insoluble materials. The soluble material was transferred to a new tube and filtered using 0.2 µm filters to remove any remaining cell debris. The supernatant was then placed in a beaker and 0.2 g/mL of solid ammonium sulphate (as determined by the ammonium sulphate precipitation trial in Section 2.2.2.4) was added slowly to precipitate the target protein, while the solution was stirred slowly using a magnetic stirrer; the process was conducted at 4°C. Once all the solid ammonium sulphate was added, the solution was left stirring for 20 min before centrifugation at 9,300 xg for 20 min at 4°C. Afterwards, the ammonium sulphate precipitate was re-solubilised in 30 mL of anion exchange buffer A (*A. baylyi* untagged FtsZ purification anion exchange buffer in Section 2.1.2) and dialysed overnight with gentle stirring against 5 L of the same buffer to remove the ammonium sulphate in the sample. After dialysis, the sample was centrifuged at 9,300 xg for 20 min to remove any insoluble material and the supernatant was immediately applied to the anion exchange column HiTrap Q HP 5 mL (GE Healthcare) which is connected to the AKTA PURE system. The target protein was eluted from the column using elution buffer (*A. baylyi* untagged FtsZ purification

anion exchange buffer B in Section 2.1.2) in a gradient manner (10 column volumes with a flow rate of 2 mL/min). The eluent was collected as 2 mL fractions and fractions corresponding to the elution peak of the chromatogram (absorbance at 280, 254 and 215 nm were measured) were collected and analysed on a 10% SDS-PAGE gel. Fractions showing high purity of the desired protein were pooled and applied to the size exclusion column HiPrep 26/60 Sephacryl S300 HR (GE Healthcare) for further purification (*A. baylyi* untagged FtsZ purification gel filtration buffer in Section 2.1.2). The purification was conducted over 1 column volume with a flow rate of 0.3 mL/min. The eluent was collected as 10 mL fractions and fractions corresponding to peaks detected on the chromatogram (absorbance at 280, 254 and 215 nm were measured) were collected and analysed on 10% SDS-PAGE gel. Fractions containing the target protein (~42 kDa) were concentrated at 4°C to 10 mg/mL using the vivaspin column with a 10,000 Da MWCO (GE Healthcare) and stored at -80°C.

Overproduction and purification of the wild-type *B. subtilis* FtsZ¹²⁻³¹⁵ follows the protocol used for the full-length *A. baylyi* untagged FtsZ with slight modifications (refer to Section 2.2.2.6). Overproduction strain used was BL21-AI. Induction temperature used was at 10°C and the cells were left for 4 days. Lysis buffer used refer to *B. subtilis* 6xhis-FtsZ purification lysis buffer in Section 2.1.2. Ammonium sulphate precipitation was achieved by adding 0.35 g/mL of solid ammonium sulphate. Anion exchange buffer used was the same as the one used for purification of the A182E version of the protein. The size exclusion column used was the HiLoad 26/600 Superdex 75 pg and the sample was collected as 1 mL fraction. The size exclusion buffer used was 20 mM Tris, 100 mM NaCl pH 7.74. The column was run at 0.5 mL/min during the purification for 1 column volume.

Overproduction and purification of full-length *A. baylyi* C-terminus hexahistidine tagged FtsA followed the same protocol with slight changes. Changes are as follows. Overproduction strain used was BL21-AI. For cell lysis buffer refer to *A. baylyi* untagged FtsZ and FtsA-6xhis purification lysis buffer in Section 2.1.2. The insoluble material containing the insoluble protein inclusion bodies was recovered, resuspended in 50 mL inclusion bodies wash buffer (refer to *A. baylyi* FtsA-6xhis purification inclusion bodies wash buffer in Section 2.1.2) and kept stirring at 4°C for 45 min. The solution was then homogenised with a homogeniser (Heidolph DIAX 600; John Morris Scientific Pty. Ltd.), followed by centrifugation at 39,856 xg for 20 min to remove the supernatant. The inclusion bodies were washed for a further three times. The subsequent two washes used the wash buffer containing 1 M NaCl, while the final wash step used the initial inclusion bodies wash buffer. The pellet was resuspended in the smallest possible volume of wash buffer (about 500 µL to 1 mL) and afterward solubilised by resuspending them in 30 mL his trap wash buffer per 1 mL of inclusion bodies (refer to *A. baylyi* FtsA-6xhis purification his trap wash buffer in Section 2.1.2) and stirring at 4°C for 60 min. The solubilised protein was then applied to HisTrap HP 5 mL (GE Healthcare) and the protein was allowed to refold on-column by slowly changing the buffer on the column to the refolding buffer (refer to *A. baylyi* FtsA-6xhis purification refolding buffer in Section 2.1.2) in a linear gradient manner (10 column volumes with a flow rate 1 mL/min). The column was further washed with five column volumes of the refolding buffer and the protein was eluted with the elution buffer (refer to *A. baylyi* FtsA-6xhis purification his trap elution buffer in Section 2.1.2) in a stepwise elution. 2 mL fractions containing the target protein were combined and dialysed overnight against 1 L storage buffer (refer to *A. baylyi* FtsA-6xhis purification storage buffer in Section 2.1.2). After 16 hours, the sample was concentrated by placing the sample in a

3,500 MWCO dialysis tube (Thermo Scientific) and dialysing it against 800 mL of the concentrating buffer (refer to *A. baylyi* FtsA-6xhis purification concentrating buffer in Section 2.1.2). This method of concentrating is a slow process, but once the sample reached the desired concentration, it was again dialysed against the storage buffer to remove any PEG that might have diffused through during the concentration.

Overproduction and purification of *B. subtilis* FtsZ¹⁻³¹⁵ A182E followed a similar protocol with a number of changes and these are summarised here. Plasmid containing the protein construct was transformed into BL21 (DE3) and grown in M9 media in the presence of 50 µg/mL of Kanamycin. Induction was achieved through the addition of 0.5 mM IPTG at 10°C and the cells were left for 4 days. Cell lysis was carried out by incubation in lysis buffer (refer to *B. subtilis* 6xhis-FtsZ purification lysis buffer in Section 2.1.2) for 30 min, followed by 6 min of sonication using 30 sec bursts and 30 sec intervals on ice slurry. The soluble and insoluble materials were separated by centrifugation of lysate at 42,200 xg for 90 min. Following that, the supernatant was applied to the nickel affinity column HisTrap HP 5 mL (GE Healthcare) which was connected to the AKTA PURE system. The target protein was eluted from the column using the elution buffer (refer to *B. subtilis* 6xhis-FtsZ purification his trap buffer B in Section 2.1.2) in a gradient manner (10 column volumes with a flow rate of 2 mL/min). Fractions showing high purity of the desired protein were pooled together and diluted to 45 mL with buffer A (*B. subtilis* N-his FtsZ purification his trap and ion exchange buffer A in Section 2.1.2). 2 U/mL of Thrombin was subsequently added and incubated at 4°C overnight with gentle agitation to cleave off the hexa-histidine tag. The next day, 1 mL of Ni-NTA Agarose resin (Thermo Scientific) was added and the solution was further incubated for 30 min at 4°C with gentle agitation to remove the cleaved hexahistidine tags. The resin was separated from the protein solution by 1 min

centrifugation at 800 xg twice, with the soluble material transferred to a fresh tube between centrifugations. Solution containing the protein was purified further using anion exchange and refer to *B. subtilis* N-his FtsZ purification anion exchange buffer B in Section 2.1.2 for the buffer used. Final purification was achieved through size exclusion chromatography using HiPrep 26/60 Sephacryl S300 HR (GE Healthcare). The purification was conducted in 1 column volume with a flow rate of 0.3 mL/min and the eluent was collected as 10 mL fractions. Refer to *B. subtilis* N-his FtsZ purification size exclusion buffer in Section 2.1.2 for buffer used. The purification of the ^{15}N labelled version of the protein also follows this protocol, with the exception of using ^{15}N labelled ammonium chloride in the M9 salts.

Table 2.7: The molecular weight, pI and extinction coefficient of proteins used in this study.

Protein	Molecular Weight (Da)	pI	Extinction Coefficient ($\text{M}^{-1} \text{cm}^{-1}$)
Full-length <i>A. baylyi</i> untagged FtsZ	41,782.54	5.11	7,450
Full-length <i>A. baumannii</i> untagged FtsZ	41,997.55	4.85	7,575
Full-length <i>A. baylyi</i> FtsA-6xhis	45,612.2	5.50	37,150
<i>B. subtilis</i> FtsZ ¹⁻³¹⁵ A182E	33,211.8	4.55	2,980
Wild-type <i>B. subtilis</i> FtsZ ¹²⁻³¹⁵	31,379.92	4.68	2,980

2.2.3 Functional assays

2.2.3.1 GTPase assay using wild-type *B. subtilis* FtsZ¹²⁻³¹⁵

To determine the GTPase activity of the wild-type *B. subtilis* FtsZ¹²⁻³¹⁵, a standard curve was initially created as written in the instruction manual of Innova Biosciences GTPase assay kit (181). In short, this was carried out by setting up a triplicate of each known phosphate concentration in a 96-welled plate and measuring the absorbance at 650 nm. The absorbance values of the triplicates were averaged and then graphed against the phosphate concentrations to produce a linear curve (Figure 2.1).

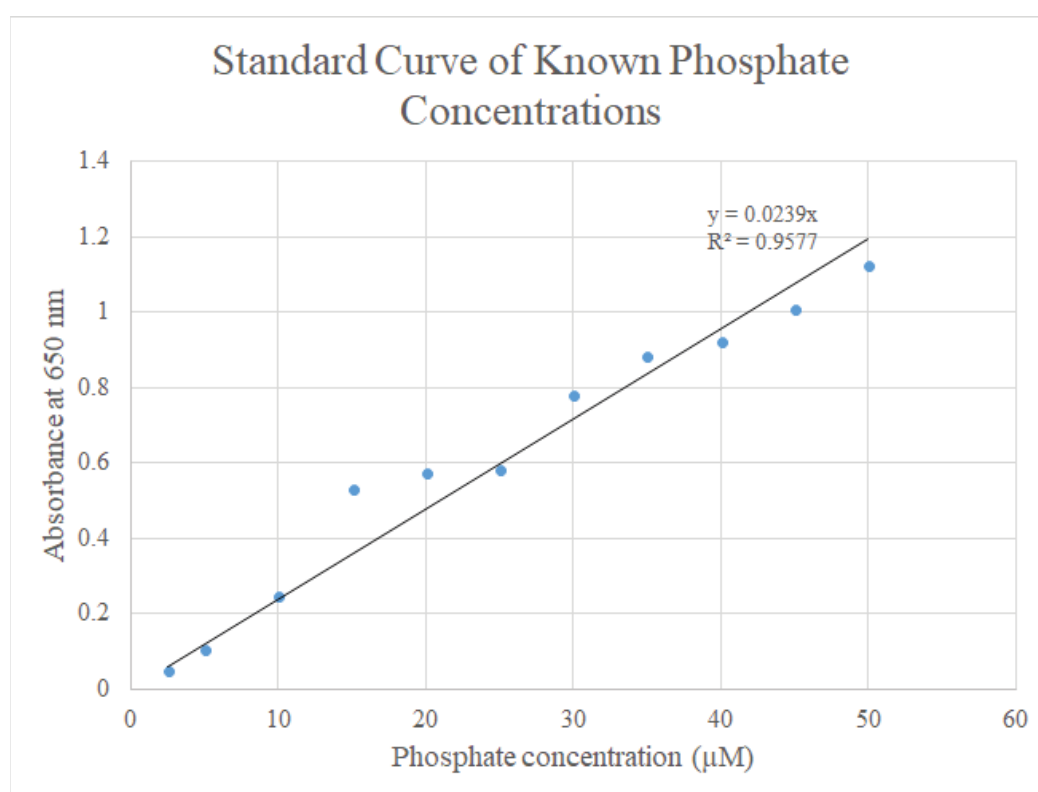


Figure 2.1: Standard curve of known phosphate concentration vs absorbance at 650 nm. This linear standard curve was used to calculate the released of free phosphate from three different concentrations of *B. subtilis* FtsZ¹²⁻³¹⁵.

To obtain the GTPase activity of the wild-type *B. subtilis* FtsZ¹²⁻³¹⁵, the protein concentration was adjusted to 2.7 μ M, 5.4 μ M and 10.8 μ M in 100 μ L buffer (20mM Tris, 100mM NaCl pH 7.74). Each protein concentration was then mixed with 100 μ L of substrate/buffer (SB) mix provided by the kit (50 mM Tris pH 7.5, 2.5 mM MgCl₂). Since the SB mix already contain 0.25 mM GTP as a part of its component, the samples were subsequently incubated at 37°C for 15 minutes. The reaction is stopped upon the addition of 50 μ L of PiColorLock™ mix. After 2 minutes, 20 μ L of the Stabiliser solution was added and each of the samples were mixed well by thoroughly pipetting up and down. Following that, the reactions were incubated for a further 30 minutes at 37°C for colour development and the absorbance were read at 650 nm. Triplicates were set up for each protein concentrations and the experiment were repeated three times.

The absorbance from each of the protein concentrations were averaged and the amount of phosphate released in the reaction was calculated by using the equation of the line from the standard curve ($y = 0.0239x$). Enzyme activity was calculated as *per* manufacturer's guideline using the equation; Activity (units/mL) = (AxC)/500B, where, A = concentration of free phosphate (Pi) in μ M, determined from the standard curve (22.1, 32.9 and 48.6 for 2.7 μ M, 5.4 μ M and 10.8 μ M, respectively); B = assay time is in minutes (15 minutes for this study); C = enzyme dilution factor (126, 63 and 32 for 2.7 μ M, 5.4 μ M and 10.8 μ M, respectively).

2.2.4 Nuclear Magnetic Resonance

2.2.4.1 Competition experiment using HSQC

Fragments needed for the HSQC competition experiments were bought from MolPort and the GDP from Sigma Aldrich. Prior to conducting the experiment, the fragments were made up to 50 mM in 100% dimethyl sulfoxide (DMSO). When conducting the experiment, each fragment was diluted to a final concentration of 1mM in 50 mM sodium phosphate, 200 mM sodium chloride pH 7.4, 10% D₂O and 100 µM 4,4-dimethyl-4-silapentane-1-sulfonic acid (DSS), along with 100 µM ¹⁵N-labelled *B. subtilis* FtsZ¹⁻³¹⁵ A182E. Control experiments of FtsZ with 1% DMSO and with GDP were prepared to account for any peaks shifting due to DMSO and GDP.

The competition experiment itself was conducted by firstly obtaining the spectra of FtsZ with fragment, followed by the spectra acquisition of FtsZ with fragment and GDP. After obtaining the four spectrum (FtsZ with 1% DMSO, FtsZ with GDP, FtsZ with fragment and FtsZ with fragment/GDP), each spectra was processed using the software TopSpin 3.5 (Bruker) (182). Once processed, the four spectrum for each fragment were then overlayed and analysed using the software Sparky (183). This process was repeated for all three fragments.

2.2.5 Crystallography

2.2.5.1 Setting up crystal trays

The wild-type *B. subtilis* FtsZ¹²⁻³¹⁵ were firstly purified as stated in Section 2.2.2.6. Initial screening was conducted using crystal screening kits purchased from Jena Bioscience: JBS Classic 1-10, JBS JCSG++ 1-4, JBS Membrane 1-4, JBS PACT++ 1-4 and JBS PEG Salt 1-4. Preparation of the crystal trays were carried out by firstly

pipetting 85 μL of the screening buffer provided by the kit into a 96-welled MRC plate, followed by the dispensing of the protein with the buffer into the crystal well (Figure 2.2). Protein dispensing was carried out using the programmable robot FORMULATRIX[®] and the drop size was set to 200 nL, containing 100 nL of protein and 100 nL of buffer. Protein concentration during screening was set to 10 mg/mL and 5 mg/mL. Once set, the crystal trays were incubated at room temperature (25°C) and checked on day 1, 3, 5, 7 and then at day 14. Crystals with sharp edges usually formed by day 7 and conditions which formed such crystals were pursued further by setting a gradient tray, whereby the parameters of the initial conditions are halved and doubled, to provide a gradient.

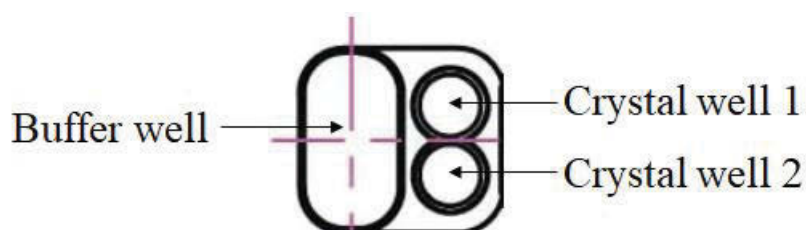


Figure 2.2: An example of a well set up in the 96-welled MRC plate for crystallography. Crystallization buffer are aliquoted into the buffer well (75 to 85 μL) and the protein is dispensed and mixed with the buffer in a 1:1 ratio in either crystal well 1 or crystal well 2. The drop size of the protein/buffer mix is typically 200 or 400 nL.

2.2.6 Molecular modelling

2.2.6.1 Creating a protein homology model of *Staphylococcus aureus* FtsZ and *Acinetobacter* FtsA

Amino acid sequence of *S. aureus* FtsZ and *Acinetobacter* FtsA were downloaded from National Center for Biotechnology Information (NCBI) and these sequences are termed the query sequence. The query sequence was then BLAST-searched against protein X-

ray crystal structure database using Discovery Studio 4.5 (DS 4.5). Protein X-ray structures identified by BLAST which have an E-value $< 1 \times 10^{-5}$ were chosen for use as the template for creating homology models. The amino acid sequence of these structures is termed the template sequence and the crystal structure itself is termed the template structure. The query sequence was then aligned to the template sequence in DS 4.5 by using the **Align Sequence to Templates**. The templates with E-value $< 1 \times 10^{-5}$ were selected in the **Input Template Structures** parameter and the query sequence was selected in the **Input Model Sequence** parameter. This was followed by the creation of the homology models based on amino acid sequence alignment by going using **Build Homology Models**. Again, the templates with E-value $< 1 \times 10^{-5}$ were selected in the **Input Template Structures** parameter and the query sequence was selected in the **Input Model Sequence** parameter. **Number of Models** parameter was set to 5 to create five homology models.

2.2.6.2 Assessing the validity of the homology models

The validity of the five newly-created homology models were assessed by using **Verify Protein (Profiles-3D)**. The five homology models were selected in the **Input Protein Molecules** parameter. The result of the process produced scores termed *Verify Expected High Score*, *Verify Expected Low Score* and *Verify Score*. In general, if the *Verify Score* result of the model protein is higher than the *Verify Expected Low Score* value, then the model is of acceptable quality. The closer the *Verify Score* result is to the *Verify Expected High Score* value, the better the quality of the model. The process also colour code the homology protein structures into red, white and blue. Regions colored blue signifies high-quality prediction, while red signifies low-quality prediction and white signifies a medium-quality prediction.

2.2.6.3 Protein-protein interaction using docking

The interaction of the *Acinetobacter* spp. FtsA protein and FtsZ peptide was firstly analysed using ZDOCK in DS 4.5. The ZDOCK protocol is usually used to perform rigid body docking of two proteins (184, 185). This was access by using **Dock Proteins (ZDOCK)**. The FtsA homology model was set as the receptor protein, while the FtsZ peptide was set as the ligand protein. The **Angular Step Size** was set to 6 degrees. The software provides two values for the **Angular Step Size**; 6 and 15 degrees. 6 degrees was chosen as it performs finer conformational sampling and thus typically results in more accurate predictions. However, 15 degrees can also be selected for a faster analysis, but the result will not be as accurate. The **RMSD Cutoff** and **Interface Cutoff** values were set at 6.0 Å and 9.0 Å, respectively. The **Maximum Number of Clusters** was set to 60.

Since there is a published co-crystal structure of *T. maritima* FtsA binding to the C-terminus peptide of *T. maritima*, the amino acid residues responsible for the interaction can be selected in the **Receptor Binding Site Residues** parameter and the other amino acid residues selected in the **Receptor Blocked Residues**. Similarly, amino acid residues of the FtsZ peptide known to be involved in the interaction were selected in the **Ligand Binding Site Residues** parameter, while residues that are not involved in the interaction were selected in the **Ligand Blocked Residues**. This blocking and filtering option allow the software to perform gating processes instead of making the software dock the FtsZ peptide all over the FtsA protein.

Following the ZDOCK run, the software will group the docked poses as clusters. The screening process involves viewing the docked poses in these clusters. Clusters with poses observed to be similar to the co-crystal structure of the *T. maritima* FtsZ peptide with FtsA were then taken forward and refined further using the RDOCK protocol (186).

Again, FtsA was set in the **Input Receptor Protein** parameter and the FtsZ peptide was set in the **Input Ligand Protein** parameter. Clusters with poses similar to the co-crystal structure were set in the **Input Poses** parameter. The RDOCK run produced values for the selected poses termed the E-RDOCK, which are used to determine the likelihood of the prediction to be near the native docking conformation *in vivo*.

2.2.6.4 Superimposition of multiple crystal structures

Crystal structures of human α - and β -tubulin, along with the GDP-bound FtsZ structures of *Staphylococcus aureus* (PDB: 3VOA and 3VO8 (93)), *Staphylococcus epidermidis* (PDB: 4M8I (187)), *Mycobacterium tuberculosis* (PDB: 1RQ7 (188) and 4KWE (189)), *Bacillus subtilis* (PDB: 2RHL (190)), *Pseudomonas aeruginosa* (PDB: 2VAW (191)) and *Aquifex aeolicus* (PDB: 2R6R (191)) were obtained from the Protein Data Bank (PDB) (192). These structures were chosen based on the following criteria: (1) their structure was solved using X-ray crystallography with good resolution (2 - 3 Å); (2) they contain GDP but no inhibitor; and (3) they are the wild-type version of the protein from either Gram-positive or Gram-negative bacterial species. The structures were loaded into DS 4.5. Initially, the crystal structures of the human tubulin and some FtsZ proteins included multiple chains, however, only chain A of each protein was used for the alignment in this analysis. The protein structures were then loaded into the same Molecule Window. The amino acid sequences were opened and aligned within the DS software. Sequence alignment in DS 4.5 uses the Align123 algorithm, a progressive pairwise alignment algorithm modified from the CLUSTAL W program (193).

The protein structures were superimposed based on the sequence alignment. The reference protein used for the superimposition was the GDP-bound *S. epidermidis* FtsZ

structure as it is a high-resolution structure with a resolution of 1.43 Å (PDB: 4M8I (187)). The root-mean-square deviation (RMSD) values of the C α atoms were obtained after superimposition.

2.2.6.5 Identification of Accessible Binding Spheres

Prior to identifying accessible binding spheres on the protein structures, the protein structures were prepared using the **Prepare Protein** function in DS 4.5. The **Prepare Protein** function is an optimisation step which corrects structural, atomic and bond length anomalies. Following protein preparation, using the “eraser” algorithm (194), accessible binding spheres were identified and the radius of the spheres was calculated by DS 4.5.

2.2.6.6 Molecular Dynamics Simulations

Before conducting molecular dynamics (MD) simulations, the structures were corrected using the Prepare Protein function in DS 4.5. The CHARMM forcefield version 40.1 (195, 196) was chosen and water molecules were added. The solvation model used was the Explicit Periodic Boundary (197, 198) in an orthorhombic cell filled with water molecules. Neutralization was achieved by the addition of Na⁺ and Cl⁻ ions.

Once the solvent environment was set, 500 ps of isothermal-isobaric ensemble (NPT) molecular dynamics simulation was conducted using a Standard Dynamic Cascade in DS 4.5. The initial system was minimised by 1000 steps of Steepest Descent, followed by 2000 steps of Adopted Basis Newton-Raphson. After the minimisation, the system was heated from 50 to 300 K over 10 ps and then equilibrated for 100 ps. Finally, a 500 ps molecular dynamics simulation was performed under a constant temperature of 300

K. Trajectory snapshots were taken every 50 ps during the production step. In all the simulations, the SHAKE constraint, which fixes all bonds involving hydrogens, was applied by default by DS 4.5 and the reference pressure was kept constant at 1.0 atmospheric pressure.

Chapter 3 - Understanding the interaction of *Acinetobacter* FtsZ and FtsA using *in silico* methods

3.1 Introduction

In the past, bacterial infections were once easily controlled *via* the use of antibiotics. However, the increase in antibiotic resistant bacteria is threatening human health, especially in hospitals (199-203). The most concerning issue is the emergence of multidrug resistant (MDR) strains, as they are un-treatable with currently available antibiotics. Over the last decade, multidrug resistant Gram-negative bacteria, including MDR-*Pseudomonas aeruginosa*, MDR-*Acinetobacter baumannii* and *Enterobacteriaceae* producing extended-spectrum β -lactamases (ESBL) and carbapenemases, have been associated with hospital-acquired infections and the numbers of infections caused by these pathogens are steadily rising (204). This is largely because they have an outer-membrane which acts as a permeable barrier to antibiotics, β -lactamases that inactivate β -lactams and multiple drug efflux systems that pumps antibiotics out of the cells faster than they can act on their target (205, 206). Added to this is the ability of bacteria to transfer genes coding for these resistance to susceptible bacterial populations through plasmid and lateral gene transfer (29).

Acinetobacter spp. are nonmotile γ -proteobacteria (79), that have now become one of the new emerging Gram-negative pathogens that cause hospital-acquired infections such as, pneumonia, wound and urinary tract infections, post-surgery complications and blood stream infections in severely ill and immuno-compromised people (207, 208). The most clinically relevant species is *A. baumannii*, although pathogenic strains of *Acinetobacter lwoffii* and *Acinetobacter baylyi* have also been reported (209-211). Of greatest concern is the rapid emergence of recently reported multidrug resistant strains

of *A. baumannii* (212), which are resistant to all currently available antimicrobials, including recently approved ones such as tigecycline (79). This has resulted in the World Health Organisation putting this organism in the priority 1: critical category in their priority pathogen list (213). Thus, there is an urgent need for the development and production of new classes of antimicrobials that target essential processes in this pathogen.

Cell division is an essential process in bacteria that could be targeted to generate a new class of antibiotics. The process involves many protein-protein interactions to form the divisome, and carry out its function (67). The inhibition of these interactions will no doubt be detrimental to the cell since the division proteins are known to be essential and that their roles appear to be structural (stabilizing the divisome), rather than enzymatic, therefore, targeting the interacting sites is likely to be highly effective (68). This approach will also arguably, have a lower rate of resistance since the cell will need to accommodate and balance the change in amino acids between multiple proteins to maintain its interactions. Two of the most highly conserved bacterial cell division proteins, FtsZ and FtsA, have been recognised as promising drug targets in *Acinetobacter* spp. and other bacteria (65). FtsZ is an essential protein in bacteria, while FtsA is essential in most bacteria but not all species, for example *B. subtilis* (214-216). Studies in *E. coli* have shown that FtsA is essential (67) and a mutant library of *A. baylyi* also suggests that FtsA is essential in this organism (217).

3.1.1 Interaction between FtsZ and FtsA

The interaction between FtsZ and FtsA has been known for over a decade (114). Studies involving yeast two-hybrid assays (115, 116) and systematic deletion mutagenesis analysis (116, 117) in several organisms has shown that FtsZ interacts with FtsA *via* conserved amino acid residues within the very extreme C-terminus of FtsZ (last 70 amino acids in the *E. coli* protein) (218). The mechanism of interaction between this FtsZ peptide and FtsA was discovered by Szwedziak *et al* (110) using proteins from *T. maritima*. They showed that the FtsZ C-terminal peptide of *T. maritima* (amino acid 337 – 351) interacts with FtsA by binding to helices H6 and H8 in the FtsA 2B domain while facing away from the nucleotide-binding domain of FtsA (Figure 3.1). Several salt bridges involved in the interaction of the C-terminal peptide of FtsZ with helix H8 of the 2B domain of FtsA were also identified; FtsA (Arg301) to FtsZ (Asp338), FtsA (Glu304) to FtsZ (Arg344) and FtsA (Lys293) to FtsZ (Leu351) (Figure 3.1).

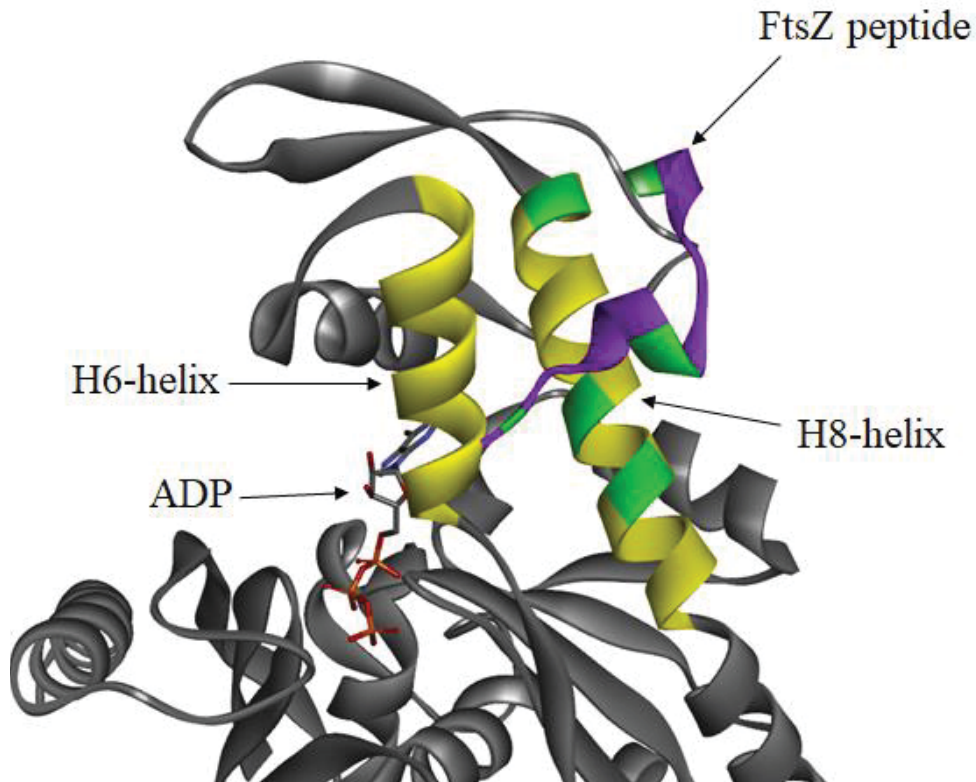


Figure 3.1: Crystal structure of FtsA from *T. maritima* bound to FtsZ C-terminal peptide. Protein Data Bank entry 4A2A (110). The FtsA 2B domain is highlighted in yellow with helix H6 and H8 at the front (arrow showing the position of H6 and H8) and FtsZ C-terminal peptide is highlighted in purple. The other parts of FtsA are in gray. Salt bridges are highlighted in green on H8 of the 2B domain of FtsA and the FtsZ C-terminal peptide (last 8-16 residues). Amino acid residues identified to form salt bridges were: FtsA (Arg301) to FtsZ (Asp338), FtsA (Glu304) to FtsZ (Arg344) and FtsA (Lys293) to FtsZ (Leu351). The ADP is located on the other side of the structure and is shown in stick form. The image was generated using Discover Studio 4.5 (219).

In *E. coli* and other γ -proteobacteria, the amino-acid sequence of the C-terminal peptide of FtsZ that interacts with FtsA is DIPAF LRKQ (79). This sequence is well conserved in most other γ -proteobacteria as shown in Figure 3.2. In *E. coli*, the aspartate and proline at position 1 and 3 of this peptide, respectively, are found to be the most important residues for interaction with FtsA and ZipA (Figure 3.2) (220). Alteration at these two positions in *E. coli* FtsZ results in a disruption of the FtsZ/ZipA interaction (218), and a change of the proline alone led to reduced binding of FtsA to FtsZ (114). Further evidence which suggests that interaction of FtsZ with other proteins requires

these two amino acids was shown in the co-crystallization of FtsZ C-terminal peptide with FtsA in *T. maritima* (110). Currently, it is yet to be understood whether *Acinetobacter* FtsZ contains the conserved C-terminal peptide and if the FtsZ in this organism interact with FtsA.

Early *Acinetobacter* FtsZ and FtsA interaction study was conducted by a member of the Harry laboratory, Dr Amy Bottomley, using the bacterial two-hybrid system. However, she found that the proteins were non-functional when tagged with the reporter protein for the assay. Therefore, it was decided that the interaction study be conducted using both computational and also *in vitro* approaches. The aim of this chapter is to identify the peptide sequence of *Acinetobacter* FtsZ by conducting amino acid sequence alignment analysis using Clustal Omega (221, 222). This will be followed by predicting the interaction between FtsZ and FtsA in *Acinetobacter* using an *in silico* method known as “dock proteins” (184, 185, 223), which is a module in the molecular modelling software Discovery Studio 4.5 (DS 4.5). Understanding this could potentially be used to develop new narrow-spectrum antimicrobials to specifically treat *Acinetobacter* infections, which is a big problem in hospital settings because of its ability to resist all of the currently available antimicrobials.

3.2 Results: *In silico* investigation of the interaction between FtsZ and FtsA in *Acinetobacter*

3.2.1 Analysis of full-length FtsZ amino acid sequence alignment to identify the conserved C-terminal peptide in *Acinetobacter* FtsZ

Identification of the peptide sequence in *Acinetobacter* FtsZ was initially conducted through the analysis of amino acid sequence alignment using Clustal Omega (221, 222) of full-length FtsZ from a variety of organisms. The alignment revealed two possible locations for the FtsZ conserved C-terminal peptide in *Acinetobacter* (Figure 3.2). One possibility is at the very end of the C-terminus with the sequence SIQDYLNQQRK and the other located upstream with the sequence DVPAINKRQNAE. From this point onwards, peptide with the sequence DVPAINKRQNAE and SIQDYLNQQRK will be referred to as peptide 1 and peptide 2, respectively. The possibility of these two being the conserved C-terminus peptide is intriguing. Peptide 1 contains the conserved amino acid residues which are important for the interaction of FtsZ with its protein partners, FtsA and ZipA, but this makes the linker length very short for a bacterial species in the γ -proteobacteria class, which usually have linkers from 52 to 81 amino acids in length (125). Contrarily, amino acid changes are expected with peptide 2 but, the linker is of the expected length for a bacterial species in the γ -proteobacteria class. This is discussed further below.

Peptide 1	<i>Acinetobacter baumannii</i>	---DVPAINKRQNAENDVNNAPSSTPRSSPMSIQDYLNQQRK	391
	<i>Escherichia coli</i>	PDYLDIPAFLRKQAD-----	383
	<i>Salmonella typhi</i>	PDYLDIPAFLRKQAD-----	383
	<i>Shigella flexneri</i>	PDYLDIPAFLRKQAD-----	383
	<i>Yersinia pestis</i>	PDYLDIPAFLRKQAD-----	383
	<i>Vibrio cholerae</i>	SGYLDIPAFLRKQAD-----	398
	<i>Pseudomonas aeruginosa</i>	LDYLDIPAFLRKQAD-----	394
	<i>Neisseria meningitidis</i>	LDDFEIPAILRRQHNSDK-----	392
	<i>Rickettsia typhi</i>	SDIHDIPAFLRKKRD-----	452
	<i>Bacillus anthracis</i>	SDDIDIPAFLRNRRRR-----	386
	<i>Bacillus subtilis</i>	DDTLDIPTFLNRNKRK-----	382
	<i>Clostridia botulinum</i>	ENDLEIPAFLRKQK-----	369
	<i>Leptospira interrogans</i>	VEDYDIPAYLRNNSGP-----	400
	<i>Helicobacter pylori</i>	EEELSIPTTIRIQD-----	385
	<i>Staphylococcus aureus</i>	TKEDDIPSFIRNREERSRTR-----	390
	<i>Listeria monocytogenes</i>	SSDVDVPAFIRNRRRG-----	391
	<i>Mycobacterium tuberculosis</i>	DDDVDVPPFMR-----	379
	<i>Streptococcus pneumoniae</i>	EDELDTPPFFKNR-----	419
	<i>Campylobacter jejuni</i>	MAQIETPTFLRRQMD-----	370
	<i>Thermotoga maritima</i>	---DIPAIYRYGLEGL-----	351
Peptide 2	<i>Acinetobacter baumannii</i>	SSPMSIQDYLNQQRK--	391
	<i>Escherichia coli</i>	PDYLDIPAFLRKQAD--	383
	<i>Salmonella typhi</i>	PDYLDIPAFLRKQAD--	383
	<i>Shigella flexneri</i>	PDYLDIPAFLRKQAD--	383
	<i>Yersinia pestis</i>	PDYLDIPAFLRKQAD--	383
	<i>Vibrio cholerae</i>	SGYLDIPAFLRKQAD--	398
	<i>Pseudomonas aeruginosa</i>	LDYLDIPAFLRKQAD--	394
	<i>Neisseria meningitidis</i>	LDDFEIPAILRRQHNSD	391
	<i>Rickettsia typhi</i>	SDIHDIPAFLRKKRD--	452
	<i>Bacillus anthracis</i>	SDDIDIPAFLRNRRRR--	386
	<i>Bacillus subtilis</i>	DDTLDIPTFLNRNKRK	382
	<i>Clostridia botulinum</i>	ENDLEIPAFLRKQK--	369
	<i>Leptospira interrogans</i>	VEDYDIPAYLRNNSGP	400
	<i>Helicobacter pylori</i>	EEELSIPTTIRIQD--	385
	<i>Staphylococcus aureus</i>	TKEDDIPSFIRNREER	384
	<i>Listeria monocytogenes</i>	SSDVDVPAFIRNRRRG	391
	<i>Mycobacterium tuberculosis</i>	DDDVDVPPFMR-----	379
	<i>Streptococcus pneumoniae</i>	EDELDTPPFFKNR-----	419
	<i>Campylobacter jejuni</i>	MAQIETPTFLRRQMD--	370
	<i>Thermotoga maritima</i>	---DIPAIYRYGLEGL	350

Figure 3.2: Full-length FtsZ amino acid sequence alignment using Clustal Omega. Full-length FtsZ amino acid sequence alignment from a range of bacteria with only the C-terminal sequence shown in the figure. The most important residues in *E. coli* have been determined to be at position 1 (aspartate, D) and 3 (proline, P); boxed in red. Additionally co-crystal structure of *T. maritima* FtsZ peptide with FtsA identified the arginine at position 7 to also be a player between the interactions of the two proteins; boxed in red. Peptide 1 of *A. baumannii* contain the conserved aspartate and proline, while the arginine is changed to a lysine. Peptide 2 shows the aspartate and proline changed to serine (S) and glutamine (Q), respectively. The arginine has also been changed to a lysine in peptide 2.

Amino acid sequence alignment with peptide 1 was observed to align the essentially-conserved aspartate and proline (Figure 3.2). Added to that, based on the co-crystal structure of *T. maritima* FtsZ peptide and FtsA, the arginine is also important for the interaction of the FtsZ peptide to FtsA in this organism through the formation of a salt-

bridge and the amino acid sequence alignment shows that this arginine is conserved in many bacterial species. In *Acinetobacter*, this arginine is changed to a lysine, which is an amino acid that is similar in nature to arginine. Having peptide 1 as the conserved peptide would suggest that FtsZ and FtsA do interact in *Acinetobacter* and possibly utilize a very similar, if not, the same mechanism of interaction that has been reported in literature.

Amino acid sequence alignment with peptide 2, on the other hand, suggests the aspartate and proline be changed to a serine and glutamine, respectively, while the arginine is changed to a lysine (Figure 3.2). Having peptide 2 as the conserved peptide raises the possibility of a different mode of interaction between FtsZ and its binding partners, ZipA and FtsA, in this organism (79). This finding could reflect a difference in affinity and/or the interacting surfaces between FtsZ and its binding partners, FtsA and ZipA, in *A. baumannii* compared to other bacteria. However, there is also a possibility that, unlike in other bacteria, the C-terminal end of FtsZ is not required for an FtsZ and FtsA interaction in *Acinetobacter*. It is also possible that FtsZ and FtsA do not interact at all in *Acinetobacter*. Although this latter possibility is rather unlikely, it is certainly worth examining.

Further sequence analysis was conducted to understand the effect of the peptide location on the linker length of the *Acinetobacter* FtsZ (Figure 3.3). Having peptide 1 and 2 in their respective places sets the linker of the *Acinetobacter* FtsZ at 24 and 52 amino acids in length, respectively (Figure 3.3). Although peptide 1 contains the conserved amino acid residues which are important for the interaction of FtsZ with its protein partners, FtsA and ZipA, the linker length is very short for a bacterial species in the γ -proteobacteria class, which usually have linkers from 52 to 81 amino acids in length (125). Contrarily, amino acid changes are expected with peptide 2 but, the linker is of

the expected length for a bacterial species in the γ -proteobacteria class. In order to predict which of the two peptides is the probable *Acinetobacter* FtsZ peptide it was decided that an *in silico* method be used.

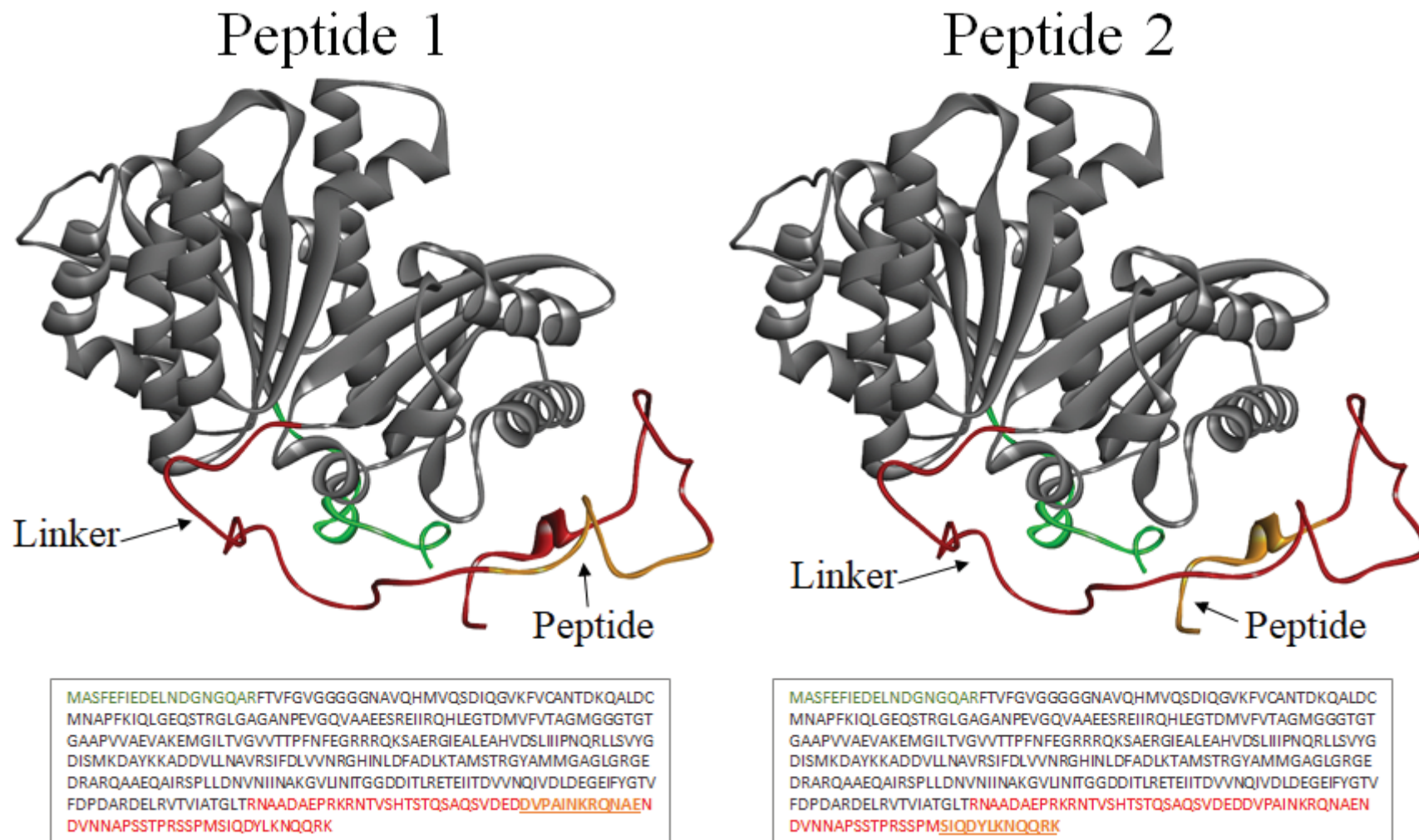


Figure 3.3: Peptide location affects linker length. Having peptide 1 as the binding region sets the linker region at 24 amino acids in length. Meanwhile, with peptide 2 as the binding region sets the linker region at 52 amino acids in length.

3.2.2 Accuracy validation of the 3D modelling program through the re-construction of the published *Staphylococcus aureus* FtsZ structure

The interaction of *Acinetobacter* FtsZ and FtsA was initially investigated *in silico* using the software DS 4.5. This software is state-of-the-art and has been used extensively in different scientific fields; including immunology (224), cancer (225), drug discovery (226) and interaction studies (227). One of the modules in the software called “dock proteins” (184, 185, 223) was used as it allows for the *in silico* investigation of protein-protein interactions using available X-ray crystal structures of interacting proteins, in this study, FtsZ and FtsA.

Currently, there is only one available X-ray crystal structure that illustrates the interaction of the FtsZ peptide with FtsA and this is from *T. maritima* (110). Since there are no available *Acinetobacter* FtsA structures, a homology model needed to be made. However, prior to that, as a personal learning process and to test the accuracy of the software, the ability of DS 4.5 to create homology models was validated by making *S. aureus* FtsZ homology models and comparing that to the *S. aureus* FtsZ X-ray crystal structure with a resolution of 1.73 Å (PDB: 3VOA (93)). This structure was chosen as a model due to its high-resolution. The full-length FtsZ amino acid sequence of the *S. aureus* Mu50 strain was downloaded from NCBI and then used as the sequence of interest, termed the query sequence. A BLAST search was conducted with the DS 4.5 software and ten FtsZ crystal structures from a variety of organisms were identified. The amino acid sequence of these crystal structures, termed the template sequence, was aligned with the query sequence using the sequence alignment modules in DS 4.5. The alignment of the query sequence to the template sequence was to ensure that the secondary structure predicted for the query sequence is as close as possible to that of the template sequence secondary structure. From this, homology models were created.

There are theoretically infinite numbers of homology models able to be created, the limiting factor being the processing power available. In this case, ten homology models were created.

The first initial screen to determine the quality of the five homology models was to investigate the **Probability Density Function (PDF)** total energy and the **Discrete Optimized Protein Energy (DOPE)** score (228). The PDF total energy equates to the probable total amount of energy required for the protein to adopt the predicted structure. While the DOPE Score signifies the statistical score created by the software through the calculation of atomic spatial restraints set up by DS 4.5. The general rule is that the lower the PDF Total Energy is, the better the quality of the created homology model. When the PDF Total Energy scores between the created models are similar, the DOPE score is used to gauge the quality of the model. Similarly, the lower the DOPE score, the better the quality of the created homology model. The PDF Total Energy and DOPE score of the ten homology models were comparable, with values ranging from 17,420 to 18,292 and -37,782 to -37,734, respectively. There is no simple interpretation of the absolute value of the energy because parts of a model (for example residues adjacent to an insertion or deletion) are almost certain to have higher restraint violations (229). The energies are useful in making comparisons between different homology models of the same protein. Both the PDF Total Energy and DOPE score are calculated using mathematical equations based on the likelihood for a random variable to occur at a given point; in other words, the relative stability a given amino acid adopts a certain conformation with respect to other conformations of the same amino acid in the same protein. These values are a measure of a comparison of homology models of a single protein, and different values will be generated with different proteins.

The ten homology models were then further validated for their quality through a homology model quality assessment function in DS 4.5. The analysis generates values termed Verify Score, Verify Expected High Score and Verify Expected Low Score. The values generated focus on the likelihood of each residue in the protein being found in its specific local environment. A Verify Score higher than or close to the Verify Expected High Score indicates that the quality of the model is good. The Verify Scores of the ten *S. aureus* FtsZ models are higher than the Verify Expected High Scores, signifying all ten homology models are of high quality (Table 3.1).

The last validation to check the accuracy of the software was to superimpose *S. aureus* FtsZ homology model with the published *S. aureus* FtsZ X-ray crystal structure (PDB: 3VOA). Since all of the created homology models are of high quality, one model (Model 1) was chosen to be used in the superimposition. The superimposition gave a C α atom RMSD value of 2.97 Å (Figure 3.4). This indicates that the homology model is similar to the X-ray structure and that the software can produce homology models fairly accurately.

Table 3.1: *S. aureus* FtsZ homology model analysis.

Model	PDF Total Energy	DOPE Score	Verify Score*	Verify Expected High Score*	Verify Expected Low Score*
1	17,420.90	-37,782.10	173.38	153.03	68.86
2	17,485.60	-37,821.10	176.18	153.03	68.86
3	17,493.10	-37,818.00	180.88	153.03	68.86
4	17,717.30	-37,740.80	173.82	153.03	68.86
5	17,748.60	-37,720.50	169.91	153.03	68.86
6	17,896.40	-37,536.20	168.21	153.03	68.86
7	18,007.10	-37,408.30	168.32	153.03	68.86
8	18,014.20	-37,497.80	181.93	153.03	68.86
9	18,051.80	-37,826.90	176.86	153.03	68.86
10	18,292.60	-37,734.10	176.11	153.03	68.86

* The “Verify Expected High Score” and “Verify Expected Low Score” is a gauging meter for the quality of homology models created. The “Verify Score” can be in between the “Verify Expected High Score” and “Verify Expected Low Score”; indicating medium quality models. The “Verify Score” above the “Verify Expected High Score” indicate high quality models.

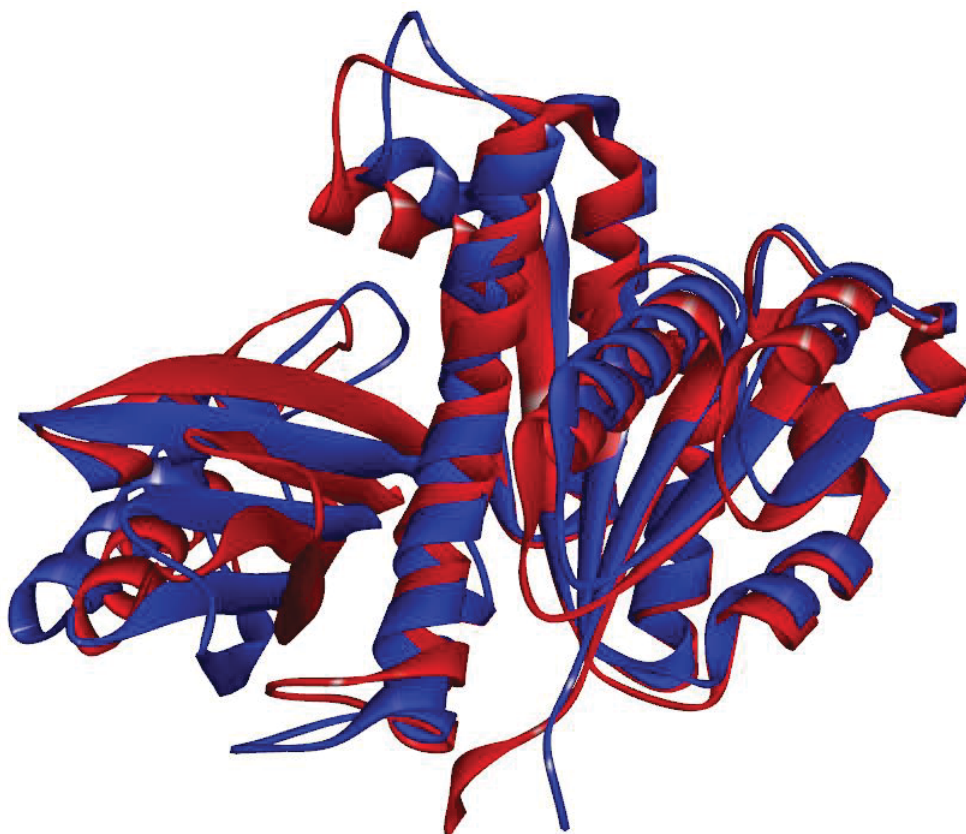


Figure 3.4: Superimposition of *S. aureus* FtsZ homology model to that of the *S. aureus* FtsZ X-ray crystal structure using Discovery Studio 4.5. The *S. aureus* FtsZ X-ray crystal structure was used as the reference protein (PDB: 3VOA). Superimposing the homology model to the crystal structure gave a C α atom root mean square deviation (RMSD) value of 2.97 Å, indicating similarity. The homology model is coloured red and the X-ray crystal structure coloured blue.

3.2.3 *In silico* reconstruction of *Acinetobacter* spp. FtsA tertiary structure

Creating the homology models of the *Acinetobacter* FtsA adhered to the workflow outlined in Figure 3.5 (refer to Chapter 2 Section 2.2.3). The FtsA amino acid sequence from *A. baylyi* ADP1 and *A. baumannii* ATCC19606 was BLAST searched to yield one hit and used as a template. This is because there is only one published FtsA crystal structure from *T. maritima* and therefore, the *Acinetobacter* FtsA homology models created will have certain bias towards the *T. maritima* FtsA structure. From this, five homology models were created for both *A. baylyi* and *A. baumannii* FtsA.

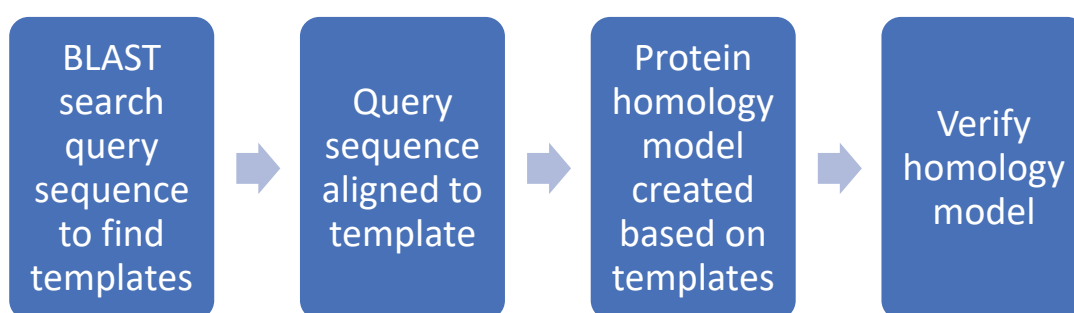


Figure 3.5: Homology modeling workflow in Discovery Studio 4.5. A typical workflow for creating homology models of the desired protein starts with obtaining the amino acid sequence of the protein of interest (termed query sequence) and then BLAST searching the query sequence against protein structure databases. This will identify proteins X-ray crystal structures (template) that have similar amino acid sequence to the query sequence. The query sequence is then aligned to the amino acid sequence of the identified-protein crystal structures (template) and homology models are created based on that alignment. The last step of building a homology model usually involves the verification of the created models. In the case of this study, the query sequence was the *A. baumannii/baylyi* FtsA sequence.

PDF Total Energy of the FtsA model from both *A. baylyi* and *A. baumannii* were alike with values around 2,000 and 2,500, respectively. Similarly, the DOPE score of the *A. baylyi* and *A. baumannii* FtsA models were comparable with values around -39,000 and -40,000, respectively. The RMSD value of the models was calculated to be around 3 Å, which is equivalent to that of medium quality X-ray crystal structures. Usually, X-ray crystal structures with a RMSD, also known as its resolution, at 3 Å is most likely to have the correct folding of its tertiary structure (230, 231). However, with this value, there is a high possibility that some amino acids, such as lysine, glutamate and valine are in the wrong orientation (230, 231). However, one model from both *A. baylyi* and *A. baumannii* had calculated RMSD values of 0.84 Å and 0.83 Å, respectively (Table 3.2). These values indicate that the placement of the atoms in the model is very close to the reference protein *T. maritima* FtsA.

Further validation of the quality of the models was conducted through generation of the Verify Score; Verify Expected High Score and Verify Expected Low Score. The Verify Score of all five FtsA models for both *A. baylyi* and *A. baumannii* are in between the Verify Expected High Score and Verify Expected Low Score range (Table 3.2). This signifies that the created models are of medium quality where some of the amino acids are possibly not oriented correctly. The quality of the model can be further visualized by using a 3D-Profile Verification function within DS 4.5. This function divides the protein into three colours; blue, white and red. The blue colour signifies high-quality prediction, while red signifies low-quality prediction and white signifies a medium-quality prediction. Using this function, the FtsA model showed majority of the protein coloured in red (Figure 3.6). Regardless of many parts of the whole protein having a low predicted quality, the region of interest, the 2B domain, of which is currently known to be the responsible site for FtsZ binding, is of reasonable quality for use in further

studies (circled in green in Figure 3.6). Therefore, the 2B domain section of the model will be used in the *in silico* interaction study with the FtsZ peptide. Based on the lowest PDF Total Energy, lowest DOPE Score, and good Verify Score, the FtsA 2B domain from model 5 was selected for use in the *in silico* interaction study of both *A. baylyi* and *A. baumannii*.

Table 3.2: *Acinetobacter* spp. FtsA homology model analysis.

Organism	Model Name	PDF Total Energy	DOPE Score	Verify Score	Verify Expected High Score	Verify Expected Low Score
<i>A. baumannii</i>	1	2,746.40	-40,936.20	148.97	189.79	85.40
	2	2,798.56	-40,755.30	140.18	189.79	85.40
	3	2,641.85	-40,838.10	140.74	189.79	85.40
	4	2,315.03	-41,402.80	144.30	189.79	85.40
	5	2,314.00	-41,365.50	146.75	189.79	85.40
<i>A. baylyi</i>	1	2,295.00	-39,322.50	136.06	183.35	82.50
	2	1,901.86	-39,585.60	129.00	183.35	82.50
	3	2,016.22	-40,201.40	141.93	183.35	82.50
	4	2,307.89	-39,641.10	134.87	183.35	82.50
	5	1,893.21	-39,879.90	137.30	183.35	82.50

Coloured boxes are determined to be the best homology model based on the lowest PDF Total Energy, lowest DOPE Score and a high Verify Score.

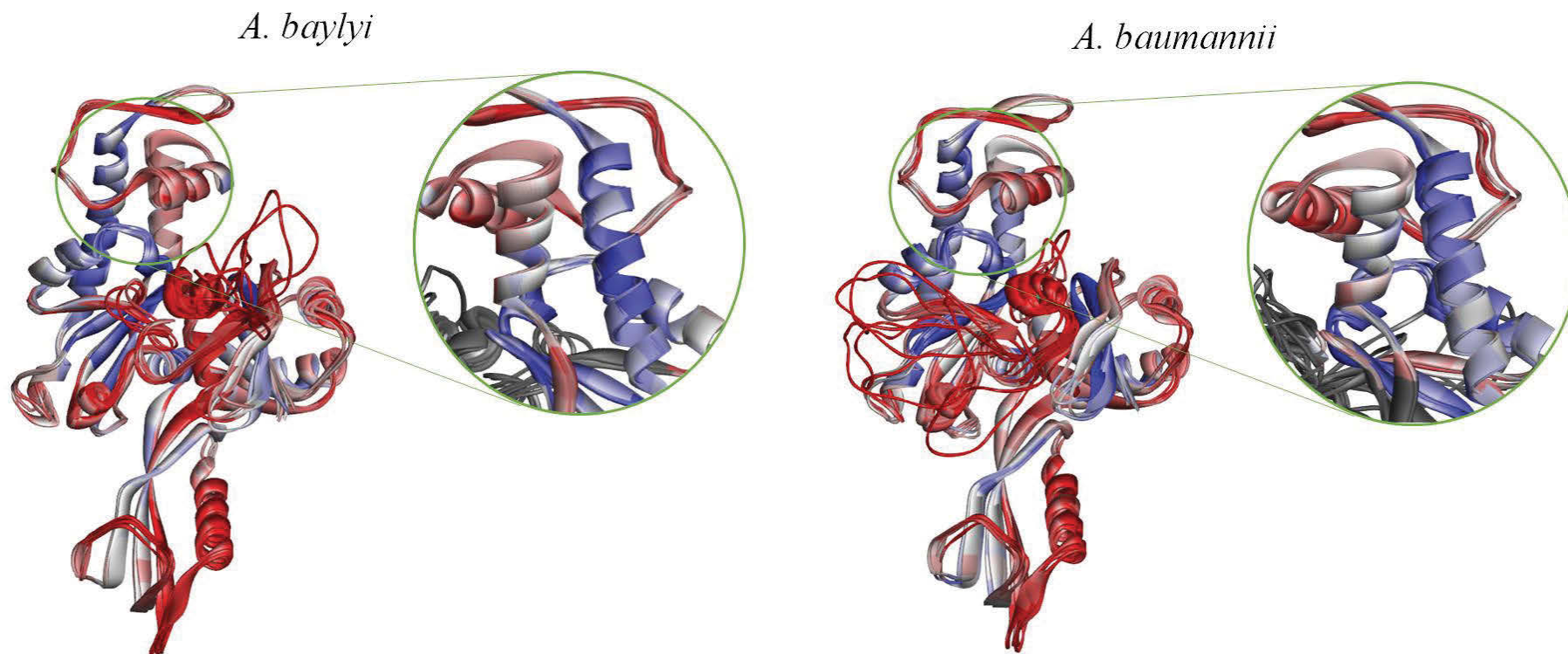


Figure 3.6: 3D-Profile Verification of the *Acinetobacter* spp. homology FtsA model using Discovery Studio 4.5. Five FtsA homology models of both *A. baylyi* and *A. baumannii* were created and the 3D structure of the model was verified alongside statistical test (Verify Score, Verify Expected High Score and Verify Expected Low Score). The predicted confidence of the created FtsA homology model from both organisms is low; this is depicted by red colouring on the majority of the protein. Nevertheless, the 2B domain of the model is still able to be used in the *in silico* interaction study as this region has a good predicted confidence. This is evident by the blue colouring of the 2B domain (area circled in green).

3.2.4 *In silico* model of *Acinetobacter* spp. FtsZ and FtsA interaction

In *E. coli* and most γ -proteobacteria, the sequence of the FtsZ C-terminal region responsible for binding is DIPAFRLRKQ. This region is conserved in many bacterial species (Figure 3.2). The aspartate and proline play important roles in the interactions of FtsZ with its partner proteins; FtsA and ZipA. There is a possibility that *Acinetobacter* may use the same sequence (peptide 1) or use a different sequence (peptide 2). The sequence of peptide 2 in *Acinetobacter* is different and the aspartate and proline been replaced with serine and glutamine, respectively. Moreover, the nature of amino acids in these two positions in peptide 2 of the *Acinetobacter* FtsZ protein have been changed from acidic to neutral and from cyclic to linear amino acid. Having peptide 2 as the actual FtsZ peptide in *Acinetobacter* suggest that the interaction of *Acinetobacter* FtsZ and FtsA are different to other bacterial species. In order to identify which of two peptides is probable for the FtsZ and FtsA interaction in *Acinetobacter*, both peptides were investigated in a *in silico* interaction study using the software DS 4.5.

To study protein-protein and protein-ligand interactions, a function called ‘Docking’ in DS 4.5 was used. The interaction between two proteins at the molecular level was examined. In this case a function called the refined docked proteins (RDOCK) was chosen for studying protein-protein interaction. The docking experiments were performed at two-stage energy minimizations. The first involves the evaluation of electrostatic (electrical repulsion) energies, and subsequently the desolvation (amount of energy taken for a molecule to be displaced by water molecules) energies. The 2B domain of FtsA was assigned as the receptor protein and FtsZ peptide as the ligand protein. The extreme C-terminal FtsZ peptide was used here because this is the only part of FtsZ present in the FtsZ-FtsA complex structure determined previously for the

T. maritima proteins (110). This FtsZ peptide is the only part of FtsZ currently known to bind to both FtsA and ZipA. Using the *T. maritima* X-ray crystal structure of the FtsZ-FtsA complex as the basis of this analysis, the FtsZ peptide was docked onto the FtsA region known to interact with the FtsZ peptide in the crystal structure. Once the docking was completed, further refinement was conducted by applying physical restraints to the model and producing a scoring function value called E-RDOCK. This was derived from the desolvation and electrostatic energy of the RDOCK method. The E-RDOCK value determines if a given interaction-pose is likely to be the probable docking conformation *in vivo*. Usually, the smaller the 'E-RDOCK' value, the higher the probability the *in vivo* interaction will look like the predicted model (E-RDOCK < 0). Note that, just like the PDF Total Energy and DOPE score, the E-RDOCK value is also a measure of comparison of homology models of a single protein. E-RDOCK values are listed in Table 3.3.

Table 3.3: Simulated interactions of *T. maritima* FtsZ to *A. baumannii*/baylyi FtsA.

Interaction poses	E-RDOCK
Tm FtsZ - Tm FtsA	-9.80
Peptide 1 - Tm FtsA	-3.18
Peptide 2 - Tm FtsA	7.09
Tm FtsZ - Bm FtsA	-0.05
Tm FtsZ - By FtsA	0.19
Tm FtsZ (D to S) - Bm FtsA	-6.90
Tm FtsZ (D to S) - By FtsA	-3.63
Tm FtsZ (R to K) - Bm FtsA	-3.88
Tm FtsZ (R to K) - By FtsA	-5.58
Tm FtsZ (D to S, R to K, P to Q) - Bm FtsA	-9.74
Tm FtsZ (D to S, R to K, P to Q) - By FtsA	-8.07

Tm = *T. maritima*; Bm = *A. baumannii*; By = *A. baylyi*; D = aspartate; S = serine; R = arginine; K = lysine; P = proline; Q = glutamine. The E-RDOCK value determines if a given simulated interaction poses is likely to be the docking conformation *in vivo*. The lower the E-RDOCK value the higher the probability the *in vivo* interaction will look like the predicted model.

As an initial test for the accuracy of the software in predicting interactions and at the same time provide a control value which signifies a predicted interaction for the *in silico* experiments, the co-crystal of *T. maritima* FtsZ peptide and FtsA was used in a docking experiment. The *T. maritima* FtsZ peptide was docked onto *T. maritima* FtsA and it produced an E-RDOCK value of -9.80, meaning the two proteins are highly-likely to interact and this also illustrates the accuracy of the software to predict a protein-protein interaction. This value (-9.80) also becomes a control value that was used to compare other E-RDOCK value produced in the experiment.

The interaction of the *T. maritima* FtsZ peptide to *Acinetobacter* spp. FtsA was tested by docking the *T. maritima* FtsZ peptide to *Acinetobacter* spp. FtsA. However, no interaction was predicted, evident by the produced E-RDOCK value close to zero (Table 3.3). Interestingly, an interaction was predicted when the *Acinetobacter* FtsZ peptide 1 was tested against *T. maritima* FtsA with the RDOCK protocol (-3.18). However, no interaction was predicted when the *Acinetobacter* FtsZ peptide 2 was tested against *T. maritima* FtsA with the RDOCK protocol (7.09).

Since the amino acid sequence of peptide 1 is the same as the *T. maritima* peptide and since, the *T. maritima* peptide was not predicted to bind the *Acinetobacter* FtsA, it suggests that *Acinetobacter* spp. might use peptide 2 for the FtsZ/FtsA interaction. To further understand the effect of the amino acid differences, the *T. maritima* FtsZ peptide was mutated with the *Acinetobacter* peptide 2 sequence and used in the RDOCK protocol with *Acinetobacter* spp. FtsA.

In the *T. maritima* crystal structure, three amino acid residues of the FtsZ peptide were identified for the formation of the salt bridges between FtsZ and FtsA. Two of these are part of the conserved region in the FtsZ peptide; aspartate (D338) and arginine (R344). In *Acinetobacter* these have been changed to serine and lysine, respectively. To understand the effect of these changes on the interaction of FtsZ and FtsA, a simulation was conducted whereby both the aspartate and arginine in the *T. maritima* FtsZ peptide was changed to a serine and lysine, respectively. The simulated interaction of *A. baumannii* FtsA with mutated *T. maritima* FtsZ (D338 to S338) predicted that the two are likely to interact because the E-RDOCK value (-6.90) is much lower compared to the interaction of *A. baumannii* FtsA with un-mutated *T. maritima* FtsZ (-0.05). Similarly, simulation with *A. baylyi* FtsA and mutated *T. maritima* FtsZ (D338 to S338) predicts an interaction between the two. This is supported by the calculated E-RDOCK

value -3.63, in comparison to the E-RDOCK value of 0.19 for the simulation of un-mutated *T. maritima* FtsZ with *A. baylyi* FtsA. Again, a similar result was observed with the docking of mutated *T. maritima* FtsZ (R344 to K344) onto *A. baumannii/baylyi* FtsA, since the E-RDOCK value of mutated *T. maritima* FtsZ (R344 to K344) interacting with *A. baumannii/baylyi* FtsA is much lower compared to the E-RDOCK value of un-mutated *T. maritima* FtsZ interacting with *A. baumannii/baylyi* FtsA. The result from the simulation implies that the serine and lysine are important for the interaction between FtsZ and FtsA in *Acinetobacter*. Assuming that the FtsZ and FtsA interaction of *Acinetobacter* spp. also uses the FtsZ C-terminal peptide and FtsA 2B domain, based on the E-RDOCK values obtained between the docking of the mutated and unmutated *T. maritima* FtsZ peptide, it is probable that the binding affinity of FtsZ and FtsA in *Acinetobacter* is less than the binding affinity observed between the *T. maritima* FtsZ peptide and FtsA ($K_d = 45 - 58 \mu\text{M}$) (110). If the interaction of *Acinetobacter* FtsZ and FtsA were to utilise a different site, the E-RDOCK value of around 0 and/or positive values would be expected during the docking of mutated *T. maritima* FtsZ peptide onto *Acinetobacter* FtsA, indicating no interaction is predicted between the FtsZ peptide and FtsA.

Another conserved amino acid within the FtsZ C-terminus region is the proline (P340) and in *E. coli*, the alteration of it resulted in reduced binding of FtsZ to FtsA (114). In the *T. maritima* X-ray crystal structure, this proline was not observed to form a salt bridge in the interaction with FtsA. However, this residue is conserved in all FtsZ proteins and the *E. coli* study suggested the importance of it in the interaction with FtsA. A simulation was conducted to understand the effect of changing this proline (P340) to glutamine (Q340). Substituting the proline to glutamine in the *T. maritima* FtsZ peptide and docking it to the *T. maritima* FtsA, did not reveal any predicted-interaction, evident

by the software producing only positive E-RDOCK value for the simulated interaction. When the mutated *T. maritima* FtsZ (P340 to Q340) was docked onto the *Acinetobacter* FtsA, the interaction conformation from the *T. maritima* crystal structure was replicated, but the produced E-RDOCK value suggests that the interaction is unlikely (E-RDOCK > 0). Mutating the *T. maritima* FtsZ peptide to that of the *Acinetobacter* sequence (D338 to S338, R334 to K334 and P340 to Q340) and docking it onto the *Acinetobacter* FtsA predicted binding. E-RDOCK values of -8.07 and -9.74 was obtained when the triple-mutated *T. maritima* FtsZ peptide was docked onto *A. baylyi* FtsA and *A. baumannii* FtsA, respectively. This indicates the possibility that the glutamine acts like the proline to stabilise the interaction of FtsZ to FtsA.

To summarise, the *in silico* interaction study suggests that FtsZ and FtsA are likely to interact in *Acinetobacter*, which was predicted through the docking of the *Acinetobacter* FtsZ peptide onto *Acinetobacter* FtsA. The obtained data also suggests a possibility that *Acinetobacter* FtsZ uses peptide 2 and that the three FtsZ residues of *Acinetobacter* that are different in other bacterial species are required for binding with FtsA in this organism

3.3 Discussion

The interaction between FtsZ and FtsA in *E. coli* has been known for quite some time. Utilizing methods such as yeast two-hybrid assays (115, 116) and systematic deletion mutagenesis analysis (116, 117) has shown that in several organisms, FtsZ interacts with FtsA *via* conserved amino acid residues on the very extreme of the C-terminal region of FtsZ. Initial amino acid sequence alignment of full-length FtsZ from various bacterial species identified two possible locations of this conserved peptide in *Acinetobacter*. One being upstream the extreme C-terminus (peptide 1) and the other at the very end of the C-terminus (peptide 2). Peptide 1 was seen to contain the conserved amino acid residues important for FtsZ and FtsA interactions; aspartate and proline. However, in peptide 2 these aspartate and proline, are replaced by serine and glutamine, respectively, in the C-terminal region of FtsZ from *A. baumannii/baylyi*. This study therefore aimed at understanding the interaction between *Acinetobacter* FtsZ and FtsA; being the first stage in identifying this interaction as a possible drug target for the development of a new class of antibacterials to treat infections caused by this organism.

The identification of the two possible peptide sequences was stimulating. Considering the effect of the peptide location to the linker length, although peptide 1 contains all the necessary amino acids important for the interaction of FtsZ and FtsA, mainly the aspartate and proline, this sets the *Acinetobacter* FtsZ linker to be 24 amino acids in length, which is far shorter than any other bacteria in the γ -proteobacteria class (125). On the other hand, the important amino acids for the FtsZ and FtsA interaction is changed in peptide 2, but having peptide 2 as the interaction region sets the *Acinetobacter* FtsZ linker at 52 amino acids in length. A bioinformatics study by Vaughan *et al.* found that the linker length from FtsZ across archaea, bacteria and eukaryota can span between 2-330 amino acid in length (125). However, specific to the

γ -proteobacteria, their linker length were identified to be 52-81 amino acids in length (125). A protein *in vitro* and *in vivo* study in *E. coli* by Gardner *et al.* found that the FtsZ linker in *E. coli* have a lower and upper limit of linker length, whereby 43 and 95 amino acids length is the limit, respectively (232). Meanwhile, Vaughan *et al.* identified Firmicutes can have linker length spanning from 26-133 amino acids. A study in *B. subtilis* suggested that a 50% shorter linker of ~25 amino acids in length is still functional for cell division (233), confirming the study conducted by Vaughan *et al.* for Firmicutes being able to tolerate a shorter linker length than the γ -proteobacteria. While perhaps it is possible for *Acinetobacter* FtsZ to contain a linker with only 24 amino acids in length, it will certainly be the odd one out as *A. baumannii* is part of the γ -proteobacteria class. To further understand the possibility of these two peptides being more significant than the other, an *in silico* interaction study was conducted.

The *Acinetobacter* FtsZ and FtsA interaction was first studied *in silico*, using the software DS 4.5. There is currently only one available FtsA X-ray crystal structure known and this is from *T. maritima*. Thus, a homology model of the *Acinetobacter* FtsA was created for this *in silico* study. As a personal learning process and an initial check of the software's accuracy to create homology models, homology models of the *S. aureus* FtsZ was created and then compared with the GDP-bound *S. aureus* FtsZ X-ray crystal structure with a resolution of 1.73 Å (PDB: 3VOA) using DS 4.5. Ten homology models of the *S. aureus* FtsZ protein were created and the accuracy of the models were validated by superimposing the models with the *S. aureus* FtsZ X-ray crystal structure, giving a Ca atom RMSD value of 2.97 Å. The low value of the RMSD indicates that the orientations of the atoms in the created models are very close to that of the original X-ray structure. This also indicate that the software is able to fairly accurately create homology models.

The quality of homology models is also dependent on the level of amino acid sequence identity between the protein of known structure and the protein to be modelled (234). Usually the higher the sequence identity, the better it is. This was the case with the FtsZ homology modelling and the reason the software was able to replicate the X-ray crystal structure. On the other hand, the creation of the *Acinetobacter* FtsA homology models did not provide that luxury. The creation of the *Acinetobacter* FtsA models was based on the *T. maritima* FtsA as the template protein and the FtsA amino acid sequence identity from the two organisms is only 26%. This level of amino acid sequence identity is usually not sufficient to be reliable (235) and because of that, future studies will include other FtsA structures for the alignment and homology models creation. Nevertheless, another validation function within DS 4.5, known as 3D-Profile Verification, whereby the 3D structure of the protein is colour coded into blue, white and red, suggests that the created FtsA homology models can be used for downstream analysis. This is supported by the blue and white colouring in the 2B domain of the *Acinetobacter* FtsA model corresponding to the *T. maritima* FtsA region identified to bind to the FtsZ peptide (Figure 3.6). The blue and white colouring suggests that the atoms in this area are properly oriented in comparison with the *T. maritima* FtsA X-ray crystal structure.

With the completion of the *Acinetobacter* FtsA homology models, docking experiments were conducted in DS 4.5 to identify the possible peptide of the very extreme C-terminus region of *Acinetobacter* FtsZ. In the co-crystallography data using the *T. maritima* FtsZ peptide and FtsA, three FtsZ residues were identified that form salt bridges during the interaction of the FtsZ peptide with FtsA (110). Two of these residues in the *T. maritima* FtsZ, aspartate and arginine, are part of the conserved region. The initial test was conducted to try and dock the wild-type *T. maritima* FtsZ peptide

onto the *T. maritima* FtsA, which predicted binding. Interestingly, docking peptide 1 onto the *T. maritima* FtsA also predicted binding. However, when the wild-type *T. maritima* FtsZ peptide and peptide 1 was docked onto the *Acinetobacter* FtsA, the result predicted no binding. In contrast, when the *T. maritima* FtsZ peptide was mutated to contain all three of the *Acinetobacter* sequence (peptide 2), binding was predicted between the mutated *T. maritima* FtsZ peptide and *Acinetobacter* FtsA. The obtained data suggests a possibility that *Acinetobacter* FtsZ uses peptide 2 and that the three FtsZ residues of *Acinetobacter* that are different in other bacterial species are required for binding with FtsA in this organism.

In *T. maritima*, the FtsA amino acid residues that formed the salt bridges are Lys293, Arg301 and Glu304. FtsA amino acid sequence alignment between *T. maritima* and *Acinetobacter* showed that Arg301 and Glu304 are conserved, while Lys293 in *Acinetobacter* is changed to glutamate. Having two of the three amino acids responsible for the formation of the salt bridges conserved on the *Acinetobacter* FtsA should allow some degree of interaction with the wild-type *T. maritima* FtsZ peptide and peptide 1, based on the systematic deletion mutagenesis studies of FtsZ (116, 117). Since no interaction was predicted from the docking experiment of wild-type *T. maritima* FtsZ peptide and peptide 1 with *Acinetobacter* FtsA, it points to a possibility of different amino acid residues playing a role in the formation of salt bridges during the interaction of FtsZ and FtsA in *Acinetobacter*; assuming the mechanism of interaction is the same. However, it is also possible that an entirely different mode of interaction exists for the *Acinetobacter* FtsZ and FtsA.

In the future it would be interesting to systematically mutate the *Acinetobacter* 2B domain and again conduct the docking experiment as this might possibly give an insight as to which amino acids are important in *Acinetobacter* FtsA for the interaction with

FtsZ. It would also be helpful to have more FtsA X-ray crystal structures to be used as a template to create homology models from as it would decrease the structural bias of the created homology models towards a certain species, as in the case of this study.

Thus far, this study has predicted that peptide 2 might be responsible for the FtsZ and FtsA interaction in *Acinetobacter*. Furthermore, the data predicts that the serine and lysine in the extreme C- terminal region of FtsZ are important for the FtsZ/FtsA interaction in *Acinetobacter* and that the glutamine acts as a stabilizer for this interaction in *Acinetobacter*. To further clarify the *in silico* data obtained and understand the interactions of the *Acinetobacter* FtsZ and FtsA, we aim to investigate the interactions of these proteins using X-ray crystallography. To achieve this endeavour, pure full-length FtsZ and FtsA protein are needed and the process of obtaining these necessary proteins is detailed in Chapter 4.

Chapter 4 – Protein purification of full-length *Acinetobacter* FtsZ and FtsA for *in vitro* interaction study

4.1 Introduction

As previously mentioned in Chapter 3 Section 3.1.2, the interaction between FtsZ and FtsA in *E. coli* has been known for over a decade (114). The mechanism of interaction was elucidated by Szwedziak *et al.* (110) through the co-crystallization of *T. maritima* FtsA with a *T. maritima* FtsZ peptide that is known to bind to FtsA; termed the C-terminal peptide. The co-crystal structure indicated that the two proteins interact through a series of salt-bridges. In *E. coli* and other γ -proteobacteria, the amino-acid sequence of the C-terminal peptide of FtsZ that interacts with FtsA is DIPAFLRKQ (79). Through a mutational study in *E. coli*, it was found that the aspartate and proline at position 1 and 3 of this peptide, respectively, are found to be the most important residues for the interaction of FtsZ with FtsA and ZipA (220). Amino acid sequence alignment of the C-terminal peptide from various organisms shows two possible locations of this peptide in *Acinetobacter* (refer to Peptide 1 and Peptide 2 in Figure 3.2 in Chapter 3). Peptide 1 contains the conserved sequence which exists in other bacterial FtsZ. On the other hand, in peptide 2, the aspartate and proline have been changed to serine and glutamine, respectively.

Currently there is only one co-crystal structure FtsZ and FtsA and that is through the use of proteins from the organism *T. maritima*. The FtsZ peptide of *T. maritima* contains the conserved aspartate and proline, which might indicate that the FtsZ peptide from other organisms that contain these conserved residues interact similarly. Analysis of amino acid sequence alignment of full-length FtsZ identified two possible peptides which may be the FtsA interacting region in *Acinetobacter* FtsZ. This begs the question,

which of these two is the sequence responsible for the FtsZ and FtsA interaction in *Acinetobacter*? If *Acinetobacter* uses peptide 1, does that mean the FtsZ and FtsA interaction in this organism is the same as the currently known mechanism of interaction? However, if *Acinetobacter* uses peptide 2 for the FtsZ and FtsA interaction, do the change in the aspartate and proline to serine and glutamine, respectively, translates to the same mechanism of interaction as currently understood? Or perhaps a different mode of FtsZ/FtsA interaction is used by *Acinetobacter*? In fact, do FtsZ and FtsA interact directly at all in *Acinetobacter*?

To answer these questions and gain a further understanding of the interactions of the divisome in *Acinetobacter*, with a long-term view to targeting these interactions with new antibiotics, the aim of the work presented in this chapter was to purify the full-length version of these two proteins, determine the structures using crystallography, test for their interaction and attempt to co-crystallize them to identify the chemical nature of this interaction.

4.2 Results: Overproduction and purification of the full-length *Acinetobacter* FtsZ and FtsA proteins

4.2.1 Overproduction and solubility analysis of *Acinetobacter baumannii* and *Acinetobacter baylyi* full-length FtsZ

Full-length FtsZ has not been crystallized and this is due to the presence of the disordered region in the C-terminus of the protein (81). However, since this region is different in *Acinetobacter* FtsZ and because no one has ever crystallized FtsZ and FtsA interacting together, it was decided that purification and an attempt at crystallization of the full-length FtsZ and FtsA should be made. This would allow examination of all the details of the *Acinetobacter* FtsZ and FtsA interaction.

To produce sufficient quantities of FtsZ from both *A. baumannii* and *A. baylyi* for structure determination using X-ray crystallography, it is necessary to overproduce the protein in an *E. coli* host for purification. The cloning of the *Acinetobacter ftsZ* genes was conducted by a member of the Harry laboratory, Dr Amy Bottomley. The *A. baumannii/baylyi ftsZ* genes were cloned into the plasmid, pETMCSITwo *ftsZ* constructs from each organism, *A. baylyi* and *A. baumannii*, were made with this plasmid. This enabled production of an untagged wild-type FtsZ and a C-terminal hexahistidine-tagged wild-type FtsZ from each species. Several constructs were made because it is not possible to predict which constructs would: (i) produce high quality, diffractive crystals; (ii) be active and interact with FtsA *in vitro*; (iii) co-crystallize with FtsA. Initially, the N-terminal tagged full-length FtsZ was also cloned but was unsuccessful. Meanwhile cloning of the untagged and C-terminal tag full-length protein was successful.

This project started with the transformation of the four newly-constructed plasmids into five different *E. coli* protein-overproduction strains *via* electroporation, as it is well

documented that some strains handle toxic foreign proteins better than other strains, while some strains are better at increasing the solubility of the foreign protein (236). Overproduction of the proteins was examined in all strains at several induction temperatures (37°C, 30°C, 25°C, 10°C) to overproduce soluble FtsZ species; both untagged and C-terminus hexahistidine-tagged. This is because proteins can be insoluble as a result of overproduction in a host (237) and lowering the induction temperature can increase the solubility of an overproduced protein (238). The screening result of the overproduction is shown in Table 4.1.

Table 4.1: Examination of strains and induction temperatures to overproduce soluble *A. baumannii* and *A. baylyi* FtsZ.

Temperature (°C)	<i>E. coli</i> overproduction strains	<i>A. baylyi</i>		<i>A. baumannii</i>	
		Untagged FtsZ	C-hexahistidine FtsZ	Untagged FtsZ	C-hexahistidine FtsZ
37	C41 (DE3)	Overproduced; insoluble	Overproduced; insoluble	Overproduced; insoluble	No overproduction
	BL21-AI	Overproduced; insoluble	Overproduced; insoluble	Overproduced; insoluble	Overproduced; insoluble
	B834 (DE3)	No overproduction	No overproduction	Overproduced; insoluble	No overproduction
	BL21 codonplus (DE3) RIPL	No overproduction	No overproduction	N/A	No overproduction
	BL21 (DE3) recA-	Overproduced; insoluble	No overproduction	Slight overproduction; insoluble	Overproduced; insoluble
30	C41 (DE3)	No overproduction	Overproduced; insoluble	No overproduction	N/A
	BL21-AI	Overproduced; insoluble	Not tested	Overproduced; insoluble	Overproduced; insoluble
	B834 (DE3)	N/A	N/A	No overproduction	N/A
	BL21 codonplus (DE3) RIPL	N/A	N/A	N/A	N/A
	BL21 (DE3) recA-	Not tested	N/A	Not tested	Overproduced; insoluble
25	C41 (DE3)	No overproduction	Overproduced; soluble	No overproduction	N/A
	BL21-AI	Overproduced; soluble	Not tested	Overproduced; soluble	Overproduced; insoluble
	B834 (DE3)	N/A	N/A	No overproduction	N/A
	BL21 codonplus (DE3) RIPL	N/A	N/A	N/A	N/A
	BL21 (DE3) recA-	Not tested	N/A	Not tested	Overproduced; 50% soluble
10	C41 (DE3)	No overproduction	Overproduced; soluble	No overproduction	N/A
	BL21-AI	Overproduced; soluble	Not tested	Overproduced; soluble	Overproduced; soluble
	B834 (DE3)	N/A	N/A	No overproduction	N/A
	BL21 codonplus (DE3) RIPL	N/A	N/A	N/A	N/A
	BL21 (DE3) recA-	Not tested	N/A	Not tested	Overproduced; 50% soluble

Strains and induction temperatures that overproduced soluble FtsZ are coloured green. Further tests were not conducted when the initial test at 37°C gave ‘No overproduction’. Also, once optimum conditions were identified for a particular construct, further tests were not conducted (N/A = Not tested).

After the optimum conditions to overproduce soluble FtsZ were determined (green coloured in Table 4.1), each of the strains was grown in 5 L of LB broth to produce large quantities of protein for purification. During the harvesting, the cells were divided into four cell pellets for use in multiple purification trials. The protein purification protocol followed is summarised in Figure 4.1 (refer to Chapter 2 Section 2.2.2 for the detailed protocol) and this was developed by our collaborator who have been specifically working with *Acinetobacter* proteins for *in vitro* studies. Therefore, after careful consideration, it was deemed appropriate to follow in their protocol instead of developing a new protocol from the start.

At this stage, it was decided that the purification of the full-length untagged FtsZ protein be pursued first instead of the C-terminus hexahistidine tagged because it is more desirable to use the untagged version of the protein for interaction studies, and also because the histidine tag in the C-terminus might affect the FtsZ-FtsA protein-protein interaction.

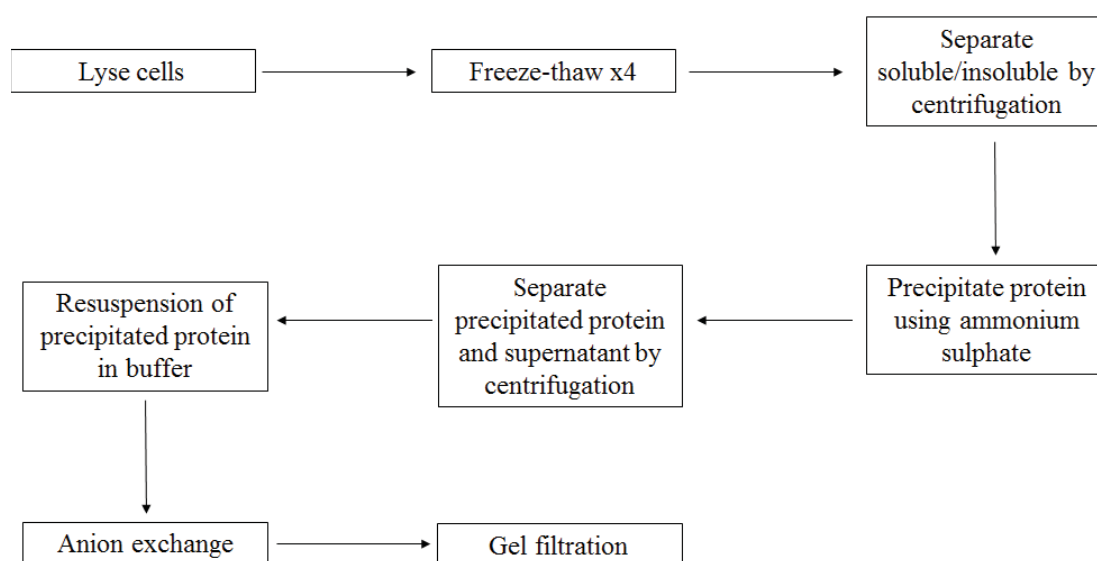


Figure 4.1: *A. baylyi/baumannii* untagged FtsZ purification workflow. A diagrammatical summary of the protein purification protocol used to purify *A. baylyi* and *A. baumannii* untagged FtsZ.

Having established the strains and induction temperature to produce soluble *A. baumannii*/*baylyi* FtsZ, one of the cell pellets containing the overproduced FtsZ was first lysed by the freeze-thaw method, followed by centrifugation to separate the soluble and insoluble materials. The supernatant was transferred to a new tube, filtered and then used in ammonium sulphate precipitation trials.

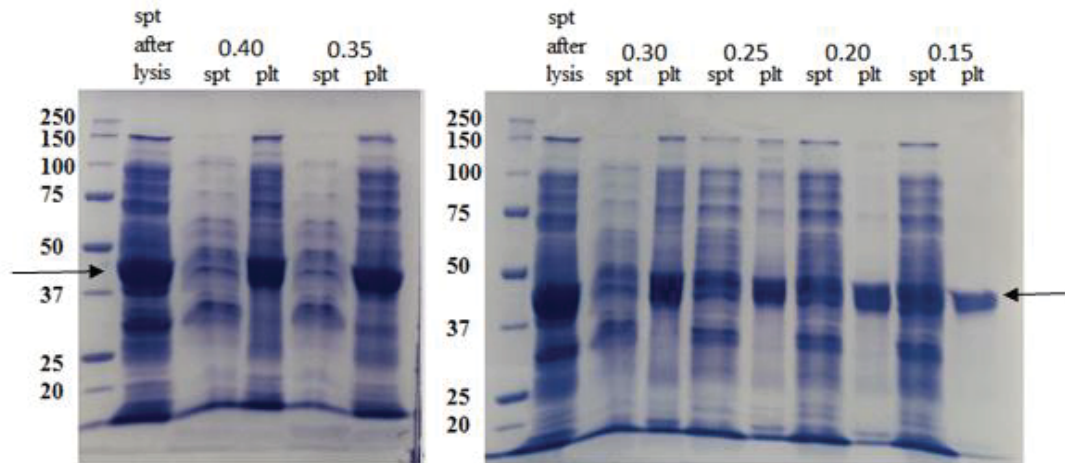
4.2.2 Ammonium sulphate precipitation trial of untagged *Acinetobacter* full-length FtsZ

Initially, ammonium sulphate precipitation trials were conducted to determine the best ammonium sulphate concentration to precipitate the untagged *A. baumannii* FtsZ, and at the same time provide an effective first-step purification of FtsZ. The result in Figure 4.2 shows that the best ammonium sulphate concentration to use is 0.2 g/mL, as it gives optimum yield with minimum contamination of other proteins.

The next step of the purification involves the use of an anion-exchange column and this requires the buffer to contain little or no sodium chloride, as sodium chloride is used for eluting the protein off the column. For this, the second cell pellet was lysed, precipitated with ammonium sulphate and then the solubility of untagged *A. baumannii* FtsZ was tested by dialysis with varying concentrations of sodium chloride (0 to 0.3 M). *A. baumannii* FtsZ was found to be soluble at all concentrations tested (Figure 4.3).

Similarly, initial ammonium sulphate precipitation and dialysis trials were conducted on untagged *A. baylyi* FtsZ. As with the *A. baumannii* FtsZ protein, the best ammonium sulphate concentration to use for the *A. baylyi* FtsZ is 0.2 g/mL (Figure 4.2), and untagged *A. baylyi* FtsZ is soluble in solutions containing 0 M to 0.3 M sodium chloride (Figure 4.3).

A. baumannii



A. baylyi

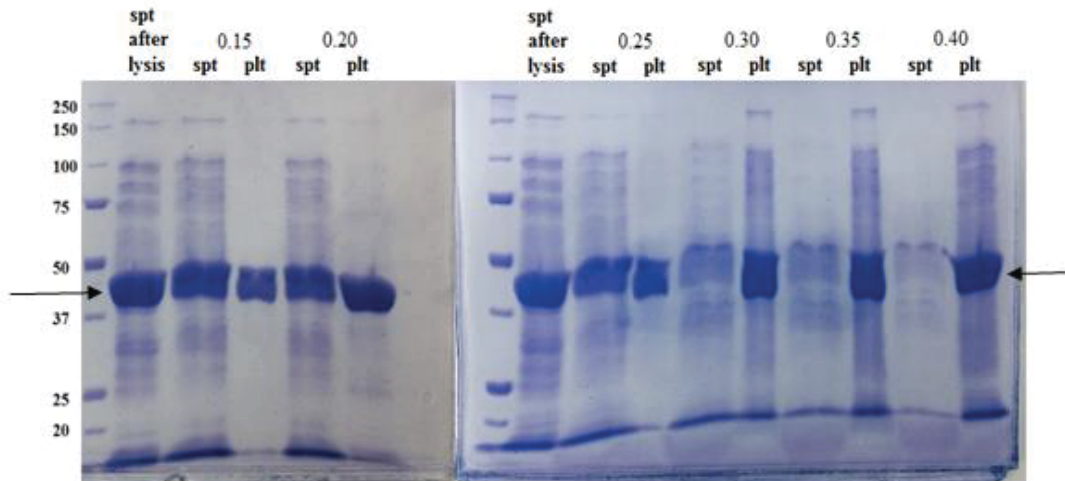
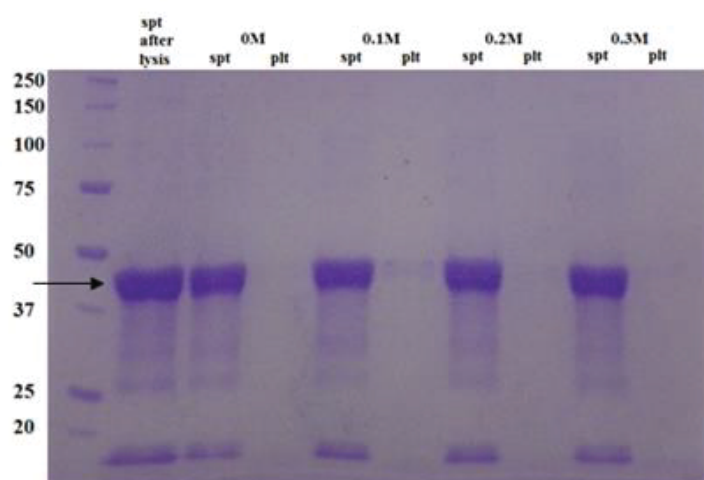


Figure 4.2: Ammonium sulphate precipitation trials of untagged *A. baumannii* and *A. baylyi* FtsZ. Coomassie-stained 10% SDS-PAGE gel showing untagged *A. baumannii* and untagged *A. baylyi* FtsZ (expected size of 40 kDa is denoted by the arrow) precipitating in a range of ammonium sulphate concentrations, from 0.15 g/mL up to 0.4 g/mL. The best yield-purification outcome for FtsZ from both *Acinetobacter* species is obtained with 0.2 g/mL. spt = supernatant and plt = pellet. Numbers on the left side of the figure represent the protein standard in kDa (*A. baylyi* FtsZ: 41.78 kDa; *A. baumannii* FtsZ: 42.00 kDa).

A. baumannii



A. baylyi

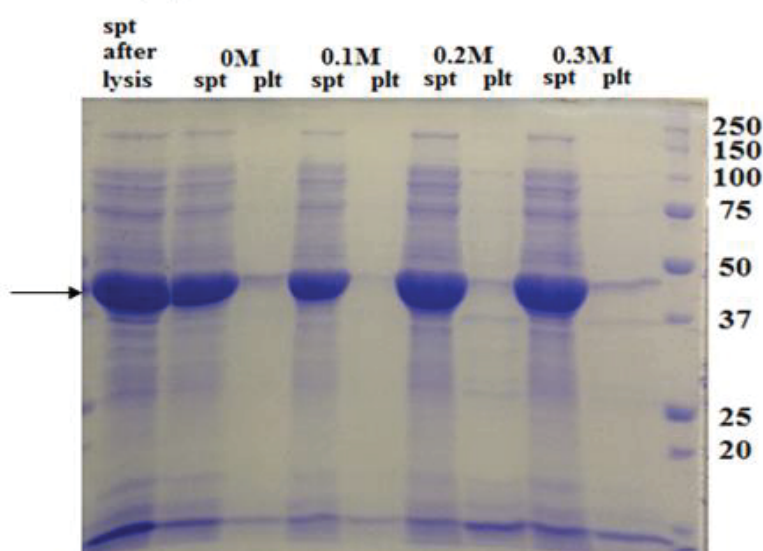


Figure 4.3: Testing of untagged *A. baumannii* and *A. baylyi* FtsZ stability in a range of sodium chloride concentrations. Coomassie-stained 10% SDS-PAGE gel showing untagged *A. baumannii* and *A. baylyi* FtsZ (expected size of 40 kDa is denoted by the arrow) in a range of sodium chloride concentrations ranging from 0 M to 0.3 M, to determine the solubility of the protein in those solutions. The result shows that both the untagged *A. baumannii*/*baylyi* FtsZ is soluble in solutions containing the tested sodium chloride concentrations as seen by the presence of the protein in the supernatant fraction. spt = supernatant and plt = pellet. Numbers on the side of the gel image are the protein standard in kDa (*A. baylyi* FtsZ: 41.78 kDa; *A. baumannii* FtsZ: 42.00 kDa).

4.2.3 Purification trial of full-length *Acinetobacter* untagged FtsZ

After ammonium sulphate precipitation, the next step was anion-exchange chromatography followed by gel filtration. One interesting observation was made during the gel filtration trials and that was the appearance of a double band at the size of the untagged FtsZ for both *A. baylyi* and *A. baumannii* (denoted by the arrows in Figure 4.4); suggesting proteolysis of the protein. The precise identity of each band was determined by cutting the bands out of the gel, trypsin-digesting and then analysing it by mass spectrometry to calculate their molecular mass.

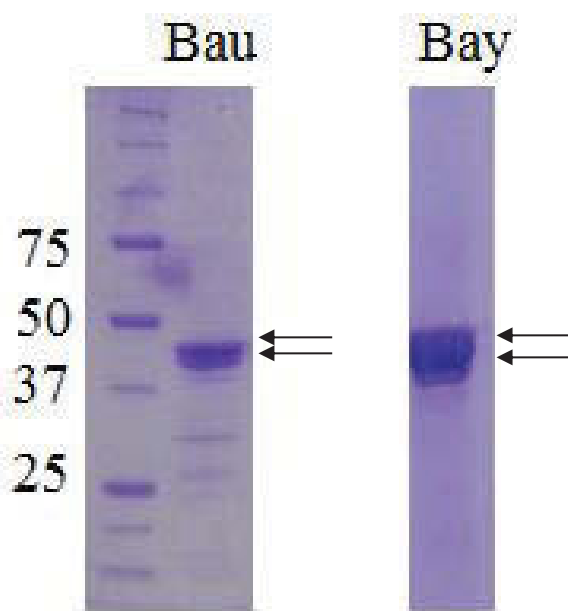


Figure 4.4: Testing gel filtration method using *A. baylyi* and *A. baumannii* untagged FtsZ revealed a double band. Gel filtration method was tested using both *A. baylyi* (Bay) and *A. baumannii* (Bau) untagged FtsZ. An interesting double band around the size of the untagged FtsZ, as denoted by the arrows, appeared after the samples were run through the gel filtration column. Numbers on the side of the figure is the protein standard in kDa (*A. baylyi* FtsZ: 41.78 kDa; *A. baumannii* FtsZ: 42.00 kDa).

The two bands denoted by the arrow in Figure 4.4 from both *A. baylyi* and *A. baumannii* FtsZ preparations were cut out from the gel, separated and an in-gel digestion of the protein was performed using trypsin. Liquid chromatography-mass spectrometry/mass spectrometry (LC-MS/MS) showed that the bottom and top band in the gel have essentially identical molecular masses: 42,039 Da and 41,838 Da for *A. baumannii* and *A. baylyi*, respectively. The molecular weight obtained is consistent with the theoretical molecular weight calculated for untagged FtsZ in *A. baumannii* (42,065.08 Da) and *A. baylyi* (41,864.08 Da). However, since the two bands are so close together in the gel, cross-contamination may occur and possibly yielding a false positive mass for the lower band. The LC-MS/MS result was, therefore, re-analysed by Electro Spray Ionisation-Mass Spectrometry (ESI-MS⁺) using the whole FtsZ purified sample. Since the ESI-MS⁺ uses an intact protein and not a trypsin-digested protein like in LC-MS/MS, this method better indicates if two protein species exist in the sample, as two different sized proteins would have a different time of flight. The ESI-MS⁺ experiment was conducted by Dr Nan Li; a member of Professor Nick Dixon's laboratory at the University of Wollongong. The ESI-MS⁺ data showed that there is only a single species of FtsZ in the sample; *A. baumannii* (41,997.55 Da) and *A. baylyi* (41,782.54 Da). The agreement in mass between the two MS methods confirms that the FtsZ protein exists as a single species and is not being proteolysed.

Having optimized the ammonium sulphate concentration, the solubility of FtsZ at various salt concentrations, and demonstrated the homogeneity of the FtsZ samples, it was decided that purification of FtsZ from both *Acinetobacter* species be conducted one at a time and for this, the *A. baylyi* FtsZ was chosen to be the first protein fully purified.

4.2.4 Analysis and prevention of proteolysis of full-length *A. baylyi* untagged FtsZ during purification

The *A. baylyi* untagged FtsZ was purified by following the protocol outlined in Figure 4.1. During the purification of the *A. baylyi* untagged FtsZ, aliquots were taken before and after each step and analysed by SDS-PAGE. SDS-PAGE analysis of the samples going through the different purification steps (after ammonium sulphate precipitation, ion exchange and gel filtration) showed the presence of the same lower molecular weight contaminating bands, preventing further purification of *A. baylyi* full-length untagged FtsZ (brackets in Figure 4.5). To stop proteolysis of FtsZ during the protein purification protocol, the cells were grown again and this time, a small sample was taken after induction and the cells lysed using two different lysis buffers: buffer A (the lysis buffer that had been used up to this point which contained 25 mM Tris, 2 mM DTT, 1 mg/mL lysozyme, 50 µg/mL DNase, 1 Roche protease inhibitor tablet) and buffer B (the same as buffer A, but contains two extra protease inhibitors; 2 mM 1,10-Phenanthroline, 1 mM PMSF). Buffer A is a typical lysis buffer that had been used to purify a number FtsZ from several organisms, for example, *S. aureus* (82), *M. jannaschii* (80), and *P. aeruginosa* (239). However, buffer B had also been used to purify FtsZ from the bacteria *M. tuberculosis* (240). To test the two buffers, one cell pellet containing the untagged FtsZ of *A. baylyi* was resuspended in buffer A and another in buffer B. The cells were lysed and centrifuged to separate the insoluble and soluble components. The soluble fraction was precipitated using 0.2 g/mL solid ammonium sulphate and analyzed by SDS-PAGE gel (Figure 4.6). Samples treated with buffer A showed proteolysis was apparent after the ammonium sulphate precipitate was re-solubilized, as evidenced by the triplet bands in the 40 kDa region and four additional bands in the 25-30 kDa region of the gel in Figure 4.6 A (lane 4 and 5; arrows). However, no proteolysis was observed when buffer B was used as a lysis

buffer, as seen by the absence of the four bands in this region of the gel (Figure 4.6 B). Therefore, buffer B was used from this point on in the protocol.

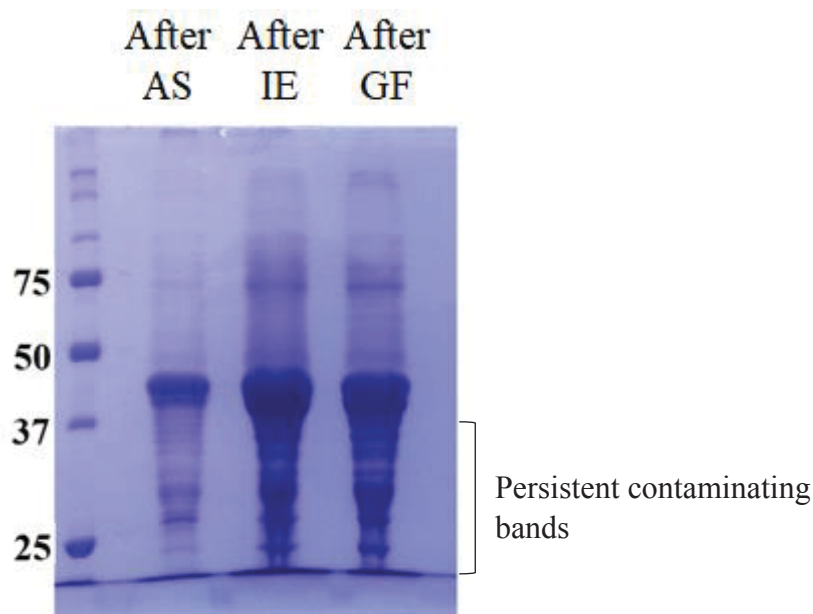


Figure 4.5: *A. baylyi* untagged FtsZ purification. Samples were taken before and after each step outlined in Figure 3.6 and analysed on a 10% SDS-PAGE gel. AS = ammonium sulphate precipitation, IE = ion exchange, GF = gel filtration. The gel analysis suggests that the *A. baylyi* untagged FtsZ was proteolysed already at the stage of ammonium sulphate precipitation and before ion exchange as evident by the samples having the same profile even after undergoing the different purification method. Numbers on the side of the figure indicate the protein standards in kDa (*A. baylyi* FtsZ: 41.78 kDa).

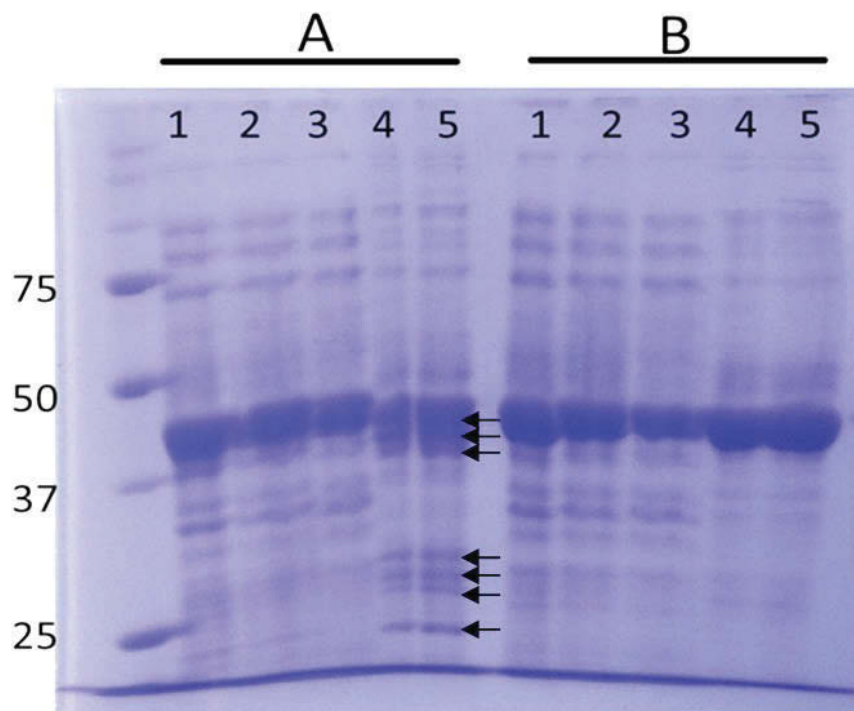


Figure 4.6: Test to see if proteolysis happens during cell lysis for *A. baylyi* FtsZ. 1= cell lysis, 2= ammonium sulphate precipitation of lysate, 3= supernatant after ammonium sulphate protein pellet is separated, 4 and 5= re-suspended ammonium sulphate protein pellet (duplicate). A = samples that were treated with buffer A, B = samples that were treated with buffer B. Proteolysis is observable in the ammonium sulphate protein pellet of buffer A (arrows) but is not evident in the ammonium protein sulphate pellet of buffer B. Numbers on the side of the figure are the protein standards in kDa (*A. baylyi* FtsZ: 41.78 kDa).

4.2.5 Purification of full-length A. baylyi untagged FtsZ leading to X-ray crystallography trials

The proteolysis problem was solved by using lysis buffer B instead of A. The *A. baylyi* untagged FtsZ purification was therefore repeated by following the method outlined in Figure 4.1 and using buffer B as the lysis buffer. This time the protein was not proteolysed; evidenced by the presence of only one major band of ~40 kDa in lane 4 of Figure 4.7 and the absence of the lower molecular mass bands seen in lane 4 of Figure 4.6 A. The purification worked very well as there was very little of any other bands apart from FtsZ using SDS-PAGE (see lane 4 of Figure 4.7). The molecular mass of the purified FtsZ was determined using ESI-MS⁺ to be 41,729.29 Da (theoretical mass was 41,864.08 Da). The difference in the molecular mass obtained from the MS and the theoretical mass is most likely due to the pure protein missing the first methionine on the N-terminus as it is quite common to lose this residue when it is followed by alanine, as seen with this protein (241, 242). The purified protein was concentrated to 24.5 mg/mL using a vivaspin column and then subjected to crystallography trials at the laboratories of Associate Professor Aaron Oakley and Professor Nick Dixon at the University of Wollongong.

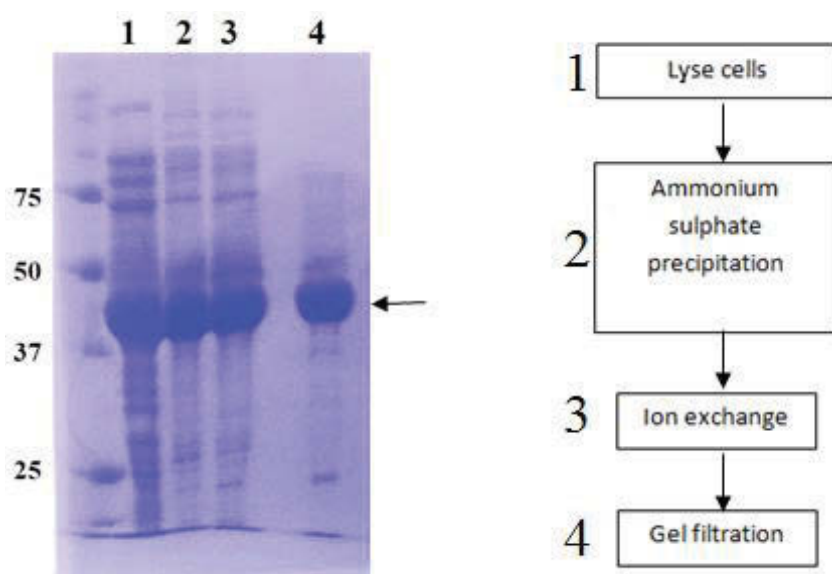


Figure 4.7: Successful *A. baylyi* untagged FtsZ purification. Samples were taken before and after each purification step and analysed on a 10% SDS-PAGE gel. Lane 1: whole cell lysis; lane 2: after ammonium sulphate precipitation and before ion exchange; lane 3: after ion exchange and before gel filtration; lane 4: after gel filtration. No proteolysis can be seen, as only one band of ~40 kDa (arrow) in lane 4 is observable and the four bands in the range of 25-30 kDa are absent (refer to the bracket in Figure 3.10). The methods utilised in the purification were able to remove many of the contaminating proteins as most of the bands observable in lane 1, 2 and 3 are not present in lane 4. Numbers on the side of the gel image are the protein standard molecular masses in kDa (*A. baylyi* FtsZ: 41.78 kDa).

4.2.6 Crystallography trials using full-length *A. baylyi* untagged FtsZ

For crystallography trials, the 24.5 mg/mL solution of FtsZ was diluted to 9.15 mg/mL by dialysing the protein sample against a buffer (20 mM Tris, 200 mM NaCl pH 7.6) overnight. This is because the FtsZ protein was stored in a storage buffer containing 20% glycerol, which needed to be removed for crystallography trials. The following day, two-hundred crystallization conditions were set up manually by mixing 1 μ L of protein with 1 μ L of buffer from the crystallography kits (JCSG+ and PEGs II) and then stored at 12°C to await possible crystallization. Since the crystallization trials were set up at the Dixon laboratories at the University of Wollongong, a member of that lab, Dr Nan Li, helped monitor the crystallization process. After two weeks of incubating the

protein mixture with JCSG+ and PEGsII kits, Dr Nan Li had observed that 30% of the conditions had precipitated and no crystals had formed. Following the first crystal trials that produced no crystals, another trial using another kit (PACT kit) was set up by Dr Nan Li and after one week of incubation at 20°C, four crystals formed under conditions with 0.2 M ammonium chloride, 0.1 M HEPES pH 7.0 and 20% PEG 6000 (Figure 4.8). The crystals, however, were too small to be X-rayed and optimisation around the said condition was needed to form crystals with acceptable size for X-ray. Dr Nan Li performed the optimisations, but she was not able to obtain acceptable crystals for X-ray. As full-length *Acinetobacter* FtsZ was predicted to have a disordered region and in other species FtsZ is known to contain a disordered region following the C-terminus globular domain of the protein; this might have affected the crystallization of the protein. However, as previously mentioned, since the primary aim was to understand and characterize the *Acinetobacter* interaction between full-length FtsZ and FtsA proteins, the starting point was to use the full-length protein.

Since the disordered region was suspected to have impacted in the crystallization of the full-length protein, Dr Nan Li removed this region by performing a trypsin digestion of the full-length protein. Using the digested protein, Dr Nan Li set up another crystal screen using the PEGs II kit. Microcrystals and needle crystals were observed under two conditions: 0.2 M ammonium sulfate, 0.1 M sodium acetate, 22% PEG 4000 and 0.2 M ammonium sulfate, 0.1 M MES pH 6.5, 30% PEG 5000MME. These, however, were not crystals of acceptable size for X-ray analysis. Dr Nan Li observed a drop in the protein concentration after performing the trypsin digest (less than 5 mg/mL), suggesting that the reason for the inability of the protein to form suitable crystal is because the protein concentration was simply too low, as protein concentration is one of the key variables that affects crystallization (243). Future crystal trials using

Acinetobacter FtsZ would need to be constructed without the disordered region in the C-terminal part of the protein to prevent the need of trypsin digest and consequently diluting the protein concentration. Since the project aimed at characterizing the interaction of the *Acinetobacter* FtsZ and FtsA using full-length proteins, FtsZ crystallization and purification of the *A. baumannii* FtsZ were put on-hold and the focus shifted towards purifying the FtsA protein that is needed for examining the interaction with FtsZ.

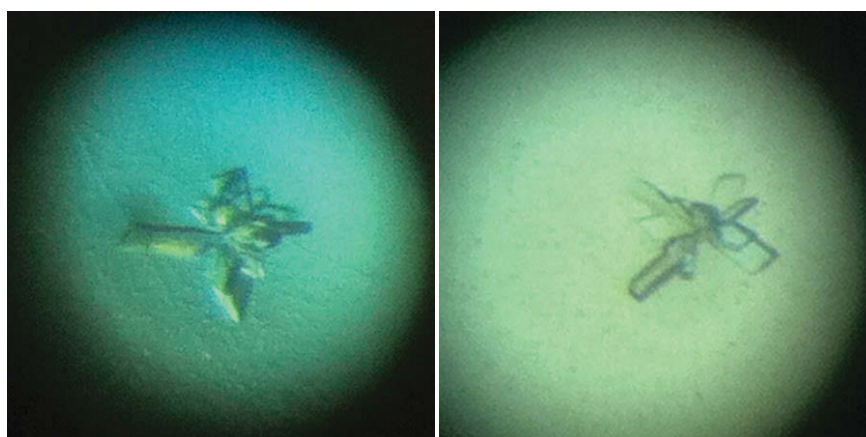


Figure 4.8: Microcrystal formation of *A. baylyi* untagged full-length FtsZ. The full-length untagged FtsZ of *A. baylyi* was subjected to crystal screen using the PACT kit. Microcrystals were observed under the condition with 0.2 M ammonium chloride, 0.1 M HEPES pH7.0, and 20 % PEG 6000.

4.2.7 Overproduction analysis of full-length *A. baylyi* N-terminus and C-terminus hexa-histidine-tagged FtsA

To understand the interaction between FtsZ and FtsA from *Acinetobacter*, it is essential that sufficient quantities of full-length *Acinetobacter* FtsA are produced for co-crystallization with FtsZ for structural determination. Reason for using the full-length FtsA construct, apart from being the aim of the study, was also because the *T. maritima* and *S. aureus* FtsA crystal structures were made with full-length proteins (244,

245). Similar to FtsZ, the full-length *A. baumannii/baylyi ftsA* gene was cloned into pETMCSI and pETMCSIII by Dr Amy Bottomley. Three *ftsA* constructs from each organism (*A. baylyi* and *A. baumannii*) were made with these plasmids. pETMCSI allowed the construction of an untagged (wild-type) *ftsA* gene and a C-terminal hexahistidine-tagged FtsA from each species, while pETMCSIII allowed the construction of an N-terminal hexahistidine-tagged FtsA from each species. In the interest of time, initial screening was conducted by Dr Amy Bottomley, and she found that all of the constructs produced insoluble protein and therefore FtsA had to be purified from inclusion bodies. From the screen, the best *E. coli* overproduction strain was found to be BL21-AI and C41 (DE3). The overproduction screen also found the most stable FtsA protein; one that does not degrade; was the *A. baylyi* N-terminal and C-terminal hexahistidine-tagged FtsA. Dr Amy Bottomley also found that purification of the protein needs to be in buffers containing 20% glycerol as it assists in the stabilization of the protein in aqueous solution and therefore, keeping it soluble once the protein is out of the inclusion bodies (246).

This part of my project started by re-transforming the plasmids (pETMCSI *A. baylyi* FtsA-6xhis and pETMCSIII *A. baylyi* 6xhis-FtsA) into competent *E. coli* overproduction strains BL21-AI and C41 (DE3). To confirm the overproduction capability of the transformants, the newly transformed cells were grown in 5-mL LB broth, overproduction of the protein was induced and cell lysates analysed using SDS-PAGE. The result showed overproduction of the target protein (expected size of ~45 kDa denoted by the arrow in Figure 4.9). One interesting observation made was that the location of the hexa-histidine tag slightly changes the migration of the FtsA band, with N-terminal tagged FtsA migrating slightly further than the C-terminal tagged FtsA (denoted by arrows in Figure 4.9). To scale this up, a 1-L culture was grown and, since

the protein is insoluble, the first part of the purification involved purifying the inclusion bodies containing the insoluble FtsA. The purification protocol is summarized in Figure 4.10. For the inclusion bodies purification trial, a small sample was taken during each step (Figure 4.11) and analysed using SDS-PAGE. The result showed the protein has not been degraded and is in the inclusion bodies (denoted by the arrow in Figure 4.11). Also, the strain BL21-AI was seen to overproduce more of the target protein compared to the strain C41 (DE3) (AI and C41 lanes in Figure 4.9). Therefore, from this point on, both the N- and C-terminal hexa-histidine tagged FtsA protein was overproduced using the BL21-AI strain.

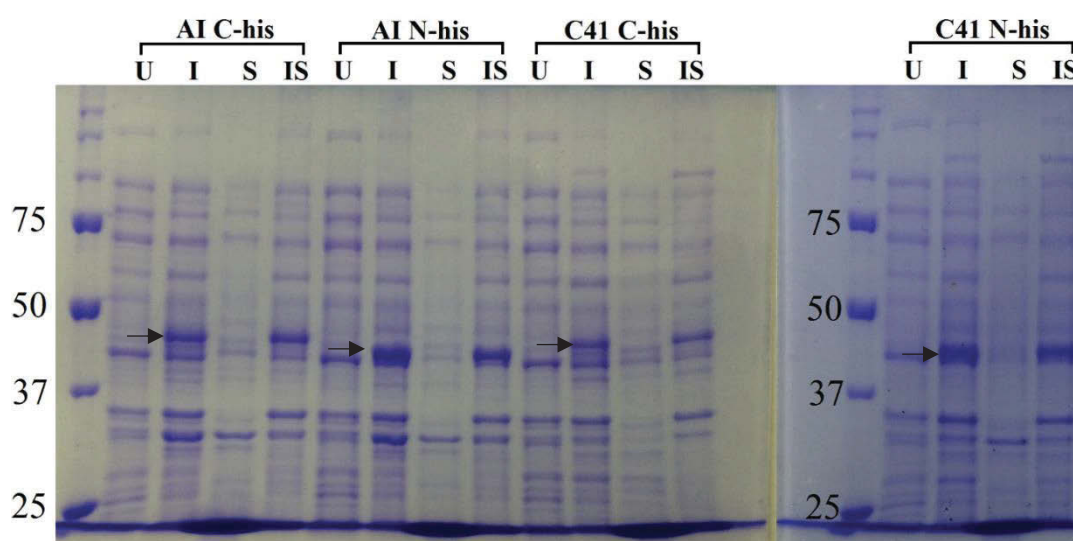


Figure 4.9: Overproduction screening of full-length *A. baylyi* N-terminus and C-terminus hexa-histidine-tagged FtsA. The two FtsA constructs were transformed into two protein overproduction strains (BL21-AI and C41(DE3)) and the cells were grown and induced at 37°C. The overproduction and solubility of the protein in those strains were analyzed on a 10% SDS-PAGE gel. The protein was overproduced with an expected size of ~45 kDa (denoted by arrow). U = uninduced cell lysate; I = induced cell lysate; S = induced soluble cell lysate; IS = induced insoluble cell lysate. Numbers on the side of the figure is the protein standard in kDa. Location of the hexa-histidine tag slightly changes the migration of the FtsA band (denoted by arrows).

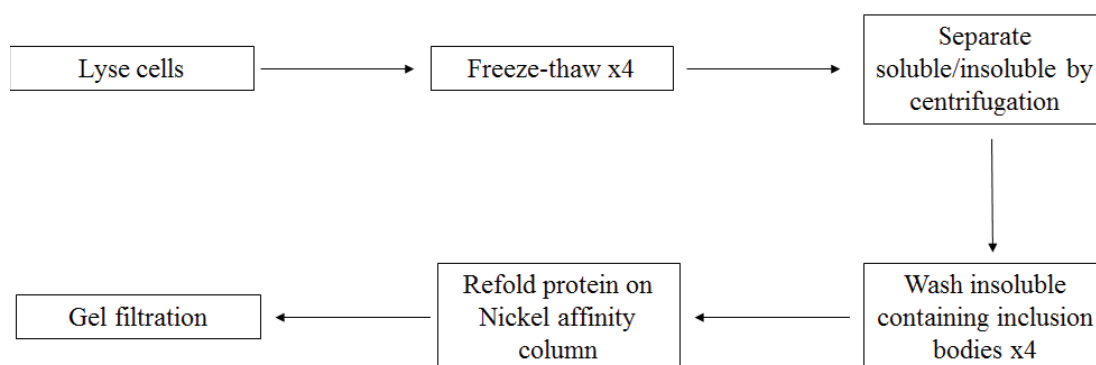


Figure 4.10: *A. baylyi/baumannii* N- and C-hexahistidine tagged FtsA purification workflow. A diagrammatical summary representation of the protein purification protocol used to purify *A. baylyi* and *A. baumannii* N- and C-hexahistidine tagged FtsA.

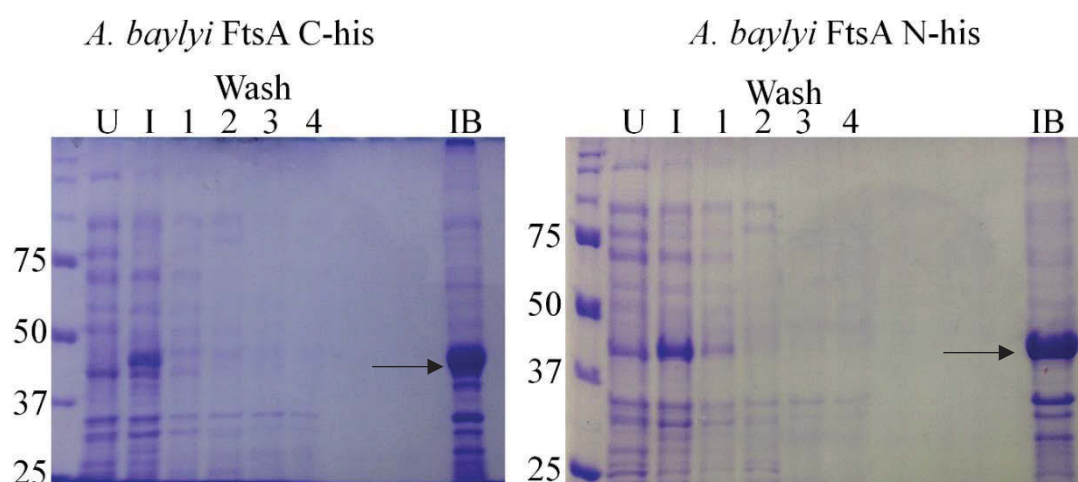


Figure 4.11: Inclusion bodies purification trial of N-terminus and C-terminus his-tagged *A. baylyi* full-length FtsA from 1L culture. Inclusion bodies purification trial of the two *A. baylyi* FtsA constructs was conducted after the *E. coli* overproduction strain AI was freshly-transformed with plasmids harbouring the two ftsA constructs. The cells were grown and induced at 37°C. The inclusion bodies purification involves washing the pellet obtained after lysing the cells with the lysis buffer four times. The overexpressed protein (expected size of ~45 kDa denoted by arrow) was seen to be in the inclusion bodies fraction and was not lost during the wash steps. U = uninduced cell lysate; I = induced cell lysate; Wash 1- 4 = cell pellet wash step after cell lysis; IB = inclusion bodies. Numbers on the side of the gel images are the protein standard in kDa.

4.2.8 Purification trial of full-length A. baylyi C-terminal hexa-histidine-tagged FtsA using nickel affinity chromatography

After observing that the *E. coli* BL21-AI strain overproduces more of the target protein compared to C41 (DE3) strain, a 1-L upscale of FtsA production with the BL21-AI strain was carried out and the inclusion bodies purified. No degradation of FtsA was observed during the inclusion bodies purification (data not shown) and the 1-L upscale produced 6 mL of inclusion bodies. Since both FtsA protein constructs are of *A. baylyi* origin, the C-terminal hexa-histidine tagged version of the protein was chosen to be purified first. 1 mL of the inclusion bodies was used in a protein purification trial. The 1-mL inclusion bodies were firstly dissolved in a washing buffer containing 6 M urea. The supernatant containing the solubilized protein was then applied to a nickel affinity column and the protein refolded on the column by gradually decreasing the concentration of urea. This can allow the protein to refold into its native conformation while remaining soluble. Once the protein was refolded, it was eluted from the HisTrap column using elution buffer containing 1 M imidazole in one-step. Small volume samples were taken at each step of the purification and analyzed on a 10% SDS-PAGE gel. The protein was eluted into one 10-mL fraction to keep it soluble (denoted by the arrow in Figure 4.12).

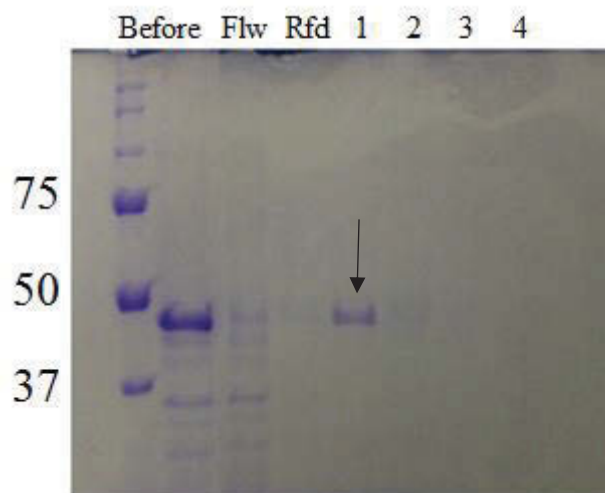


Figure 4.12: Purification trial of *A. baylyi* C-terminal hexahistidine-tagged full-length FtsA. The protein was firstly purified in inclusion bodies and the inclusion bodies were dissolved in a buffer containing 6 M urea. The dissolved inclusion bodies were applied to a nickel affinity column and the protein was refolded on the column and eluted. The protein was eluted into one fraction (denoted by arrow). Flw = the flow-through during application of protein sample onto the column, Rfd = flow-through collected during the on-column refolding step. Numbers on the side of the figure are the protein standard in kDa.

Since the protein was eluted into a 10-mL fraction, dilution of the protein was inevitable. The final step of purification was to use a size exclusion column. This step also allows assessment of the homogeneity of the protein sample. For sufficient resolution using the size exclusion column (HiPrep 26/60 Sephacryl S300 HR), the sample being applied needs to be 2% of the column volume (in this case 6 mL), hence it was necessary to concentrate the protein sample before applying to the gel-filtration column.

4.2.9 Concentrating full-length *A. baylyi* C-terminal hexa-histidine-tagged FtsA using various methods

The primary aim of this project was to understand and characterize the *Acinetobacter* FtsZ and FtsA interaction. It was therefore determined to be essential to use the full-length FtsA protein. FtsA in *E. coli* and *B. subtilis* is known to have a MTS (247). However, at the start of the project it was not assumed that the *Acinetobacter* FtsA also

contained a MTS. Furthermore, since the project was aimed at understanding the interaction of the *Acinetobacter* FtsZ and FtsA, it was deemed important to take the challenge and use the full-length proteins in the first instance.

Initially, Dr Amy Bottomley had attempted to concentrate the protein sample using a vivaspin column with 10,000 Da MWCO. However, she found that it was too time consuming and she also identified that the protein adheres to the filter membrane of the column and is un-recoverable. Therefore, using the sample that originated from the 1-mL inclusion bodies, which had been used up to this point, concentrating *via* anion exchange was attempted. This was carried out by a one-step elution into a 2-mL fraction. The result from the trial suggested that the method is problematic, with FtsA being lost during the process; either from the protein precipitating on the column or the protein adhering to the column and not eluting (protein observed when elution during column clean up with sodium hydroxide was analysed on SDS-PAGE; data not shown). The protein sample was therefore concentrated using PEG 20,000 (polyethylene glycol). To concentrate using PEG 20,000, another 1-mL inclusion body was used and at this step, to test the method, 2 mL of the 10-mL protein sample was transferred into a dialysis tube with 3,500 Da MWCO and then dialysed against a 20% PEG 20,000 solution for two hours. Small samples were taken pre- and post- dialysis with PEG 20,000 and analyzed on a 10% SDS-PAGE gel. This method appeared to result in an increase in protein concentration post-dialysis with PEG 20,000 (denoted by the arrow in Figure 4.13). The protein concentration of pre- and post-dialysis was also checked using a nanodrop. This confirmed an increase in concentration of FtsA from 0.67 mg/mL to 0.91 mg/mL but, it is not enough for the protein to be used in protein crystal trials as the protein usually needs to be in the concentration of 10 mg/mL for setting crystal trays.

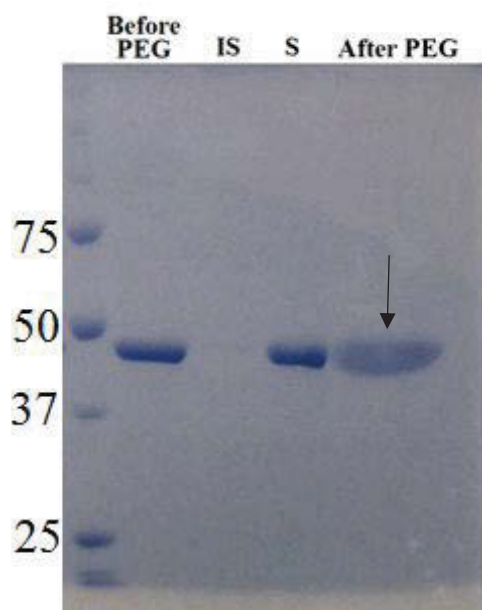


Figure 4.13: Concentrating full-length *A. baylyi* C-terminal hexahistidine-tagged FtsA via dialyzing against PEG 20,000. Once the protein was refolded and purified using affinity chromatography column, it was concentrated by dialyzing against a solution containing 20% PEG 20,000. The protein was able to be concentrated using this method (denoted by arrow). IS = insoluble fraction after dialysis; S = soluble fraction after dialysis containing the protein. Numbers on the side of the figure are the protein standard in kDa.

4.2.10 Confirming full-length A. baylyi C-terminal hexahistidine-tagged FtsA polymeric state via size exclusion chromatography

Once the protein was concentrated, a size exclusion column was used to check the homogeneity of the sample. Homogeneity of the sample is essential as aggregation of the protein in the sample would not create good diffracting crystals and also would not give the correct conclusion from any interaction studies. To check this, the concentrated sample of *A. baylyi* C-terminal hexa-histidine-tagged FtsA protein was applied to the size exclusion column and the protein eluted from the column in 314 minutes. For comparison, a standard curve was constructed by using four proteins of known molecular mass; lysozyme (14.3 kDa), proteinase K (28.93 kDa), bovine serum

albumin (BSA) (66.464 kDa) and catalase (250 kDa). Since size exclusion chromatography works by the principle of separating protein based on size, the standard proteins eluted with time 1110 (lysozyme), 877 (proteinase K), 560 (BSA), 489 (catalase) minutes. Comparing the elution time of the purified *A. baylyi* C-terminal hexa-histidine-tagged FtsA (314 minutes) with the four standard proteins, the FtsA protein eluted outside the range of the standard proteins. This shows that the FtsA protein is forming a high-order structure that is bigger than 250 kDa. This is an indication that the full-length *Acinetobacter* FtsA protein is aggregated and is likely caused by the presence of a MTS. This might also explain why Dr Amy Bottomley found some of the protein sticking to the membrane filter of the vivaspin column she used for concentrating proteins.

At this time, the purification protocol of *A. baylyi* C-terminal hexahistidine-tagged FtsA had been optimized. Unfortunately, the size exclusion chromatography data suggests that the protein is aggregated and had formed high-ordered structure. Therefore, the protein is unsuitable to be used for further *in vitro* studies. At this stage of the project, I had spent about two years into my PhD candidature attempting to purify full-length FtsZ and FtsA from *A. baylyi*. In the interests of time and gaining positive results, a change in the focus of the project was required. The focus then became: understanding the potential of FtsZ as drug target through *in silico* analysis and conducting fragment-based drug discovery using FtsZ as the target. The former will be discussed in Chapter 5 and the later in Chapter 6.

4.3 Discussion

The protein side of the project started with creating several constructs of the *Acinetobacter* FtsZ and FtsA to optimize the chances of obtaining overexpression constructs that would: (i) produce high quality, diffractive crystals; (ii) be active and interact with FtsA/FtsZ *in vitro*; (iii) co-crystallize with FtsA/FtsZ. It was decided that full-length FtsZ and FtsA be used in the co-crystallization experiment because, apart from the published interaction of *T. maritima* FtsZ peptide with FtsA, there is no published data showing a direct interaction between the two full-length proteins. Added to that, it cannot be assumed that FtsZ in *Acinetobacter* only interacts with the extreme C-terminal region and that the *Acinetobacter* FtsA contains a MTS. Since the aim of the project was to understand the interaction of the *Acinetobacter* FtsZ and FtsA in detail, it was deemed appropriate to use the full-length proteins.

In this project, the purification protocol for both the *Acinetobacter* FtsZ and FtsA proteins was successfully optimized and both proteins were purified. The purified FtsZ was used in a crystal trial but no acceptable-sized crystal for X-ray analysis was obtained. It was postulated that this is due to the presence of the disordered region in the C-terminus of full-length FtsZ possibly interfering with the packing of the protein to form crystals. Such phenomena are often observed for proteins that bind DNA or RNA, as they contain many disordered or flexible loops that interfere with the formation of a well-ordered crystal lattice (248). Bioinformatic prediction using PONDR suggested a presence of a disordered region in the C-terminus of the full-length *Acinetobacter* FtsZ protein (249). Attempts to remove the predicted disordered region was by conducting limited proteolysis in a trypsin digest experiment. This is a common solution for proteins with disordered regions, whereby removing the disordered region will allow the protein to pack together, forming a well-ordered crystal lattice (250).

This, however, still did not produce FtsZ crystals of acceptable size for structural analysis. Since the project aimed at characterizing the interaction of the *Acinetobacter* FtsZ and FtsA using full-length proteins, FtsZ crystallization was put on-hold and the focus was shifted to purifying the FtsA protein that is needed for examining the interaction with FtsZ.

Acinetobacter FtsA involved purifying the protein from insoluble aggregates known as inclusion bodies. It is not uncommon for proteins being overproduced in *E. coli* to accumulate and form these dense, insoluble aggregates (251). This is perhaps the main limiting factor of the *E. coli* expression system (252). After inclusion bodies were obtained, the most critical step in purifying proteins from these aggregates is the inclusion body solubilisation and protein refolding step (253). As this type of purification process is still mostly dependent on trial-and-error strategies (254), there is no standard protocol for this process. The protein purification protocols used in this study were developed at the laboratory of Professor Nick Dixon. The solubilisation and refolding buffer usually contains a chaotropic agent (253); in this case, urea. The refolding process on the nickel affinity column was conducted by slowly decreasing the amount of urea present in the sample, allowing the bound protein to refold slowly. Once the protein was refolded and eluted from the column, it was dialysed into a buffer containing 20% glycerol. It is reported in the literature that glycerol aids in the stabilization of proteins and prevention of their aggregation (246). Furthermore, glycerol also aids in refolding proteins. In this study, glycerol was not included in the refolding buffer but the protein was transferred into a buffer containing glycerol once it was refolded and this might have caused the protein to aggregate, evident in the subsequent size exclusion data. In the future it would be good to include glycerol in the refolding buffer.

An alternative solution to obtaining soluble overproduced FtsA would be to use certain fusion tags. Examples include the IMPACTTM (Intein Mediated Purification with an Affinity Chitin-binding Tag) system and His-SUMO (Small Ubiquitin-like Modifier) tag. The IMPACTTM system was used to purify full-length soluble *T. maritima* FtsA which was used in the interaction study with the *T. maritima* FtsZ peptide using both NMR and crystallography (110), while the His-SUMO tag was used to successfully to purify full-length soluble *E. coli* FtsA, and used in an interaction study with full-length *E. coli* FtsZ (255). The IMPACTTM system was initially tried by an honours student in the Harry Laboratory to purify full-length *Acinetobacter* FtsZ but was unsuccessful. Meanwhile, in this study full-length *Acinetobacter* FtsZ was successfully purified without the use of a protein tag. This indicates that when a certain tag is used to successfully purify FtsA of one species, it does not mean that the same tag can also be used to successfully purify FtsA from another species. Alternatively, different detergents in the purification buffer can also be tested to solubilise full-length *Acinetobacter* FtsA.

Another approach for understanding the *Acinetobacter* FtsZ and FtsA is to produce the *Acinetobacter* FtsZ peptide and also overproduce and purify only the 2B domain of the *Acinetobacter* FtsA. It is also possible to delete the MTS from the *Acinetobacter* FtsA and purify the cleaved protein for use in the interaction studies. As indicated in the result, it is possible that the MTS is the cause of the aggregation of the purified full-length *Acinetobacter* FtsA in this study. Deleting the MTS from the full-length FtsA protein should not cause a disruption for the *in vitro* interaction studies since the interaction of FtsZ and FtsA does not involve the MTS. Rather, the MTS is thought to act as an anchoring point for FtsZ to the cell membrane *in vivo* (247). In *E. coli*, the

MTS has also recently been shown to be involved in reshaping membrane architecture *in vitro* (256).

For years, targeting protein-protein interactions has been considered as a very difficult, if not impossible task (257). This chapter has revealed a small snapshot of the challenges associated with attempting to target protein-protein interaction. These include the need to: (i) purify full-length protein that is well-behaved, (ii) understand the details of the protein-protein interaction of interest and (iii) have the correct protein construct for structure determination using X-ray crystallography. Overall, both chapter 3 and chapter 4 have been a great learning experience in both the *in silico* and *in vitro* approaches for understanding protein-protein interactions. However, in the interest of time and for gaining positive result, the project focus was switched from targeting protein-protein interaction to a single target approach, which will be discussed in the next chapter.

Chapter 5 - *In silico* analysis of FtsZ crystal structures to better understand its potential as a drug target

Preface

Prior to reading this chapter, the reader should know that this chapter has now been accepted for publication by the “Australian Journal of Chemistry”. The formatting used in this chapter is like the submitted manuscript with slight changes to suite the thesis style of writing. These changes include the incorporation of a chapter and numbering system, as well as the methodology section used in this chapter being moved to Chapter 2 – Materials and Methods.

5.1 Introduction

Antibiotics underpin modern medicine; their use has reduced childhood mortality and increased life expectancy, and they are crucial for invasive surgery and treatments such as chemotherapy (34). However, the number of infections caused by multidrug-resistant bacteria is increasing globally, and the spectre of untreatable infections is becoming a reality. One measure to help alleviate this crisis is to develop new antimicrobials, with novel mechanisms of action. A process that is yet to be targeted by any of the clinically approved antibiotics is bacterial cell division, whereby one cell grows and replicates its genetic content, eventually splitting into two identical daughter cells. It has been shown that compounds which target this process, such as **PC190723**, are efficacious in clearing infections in animals (93, 143, 147, 156, 157).

Studies attempting to identify inhibitors of the bacterial cell division process have mainly focused on targeting the prokaryotic tubulin homologue (80), FtsZ, as it is an essential cell division protein (258) and is highly conserved among bacteria (125).

During cell division FtsZ is the first protein to be recruited to midcell to form a structure known as the Z-ring *via* self-polymerisation, which is promoted by the hydrolysis of GTP to GDP. The formation of the Z-ring is essential for the recruitment of downstream division proteins involved in splitting the dividing cell into two new cells. Inhibiting the polymerisation of FtsZ into the Z-ring has proved fruitful in the development of bacterial cell division inhibitors. However, whilst FtsZ has 40 – 50% amino acid sequence identity between different bacterial species (154), species-specific activity of FtsZ inhibitors, including PC190723, has been observed (93, 143, 147, 156, 157). This raises the possibility of inherent differences in the structure of FtsZ from one bacterial species to another, which may have implications in the development of a commercially viable broad-spectrum FtsZ inhibitor.

Currently, there appear to be three protein pockets within FtsZ that can bind molecules, collectively termed the druggable regions. They are the nucleotide-binding domain (NBD) (131), the synergistic T7-loop (132) and the interdomain cleft (133) (Figure 5.1). The nucleotide-binding domain has been successfully targeted by a C8-substituted GTP analogue that could selectively inhibit the GTPase activity of FtsZ, while having no effect on tubulin (131). The second druggable protein cleft, the T7-loop, has also been shown to bind small molecules, as predicted by the *in silico* modelling and STD-NMR studies for the binding of non-toxic cinnamaldehyde to FtsZ (132). The final druggable region, the interdomain cleft between the central core helix (H7-helix) and the C-terminal domain (Figure 5.1), has also been successfully inhibited by the compound, **PC190723** (80). A computational study conducted by Ballu *et al.* found that Val 207, Leu 209 and Asn 263, which are located in the interdomain cleft are very important for the binding of inhibitors in this region of the protein (259).

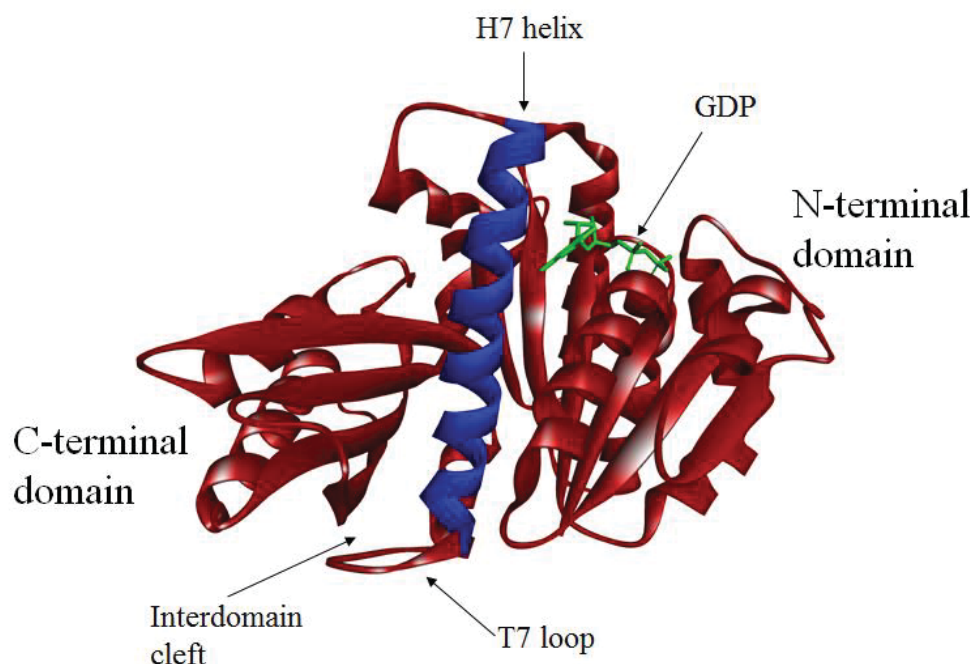


Figure 5.1: Druggable regions of FtsZ. Protein Data Bank entry 2VAP (81). Cartoon representation of *M. jannaschii* GDP-bound FtsZ resolved at 1.7 Å. FtsZ consists of N- and C-terminal domains (coloured red) that are divided by a central helix called the H7 helix (coloured blue). The NBD of the protein is located in the N-terminal domain and the protein is bound to GDP (green sticks).

In this chapter, the molecular modelling software Discovery Studio 4.5 (DS 4.5) (229) was used to examine published FtsZ X-ray crystal structures from both Gram-positive and Gram-negative bacterial species to firstly, closely examine the structural differences and similarities between multiple FtsZ proteins and secondly, to identify species specific and conserved pockets within FtsZ across different species that can potentially be targeted by narrow- and broad-spectrum antibiotics, respectively. Thirdly, the effect of **PC190723** on the structure and dynamics of FtsZ will also be examined.

5.2 Results and Discussion: *in silico* analysis of FtsZ structures from different bacterial species

5.2.1 Comparison of GDP-bound FtsZ structures from different bacterial species

5.2.1.1 Superimposition of published FtsZ X-ray crystal structures

Crystal structures of GDP-bound FtsZ of *Staphylococcus aureus*, *Staphylococcus epidermidis*, *Mycobacteria tuberculosis*, *Bacillus subtilis*, *Pseudomonas aeruginosa* and *Aquifex aeolicus* were obtained from the Brookhaven Protein Data Bank (PDB), imported into DS 4.5 and their amino acid sequences aligned. GDP-bound FtsZ were used because many FtsZ crystal structures are bound to GDP and this would be the closest representation of *in vivo* FtsZ. Following the amino acid sequence alignment, the tertiary structures of these FtsZ proteins and human tubulin were compared and analysed. Comparison of the tertiary structure of the various FtsZ proteins showed differences between species. C α atom superimposition of the FtsZ structures onto the crystal structure of *S. epidermidis* FtsZ (PDB: 4M8I (187)), which was used as a reference due to its high resolution (R = 1.43 Å), showed the staphylococcal FtsZ to be structurally similar to each other, while the non-staphylococcal slightly differ to that of the staphylococcal FtsZ (Figure 5.2A). The major difference between them lies in the β -sheet organisation at the C-terminus (region circled in red in Figure 5.2A). The C-terminal β -sheets of FtsZ from the staphylococcal genus are well-aligned, while the β -sheets in non-staphylococcal FtsZ have a degree of curvature and disorganisation. The C α RMSD, which is defined as the measure of the average distance between the alpha-carbon atoms of the superimposed FtsZ species, is ~ 3 Å, indicating a degree of variability between the tertiary structures of the multiple FtsZ species (Table 5.1). A low RMSD value of 0.3 Å was obtained from the superimposition of the staphylococcal FtsZs, while an RMSD value of ~ 1.3 Å was obtained when the non-staphylococcal

FtsZs were superimposed (RMSD^a and RMSD^b in Table 5.1). This indicates very low degree of variability between the staphylococcal FtsZ, while more variability exists between the non-staphylococcal FtsZ proteins, which are, however, still quite similar to each other.

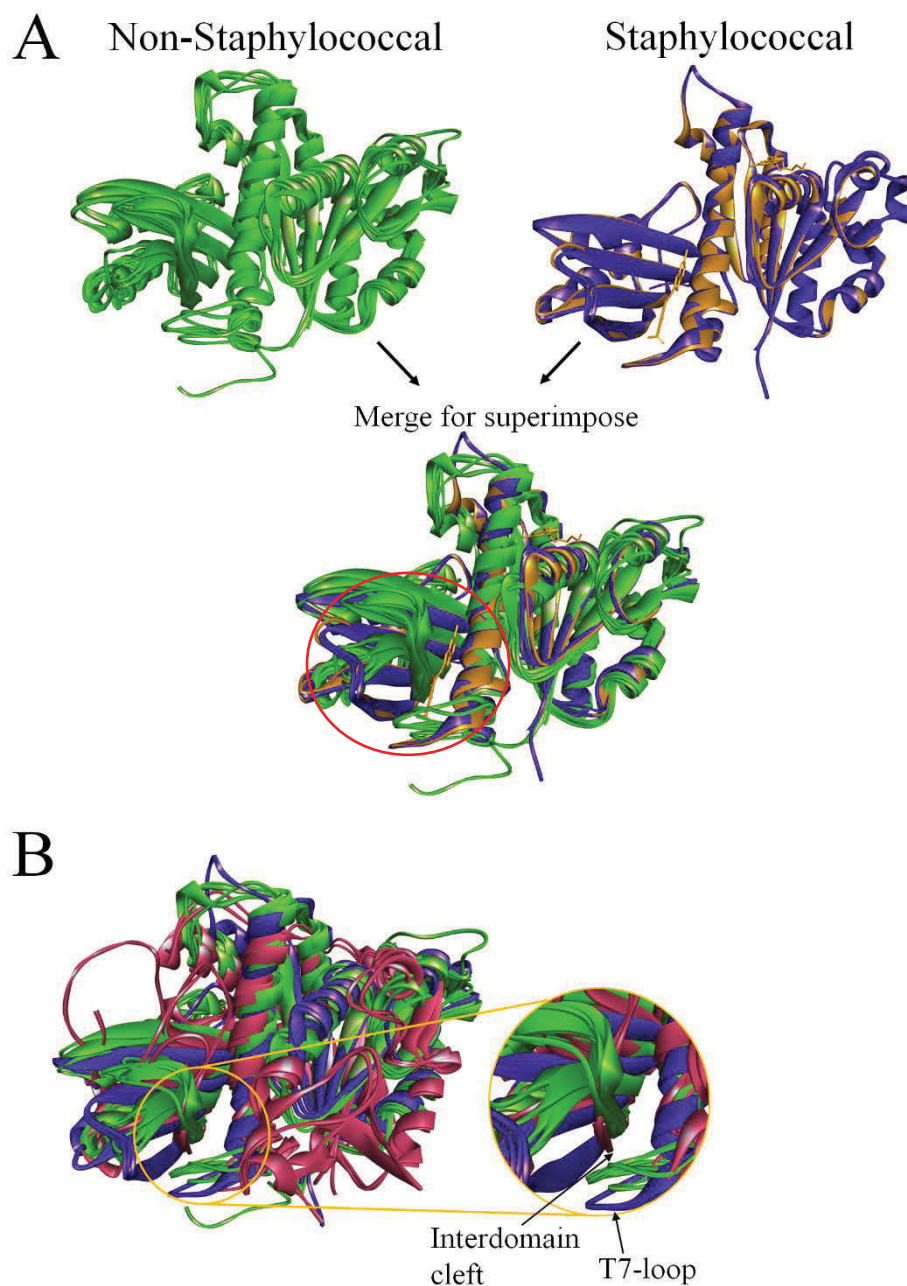


Figure 5.2: Superimposition of FtsZ from various organisms and of FtsZ structures with human α - and β -tubulin. (A) FtsZ structures can be classified into two categories: staphylococcal (purple is GDP-bound and gold is the *S. aureus* GDP-bound FtsZ structure co-crystallized with PC190723) and non-staphylococcal class (green). Superimposing the two different FtsZ groups (staphylococcal and non-staphylococcal) showed non-overlapping region at the C-terminus and later half of the H7-helix (region circled in red). (B) Superimposing eight bacterial FtsZ proteins (non-staphylococcal and staphylococcal class coloured in green and purple, respectively) with human α - and β -tubulin (coloured in pink) shows that there are structural differences between the two. The main difference between the FtsZ and tubulin can be seen in the presence of the interdomain cleft in FtsZ and also the T7-loop, which are absent in tubulin (denoted by arrows).

Table 5.1: RMSD values obtained from the superimposition of FtsZ and tubulin structures.

Organism	PDB ID	R (Å)	Wilson B-factor (Å ²)	RMSD ^a (Å)	RMSD ^b (Å)	Number of Residues used in superimposition
<i>M. tuberculosis</i>	1RQ7	2.60	33.70	3.02	N/A	300
<i>M. tuberculosis</i>	4KWE	2.91	108.20	3.19	0.97	305
<i>P. aeruginosa</i>	2VAW	2.90	51.80	2.80	1.24	305
<i>A. aeolicus</i>	2R6R	1.70	16.60	3.82	1.71	310
<i>B. subtilis</i>	2RHL	2.45	54.20	3.20	1.34	305
<i>S. aureus</i>	3VO8	2.26	28.70	0.31	-	305
<i>S. aureus</i>	3VOA	1.73	20.00	0.27	-	305
<i>S. aureus</i>	3VOB*	2.70	25.50	0.39	-	304
<i>S. epidermidis</i>	4M8I	1.43	20.80	N/A	-	300
<i>H. sapiens</i> <i>α-tubulin</i>	5ITZ (Alpha-1B chain)	2.20	34.50	10.13	8.61	311
<i>H. sapiens</i> <i>β-tubulin</i>	5ITZ (Beta-2B chain)	2.20	34.50	9.28	8.48	311

^aThe *S. epidermidis* FtsZ structure (PDB ID: 4M8I) was used as a reference protein.

^bThe *M. tuberculosis* FtsZ structure (PDB ID: 1RQ7) was used as a reference protein.

* The *S. aureus* GDP-bound FtsZ co-crystallized with the inhibitor **PC190723**.

N/A is not applicable

FtsZ and human α - and β -tubulin are structural homologues (80). However, the superimposition revealed structural differences between FtsZ and tubulin with an RMSD value of 8 to 10 Å between the different FtsZs and tubulin (Table 5.1). The main difference consisted of FtsZ having an interdomain cleft and T7-loop, which are absent in human tubulin (Figure 5.2B). One can speculate that, as a result, the FtsZ inhibitor PC190723, which binds to the interdomain cleft and T7 loop is unable to bind tubulin.

Identified druggable binding pockets of FtsZ X-ray structures were analysed. There are three identified pockets in FtsZ: the nucleotide-binding pocket, the interdomain cleft and the T7-loop. The pockets were identified in DS 4.5 as “binding-spheres”, and the radius of the sphere was measured. Statistical analysis using the two-variance test found that the radii of the nucleotide-binding pockets between the two FtsZ classes are not significantly different ($p > 0.05$), with the staphylococcal FtsZ having a mean sphere radius value of 11 Å, and the non-staphylococcal structures having a mean value of 9 Å (Figure 5.3A). This was expected, as the site is occupied by GTP or GDP and is crucial for the function of the protein. Similarly, the radii of the binding-sphere of the T7-loops are not significantly different ($p > 0.05$), with the staphylococcal FtsZ having a mean value of 5.3 Å, while the non-staphylococcal FtsZ have a mean value of 4.9 Å (Figure 5.3B). It is worth noting that the number of amino acids that form the T7-loop is the same for all analysed FtsZ structures (six residues). These six residues are usually found in position 201 to 206 or 204 to 209 and have a consensus sequence of P(S) G X I(V) N V(L). Due to this conserved nature of both the NBD and T7-loop, the possibility arises of creating broad-spectrum antibiotics by targeting these FtsZ pockets. Molecules such as a C8-substituted GTP analogue, have been shown to selectively inhibit FtsZ without affecting tubulin (131), indicating the potential to safely use the NBD for broad-spectrum antibiotics. For now, apart from cinnamaldehyde (132), no other molecule is known to target the T7-loop.

The interdomain cleft is important and yet was not straightforward to measure by using the sphere method as it consists of multiple smaller pockets within the cleft. Alternatively, the opening size of the interdomain cleft was measured across all FtsZ structures as this provides some insight into the accessibility of the cleft for inhibition. Staphylococcal FtsZ was found to have the widest opening of the interdomain cleft at

20.53 Å (PDB: 3VO8) and 20.84 Å (PDB: 3VOA). The size of the opening of the interdomain cleft of *S. epidermidis* FtsZ was measured to be 21.33 Å (Figure 5.3C). The opening of the interdomain clefts of FtsZ from *B. subtilis*, *M. tuberculosis*, *A. aeolicus* and *P. aeruginosa* were 9 to 10 Å (Figure 5.3C). The difference observed in the opening size of the interdomain cleft could possibly explain the strong affinity **PC190723** has towards *S. aureus* FtsZ and not other FtsZ species. It has also been shown that **PC190723** can inhibit FtsZ of *B. subtilis* (157) and although the opening size of the interdomain cleft of *B. subtilis* FtsZ is different to that of *S. aureus* FtsZ, **PC190723** was able to insert itself into the interdomain cleft of *B. subtilis* FtsZ and inhibit its function. It appears that *B. subtilis* FtsZ will need to open its interdomain cleft and allow **PC190723** to insert itself. Further explanation of how the protein may allow the compound to enter the interdomain cleft is described further in the molecular dynamics simulation section (Section 5.2.3).

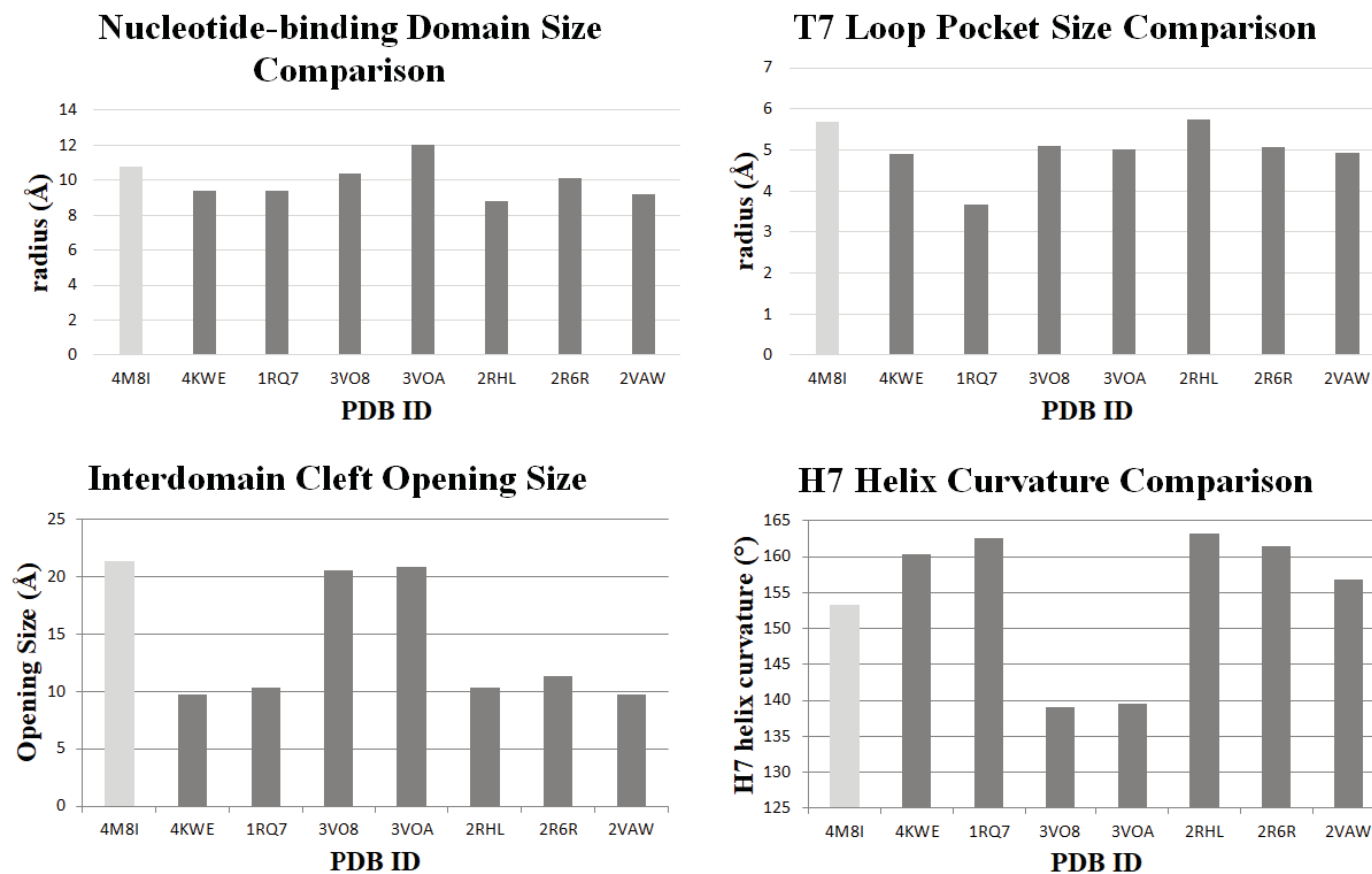


Figure 5.3: Comparison of druggable pocket sizes between FtsZ from different organisms. The size of the NBD (A) and T7-loop (B) were similar in all structures ($p > 0.05$). (C) The interdomain cleft was largest in FtsZ of the staphylococcal species. (D) The H7-helix of the staphylococcal species was the most curved, with the H7 of *S. aureus* being more curved than that of *S. epidermidis*. 4M8I: *S. epidermidis*; 4KWE and 1RQ7: *M. tuberculosis*; 3VO8 and 3VOA: *S. aureus*; 2RHL: *B. subtilis*; 2R6R: *A. aeolicus*; 2VAW: *P. aeruginosa*. The lighter coloured bar of *S. epidermidis* was used as the reference in the comparisons.

The superimposition of the FtsZ crystal structures (refer to Section 5.2.1.1), showed variation of the lower-half of the core H7-helix, towards the T7-loop, between staphylococcal and non-staphylococcal FtsZs (Figure 5.2A). To investigate this further, the angle of curvature of the H7-helix was measured (refer to Chapter 2 Section 2.2.3.5). The degree of curvature in the H7-helix can influence the size and shape of the interdomain cleft. The FtsZ structures of the staphylococcal class had a more curved central H7-helix in comparison to the non-staphylococcal FtsZ. This was particularly true for *S. aureus* FtsZ, where the angle of curvature was 139°, while FtsZ from other bacterial species had a curvature of 156 to 160°. The H7-helix in *S. epidermidis* has a lower degree of curvature than the H7-helix in *S. aureus* but is still more curved than in other FtsZ of different species (Figure 5.3D). The two-variance statistical analysis test showed that there is a significant difference in the angle of curvature between the H7-helix of the staphylococcal and non-staphylococcal FtsZ proteins ($p < 0.05$). Conducting a Pearson-Correlation test of the H7 curvature and the size of the interdomain cleft opening showed a strong inverse relationship ($p < 0.05$; correlation coefficient = -0.82), indicating that accessibility to the interdomain cleft is different for FtsZ from the two classes. Together, this data has shown that there are structural differences between FtsZ from diverse bacterial species, which may influence the binding affinity of compounds to this region. It is therefore imperative to obtain FtsZ crystallographic data for clinically-important organisms for the purpose of using the protein as a drug target.

5.2.1.3 Comparison of accessible binding sites between GDP-bound FtsZs from various bacterial species

Three locations within FtsZ are known to be druggable. However, for only one family of FtsZ inhibitor, the benzamide derivatives such as **PC190723** and **TXA707**, is there unequivocal evidence of its binding site, *via* X-ray crystal structure determination (93, 152). The structural diversity of FtsZ inhibitors points to the possibility of currently undetermined binding pockets within FtsZ. Novel accessible binding sites for the various GDP-bound FtsZ structures were identified using DS 4.5 as spheres. GDP was left in the crystal structures for this analysis to block the NBD from being identified as a binding site by the software for clarity of presentation.

This analysis identified the interdomain cleft and T7-loop as binding sites in all the GDP-bound FtsZ structures (arrow 1 in Figure 5.4). However, the spheres vary in size. This is supported by the previous results which showed different sizes and widths of the interdomain cleft. Apart from the spheres within the interdomain cleft and T7-loop, other binding spheres were found to vary in their locations for different FtsZ species.

In the *S. aureus* and *S. epidermidis* FtsZ structures, other binding spheres were detected around the α -helices near the NBD and the H7-central helix (arrow 2 in Figure 5.4). In the FtsZ structures of *B. subtilis* and *P. aeruginosa*, a sphere was seen to cover the area of α -helices towards the front of the nucleotide pocket (arrow 3 in Figure 5.4). In the *P. aeruginosa* FtsZ structure, another sphere (denoted by arrow 6) was observed below the sphere denoted with arrow 3, and this was observed only in the *P. aeruginosa* FtsZ structure. Another binding site in the *M. tuberculosis* FtsZ was identified towards the right of the nucleotide pocket (arrow 4 in Figure 5.4). Binding sites identified surrounding the NBD suggests that it is possible to target this region, without the need to target the NBD itself and hence no need to compete with GTP or GDP. Molecules

which bind these regions can be predicted to also inhibit the GTPase function of FtsZ as this region was shown to act as part of the catalytic switch in *M. tuberculosis* FtsZ (188).

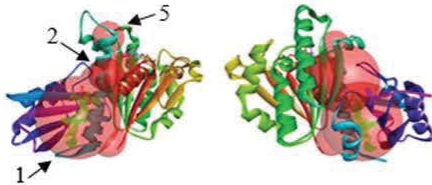
A sphere towards the left of the central H7-helix was also observed in the FtsZ structures from both *B. subtilis* and *A. aeolicus*. In *A. aeolicus*, other binding sites were suggested around the H7-helix and towards the back of the protein while the binding sites in the other FtsZ structures only covered regions on the front surface. This demonstrates that although there are conserved pockets within the different FtsZs, there could also be organism-specific pockets that might allow the creation of narrow-spectrum antibiotics for specific bacterial species. An intriguing idea for exploration is to search for druggable pockets that might exist in polymerized FtsZ, as it has never been explored previously.

One other potential binding site for a broad-spectrum antibiotic was observed at the top of FtsZ; T6-loop (arrow 5 in Figure 5.4). The sphere in this region was observed in all the FtsZ structures except *B. subtilis* and *P. aeruginosa*. Molecules which bind this pocket (arrow 5 in Figure 5.4) could possibly prevent FtsZ from polymerising entirely in a head-to-tail fashion. This could be achieved by blocking interaction between the T7-loop of one subunit with the catalytic site of another subunit (260). Amino acid sequence alignment of FtsZ from multiple bacterial species identified that this region has a different consensus sequence between Gram-positive and Gram-negative bacteria which can be exploited for therapeutic purposes (Figure 5.5). Overall, the consensus sequence that can be found in Gram-positive bacteria (more specifically, the Firmicutes) and Gram-negative bacteria (more specifically, the γ -proteobacteria) is V D K K(S/N) T P(S) and L G R G I S, respectively. Regardless, the multiple FtsZ sequence alignment also identified an FtsZ sequence from a Gram-negative bacterium

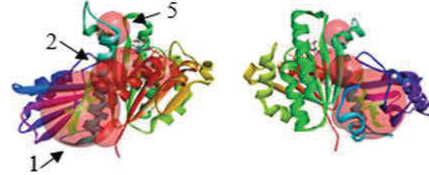
(*Leptospira interrogans*) that has the same consensus sequence as the Gram-positive Firmicutes. At present, no known FtsZ inhibitor has been shown to target this pocket.

Staphylococcal FtsZ

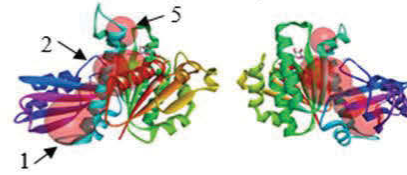
S. epidermidis (4M8I)



S. aureus (3VOA)

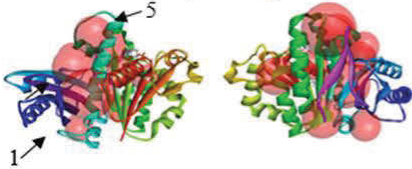


S. aureus (3VO8)

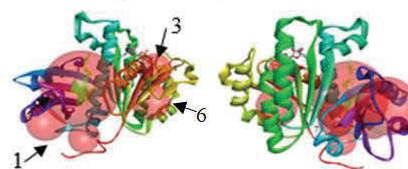


Non-Staphylococcal FtsZ

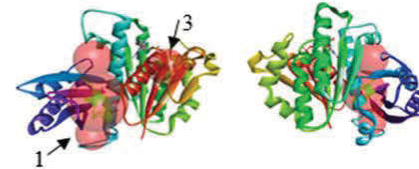
A. aeolicus (2R6R)



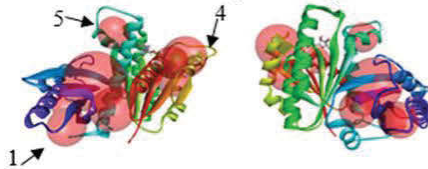
P. aeruginosa (2VAW)



B. subtilis (2RHL)



M. tuberculosis (4KWE)



M. tuberculosis (1RQ7)

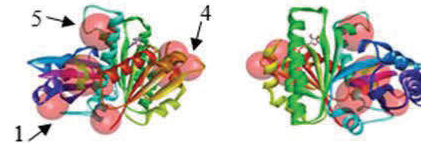


Figure 5.4: Comparison of the accessible binding sites of various GDP-bounded FtsZ structures. The available binding sites (red spheres) as identified by Discovery Studio 4.5. The locations of the spheres cover similar areas of the protein, but their sizes differ between the different FtsZ structures, especially in the area of the interdomain cleft (arrow 1). GDP was kept in the nucleotide-binding domain; hence no sphere is shown in its binding pocket.

<i>Helicobacter pylori</i>	RAEEGLKELEQSSDSILVIPNDKILLT	TMKKNASTTECYREVDDVLVRAVSGISTIITKPG	222
<i>Rickettsia typhi</i>	TADKGLIELQQFVDTLIVIPNQNLFR	IANEQTFADAFKMADDVLHAGVRGVTDLMIMPG	208
<i>Acinetobacter baumannii</i>	SAERGIEALEAHVDSLIIIPNQRLLSVYG-	DISMKDAYKKADDVLLNAVRSIFDLVVNRG	210
<i>Neisseria meningitidis</i>	VAQAGLEQLKEHVDSLIIIPNDKLM	TALGEDVTMREAFRAADNVLRDAVAGISEVVTCP	207
<i>Haemophilus influenzae</i>	FAELGIKDL SQYVDSMIIIPNQIQKVL	PKNAKLIDAFAAANDVLRNSVMGISDMITSPG	229
<i>Pseudomonas aeruginosa</i>	IADEGIRALAESVDSLITIPNEKLLT	ILGKDASLLAAFAKADDVLAGAVRGISDI	205
<i>Vibrio cholerae</i>	FAEQGIEELSKHVDSLITIPNEKLLKV	LGRGITLLEAFASANNVLKNAVQGIAELITRPG	205
<i>Escherichia coli</i>	FAEQGITELSKHVDSLITIPNDKLLKV	LGRGISLLDAFGAANDVLKGAVQGIAELITRPG	204
<i>Shigella flexneri</i>	FAEQGITELSKHVDSLITIPNDKLLKV	LGRGISLLDAFGAANDVLKGAVQGIAELITRPG	204
<i>Salmonella enterica</i>	FAEQGITELSKHVDSLITIPNDKLLKV	LGRGISLLDAFGAANDVLKGAVQGIAELITRPG	204
<i>Yersinia pestis</i>	FAEQGIAELSKHVDSLITIPNDKLLKV	LGRGISLLDAFGAANDVLKGAVQGIAELITRPG	204
<i>Campylobacter jejuni</i>	LAESGLLELKKESDSILVIQNEKLLS	IDKKAGIKDAFRLVDDILARAVKGMVSILLDNG	208
<i>Thermotoga maritima</i>	KAIEGLKKLRKHVDTLIKISNNKLMEEL	LPDRVKIKDAFLKADETLHQGVKGISELITKRG	215
<i>Leptospira interrogans</i>	FARKGIEQLRSHVDTLILINND	SIFRVVDKNTPIDLAFQVIDDILLNAV	206
<i>Mycobacterium tuberculosis</i>	QAENGIAALRESCDTLIVIPNDRLLQ	MGDAAVSLMDAFRSADENVLLNGVQG	202
<i>Streptococcus pneumoniae</i>	FAVEGINQLREHVDTLIIISNNLLEI	VDKKTPLLEALSEADNVLRQGVQG	206
<i>Clostridium botulinum</i>	HAEMGINTLKERVDTLVTIPNERLLS	VDKKTSLMDSFKLADDVLRQGVQGIS	205
<i>Staphylococcus aureus</i>	QAAAGVEAMKAAVDTLIVIPNDRLLD	IVDKSTPMMEAFKEADNVLRQGVQGIS	205
<i>Listeria monocytogenes</i>	QALTGTEAMKEAVDTLIVIPNDRLLQ	IVDKNTPMLEAFREADNVLRQGVQGIS	205
<i>Bacillus anthracis</i>	QAASGIAAFKENVDTLIVIPNDRLL	IVDKNTPMLEAFREADNVLRQGVQGIS	205
<i>Bacillus subtilis</i>	QAAGGISAMKEAVDTLIVIPNDRILE	IVDKNTPMLEAFREADNVLRQGVQGIS	205

Figure 5.5: Amino acid sequence alignment of the T6-loop from multiple bacterial species using Clustal Omega. The T6-loop region (red box) consensus sequence was seen to be conserved within the Gram-negative γ -proteobacteria (pink) and Gram-positive Firmicutes (cyan). The Gram-negative *Leptospira interrogans* has the same consensus sequence as the Firmicutes. DS 4.5 identified the T6-loop to be a possible binding site in all analysed FtsZ structures, suggesting the potential of this site as a target for broad-spectrum antibiotics.

5.2.2 Comparing GTP and GDP-bound FtsZ of various bacterial species

5.2.2.1 Comparison of GTP- and GDP-bound FtsZ structures

Polymerised FtsZ is known to undergo a curved and straight conformation in response to presence of GTP and GDP in the NBD (261), respectively, but the translation of this change to the structure of FtsZ is yet to be understood. For this, the GDP-bound FtsZ structures were compared with the corresponding GTP-bound structures. To date, there are only four GDP-bound FtsZ structures available of which the corresponding GTP-bound structures are also available. These GTP-bound structures are from *M. tuberculosis* (PDB: 2Q1Y and 1RLU (188)), *S. aureus* (PDB: 3WGN (262)), *B. subtilis* (PDB: 2RHO (190)) and *A. aeolicus* (PDB: 2R75 (131)). The opening of the interdomain cleft and the H7 helix angle of curvature were compared. The analysis did not show any changes in the angle of curvature of the H7-helix and most of the widths of the opening of the interdomain cleft showed no detectable changes between the GDP- and GTP-bound structures or for the *S. aureus* FtsZ structure bound with **PC190723** (Table 5.3). This suggests that it might not be possible to detect structural changes on FtsZ by solely analysing the crystal structures since macromolecular structure may be completely correct in crystallographic terms, yet may not correspond to the biologically relevant state of the molecule (263). Therefore, to further investigate this matter, the analysis was conducted using the “binding sphere” method and followed by molecular dynamics simulation.

Table 5.2: FtsZ structural differences between the GDP- and GTP-bound states.

Organism	PDB ID	GDP		PDB ID	GTP	
		H7 curvature (°)	Size of IDC opening (Å)		H7 curvature (°)	Size of IDC opening (Å)
<i>S. epidermidis</i>	4M8I	153.30	12.40	-	-	-
<i>M. tuberculosis</i>	4KWE	160.30	7.30	2Q1Y	160.00	9.60
	1RQ7	162.60	11.10	1RLU	159.20	10.90
<i>S. aureus</i>	3VO8	139.10	15.50	3WGN	140.30	15.90
	3VOA	139.60	16.80	-	-	-
	3VOB*	140.40	15.20	-	-	-
<i>B. subtilis</i>	2RHL	163.20	10.30	2RHO	164.50	7.50
<i>A. aeolicus</i>	2R6R	161.50	7.70	2R75	162.10	7.90
<i>P. aeruginosa</i>	2VAW	156.80	6.40	-	-	-

IDC = interdomain cleft. (-) = the structure is not available. * The *S. aureus* GDP-bound FtsZ co-crystallized with the inhibitor PC190723.

Analysis of the GTP- and GDP- bound *S. aureus* FtsZ suggests that the N-terminus of the protein shifted when occupied by the two different nucleotides and the interdomain cleft did not undergo changes when bound to either nucleotide (Figure 5.6). However, two spheres were observed to be present only in the GTP-bound structure (arrows 1 and 2 in Figure 5.6). The disappearance of these spheres further supports the movement of the N-terminus of the protein when exchanging between GTP and GDP.

This movement might be negligible in *S. aureus* FtsZ regarding access to the interdomain cleft, but it might be possible to inhibit protein function by inducing this movement and locking the protein into this conformation. Analysis of the structure of *S. aureus* FtsZ co-crystallised with **PC190723**, revealed a sphere which became larger only in the inhibitor-bound structure (arrow 3 in Figure 5.6). It should be noted that sphere 3 is positioned at the centre of the nucleotide-binding pocket, which is necessary for interlocking of the T7-loop from the upper monomer to the bottom monomer subunit

to stabilise the polymer structure. Enlargement of the sphere (arrow 3) implies that the optimum interactions of the T7-loop to the nucleotide-binding pocket might be significantly increased when *S. aureus* FtsZ is bound to **PC190723**. The resulting stronger interactions may strengthen the structural integrity of the FtsZ filaments. Supporting this idea is the GTP-dependent FtsZ polymerization assay conducted by Elsen *et al.* (156). They showed that **PC190723** causes FtsZ to lose its ability to assemble cooperatively and forces the protein to assemble in a non-cooperative manner. In the presence of the inhibitor in the interdomain cleft, the N-terminus of the protein was incapable of completing the shifting motion required during the exchange of nucleotides due to the enlargement of the pocket identified by sphere 3.

Sphere 4 is only observed for the inhibitor-bound structure and two other crystal structures of GDP- and GTP-bound FtsZ: those of *M. tuberculosis* FtsZ. Taking the two spheres (arrows 3 and 4 in Figure 5.6) into account; it is probable that the FtsZ inhibitor **PC190723** locks the *S. aureus* FtsZ into a protein state whereby FtsZ is forced to adopt the structural conformation between a GTP- and GDP-bound structural conformation. This state is termed the transition state or intermediary state.

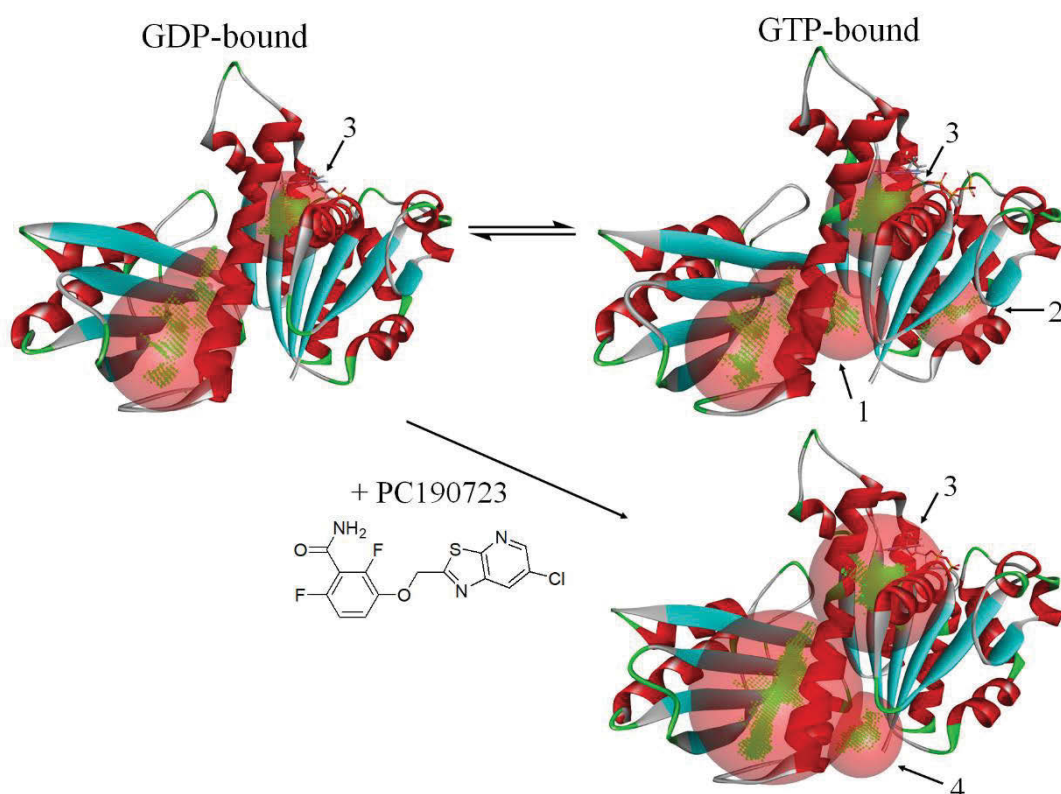


Figure 5.6: Analysis of the accessible binding sphere of *S. aureus* FtsZ when bound to different nucleotides and the FtsZ inhibitor PC190723. The interdomain cleft of the *S. aureus* FtsZ was not affected by the presence of the different nucleotides. The swapping of GTP to GDP causes structural changes at the N-terminus of the protein, seen by the disappearance of two spheres (arrows 1 and 2) when the protein is GDP-bound. Sphere 3 becomes larger in the FtsZ structure bound to the inhibitor **PC190723**. A unique sphere was observed only in the **PC190723**-bound structure (arrow 4).

5.2.2.2 Accessible binding site comparison of GTP- and GDP-bound non-staphylococcal FtsZ structures

Analysis of the accessible binding spheres from non-staphylococcal FtsZ which are bound to GDP and GTP showed differences. The sphere in the interdomain cleft of *B. subtilis* GTP- and GDP-bound FtsZ was seen to shift in position, while in the *M. tuberculosis* FtsZ the sphere was seen to change in size (arrow 1 in Figure 5.7). This suggests movement of the opening to the interdomain cleft which changes the accessibility of the pocket between the GDP- and GTP-bound states of the protein.

Furthermore, a sphere was observed to disappear between the GTP- and GDP-bound FtsZ structures from both *M. tuberculosis* and *B. subtilis* (arrow 2 in Figure 5.7). Correlating this with the shifting and size changing of the sphere in the interdomain cleft suggests that the movement of the N-terminal domain caused by the changing of nucleotides may result in the opening and closing of the interdomain cleft. The same analysis was conducted with the *A. aeolicus* FtsZ structures which are the only other non-staphylococcal FtsZ structures to have both GTP and GDP-bound to it. The analysis did not show any differences in the distribution and size of the binding spheres.

Another interesting sphere was observed at the bottom of the *M. tuberculosis* FtsZ structures; 2Q1Y and 1RQ7 (arrow 3 in Figure 5.7). This sphere was detected in GTP- or GDP-bound *M. tuberculosis* FtsZ structures but not crystal structures from other bacterial species. This, may indicate that the crystal structure with a sphere in this location might be a transitional form of the protein when switching between GTP to GDP. Another crystal structure in which this sphere is observable is PC190723-bound *S. aureus* FtsZ, suggesting that PC190723 locks *S. aureus* FtsZ in a transition state of the protein. This is further analysed in the molecular dynamics simulation section below (Section 5.2.3).

The observed changes in the binding spheres from the analysed FtsZ structures, suggest a model describing the structural changes of non-staphylococcal FtsZ upon binding to the different nucleotides (Figure 5.7). In the model, GTP-bound FtsZ has the widest opening of the interdomain cleft, allowing easy access to the interdomain cleft and T7-loop. As GTP is hydrolysed to GDP, the N-terminus of the protein shifts and results in the closing of the interdomain cleft. As long as GDP remains in the NBD, the interdomain cleft would stay closed. As a result, only the upper portion of the interdomain cleft is accessible while the T7-loop is not. However, the interdomain cleft

will revert to the open-form as soon as GTP is present in the NBD (Figure 5.7). Based on this model, the FtsZ crystal structures of *A. aeolicus* bound to GTP and GDP might both adopt the GDP-bound conformation. This is because FtsZ which has adopted the GDP-bound conformation changes to the GTP-bound conformation once GTP is present in the NBD.

The analysis of accessible binding spheres of both the staphylococcal and non-staphylococcal FtsZ crystal structures have shown that GTP and GDP cause structural changes to FtsZ which in turn affects the binding pockets located on the protein. Revealing this information for target-based drug discovery using FtsZ makes a valuable contribution to understanding the differently available binding pockets that may facilitate design and development of new FtsZ inhibitors using new chemical space groups than what has already been described in literature. The next section utilises molecular dynamics simulation to investigate the dynamics of staphylococcal and non-staphylococcal FtsZ bound to GTP and GDP and how they may differ. The next section also studies the mechanism of inhibition of **PC190723**.

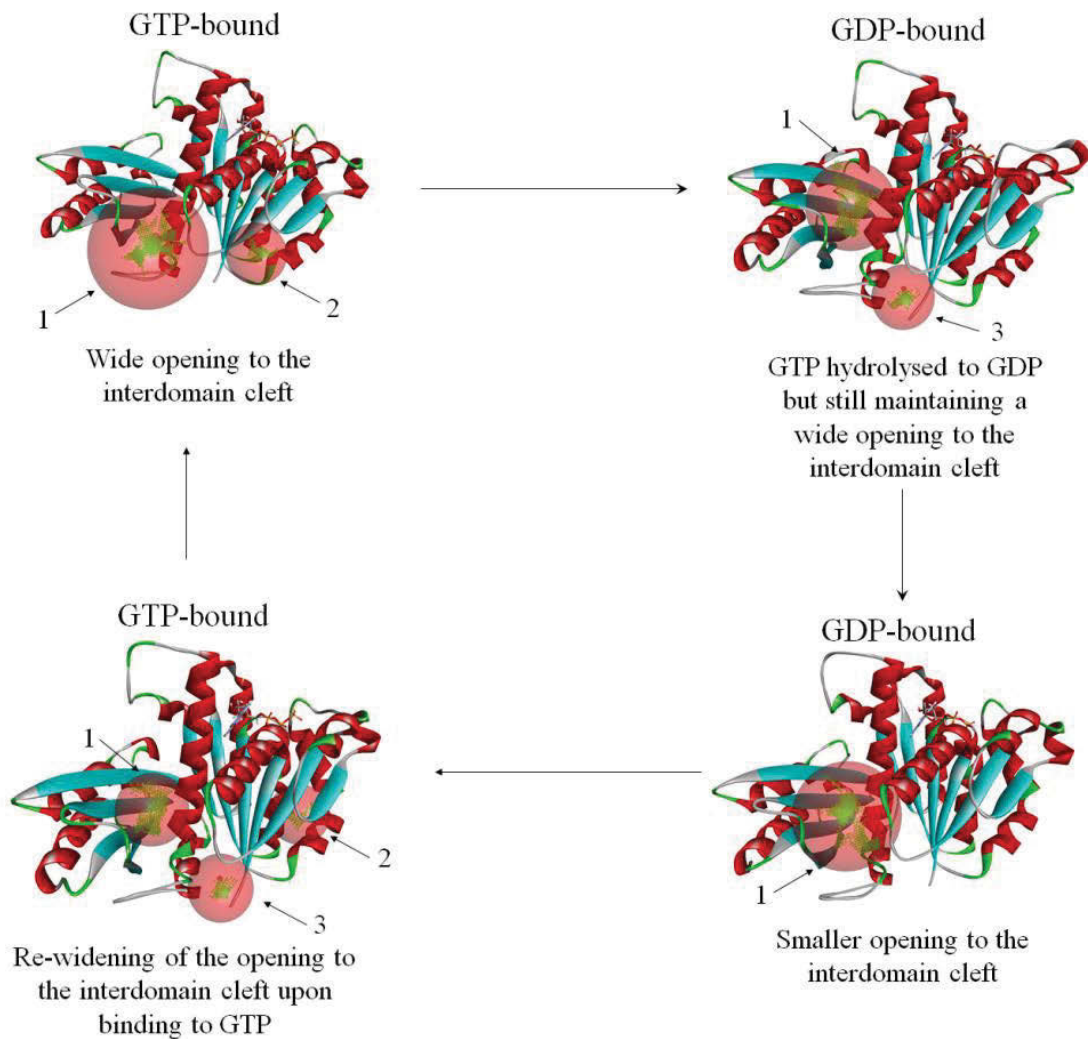


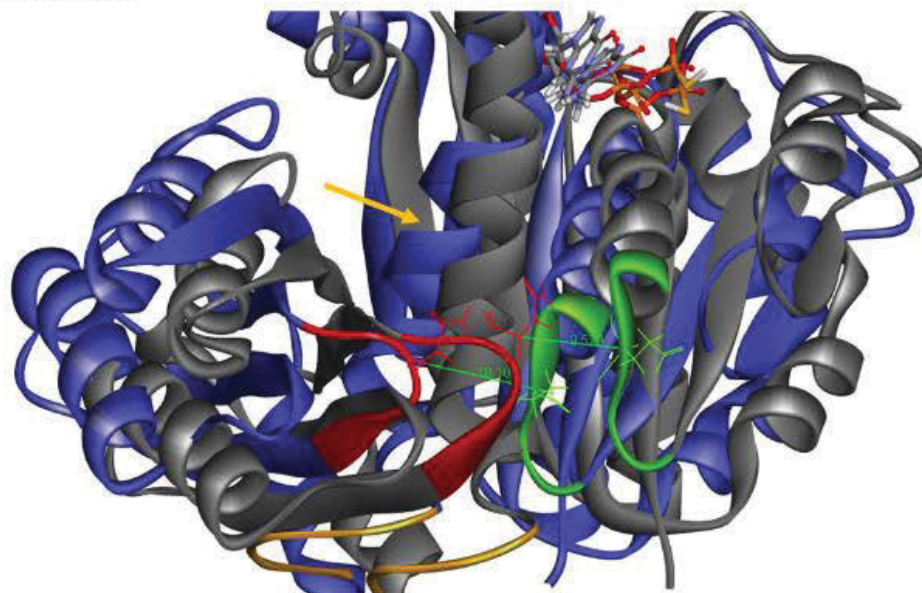
Figure 5.7: A model of structural changes in monomeric FtsZ upon binding to GDP and GTP. Both *B. subtilis* and *M. tuberculosis* FtsZ X-ray crystal structures bound to either GTP or GDP were analysed. A model of the molecular changes to the monomeric form of the protein upon binding to the different nucleotides is proposed. Upon binding to GTP, the entry to the interdomain cleft is wide open; observed as having the biggest binding sphere (arrow 1). As GTP is hydrolysed to GDP, N-terminal of the protein shifts and starts to close the interdomain cleft; observed as a narrowing of the binding sphere (arrow 1). The process of shifting in the N-terminal region sees that sphere 2 disappear upon binding to GDP and as the protein reaching equilibrium during GDP-bounded state, sphere 3 can be observed. As the protein reaches equilibrium in its GDP-bound state, the opening to the interdomain cleft is the smallest. As GTP is re-introduced to the protein, the N-terminal shifts again, allowing sphere 2 to re-emerge and as the protein is opening the interdomain cleft, sphere 3 can be seen once again. The state where sphere 3 is observed is called the transition state.

5.2.3 Molecular dynamics simulation

The changes observed in the binding sites analysis point to a possible conformational change of the protein upon binding to the different nucleotides. The phenomenon of closing and opening of the interdomain cleft of FtsZ was first described by computational analysis and mutational study of *M. jannaschii* FtsZ (264). Recently, a similar mechanism was described in the *S. aureus* FtsZ structure by Wagstaff *et al.* (265). Both studies agreed that FtsZ could exist in the two conformations; namely a closed and an open form. In this section, this knowledge was applied for understanding how **PC190723** inhibits *S. aureus* FtsZ, as well as understanding how **PC190723** is able to bind *B. subtilis* FtsZ, despite the differing accessibility to its interdomain cleft compared to the *S. aureus* FtsZ.

The open and closed conformation was observed when FtsZ was bound to GTP and GDP, respectively. Through molecular dynamics simulations in this study, two mechanisms were observed for the opening and closing, depending on the FtsZ class; staphylococcal or non-staphylococcal. Molecular dynamics simulation of *M. tuberculosis* and *B. subtilis* FtsZ structures showed that accessibility to the interdomain cleft and T7-loop might be regulated differently in the non-staphylococcal FtsZ compared to the staphylococcal FtsZ. In the molecular dynamics simulation of *B. subtilis* FtsZ, the interdomain cleft opening was maintained at ~10 Å (Figure 5.8). The opening and closing of the cleft were caused by the twisting of the H7-helix (orange arrows in Figure 5.8). Movement of the N-terminal domain of the protein allowed the H7-helix to twist and resulted in the shifting of the C-terminal domain.

Frontal



Top

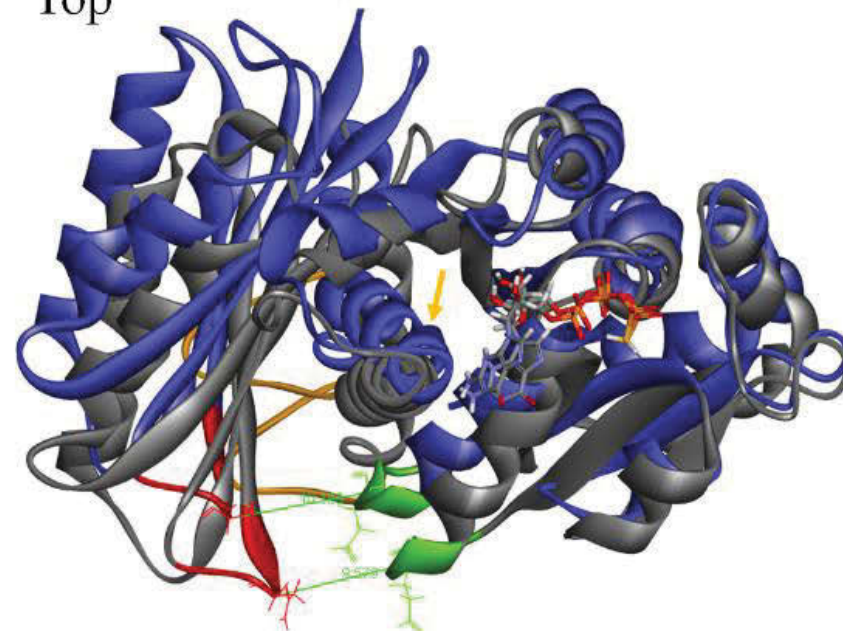


Figure 5.8: Conformational change of *B. subtilis* FtsZ. Blue and grey coloured structures represent snapshots of *B. subtilis* FtsZ taken at 100 ps and 500 ps, respectively. The opening size of the interdomain cleft was maintained at ~ 10 Å during the simulation. Twisting of the H7-helix (orange arrows) towards the back of the protein resulted in the opening of the interdomain cleft and movement of the red and green coloured loops. The H7-helix was seen to be most twisted at 100 ps and then relaxed at 500 ps. GTP is represented as coloured sticks and the T7-loop is coloured orange.

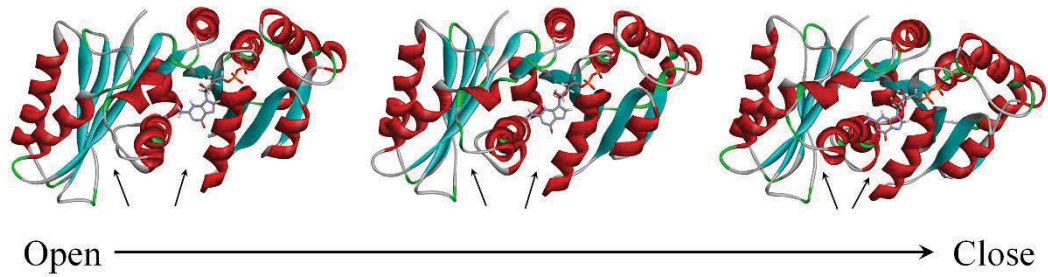
The frame collected at 100 ps during the simulation with the GTP-bound *B. subtilis* FtsZ started with a very twisted H7-helix, compressing itself towards the back of the protein (Top view in Figure 5.8). As the simulation reached 500 ps, the H7-helix was seen to relax, shifting the loop formed by amino acid residue 299-303 in *B. subtilis* FtsZ up (in *M. tuberculosis* these are amino acid residue 296-300) (red loop in Figure 5.8). Simulation with the GDP-bound *B. subtilis* FtsZ structure showed the reverse of this motion. The simulation was also conducted with the GTP- and GDP-bound *M. tuberculosis* FtsZ structures and the results obtained reflect those obtained from the simulation with GDP-bound *B. subtilis* FtsZ structures. Based on this data, it can be concluded that *B. subtilis* FtsZ is very similar to *M. tuberculosis* FtsZ. Therefore, it is possible that **PC190723** is also able to bind the interdomain cleft of *M. tuberculosis* FtsZ. This, however, is something that is yet to be tested.

The motion observed in the simulations using non-staphylococcal FtsZ might explain the method for incorporation of **PC190723** into the interdomain cleft of *B. subtilis* FtsZ. As GDP occupies the NBD, the H7-helix relaxes and the loop shifts up (red loop in Figure 5.8), blocking access to the lower part of the interdomain cleft and T7-loop and therefore would most likely block **PC190723** from entering. With the binding of GTP to the protein, the H7-helix twists towards the back of the protein and the T7-loop once again shifts down; allowing access to the lower part of the interdomain cleft and T7-loop (Figure 5.8), consequently opening up enough space for **PC190723** to slot itself in and bind. Added to that, the work conducted by Miguel *et al.* provided additional information as to why **PC190723** also binds *B. subtilis* FtsZ. They found that the interdomain cleft chemical environment of the *B. subtilis* structure is very similar to that of *S. aureus* FtsZ (135), which further facilitates the binding of **PC190723** to *B. subtilis* FtsZ. Therefore, we can conclude that the binding of **PC190723** to FtsZ species

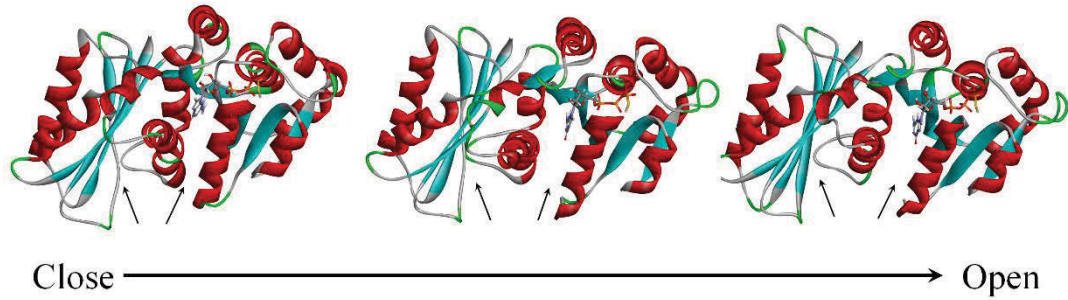
requires both sufficient accessibility of the interdomain cleft and also the appropriate chemical environment for binding.

Molecular dynamics simulation conducted with *S. aureus* FtsZ structures revealed a slightly different mechanism to that of the non-Staphylococcal FtsZ. The opening and closing movement of the *S. aureus* FtsZ protein can be described as that of a sliding door, which is also caused by the twisting of the H7-helix (Figure 5.9). The N- and C-termini were observed to move closer to the central H7-helix when bound to GDP and move away from the H7-helix when bound to GTP (Figure 5.9). As a result, the opening size of the interdomain cleft changes (Figure 5.10). A molecular dynamics study conducted by Miguel *et al.* (135) proposed that **PC190723** binds with higher affinity to GTP-bound *S. aureus* FtsZ compared to GDP-bound. The data obtained in this study provides a possible explanation for this as the GTP-bound *S. aureus* FtsZ adopted a wider opening of the interdomain cleft than the GDP-bound structure, facilitating **PC190723** binding within the cleft.

GDP-bound



GTP-bound



PC190723-bound

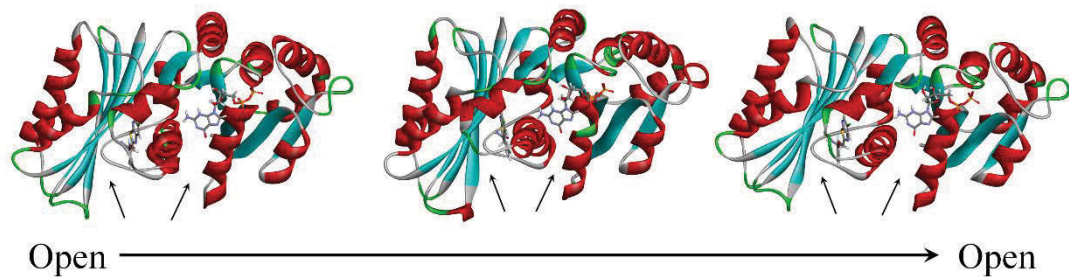


Figure 5.9: Conformational change of *S. aureus* FtsZ when bound to nucleotides and an inhibitor. Molecular dynamics simulation using the GTP- (PDB: 3WGN) and GDP-bound (PDB: 3VOA and 3VO8) *S. aureus* FtsZ structures revealed a sliding-door movement of the N- and C-terminus of the protein; opening and closing the area around the central H7-helix (indicated by arrows). The binding of **PC190723** (PDB: 3VOB) in the interdomain cleft inhibits the ability of the GDP-bound FtsZ structure to form the closed-conformation. The orientation of the protein structures is all the same, looking from the top of the protein. The structural change caused by the opening and closing movement of the protein structures could give out an illusion that the orientation in the different panels are not the same.

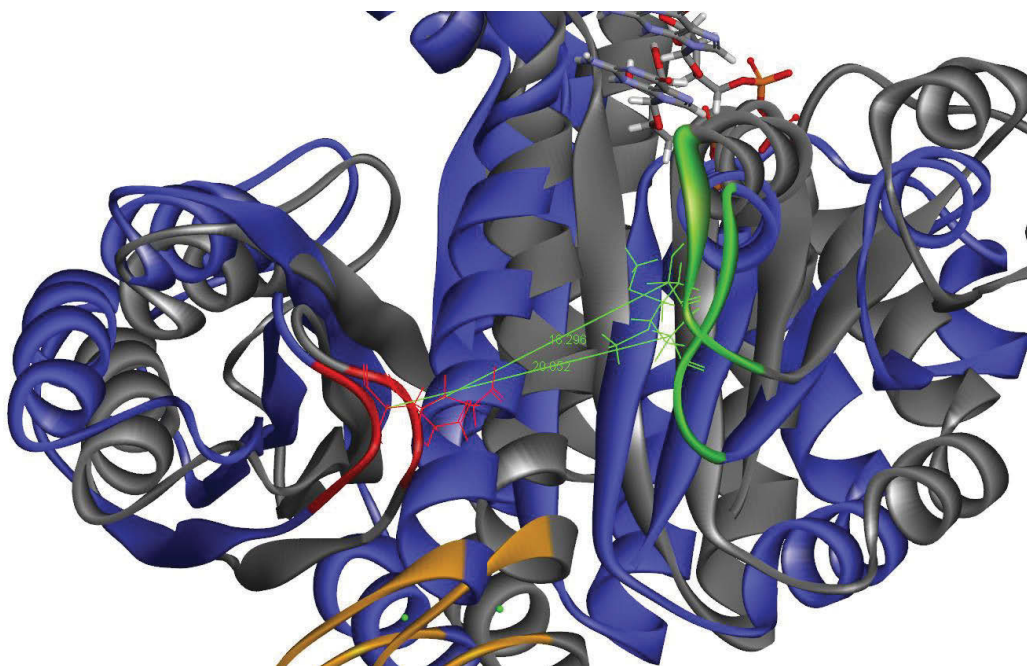


Figure 5.10: Conformational change of *S. aureus* FtsZ. Blue and gray coloured structures represent snapshots of *S. aureus* FtsZ taken at 150 ps and 300 ps, respectively. Opening size of the interdomain cleft changed from 20 Å to 18 Å (green numbers). The H7-helix was twisted at 150 ps, stretching the opening size of the interdomain cleft to ~20 Å. As the H7-helix relaxes at 300 ps, the interdomain cleft opening size decreased to ~18 Å. GDP is represented as coloured sticks and the T7-loop is coloured orange. Calcium is represented as green balls.

Molecular dynamics simulation was also conducted with the **PC190723**-bound *S. aureus* FtsZ structure. During the simulation, it was observed that the presence of **PC190723** in the interdomain cleft of *S. aureus* FtsZ did not allow the protein to form the closed conformation, forcing it to continuously adopt the open conformation (Figure 5.9). As a result, the mechanism of inhibition of *S. aureus* FtsZ by **PC190723** is proposed to entail permanently locking the protein in the open conformation.

5.3 Conclusion

In this study, superimposition of the tertiary structure of FtsZ proteins from multiple bacterial species revealed that staphylococcal and non-staphylococcal FtsZ are structurally different based on the H7 helix curvature, as well as the organisation of β -sheets at the C-terminus. This has implications in drug discovery in that it cannot be assumed that compounds which are effective against, for example, the staphylococcal FtsZ, will also hit the non-staphylococcal FtsZ. In addition, this study has also demonstrated that if a compound binds to one of the non-staphylococcal FtsZ, it does not mean that it will hit every non-staphylococcal FtsZ as binding sites are likely to vary. However, that is not to say that it is impossible to create compounds with broad-spectrum activity, as this study has also shown that some binding sites, such as the NBD, are conserved between the FtsZ proteins. Most importantly, this study has shown that there is variability in the accessibility of the interdomain cleft and T7-loop between the FtsZ proteins. Most of the published FtsZ inhibitors are known to hit one of the three known druggable regions on FtsZ, the NBD, the interdomain cleft or the T7-loop. This study has shed some light into other possible binding sites on FtsZ, such as the area surrounding the NBD and T6-loop. Such information is vital and can be utilized to produce broad-spectrum antibiotics and identify opportunities for the exploration of new chemical space which can be used to target the new binding sites proposed in this study.

Chapter 6 - Fragment-based drug discovery using FtsZ as a target

6.1 Introduction

Studies of bacterial cell division inhibitors have mainly focused around FtsZ, as it is essential and highly conserved amongst bacteria. Furthermore, there are currently three potential drug binding regions on FtsZ termed “druggable regions” (the NBD (131), the interdomain cleft (133), and the T7-loop (132); see Figure 5.1 in Chapter 5) which many of the reported FtsZ inhibitors have been shown to bind to (Refer to Table 1 of Chapter 1). Refer to Chapter 1 Section 1.6 and Chapter 5 Section 5.1 for more in-depth information on these regions.

6.1.1 Inhibitors of FtsZ

Until today, many FtsZ inhibitors have been identified using the conventional high-throughput screening (HTS) of compounds (266) or rational drug design. These method has been the go-to approach for identifying lead compounds in antibacterial drug discovery projects (267). However, the major problem was that hits identified from HTS screening are functionally complex and make numerous but low-quality interactions (268). Due to this, HTS screening provided very few hits (0.1 %) (269, 270) and yielded false positives (271). There is a high attrition rate in HTS. It is estimated that the number of possible drug-like molecules is around 10^{63} (272) and HTS typically utilises a library of 10 million compounds, which seems rather paltry (273). A review by Payne *et al.* suggested that antibacterial drug discovery shift efforts towards chemically diverse libraries as sources of new antibacterials (120) and this is where fragment-based drug discovery (FBDD) enters.

6.1.2 Fragment-based drug discovery

Rather than screening millions of compounds to find hit compounds, FBDD begins with much smaller collections of chemically diverse inactive smaller molecules termed fragments, which can subsequently be assembled into active compounds (273). The method usually has a hit-rate of 30 to 50 times-higher than HTS (270). Furthermore, since the method utilises small molecules, it is possible to take advantage of the approach for use in identifying binding pockets on a target protein in which its druggable binding pocket is yet to be determined.

To ensure the likelihood of developing a lead compound, the fragments should be compliant to the “rule of three”, which states that a fragment should not exceed a molecular weight of 300 Da. Other filtering criteria such as H-bond donors ≤ 3 and H-bond acceptors ≤ 3 and cLogP ≤ 3 should also be considered to ensure high aqueous solubility during screening (268, 274). Furthermore, this would ensure that the assembled molecule is complying with the “rule of five”. The “rule of five” is another filtering criteria developed by Lipinski and it is used to evaluate the drug-like properties of a molecule. The “rule of five” states that a compound should not exceed a molecular weight of 500 Da, have H-bond donors ≤ 5 , H-bond acceptors ≤ 10 , and high aqueous solubility (cLogP ≤ 5) (275). Since these fragments are small, it is common for them to have weak binding affinity; usually in the millimolar (mM) or high micromolar (μ M) range. Therefore, high-resolution screening methods such as NMR and X-ray crystallography can be used to provide the precise location and orientation of each binding fragment in the protein pocket (276).

6.1.3 Requirements for a successful FBDD project

A successful FBDD program needs to meet several criteria. These include the requirement of a biomolecular target protein that is relatively stable and can be produced in milligram quantities, a well-constructed fragment library (277), one or more robust biophysical screening methods (278), and access to medicinal chemistry expertise to develop promising hits. A high-resolution structure of the target protein, determined by either X-ray crystallography or NMR spectroscopy, is a significant advantage. Equally important is high-quality structural information on the binding pose(s) of elaborated fragments as this is required to guide medicinal chemistry optimization. While this information can be obtained using X-ray crystallography (279, 280), there are numerous examples where visualization of the bound ligand in this way is not feasible because crystallization of the ligand-target complex is too slow or not feasible.

Examples of successful FBDD programs can be seen in the development of the drug Vemurafenib, a B-Raf (V600E) inhibitor developed by Plexxikon (Berkeley, CA, USA) for late-stage melanoma (281), and Venetoclax (ABT-199), as shown in Figure 6.1, which inhibits the interaction of Bcl-2 with its protein partners (282, 283). The FBDD approach has mostly been utilized in the discovery of anti-cancer drugs but this approach has also been utilized in the discovery of several antibacterials (284). Such examples include the amino-oxazole inhibiting Gram-negative biotin carboxylase (285) and the inhibitors of protein tyrosine phosphatase PtpA or antigen 85C of *M. tuberculosis* (Figure 6.2) (286, 287).

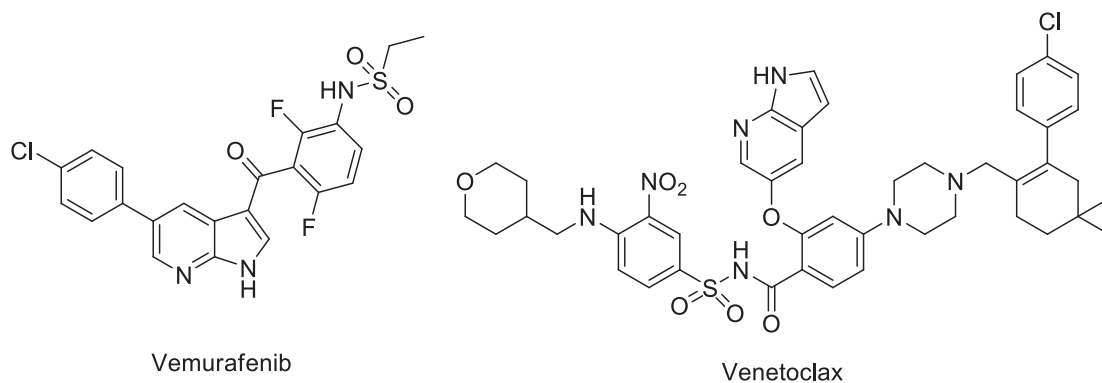


Figure 6.1: Chemical structure of Vemurafenib and Venetoclax. These two compounds were successfully created through fragment-based drug discovery as anti-cancer drugs.

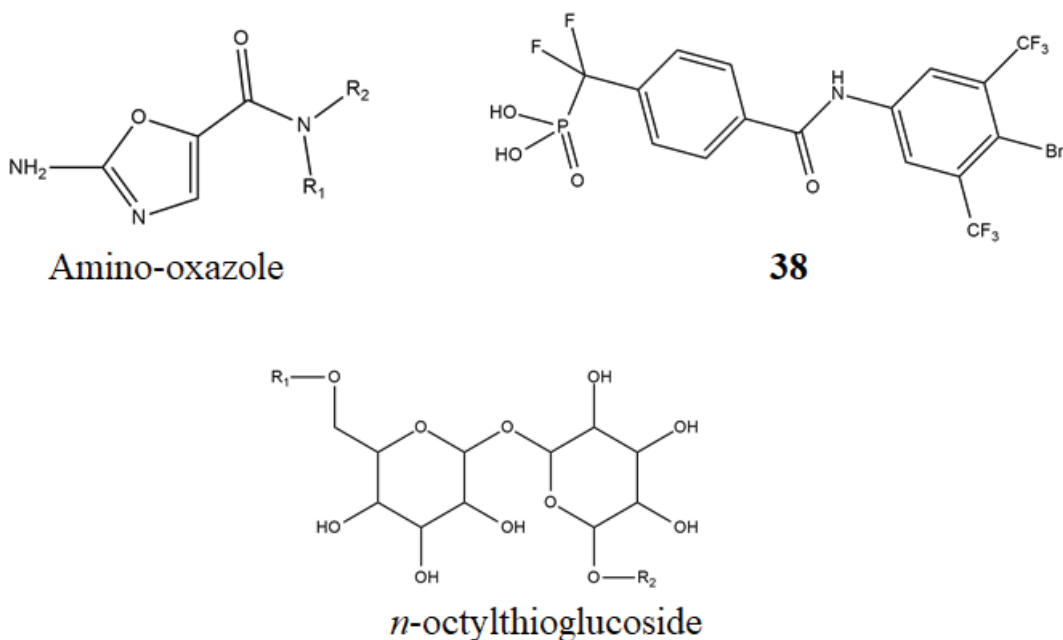


Figure 6.2: Examples of antibacterials that were developed from fragment-based drug discovery. Amino-oxazole is known to inhibit Gram-negative carboxylases. Meanwhile compound **38** and *n*-octylthioglucoside inhibits protein tyrosine phosphatase PtpA and antigen 85C of *Mycobacterium tuberculosis*.

6.1.4 Fragment-based drug screening using NMR

The FBDD process is summarized in Figure 6.3 and usually starts with screening a cocktail of ~1000 fragments for weak binding to the protein of interest using either STD-NMR or X-ray crystallography. After the first screening, the fragments carried

forward are further filtered in a follow-up screen using a method called triple-ligand detect. This method consists of three sets of independent NMR experiments: Water-Ligand Observed via Gradient Spectroscopy (Water-LOGSY); Carr, Purcell, Meibloom and Gill (CPMG) and STD; all of which record fragment spectra by utilising different properties of the sample. WaterLOGSY detects binding through the transfer of magnetisation from the water molecules to the ligand bound to the protein (288, 289). STD uses a pulse to saturate signals from methyl groups in the protein. The disturbance in magnetisation is then transferred to the bound ligand, with the resulting difference spectrum only showing a peak of the ligand when this binds to the protein target (288, 290). Finally, CPMG is a relaxation-time-edited NMR experiment that exploits differences in transverse relaxation time (T_2) (288, 291). Proteins (and bound ligands) have a small T_2 while free ligands have a large T_2 . Thus, T_2 binding can be detected when the signal of the ligand decreases. After going through the filtering process, the lead fragments are then able to be chemically linked together through a series of reactions to produce whole ligands, using methods known as ‘fragment-linking’ and ‘fragment-growth’.

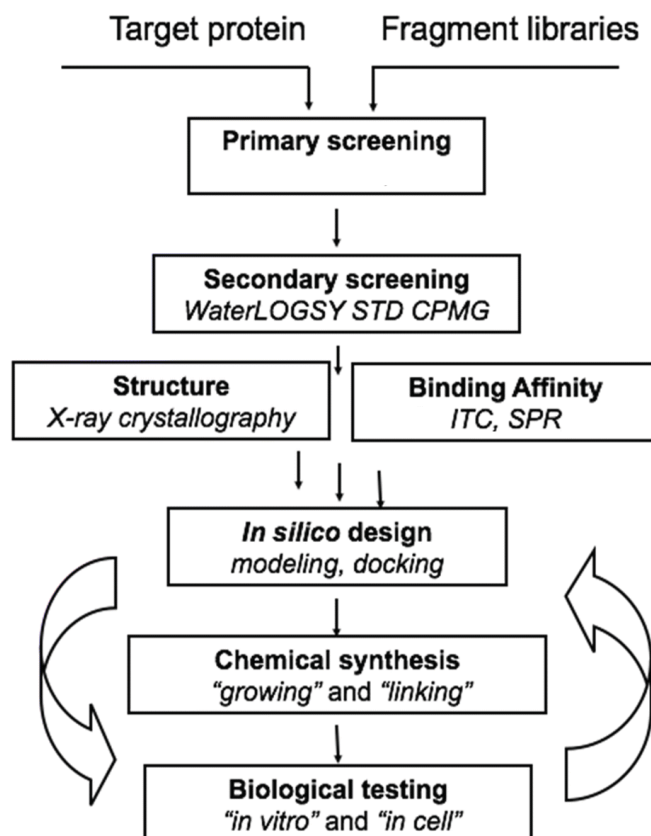


Figure 6.3: Typical schematic of fragment-based drug discovery. Primary screening is conducted by mixing the target protein to fragment libraries and then screening using several methods such as nuclear magnetic resonance (NMR) and thermal shift. Secondary screening of initial hits obtained in the primary screening is conducted with three independent NMR experiments known as Water-LOGSY, STD and CPMG. The binding affinity of the fragment leads obtained in the second screen is calculated using methods such as isothermal titration calorimetry (ITC) and surface plasmon resonance (SPR) while structure determination is carried out using X-ray crystallography. Further derivatisation of the fragments is conducted in three stages: in silico design, chemical synthesis and biological evaluation. The figure is adapted from (288).

6.1.5 Producing compounds by fragment-linking and -growing

Fragment-linking is the process whereby two or more fragments which occupy the “hot spots” in a protein binding pocket are linked together covalently, either directly or through a molecular linker, to afford a more potent compound (292) (Figure 6.4). An alternative approach known as ‘fragment-growth’ is also possible (Figure 6.5). This is

a process whereby the fragment hits are grown through chemical manipulation to fill the space within a binding pocket (292).

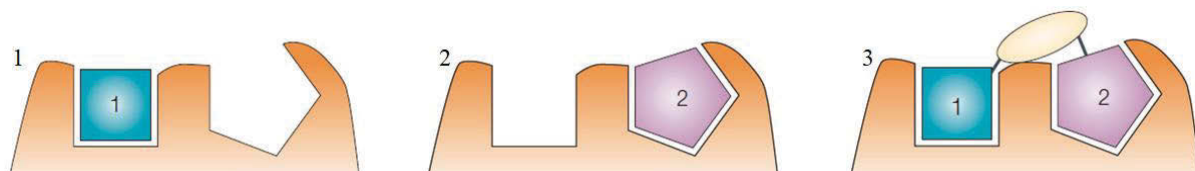


Figure 6.4: The process of fragment linking. (1) Fragment 1 binds to the receptor at “hot spot 1”. (2) Fragment 2 binds to the same receptor at an adjacent “hot spot 2”. (3) Fragments are joined by a molecular linker to form a lead molecule with high binding affinity. Figure was adapted from (292).

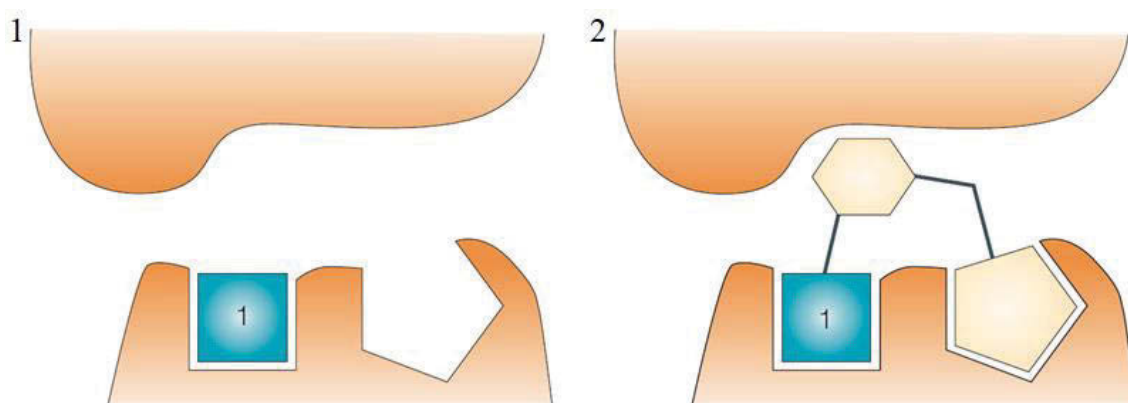


Figure 6.5: The process of fragment growth. (1) Fragment 1 binds to the receptor at “hot spot 1”. (2) The lead molecule is evolved by building away from the starting fragment (fragment 1) and making good contact with the upper surface and then by growing into a “hot spot 2”. Figure was adapted from (292).

There are two things that need to be considered before fragments can be used in the linking and/or growing process. The first is the location and orientation of the fragment binding to the protein (274). This usually needs a very well established understanding of the structural information of the target (274). Using NMR, this is identified by

mixing the fragment with a labelled protein that already had its signals identified. The other thing to consider is the synthetic feasibility of the obtained fragments to be linked or grown using chemistry approaches (274).

This chapter aimed at using a fragment-based drug discovery method to firstly identify other possible binding pockets within FtsZ which were identified in the previous chapter, as well as understand how the fragment hits bind the target FtsZ. As a proof of concept, this was carried out using NMR screening of a fragment library containing ~1000 fragments against *B. subtilis* FtsZ protein. Once the hit fragments have been identified, they will be used in subsequent X-ray crystallography structural analysis of fragment binding in the protein pocket. This would then be used in future elaboration of the fragment into active compounds which specifically target FtsZ.

6.2 Results: fragment-based drug discovery using *B. subtilis* FtsZ as the target

6.2.1 Bioinformatically identifying the mutation A182E on *B. subtilis* FtsZ structure

The initial work for this chapter was to use *B. subtilis* FtsZ in screening fragment libraries consisting of 1140 fragments *via* 3D-NMR structure elucidation. As wild-type FtsZ is known to self-associate and form polymers, it was observed by our collaborator in Brazil (Frederico José Gueiros Filho) and at University of Sydney (Joel Mackay) that this property inhibited the protein signal during data acquisition in 3D-NMR. Our collaborator in Brazil had designed a *B. subtilis* FtsZ which lacks the ability to polymerise while retaining the ability to bind nucleotides by introducing a mutation of alanine to glutamate at position 182 (A182E). As a result, this mutation causes the *B. subtilis* FtsZ to stay monomeric instead of forming polymers. The monomer of FtsZ is necessary for data collection during the TROSY- HSQC NMR experiments as it will allow the detection of the signal produced during experiment. To ensure the mutation of the *B. subtilis* FtsZ does not affect the binding of fragments in any of the druggable regions on the protein, the location of the substituted amino acid was checked (Figure 6.6). Its location was found to be at the top of the H7-helix (the yellow coloured region in Figure 6.6) and was therefore considered not to affect or interfere with binding sites as the protein is still able to bind nucleotides. The ability of the mutant protein to bind nucleotide was indeed demonstrated through TROSY-HSQC NMR experiments and is covered in a later section.

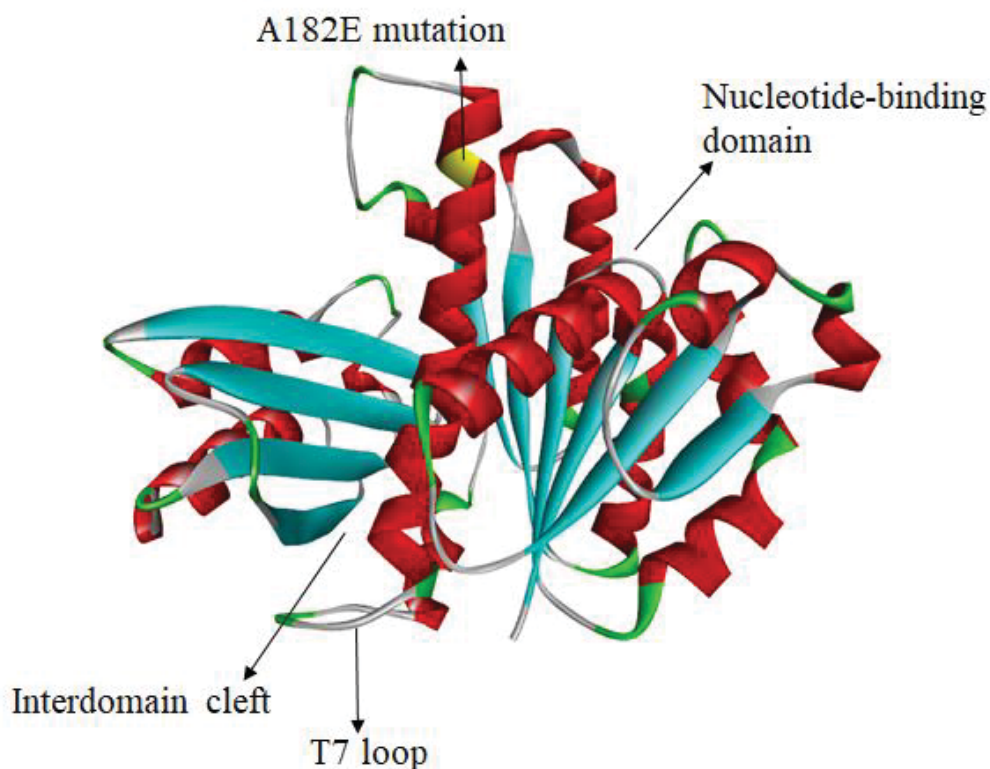


Figure 6.6: Indication of the A182E mutation position in the *B. subtilis* FtsZ. X-ray crystal structure is 2RHL (190). The mutation (yellow coloured region) on the protein is located away from the druggable regions on the protein and will most likely not affect its binding pockets, which are labelled as nucleotide-binding domain, interdomain cleft and T7-loop.

6.2.2 Initial fragment-based drug screening

The primary and secondary fragment screen was conducted at the University of Sydney using NMR as a service provided by Professor Joel Mackay and Dr Lorna Wilkinson-White (Sydney FBDD Facility within the Sydney Analytical Core Facility, University of Sydney). As stated above, wild-type *B. subtilis* FtsZ protein readily forms polymer and would hinder signal acquisition during the TROSY-HSQC NMR experiment, which was planned as a part of the screening process. Therefore, to avoid such problem, initial screening was conducted using a mutant *B. subtilis* FtsZ protein. The first fragment-screen was conducted with a purified *B. subtilis* FtsZ¹⁻³¹⁵ A182E (purified as

described in Chapter 2 Section 2.2.2.7) against a library of 1140 fragments, which was developed by the medicinal chemists at Monash Fragment Platform, Monash University. The cut-off value determining a “hit” in the first screen and subsequent screening was set based on previous experiments by the medicinal chemists at Monash Fragment Platform, Monash University. The cut-off values for STD-NMR, Water-LOGSY and CPMG-NMR are set to be in the range of saturate transfer difference percentage (STD (%)) 4 – 8%, negative-signal change to flat- and/or positive-signal and 20 – 50% signal reduction, respectively. The precise cut-off value for these three experiments is determined by strength of the ligand to bind the target protein and the signal intensity the ligands are able to produce. As the strength of the ligand used in this study were weak and the signal intensities produced by the ligand were low, cut-off values chosen in this study are that of the lower-end of the spectrum. Also, negative control for all the initial screening was just the fragment alone and signal produced from the negative control was compared with signals created by the fragment when mixed with the protein to identify binding (Figure 6.7).

In the first screening the fragments were divided into three separate 96-welled plates, with each well containing five fragments. “Hit” fragments were determined when the STD (%) of 7% and above is obtained, which indicates that the fragment interacts with the protein. From the three trays, a total of 72 fragments were identified as hits and these were subsequently refined in a second screening to confirm the validity of each fragment as a hit.

The further refinement was conducted in the second screen by utilising the *B. subtilis* FtsZ A182E protein in a method called triple-ligand detect. The fragment that shows signal changes in at least two of the three triple-ligand detect experiments are

considered to be a hit from the refinement second screening. The signal change cut-off value to be considered a hit for the three experiments are as follows (Figure 6.7);

- Water-LOGSY: the negative-signal produced by the fragment alone changes to a positive-signal when bound to the protein. A flat-signal is also an indication of binding, but strong binding will be detected as a negative- to positive-signal change.
- CPMG-NMR: a 30% decrease or more of the fragment peak size when bound to the protein. Since fragments are small moieties which bind weakly, the 30% cut-off was deemed as the appropriate amount of signal change to signify the binding of fragments to protein.
- STD-NMR: a signal change of more than and/or equal to 4% between the fragment only and fragment-protein spectra.

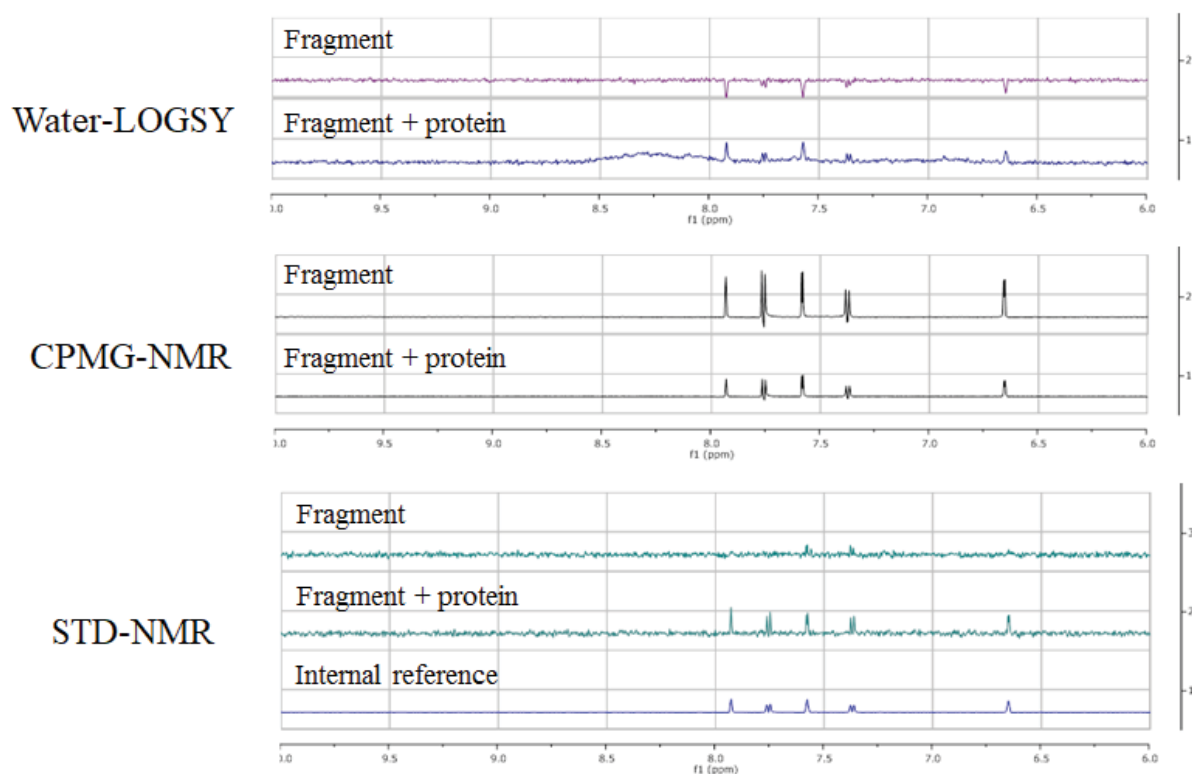


Figure 6.7: Cut-off value for determining “hit” fragments in the triple-ligand detect experiments. In Water-LOGSY NMR experiments, the binding of the fragment to protein is signified by the change of the negative signal to either a flat or positive signal, with a positive signal indicating strong binding. In CPMG-NMR binding of the fragment to protein is signified as a signal decrease by at least 30% while in STD-NMR a signal change of more than and/or equal to 5% is needed to be considered as “binding”. In STD-NMR another spectrum termed internal reference is usually included to show the expected fragment signal when binding is observed, which has a similar purpose to that of a positive control.

The second screen using the triple-ligand detect method identified 16 of the 72 fragments to be hit fragments. These 16 fragments were further refined in a transverse relaxation optimized spectroscopy-heteronuclear single quantum coherence (TROSY-HSQC) experiment using ^{15}N -labelled *B. subtilis* FtsZ A182E. The ^{15}N -labelled protein was purified by the PhD student and is described in Chapter 2 Section 2.2.2.7. TROSY-HSQC experiment requires the use of ^{15}N -labelled *B. subtilis* FtsZ, which allows for the detection of ^{15}N -chemical shifts (δ) of amino acid residues in the protein binding pocket. The change in the observed chemical shifts (δ) indicates the modified chemical

environment of the amino acid residues, and hence the conformation or environment of the pocket. This modification is due to the binding of the fragment. The experiment, therefore, directly investigates the changing of protein binding pocket due to ligand binding. Since our Brazilian collaborator has already assigned 80 % of the amino acid signals in the mutant *B. subtilis* protein, the signal change between the protein and protein-fragment spectra which indicates binding, will also inform the precise binding location of the “hit” fragments as each signal observed represents a single amino acid in the binding pocket.

For the ease of explaining the NMR experimental data, this paragraph will briefly explain the amino acids on FtsZ that are involved in both GDP- and **PC190723**-binding. GDP-binding in the *B. subtilis* FtsZ structure is facilitated by amino acids: G20 G21 G22 N25 G104 M105 G107 G108 T109 G110 E139 R143 F183 A186 D187 while **PC190723**-binding in the *S. aureus* structure is facilitated by amino acids: G196 D199 L200 V203 V207 N208 L209 M226 I228 N263 T296 V297 T309 V310 I311. The **PC190723**-binding region in the *B. subtilis* FtsZ is very similar to that of the *S. aureus* **PC190723**-binding region with a slight variation at amino acid 207 and 296. In *B. subtilis* FtsZ, V207 and T296 is changed to I207 and S296, respectively. Although these are different amino acids, the change of these amino acids does not result in the change of the chemical environment of the pocket as these are all neutral amino acids. Therefore, changes in the chemical shifts observed with these amino acids will be informative for the fragments binding in either the NBD and/or interdomain cleft.

6.2.3 TROSY-HSQC screen with ^{15}N labelled *B. subtilis* FtsZ^{I-315} A182E

The 16 fragment hits obtained in the second screening were further validated using TROSY-HSQC. The screening identified 4 of the 16 fragments causing the strongest signal change of the protein chemical signals in the TROSY-HSQC NMR. These are fragments **1**, **3**, **4** and **14** and the strong signal change indicates these four fragments are the best binders. Fragment **4** was seen to cause shifts in chemical signals similar to fragment **1**, but with a smaller change in the chemical signals. Similarly, fragment **14** has a similar signal profile to that of fragment **1**, but with a slightly weaker change in comparison to the chemical signals of fragment **1**. This indicates that both fragment **4** and **14** might bind to FtsZ with a similar affinity to fragment **1**. A list of amino acids which experienced chemical shifts upon the binding of fragment **1**, **3**, **4** and **14** are listed in Table 6.1. Mapping these amino acids signals onto the *B. subtilis* FtsZ protein structure suggests that the four fragments are binding the NBD and/or the interdomain cleft (Figure 6.8).

Table 6.1: Mutant *B. subtilis* FtsZ amino acid residues which changed upon fragment binding during the TROSY-HSQC experiment.

Fragment		
1 & 4	3	14
<p>G18 G20-23 T45 G46 K58 G62 G68 G78 G104 G106-108 T109 L127 V129 G130 V132 G193 V194 Q195 G196 S198</p>	<p>G20-23 G62 G68 G78 G104 G106-107 V129 Q192 G193 V194 Q195 G196 I197 M226 G227 I228 T265 S296 V307- T309</p>	<p>G18 G20 G22-23 G62 G68 V101 G104 G106-108 V129 G130 V132 T137 G193 V194 Q195 G196 I197 G227 I228 G229 L261 T265 G266 V308</p>

Amino acids located in the nucleotide-binding domain and interdomain cleft is coloured orange and magenta, respectively.

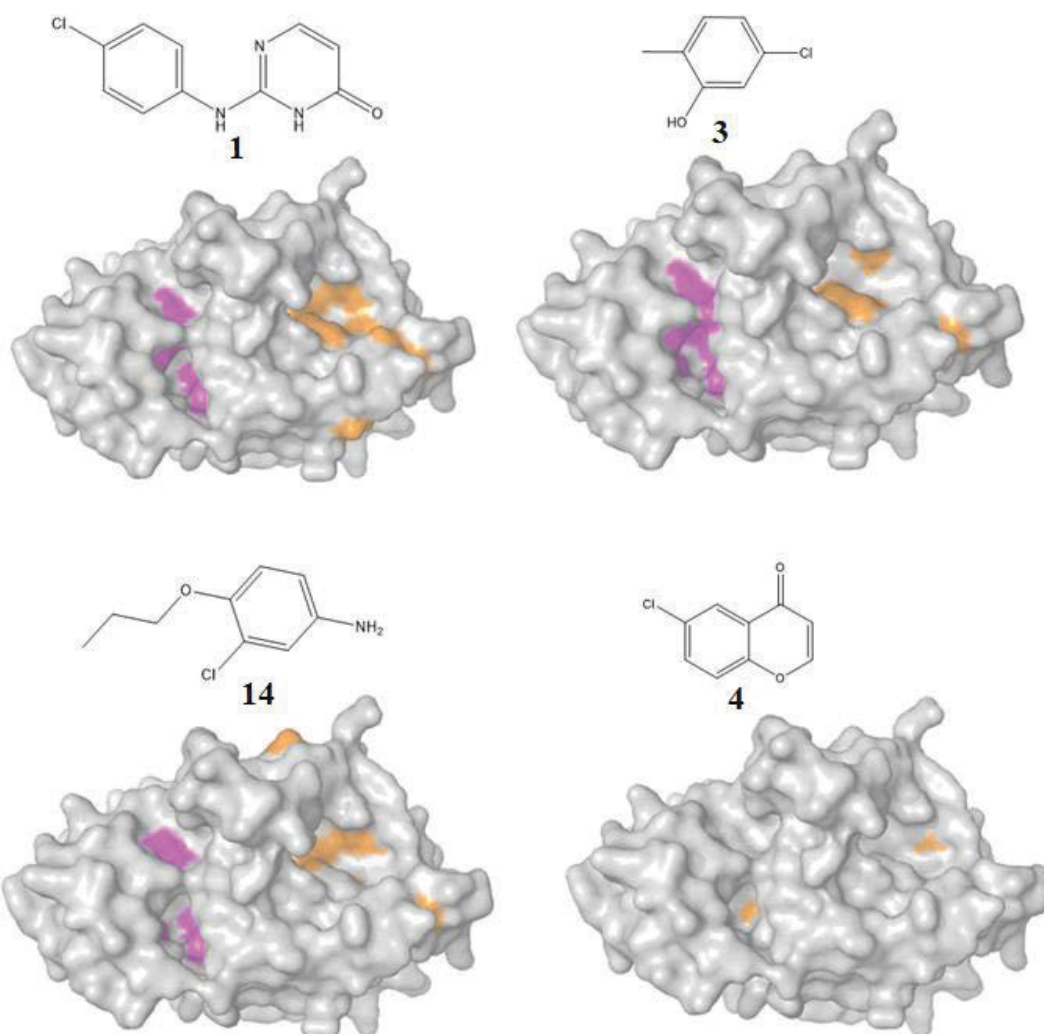


Figure 6.8: Mapping the binding location of the four hit fragments on the *B. subtilis* FtsZ crystal structure. Fragment **1**, **3**, **4** and **14** were observed to cause the strongest change in the amino acid chemical shifts (δ) in the second screening. Mapping the chemical shifts of these four fragments onto the *B. subtilis* FtsZ crystal structure suggests that they bind the nucleotide-binding domain (orange) and interdomain cleft (magenta) of the *B. subtilis* FtsZ.

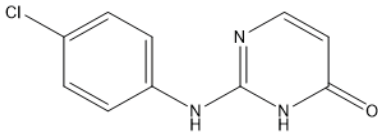
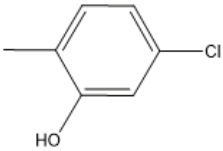
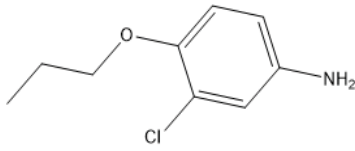
The signal change indicates that the four fragments are binding the NBD and/or the interdomain cleft. However, as the binding of molecules to proteins are usually very specific, these fragments were hypothesised to selectively bind to one pocket over the other. Therefore, to identify which of the two regions of FtsZ the four fragments prefer to occupy, competition experiments using GDP were conducted. From this point onwards, the experiments were performed entirely by the PhD student.

6.2.4 HSQC-NMR competition experiment using *B. subtilis* FtsZ¹⁻³¹⁵ A182E

To conduct the GDP competition experiment (method is described in Chapter 2 Section 2.2.4), the four fragments were obtained commercially. Unfortunately, fragment **4** was unavailable, therefore the competition experiments were conducted with only three of the fragments (fragments **1**, **3** and **14**).

Determination of fragment binding to FtsZ using TROSY-HSQC was defined as a change in FtsZ amino acid signals, determined by a difference in chemical shifts ($\Delta\delta$) created by the protein alone (negative control), protein with GDP (positive control), protein with fragment and protein with both fragment and GDP (Figure 6.9). The TROSY-HSQC experiments of protein alone, protein plus the fragment and protein plus GDP were run separately and used as references chemical shifts-map; much like that of a GPS, of the amino acids at the binding pockets. The TROSY-HSQC experiment involving protein with fragment and GDP was acquired in the fourth experiment. Amino acids observed to experience a change in their chemical shifts during the competition experiment are listed in Table 6.2.

Table 6.2: Amino acid of mutant *B. subtilis* FtsZ which experienced a change in their signals upon the addition of fragments and GDP.

Fragment 1	Fragment 3	Fragment 14
		
G21 G22 G62 G68 G95 L127 T137 I162 V163 Q195 G196 I217 S219 M226 G227 A231 T265 E300 E305 I311 A312	G21 Q36 T109 L127 V129 G130 T137 D159 V163 N176 G193 G196 S219 M226 G227 G229 T265 N299 E305 A312	G21 G22 G23 G62 G104 G106 L127 V129 I151 D159 I164 G193 G196 S219 G227 I228 E305 A312

Amino acids located in the nucleotide-binding domain and interdomain cleft is coloured orange and magenta, respectively.

Spectrum observed with fragment **1** and **3** saw that majority of changes to the protein signals are for amino acids located in the interdomain cleft and these are Q195, G196, M226, G227, G229, A231, T265, N299, E305, I311 and A312. This indicates that these two fragments prefer to occupy this druggable pocket of *B. subtilis* FtsZ¹⁻³¹⁵ A182E (Figure 6.10). Meanwhile, spectra obtained with fragment **14** showed that the signal changes were in amino acids located in both the NBD and interdomain cleft and these are G21, G22, G23, G104, G106, G193, G196, G227, I228 and A312 (purple coloured region in Figure 6.10). This indicates that fragment **14** might be utilised in creating compounds which target the NBD or interdomain cleft.

One interesting observation, however, is that the addition of GDP during the competition experiment did not hinder the binding of fragment **14** with the amino acids which are part of the NBD itself and these are G21, G22, G23, G104 and G106. Mapping these amino acids shows that they are located towards the front of the NBD (Figure 6.10). This points to the possibility that fragment **14** is binding in a newly

discovered region that is located towards the front of the NBD and therefore, confirming one of the pockets that was suggested to be a possible binding pocket in Chapter 5 (arrow 3 and 4 in Figure 5.5 of Chapter 5). This is an exciting discovery as this will be the first study to identify a new possible targetable pocket on FtsZ.

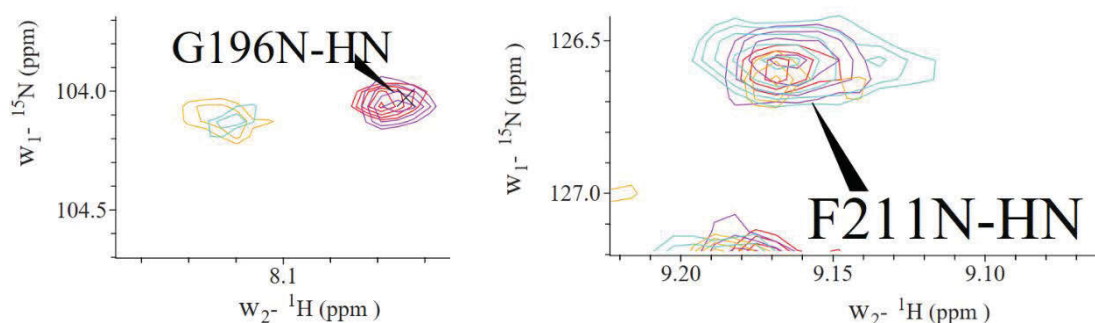


Figure 6.9: An example spectrum showing fragment binding to *B. subtilis* FtsZ¹⁻³¹⁵ A182E. Spectra coloured in red represents FtsZ amino acids and spectra coloured in purple is FtsZ bound to GDP. Orange spectra represents FtsZ with fragment and turquoise spectra represents FtsZ with fragment and GDP. Changes to chemical shift was determined when the peaks of the same amino acid between the spectrum are observed to be separated, as seen with the red and orange peaks of amino acid G196. The chemical shift of F211 is an example of the “no-change” in signal observed when no fragment is binding with the amino acid.

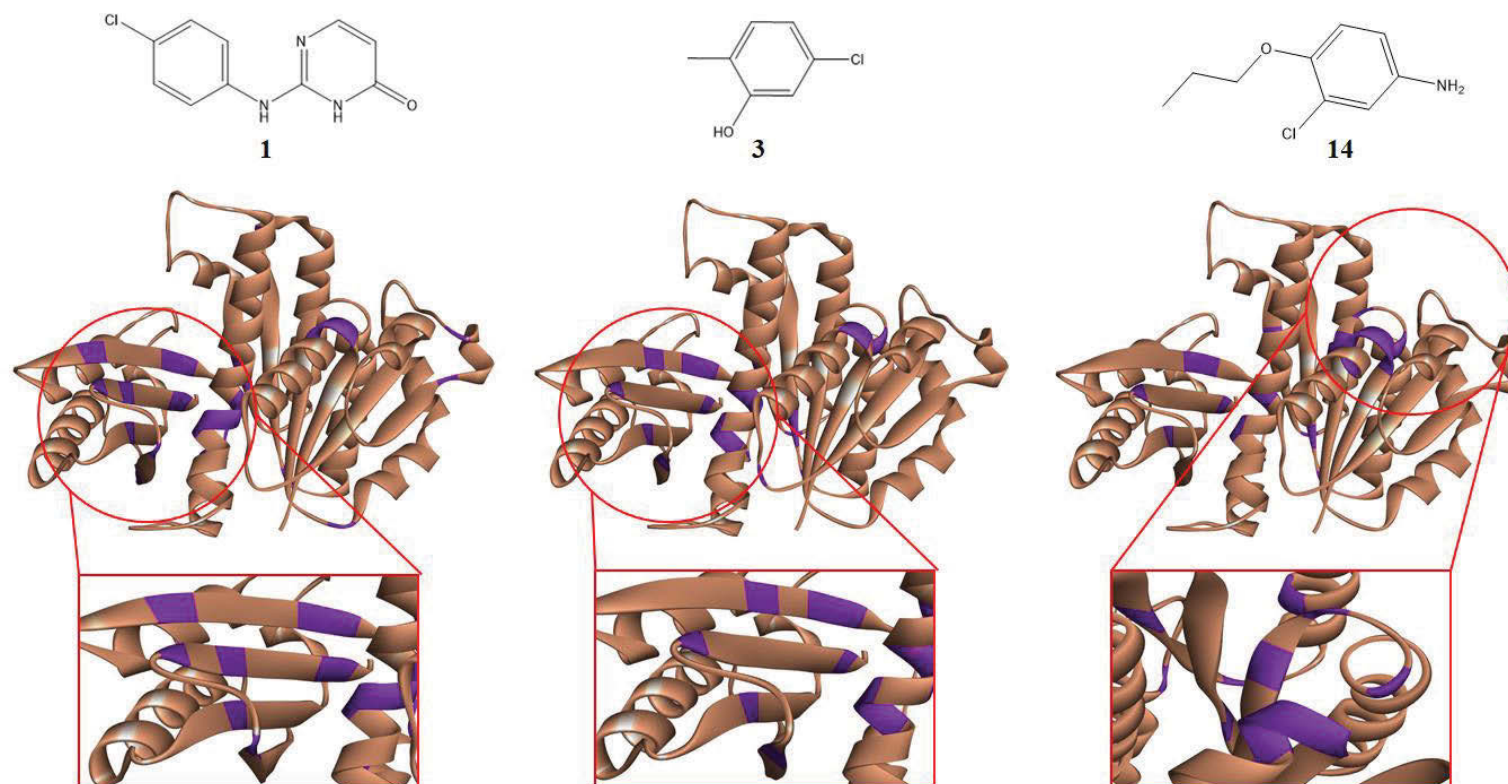


Figure 6.10: The preferred binding site of fragment 1, 3 and 14 on the *B. subtilis* FtsZ¹⁻³¹⁵ A182E. The whole protein is coloured in cream and amino acids which were observed to experience a signal change during the competition TROSY-HSQC experiment are coloured in purple. Fragment 1 and 3 prefer to occupy the interdomain cleft while fragment 14 can occupy the interdomain cleft and area towards the front of the NBD.

X-ray crystallography is the best way to identify how the fragments binds and orientate itself when bound to FtsZ and it is the wild-type not mutant protein (as was used in the NMR screening experiment) that is of interest since the goal of the project is targeting this form of FtsZ. Prior to undertaking crystallography, it is important to firstly confirm that the fragments also bind the wild-type protein and this is discussed below. In order to test this and also conduct the crystallography experiments, a wild-type *B. subtilis* protein construct is needed and, based on currently published FtsZ structures, it was deemed necessary to remove the first eleven amino acids, as well as the C-terminus disordered region as this would greatly help in the crystallization of the protein. As a result, this will allow isolation of the wild-type *B. subtilis* FtsZ¹²⁻³¹⁵ protein, which is described below. Plasmid creation is described in Chapter 2 Section 2.2.1.3 to Chapter 2 Section 2.2.1.6.

6.2.5 Overproduction and purification of wild-type *B. subtilis* FtsZ¹²⁻³¹⁵

To overproduce the *B. subtilis* FtsZ¹²⁻³¹⁵ protein, plasmid pETMCSI encoding the protein was transformed into electrocompetent *E. coli* BL21-AI cells and selected on LB plates containing ampicillin. Growth and overproduction conditions are described in Chapter 2 Section 2.2.2.7. Cell lysates prepared from cells harvested both before and after induction were analysed on a 12% SDS-PAGE (Figure 6.11). An intensely-stained band having an estimated molecular mass of ~30 kDa (denoted by arrow in Figure 6.11) was present only in the induced and soluble lane; lane denoted as I and S in Figure 6.11, respectively. With the protein being overproduced and soluble, the process was upscaled to 3 L and the protein purified.

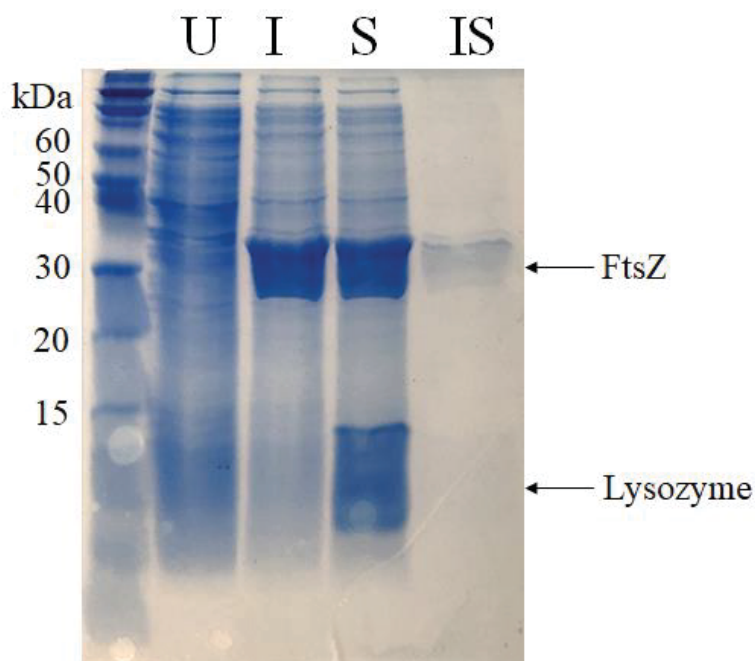


Figure 6.11: Overproduction of wild-type *B. subtilis* FtsZ¹²⁻³¹⁵. Induction to overproduce the wild-type *B. subtilis* FtsZ¹²⁻³¹⁵ was conducted at 10°C and it showed overproduction (arrow); which is depicted as a thick band at the size of ~30 kDa in the induced lane (I). The protein was also seen to be soluble as it is present in the soluble lane (S). The thick band towards the bottom of the soluble lane is lysozyme, as it was used to lyse the cells when separating the soluble and insoluble (IS) fraction of the cell lysate.

Purification of the protein is described in Chapter 2 Section 2.2.2.7. During the final purification step using the size exclusion chromatography column, two distinct peaks were observed in the chromatogram and analysing the samples corresponding to these two peaks on SDS-PAGE showed that both peaks contained the overproduced wild-type *B. subtilis* FtsZ¹²⁻³¹⁵ (pointed by the arrow in Figure 6.12). Samples from each peak was collected separately and then individually concentrated using a vivaspin column. Sample under peak 1 and 2 was concentrated to 13.5 mg/mL and 10.7 mg/mL, respectively. To understand if both samples are the same or different species, 50 µL of each concentrated sample was injected onto a small size exclusion column (Superdex™ 75 Increase 10/300 GL) (data not shown). The result showed that there are two species

of protein, with one species eluting faster than the other species. This is a common phenomenon of purifying wild-type FtsZ as it forms oligomers (293). Analysis of the concentrated protein sample on a 12% SDS-PAGE gel from both peak 1 and peak 2 showed that protein sample from peak 2 contains less contaminants than the sample in peak 1 (Figure 6.13). Therefore, samples prepared from peak 2 were tested in a GTPase assay to assess its functionality and hence its folding and subsequently used in experiments to identify binding of the hit fragments with the wild-type protein using NMR. This will be followed by a co-crystallization of the fragments with the wild-type protein to understand how the fragments bind to the protein.

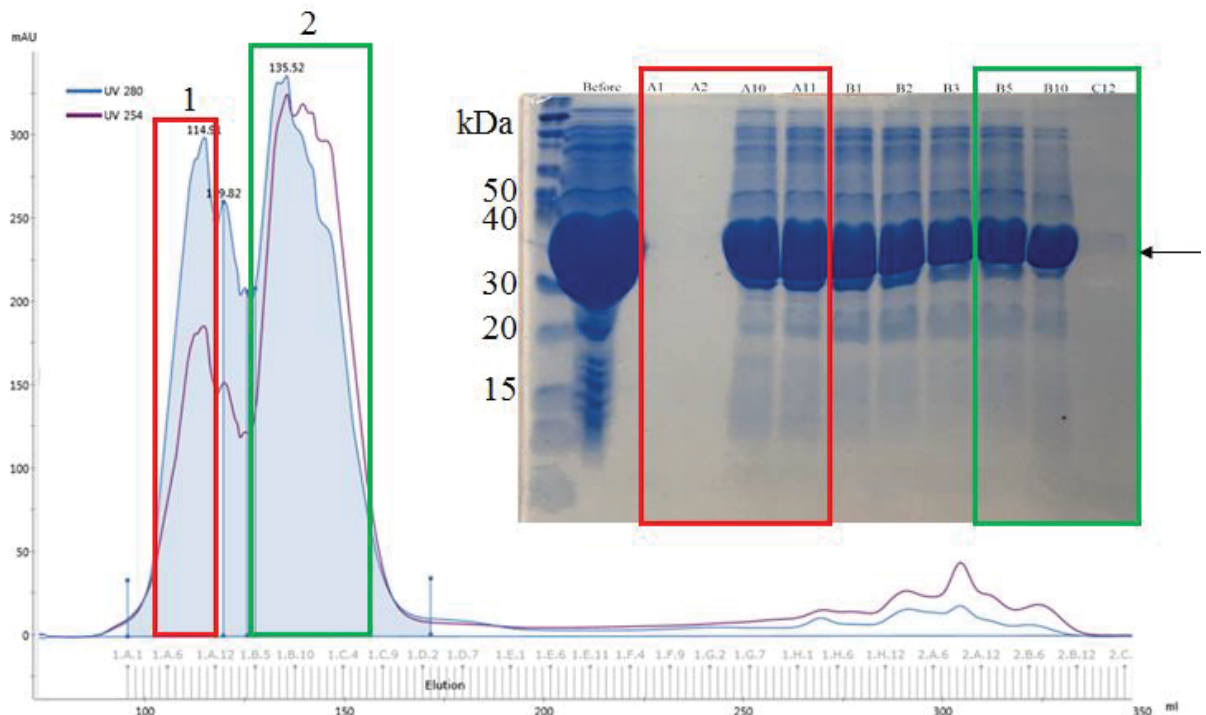


Figure 6.12: Chromatogram and SDS-PAGE of size exclusion chromatography during the purification of wild-type *B. subtilis* FtsZ¹²⁻³¹⁵. Two peaks were observed during the size exclusion step of purifying the wild-type *B. subtilis* FtsZ¹²⁻³¹⁵. Peak 1 is boxed in red and peak 2 in green. Fractions corresponding to these two peaks were analysed on SDS-PAGE gel and fractions corresponding to peak 1 and 2 are boxed in red and green, respectively. The overproduced protein (pointed by the arrow) is present in both peaks.

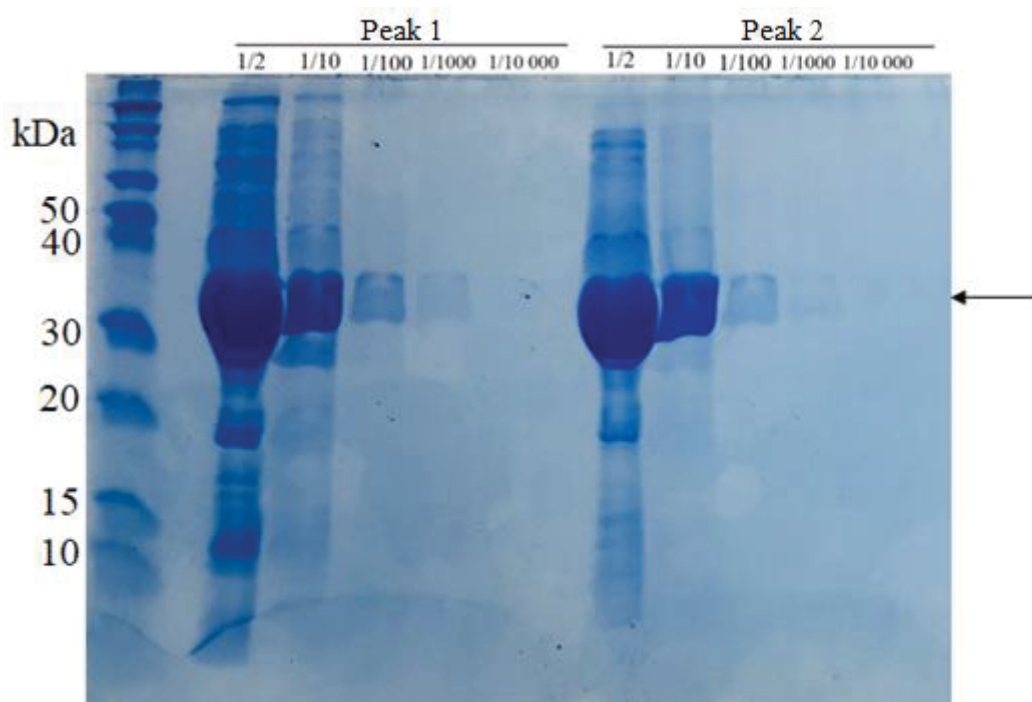


Figure 6.13: Concentrated protein sample of wild-type *B. subtilis* FtsZ¹²⁻³¹⁵ from peak 1 and peak 2. Samples from both peak 1 and peak 2 were concentrated separately and a small aliquot of it was diluted and analysed on a 12% SDS-PAGE gel to check its profile. Sample from peak 2 contained less contaminants than the sample from peak 1. The overexpressed protein is denoted by the arrow.

6.2.6 Functional assay using a GTPase kit with the wild-type *B. subtilis* FtsZ¹²⁻³¹⁵

Preceding carrying out the GTPase assay, the protein sample was tested for inorganic phosphate contamination by adding malachite green to the sample (Figure 6.14). The assay relies on the binding of the dye to the free phosphate generated when GTP is hydrolysed to GDP. The binding of the dye to the free phosphate causes a colour change from orange to green. Since the colour change is caused by the dye binding to free phosphate, this can also be used to qualitatively check for phosphate contamination in the protein sample. Addition of the dye to the purified FtsZ protein sample did not turn the sample green but stayed a yellow/orange colour, indicating that the purified FtsZ sample is free from phosphate contamination. Meanwhile, spiking the FtsZ sample with 20 μ M inorganic phosphate turned the solution green, which indicates the presence of

free inorganic phosphate. Therefore, the phosphate detected during the assay will be due to the release of free phosphate through the hydrolysis of GTP to GDP by FtsZ.

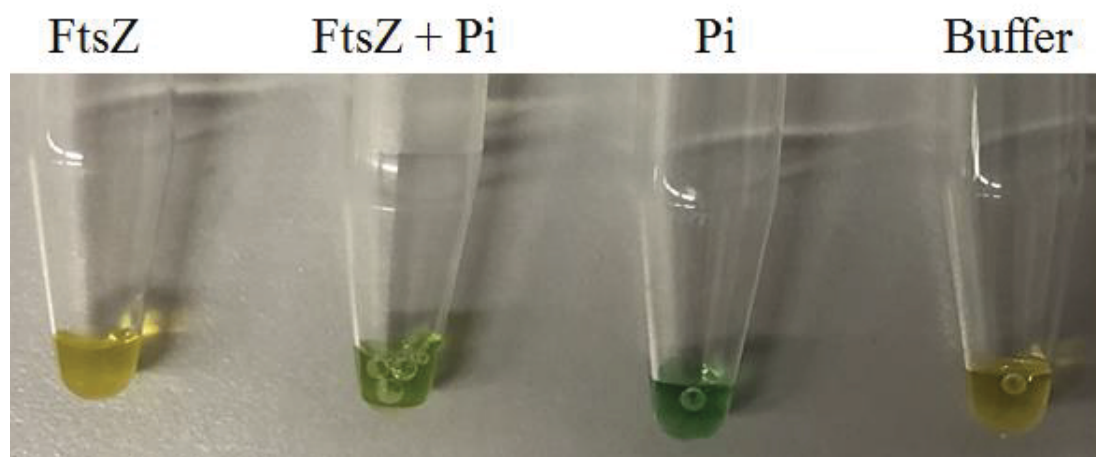


Figure 6.14: Testing the protein sample for phosphate contamination using malachite green. Addition of the malachite green dye to the protein sample (FtsZ) produced a yellow colour, indicating an absence of free inorganic phosphate, abbreviated as Pi. Meanwhile, the protein sample spiked with 20 μM Pi (FtsZ + Pi) produced a green colour when mixed with the malachite green dye, indicating the presence of free Pi. The positive control was the solution with 20 μM Pi (Pi), while the negative control was protein buffer alone (Buffer).

The GTPase assay was conducted by, firstly, creating a standard curve and conducting a comparison of free phosphate released by three different protein concentrations (2.7 μM , 5.4 μM and 10.8 μM). These concentrations were chosen based on the published study by Wang and Lutkenhaus (294), that showed 2.7 μM was the lowest *B. subtilis* FtsZ concentration for detecting GTPase activity. The absorbance values at 650 nm from the three protein concentrations (2.7, 5.4 and 10.8 μM) were within the linear portion of the constructed standard curve and correspond to the production of 21, 33 and 50 μM of free inorganic phosphate, respectively.

The specific activity of wild-type *B. subtilis* FtsZ¹²⁻³¹⁵ protein at concentrations of 2.7 μM (0.1 mg/mL), 5.4 μM (0.17 mg/mL) and 10.8 μM (0.34 mg/mL) were calculated to be 4.6, 1.6 and 0.6 $\mu\text{mol min}^{-1} \text{mg}^{-1}$ (Figure 6.15), respectively and is within the range stated in literature for *B. subtilis* FtsZ (for 0.1 – 0.18 mg/mL of *B. subtilis* FtsZ, specific activity is 1.3 – 9.3 $\mu\text{mol min}^{-1} \text{mg}^{-1}$) (294). Since the buffer used in this experiment contained no potassium chloride and only minimal amount of GTP was used (0.25 mM), the observed decrease in specific activity while increasing the protein concentration can be attributed to the bundling of FtsZ filaments under low potassium chloride concentration, as well as, low amount of GTP. This was shown to be because the subunit turnover rate of GTP-FtsZ polymer is dependent on potassium and not its hydrolysis rate (295). This can be addressed by providing excess GTP (2 mM) to the system and also increasing the potassium chloride concentration (296). This avenue, however, was not pursued further as the objective of conducting the GTPase assay was to confirm the purified wild-type *B. subtilis* FtsZ¹²⁻³¹⁵ is properly folded and functional as well as suitable for use in downstream experiments.

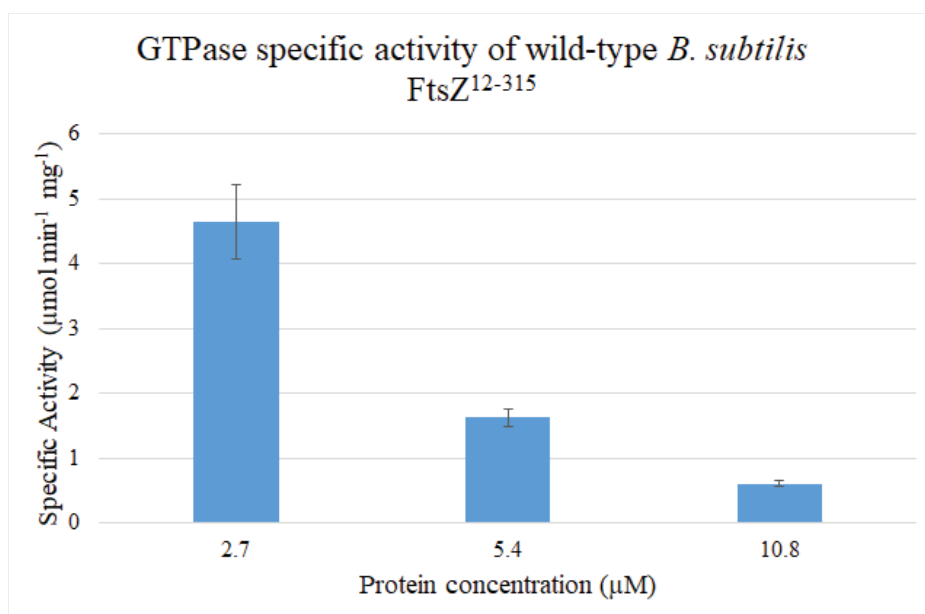


Figure 6.15: Calculated GTPase specific activity of wild-type *B. subtilis* FtsZ¹²⁻³¹⁵ at different protein concentrations. The specific activity of wild-type *B. subtilis* FtsZ¹²⁻³¹⁵ was calculated to be 4.6, 1.6 and 0.6 μmol min⁻¹ mg⁻¹ in three different protein concentrations of 2.7, 5.4 and 10.8 μM, respectively. Error bars represents standard deviation: ± 0.6 for 2.7 μM, ± 0.1 for 5.4 μM and ± 0.05 for 10.8 μM. n = 3 and N = 3.

6.2.7 Triple-ligand detect experiment using wild-type *B. subtilis* FtsZ¹²⁻³¹⁵ to confirm the binding of the fragment **1**, **3** and **14** to the wild-type protein

Thus far, it is known that fragment **1**, **3** and **14** bind the mutant *B. subtilis* protein but whether these three fragments also bind the wild-type protein needed to be tested. Since X-ray crystallography study was planned on using the wild-type *B. subtilis* FtsZ protein due to it being more biologically relevant to use than the mutant protein, it is important to know whether the three fragments also bind the wild-type protein. To answer this, the binding of the three fragments to the wild-type protein was tested using the NMR triple-ligand detect method. Since the wild-type FtsZ readily forms polymer which will hinder signal acquisition, as previously observed by both our Brazilian and USyd collaborator, the binding identification with the wild-type protein cannot be through the protein. This was achieved by using the triple-ligand detect method as it allows for the

detection of binding through the signals produced by the fragment and not through the protein. The experiment was conducted by Dr Lorna White at the University of Sydney, and this section will summarize the results obtained.

As discussed in Section 6.2.2, triple-ligand detect experiments focus on observing the change in the signal produced by the fragment with and without protein, to signify the binding of the fragment with the protein. Also, refer to Section 6.2.2 for cut-off values to determine binding. For all the three fragments, Dr Lorna White was able to observe signal changes in all three triple-ligand detect experiments (CPMG-NMR, WaterLOGSY and STD-NMR). However, the signal change produced with the wild-type protein was reduced relative to the signal change produced with the mutant protein (Table 6.3). This might be attributed to the ability of the wild-type protein to polymerise in solution and thus interfering with the signals obtained. Another possibility could be that these three fragments bind the wild-type protein with less affinity compared to the mutant protein. Nevertheless, the data obtained are suggestive of binding and therefore it can be assured that fragment **1**, **3** and **14** also bind the wild-type *B. subtilis* FtsZ¹²⁻³¹⁵. With this question answered, it is now important to understand how the fragment is binding to the protein. For this, crystallography was used and is discussed further below.

Table 6.3: Comparison of triple-ligand detect experimental data between mutant and wild-type *B. subtilis* FtsZ protein.

	Fragment 1		Fragment 3		Fragment 14	
	Mutant	Wild-type	Mutant	Wild-type	Mutant	Wild-type
CPMG-NMR*	68% reduction	50% reduction	60% reduction	60% reduction	61% reduction	55% reduction
Water-LOGSY#	Turned to a positive-signal	78% reduction	Turned to a positive-signal	56% reduction	Turned to a flat-signal	50% reduction
STD-NMR@	5%	1.1%	4.9%	3%	2.6%	1.6%

* Binding confirmation with CPMG-NMR is when signal reduction is $\geq 30\%$.

Binding confirmation with Water-LOGSY is when the initial negative signal is reduced to turn the signal into a flat- and/or positive-signal.

@ Binding confirmation with STD-NMR is when signal is $\geq 4\%$.


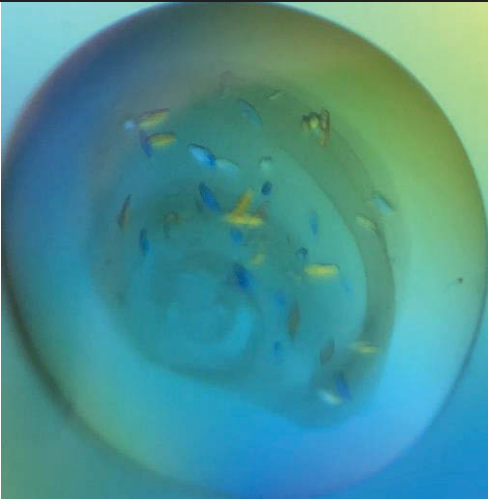
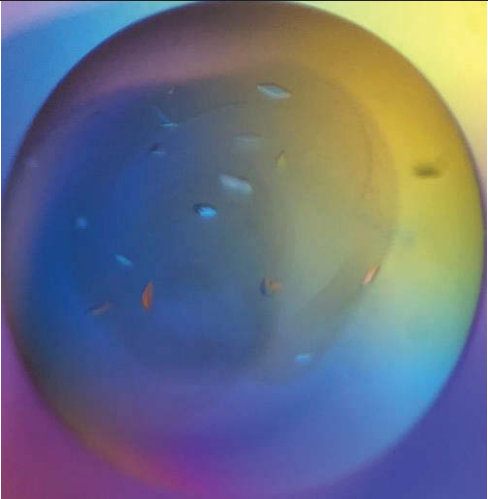
6.2.8 Crystallization of wild-type *B. subtilis* FtsZ¹²⁻³¹⁵


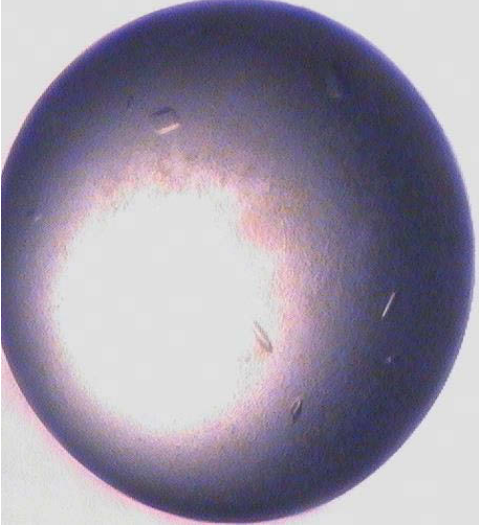
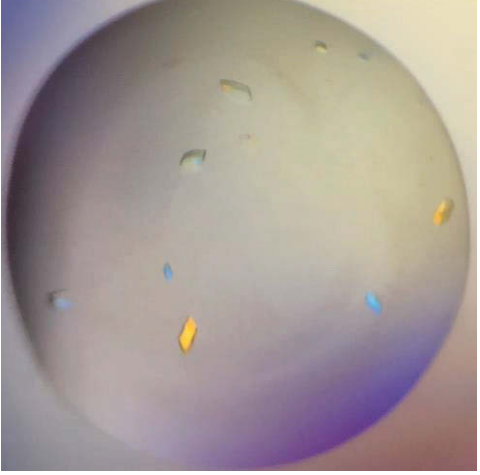
To date, there are six *B. subtilis* FtsZ structures available in the Protein Data Bank. The resolution of these structures ranged from 1.7 Å to 2.5 Å (143, 190, 191). As these structures have been solved previously and that the conditions for obtaining high-resolution structure is known, it was decided that crystallization of the wild-type protein purified in this study be conducted using conditions which previously produced the 1.7 Å *B. subtilis* FtsZ structure (0.2 M potassium citrate, 15-20% PEG 3350) (143). This was initially tried but no crystals were successfully formed. There are many parameters which affect crystallization (297). Nevertheless, there are several reasons which can explain the inability to replicate the published crystal formation. Firstly, the protein in

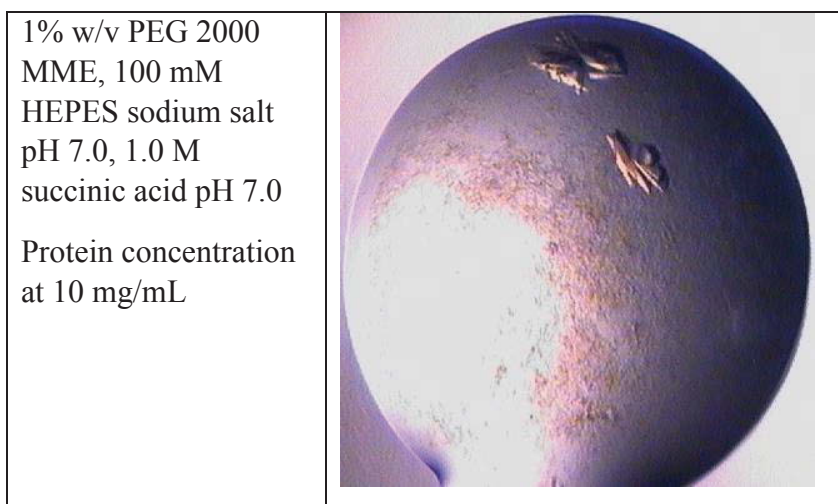
this study was purified differently from the purification method reported in the published literature. Secondly, the final storage buffer used for the protein in this study (20 mM Tris-HCl pH 7.74, 100 mM NaCl) is different to the one used in the published literature (10 mM Tris-HCl pH 8.0). Thirdly, ambient temperatures of where the crystal tray was stored also affect crystal formation and since the published literature did not specify the temperature in which the crystals formed, it is possible that the tray in this study was stored at a different temperature. Therefore, since there are practically many variable parameters to trial, in the interest of time, it was deemed necessary that a full screen be conducted using the crystal screening kits available at UTS which include: JBS Classic 1-10, JBS JCSG++ 1-4, JBS Membrane 1-4, JBS Pentaerythritol 1-2, JBS PACT++ 1-4 and JBS PEG Salt 1-4 (Jena Bioscience). This set of kits will screen 768 different crystallisation conditions. Crystal trays were set by the PhD student and is described in Chapter 2 Section 2.2.5.

Conducting the crystal screen using the available kits proved to be fruitful. Around half of the screening conditions produced crystals but only conditions which produced single crystals with sharp edges are summarized in Table 6.4 as these are the type of crystals which are of interest and more likely to diffract well.

Table 6.4: Conditions which were identified to produce *B. subtilis* FtsZ¹²⁻³¹⁵ crystal with sharp edges.

Conditions	Crystal photos
<p>45% w/v Pentaerythritol propoxylate (5/4 PO/OH), 100 mM HEPES pH 7.5</p> <p>Protein concentration at 10 mg/mL</p>	
<p>20% w/v PEG 3350, 200 mM di- Ammonium Tartrate</p> <p>Protein concentration at 10 mg/mL</p>	
<p>20% w/v PEG 3350, 200 mM di- Ammonium Tartrate</p> <p>Protein concentration at 5 mg/mL</p>	

<p>800 mM succinic acid pH 7.0</p> <p>Protein concentration at 10 mg/mL</p>	
<p>15% w/v PEG 3350, 100 mM succinic acid pH 7.0*</p> <p>Protein concentration at 5 mg/mL</p>	
<p>20% w/v PEG 3350, 200mM Lithium Acetate</p> <p>Protein concentration at 2 mg/mL</p>	



* Crystal condition which was pursued further using a gradient tray as it produced a clear initial diffraction and was approximated to be resolvable to $R = \sim 4 \text{ \AA}$.

A number of small crystals sized $\sim 10 - 30 \text{ \mu m}$ were produced from the screening and were analysed with X-ray at room temperature at University of New South Wales (UNSW) with Dr Kate Michie to determine their diffraction pattern and the resolution able to be produced by these crystals. After obtaining the diffraction pattern and calculating the resolution that is able to be produced by the crystals using the software Mosflm (298), it was determined that crystals produced under condition 15% w/v PEG 3350, 100 mM succinic acid pH 7.0 (Table 6.4) were suitable for further optimisation as they produced a strong diffraction and predicted to be able to be resolved to approximately $R = 4 \text{ \AA}$ (Figure 6.16). As this resolution is still low, further optimization of the crystal is needed to obtain crystals that will resolve to at least $R = 2 \text{ \AA}$. Such a high-resolution structure is needed to observe very detailed changes on the protein when binding to the fragments, as well as, because the subsequent handling of the crystal will decrease the resolution of the crystal, hence it would be best to start with a crystal that can produce high resolution structure.

Optimization was carried out by the PhD student by setting up a gradient tray which contained the same components as the original conditions from the screen (succinic

acid and PEG 3350) and making a range of concentrations of the components on a 96-welled MRC plate. In this case, since the original condition was 15% w/v PEG 3350, 100 mM succinic acid pH 7.0, the gradient tray was set so that it contained 7.5% - 30% w/v PEG 3350 and 50 – 200 mM succinic acid pH 7.0.

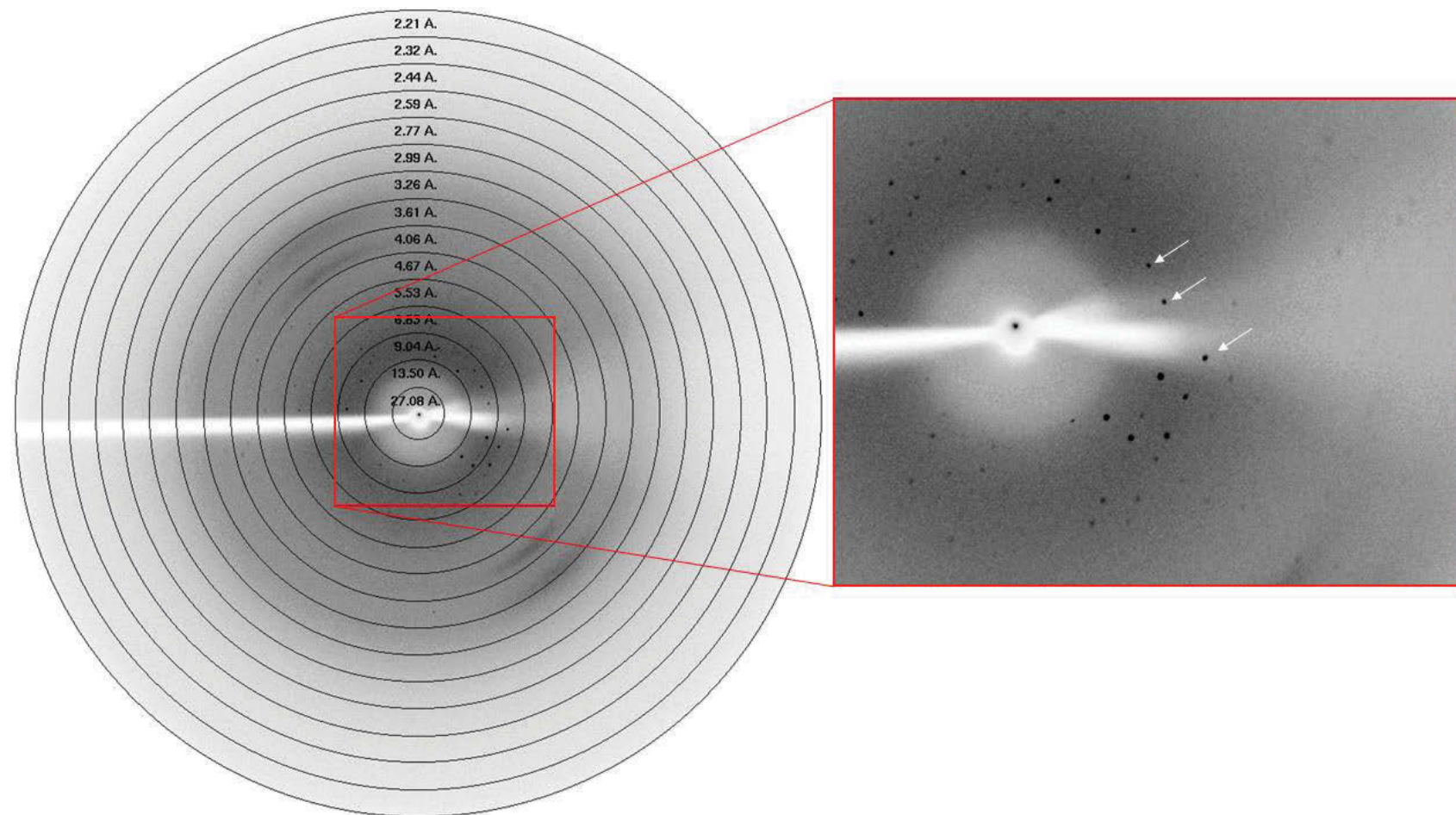


Figure 6.16: Diffraction pattern produced by wild-type *B. subtilis* FtsZ¹²⁻³¹⁵ crystal. The crystal was formed under 15% w/v PEG 3350, 100 mM succinic acid pH 7.0 and it was able to produce strong diffraction pattern (clear black spots pointed by white arrows) and resolvable to $R \approx 4$ Å.

The original condition was optimized several times using the gradient tray and the crystals were observed to increase in size with each optimization (Figure 6.17). The condition which produced consistently big crystals ($\sim 100 - 150 \mu\text{m}$), that is, a condition in which big crystals were observed in more than 90% of the well on the 96-well MRC plate, was identified to be 55 – 75 mM succinic acid pH 7.0, 15 – 16% PEG 3350.

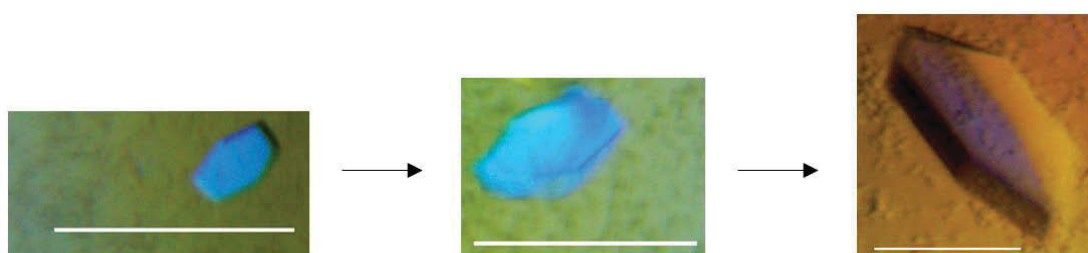


Figure 6.17: Optimization of crystallization condition of wild-type *B. subtilis* FtsZ¹²⁻³¹⁵ protein resulted in the increase of crystal size. Crystals were originally formed under 15% w/v PEG 3350, 100 mM succinic acid pH 7.0 (first panel). Optimization of the said condition resulted in an increase of the crystal size, with the biggest size crystals ($\sim 100 - 150 \mu\text{m}$) forming under 55 – 75 mM succinic acid pH 7.0, 15 – 16% PEG 3350 (last panel). Scale bar is 100 μm .

The larger crystals obtained from the optimization were analysed with the X-ray beam at UNSW at room temperature. They showed a very strong diffraction pattern which was predicted by the software Mosflm to be resolvable to approximately 3.5 Å (left panel in Figure 6.18). Indexing this data identified the crystal of having a predicted space group of P 1 and the cell dimensions of the crystal form are summarised in Table 6.5. This data indicates that this is a different crystal form than the reported ones, which mean that it might not be resolvable to the same high-resolution as structures published in the literature.

Table 6.5: Cell dimension of the crystal form pursued in this study.

Length (Å)*		Angle (°)*	
a	54.1	α	107.1
b	88.0	β	91.7
c	146.8	γ	89.9

* This crystal cell dimension is different from that of the crystal cell dimension reported in the currently published structure.

Since X-rays are very damaging to the protein crystals (299), important structural data gathering from the crystals are usually conducted in an environment under a slow stream of liquid nitrogen and the crystals pre-coated with cryoprotectant prior to data collection. In this study 20% glycerol was tested as the cryo-protectant as it was the cryoprotectant used in the study which produced the 1.7 Å *B. subtilis* FtsZ structure (143). The result, however, showed that glycerol is not the correct cryoprotectant to use as it greatly reduces the diffraction pattern of the crystal (right panel in Figure 6.18). Therefore, further study will need to include a screening process to identify the correct cryoprotectant to use.

Thus far, this result chapter has identified three lead fragments which bind to wild-type *B. subtilis* FtsZ¹²⁻³¹⁵. Competition NMR experiment suggests that two of the fragments prefer to bind the interdomain cleft while another in the interdomain cleft as well as in a newly discovered region that is towards the front of the NBD. Crystallography was undertaken with the aim to understand the binding of these fragments to the protein. Initial crystallography attempts produced good-sized crystals of wild-type *B. subtilis* FtsZ¹²⁻³¹⁵ that created strong diffraction pattern and predicted to be resolvable to R= ~3.5 Å. Unfortunately, higher resolution structure is needed to accurately solve the

fragment-protein complex. Nevertheless, this result chapter is the beginning of an exciting journey in the discovery process of new and novel antibacterials.

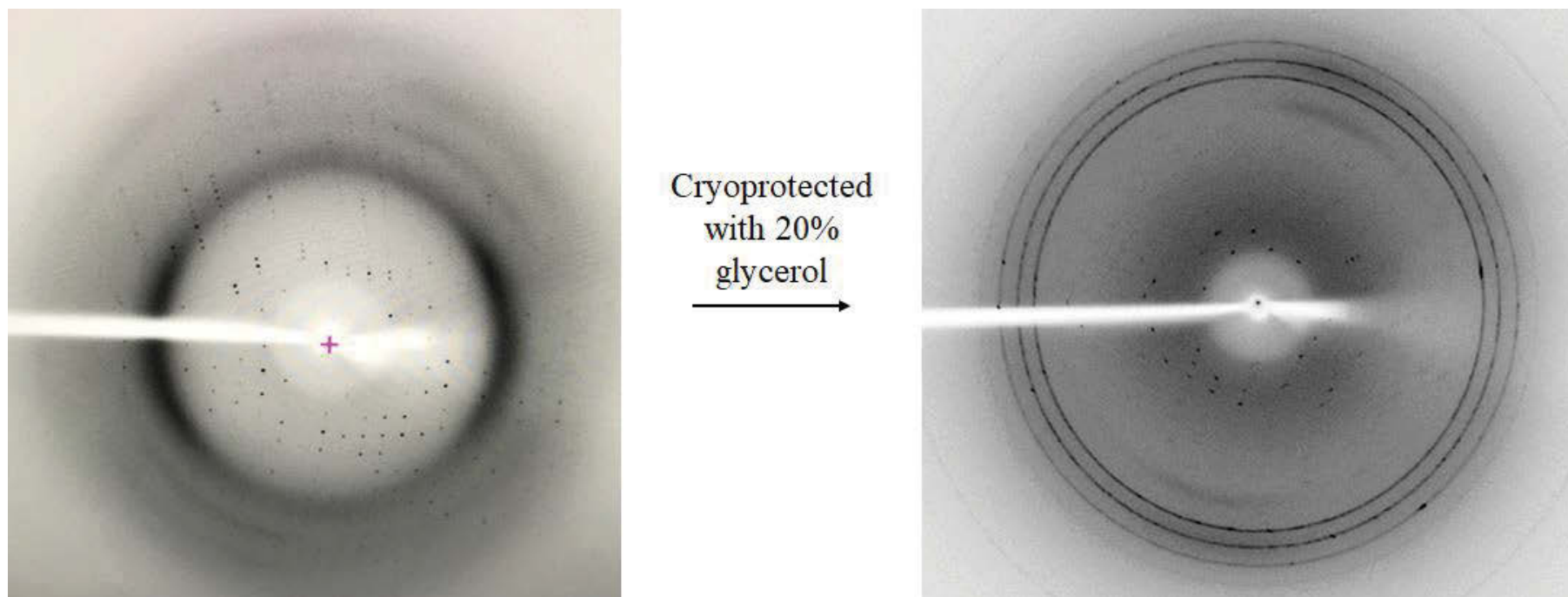


Figure 6.18: The effect of using 20% glycerol as a cryoprotectant to the crystal diffraction pattern. Initial analysis was conducted at room temperature and produced a strong diffraction pattern. The software Mosflm calculated this diffraction pattern to be resolvable to approximately $R = 3.5 \text{ \AA}$ (left panel). Diffraction pattern was greatly reduced once the crystal was coated with 20% glycerol as a cryoprotectant and the crystal analysed under a low stream of liquid nitrogen (right panel).

6.3 Discussion

The FBDD started in this project is the first of its kind to use this approach with FtsZ as the target. In this FBDD study, *B. subtilis* FtsZ was used as the target to identify firstly, other possible binding pockets on FtsZ and secondly, identify fragment leads which are able to be used for creating new antimicrobials with a novel mechanism of action. As fragments are small molecules with a size range of ~150 – 250 Da (300), it was thought that perhaps it was possible to identify other potential binding pockets within FtsZ that are yet to be reported in the literature and also confirm the suggested binding sites proposed in Chapter 5. Using NMR, four hit fragments were identified as lead fragments and by conducting a competition NMR experiment on three of the four fragments, it was shown that two of the fragments (fragment **1** and **3**) prefer to occupy the interdomain cleft while the other (fragment **14**) can occupy both the NBD and interdomain cleft. Taking into account the nature of the competition experiment with GDP, as well as analysis of the TROSY-HSQC data obtained with fragment **14**, it is possible that fragment **14** is actually binding in a new pocket that is adjacent to the NBD. Thus confirming one of the pockets suggested in Chapter 5. The next step will be to solve the fragment-protein complex using X-ray crystallography, followed by the process of fragment growing or linking which will make fragment **14** to be more selective, either towards the interdomain cleft or the NBD.

In terms of future prospect with fragment **14**, it is possible to grow this fragment to co-occupy both the NBD and the newly discovered pocket. As a result, this will potentially inhibit the ability of FtsZ to polymerize since it is located near the NBD. At the same time, any mutation obtained by the protein to combat any compound binding this region, will need to be accommodated with a mutation at the T7-loop because the catalytic site of FtsZ

is made complete through the insertion of the T7-loop of one monomer unit into the NBD of another subunit. Therefore, since mutations on two regions of the protein is needed for resistance, it will likely to decrease the rate of resistance appearing in comparison to the resistance rate of mutation in just one region of the protein, as seen with **PC190723**.

Another possibility for targeting FtsZ is potentially through its dimer interface and a pocket which may only be created through the coming together of two monomer units. These are exciting avenues that are yet to be explored in the field and have the potential for baring fruits. One may start looking into this through *in silico* analysis, like that presented in chapter 5 and start analysing possible binding pockets on FtsZ dimer instead of monomers, like in chapter 5. Another possibility is to clone and purify FtsZ dimers, which can be carried out by making a plasmid construct that has two of the FtsZ sequence linked by a linker region. The protein is then overexpressed and purified as a dimer. The protein is the subsequently crystallized and utilised in fragment screening using crystals instead of NMR as presented in this study.

The hit rate observed in this study (0.4%) was that of a typical fragment screen, which can range from 0.2% to 62% (301). Hit rates can be increased by screening larger number of fragments compared to the ones conducted in this study. Pharmaceutical companies such as Novartis and Pfizer typically conduct their screening using 2500 – 3000 fragments (302, 303), while company such as AstraZeneca can screen up to 40,000 fragments (304). Nevertheless, increasing the number of fragments being screened will not necessarily increase the hit rate, but will definitely identify more fragments belonging to other chemical space, which will allow the creation of new novel molecules that target FtsZ.

One of the major caveats in using FtsZ for screening fragments and also identification of fragment binding using 1D- and 2D-NMR was its intrinsic ability to polymerise. Therefore, a mutant version of *B. subtilis* FtsZ was used to address this problem. As shown in this chapter, the A182E mutation within the *B. subtilis* FtsZ stops the protein from polymerising and it is probable that a mutation on other FtsZ species that is equivalent to the A182E mutation on the *B. subtilis* FtsZ would be beneficial when attempting NMR studies with this protein. Furthermore, based on the triple-ligand detect experiments, fragment hits obtained through screening with the mutant version of the protein was seen to be translatable to the wild-type version of the protein, allowing for convenience in both screening and data gathering using both the wild-type and mutant version of the protein. Although the wild-type protein was able to be used in the triple-ligand detect experiment, it will not be viable to use this protein in the TROSY-HSQC NMR experiment, as its polymerisation will hinder signal acquisition and hence showing further the importance of actually using both the mutant and wild-type FtsZ in conducting FBDD with this protein.

Following identification of fragments hits, fragment optimization using fragment linking and growing require structural information of how the hit fragments bind the target protein, in this case FtsZ. This is important because high-quality structural information on the binding orientation of the fragment in the protein is required for guiding medicinal chemists during fragment linking/growing and elaboration to transform fragments into active compounds. Furthermore, as the whole concept of FBDD is to create a compound which specifically fits in the targetable pocket of the interested protein, the importance of structural information when conducting fragment optimization is even more apparent. In this study crystallography was attempted with the wild-type *B. subtilis* FtsZ¹²⁻³¹⁵ and the

crystals obtained was predicted by the software Mosflm to be able to produce a structure with a resolution of approximately $R = 3.5 \text{ \AA}$. This resolution, however, is lower than any of the published *B. subtilis* FtsZ structures ($R = 1.7 - 2.45 \text{ \AA}$) and therefore will not be adequate for undertaking structural determination of the fragment with the protein as this needs the crystal to be resolvable to $R = \sim 2 \text{ \AA}$. Since increasing the size of the crystals obtained in this study has shown to improve the diffraction and resolution obtained, attempts to make the crystal size much bigger was carried out by increasing the drop size on the gradient tray from 400 nL to 4 μL . This avenue, however, did not produce any crystals that are bigger than 100 – 150 μm , indicating the maximum size this crystal formation is able to achieve. Calculating the space group and also cell dimension of the crystal pursued in this study indicate that this is a different crystal form than the reported ones. Therefore, since this crystal formation will not produce larger crystals and possibly lessens the likelihood of obtaining higher resolution structure of the protein/fragment complex, the next step for the crystallography approach would be to screen for other crystal forms which may possibly exist in the screening trays already conducted in this study. It is possible that in-doing-so, crystal forms similar to the reported ones be identified for use in future soaking experiments.

One of the vital aspects of structural determination in X-ray crystallography is the data gathering, whereby the crystals are shot directly with an intense beam of X-ray to produce the diffraction pattern used in structural determination. For this, the crystal needs to be able to withstand the heat produced by the X-ray and withstand the radiation damage caused by the X-ray during data acquisition (299). To prevent this damage and therefore able to collect large amount of data for structural determination, the crystal is usually cryo-

protected prior to analyzing it with X-ray beam under a low-stream of nitrogen gas (299). In this study, glycerol was tested as a cryo-protectant as it is the one used in the study which produced the 1.7 Å *B. subtilis* FtsZ structure (143). This, however, was found to decrease the diffraction and approximated resolution produced by the crystal in this study. Thus, in the future, cryoprotectant screening will need to be conducted to identify the appropriate cryoprotectant which will not hinder the diffraction produced by the crystals. Rather than trying only a handful of cryoprotectant at a time, today, this can be easily conducted by purchasing a cryoprotectant screening kit containing at least 40 different cryoprotectant from companies such as Jena Bioscience and Hampton Research.

To summarise, this chapter has shown the possibility of using FBDD to identify other binding pockets within FtsZ and then subsequently to create compounds which target FtsZ. The research presented in this chapter has also shown the necessity of using a mutant FtsZ which lacks the ability to polymerize for understanding the interaction of fragment with the protein using NMR. Furthermore, the FtsZ mutation mentioned in this study may be a requirement for conducting FBDD with FtsZ originating from other bacterial species. Moreover, this mutation is advantageous as this study has shown that the fragment hits obtained from screening with the mutant *B. subtilis* FtsZ also translates to the wild-type *B. subtilis* FtsZ protein. The next step in the project will without a doubt be gathering structural data of the fragment-protein complex, followed by a structure-activity relationship study to start gaining understanding as to what part of the fragment is important for binding. It is once all those data are gathered that a medicinal chemist can go ahead in building the fragments through fragment linking and growing in order to perfectly fit the compound into the druggable protein pocket and at the same time create unique

intellectual property (IP). Overall, this chapter is only the beginning of many more new exciting discoveries and one that is urgently needed globally since many of currently approved antibiotics are failing to treat infections, due to antibiotic resistance.

Chapter 7 - General discussion

The discovery of penicillin propelled human history into the ‘Golden Age of Medicine’ and allowed many of today’s medical procedures to be routinely conducted; such as Caesarian sections, hip replacements and chemotherapy (305). However, the rise of antibiotic resistant bacteria causing infections is reverting human history into the ‘pre-antibiotic’ era, where common infections will once again be lethal, making many currently routine medical procedures very high-risk actions (2). The problem of antibiotic resistance is a complex issue and addressing it will need a concerted effort from all sectors, including agriculture, medicine, science/research, government, social science, businesses and the community (306).

While all these aspects of antibiotic resistance are being tackled globally, it is also essential that antibiotics with new and novel mechanism of actions are developed. One such process that is yet to be targeted by any of the FDA-approved antibiotics is bacterial cell division and many studies into the inhibition of this process have mainly focused on the conserved and essential protein FtsZ. This thesis attempted to tackle the problem by targeting FtsZ in two ways: inhibiting its essential interaction with its protein partner, FtsA, and by targeting the FtsZ protein itself.

Initial attempts to target the interaction between FtsZ and FtsA used these proteins from the organism *A. baumannii*. *Acinetobacter* was chosen because: (i) *A. baumannii* has been classified by the World Health Organization (WHO) to be a “priority 1” organism to which new antibiotics are urgently needed (213) and (ii) the region of FtsZ that is known to interact with FtsA in *Escherichia coli* and a range of other bacterial species is different in

Acinetobacter spp., and understanding the implications of this difference could be used to develop new narrow-spectrum antibacterials to specifically treat *Acinetobacter* infections. These infections are a particularly urgent threat because of the organism's ability to resist all of the currently available antibacterials (307).

An initial examination to understand this interaction using the amino acid sequence of the full-length proteins was carried out *in silico*. The software used predicted that the *Acinetobacter* FtsZ and FtsA interactions are similar to that of the currently known FtsZ and FtsA interactions that were shown through the co-crystallization of *T. maritima* FtsZ peptide and FtsA. However, the *in silico* study suggested that the *Acinetobacter* spp. FtsZ utilises different amino acids to interact with FtsA. In *E. coli* and other bacterial species, the aspartate (D373) and proline (P375) of the FtsZ extreme C-terminal peptide are important for the FtsZ/FtsA interaction. The *in silico* data obtained in this study for *A. baumannii* suggests that serine (S380) and lysine (K386) are important for the interaction and that the glutamine (Q382) acts as a stabilizer for the *Acinetobacter* FtsZ/FtsA interaction. Further characterisation of the *Acinetobacter* FtsZ-FtsA interaction and validation of the *in silico* data was sought through purification of the *Acinetobacter* spp. full-length FtsZ and FtsA proteins and attempting to co-crystallize and solve the structure of the complex.

Full-length protein was decided to be used for the *in vitro* study because it is unclear whether FtsZ interacts with FtsA only via the extreme C-terminal peptide or if another region on FtsZ can also interact with FtsA. Furthermore, since no one has ever crystallized FtsZ and FtsA interacting together, it was decided that purification and an attempt at crystallization of the full-length FtsZ and FtsA should be made. This would allow

examination of all the details of the *Acinetobacter* FtsZ and FtsA interaction. This, however, proved to be highly challenging in a number of steps. Full-length *Acinetobacter* FtsZ was successfully purified and mass spectrometry showed it that the purified sample was homogeneous. However, attempts to obtain crystals suitable for structure determination using purified full-length FtsZ were unsuccessful due to the presence of a disordered region on the protein. While full-length FtsA was also purified from insoluble inclusion bodies, gel filtration showed it to be aggregated, and therefore not suitable for downstream interaction studies and co-crystallization.

In hindsight, although this approach to examine the FtsZ/FtsA interaction had the potential to be highly rewarding, it was probably very ambitious and future studies will address these problems in multiple ways. For example, one could remove the MTS from the *Acinetobacter* FtsA and conduct a co-crystallization solely with the extreme C-terminal peptide of the *Acinetobacter* FtsZ, as conducted with the *T. maritima* proteins or perhaps as an initial step, only overproduce and purify the region of FtsA that is shown to interact with FtsZ, the 2B domain. Another approach would be to use certain fusion tags such as, IMPACTTM and His-SUMO, which have now been shown to results in successful purification of full-length soluble *T. maritima* FtsA and *E. coli* FtsA, respectively (110, 255). Although these tags were successfully used in purifying FtsA from both *E. coli* and *T. maritima*, this does not mean that it can be used to successfully purify *Acinetobacter* FtsA. As an example, The IMPACTTM system was initially tried by one of the honours student in the Harry laboratory for the purification of *Acinetobacter* FtsZ protein but, was not successful. Meanwhile, successful purification of *Acinetobacter* FtsZ was achieved without the use of any tag in this study. This example highlights the non-predictable nature

to successfully purify soluble proteins. An alternative approach can be to test different detergents in the purification buffer in order to solubilise full-length *Acinetobacter* FtsA. Overall, strategies to target any protein-protein interaction site is very challenging. However, since bacterial cell division is essential and is yet to be targeted by any FDA-approved antibacterials, it is of interest to scientists in the field, as the fight to provide new antibacterials with a novel mechanism of action for the whole world continues.

Targeting cell division protein-protein interactions should be of interest for researchers in the field as the cell division process is: (i) essential and is orchestrated by more than two dozen proteins that interact together to form the cell division machinery (the divisome) (67); (ii) the roles of most of the proteins appear to be structural (stabilizing the divisome), rather than enzymatic; hence targeting interacting sites to target cell division is likely to be highly effective (68) and (iii) almost all of the division proteins interact with several partners (68). Therefore, a single inhibiting molecule may simultaneously disrupt many essential interactions and lower the chance of resistance. As it currently stands, the advancement of technologies have allowed us to start probing and understanding the interaction mechanisms between these cell division proteins and further information can be found in reference (308). Both chapters 3 and 4 have revealed small snapshots of the challenges associated with targeting protein-protein interactions, which include the need to: (i) purify full-length protein that is well-behaved, (ii) understand the details of the protein-protein interaction of interest and (iii) have the correct protein construct for structure determination using X-ray crystallography. However, in the interests of time and to obtaining positive results, at this stage, the project focus was switched from targeting

the FtsA-FtsZ interaction to a single target approach which solely focus on FtsZ as the target.

The single target approach itself is not without its limitations. It is understood that the single target approach is undesirable due to the high likelihood of selecting for single-step resistance that is caused by changes in the target molecule, resulting in large increases in the minimum inhibitory concentration (MICs) (309-313). However, there are exceptions. Single target approach will be successful if: (i) resistant mutants have lower fitness, (ii) the drug has low toxicity and (iii) the drug kills very quickly, which allows for both higher dosing and preventing survival of resistant mutants (313). Examples of these two cases can be seen in the antibiotic Fosfomycin (314) and Fidaxomicin (315). Currently, no FtsZ inhibitors have shown all these characteristics. Compound **TXA709**, which is a derivative of **PC190723**, has been shown to meet criteria (ii) but, to address criteria (i) and (iii) the compound was tested in a synergistic assay with other antibiotics. The result showed that **TXA709** has synergy with other antibiotics, resulting in a lowered resistance rate. Therefore, **TXA709** will potentially be used in a combination therapy with other antibiotics to treat Methicillin-Resistant *Staphylococcus aureus* (MRSA) infections in the clinic and is now on its way to Phase I clinical trials (119, 316).

To date, there are many potential FtsZ inhibitors that have been reported in the literature. Table 1 in Chapter 1 showcases the most active compounds from a large number of derivatives in each referenced publication, including evidence that suggests FtsZ is the target. These compounds appear to bind FtsZ of certain species and not others in one of the following three known druggable protein pockets; the nucleotide-binding domain (131), the synergistic T7-loop (132) and the interdomain cleft (133). This raises several questions,

such as, how conserved are the druggable pockets of FtsZ? For example, why doesn't one compound affect *E. coli* FtsZ if it inhibits *S. aureus* FtsZ? Chapter 5 addresses these questions by conducting an *in silico* analysis of the structure of FtsZ from multiple bacterial species, as well as its three druggable pockets. The results obtained showed that FtsZ from different bacterial species could be divided into two structural categories: staphylococcal and non-staphylococcal classes. The two classes differ in their H7-helix curvature as well as the organisation of their β -sheets in the C-terminus and, as a consequence, allows staphylococcal FtsZ to have an interdomain cleft that is more open than the non-staphylococcal FtsZ. As a result, molecules will be able to more easily access the interdomain cleft and T7-loop of the staphylococcal FtsZ than the non-staphylococcal FtsZ. Perhaps this may explain why some compounds, for example, **PC190723**, bind the interdomain cleft of one FtsZ species, such as *S. aureus* and *B. subtilis* and not others. It is possible to utilise these differences in FtsZ for creating narrow-spectrum FtsZ inhibitors. Nevertheless, it is also possible to develop broad-spectrum FtsZ inhibitors since there are several common areas between different FtsZ structures that were detected by the software used in this study. For example, the T6-loop and the area in front of the nucleotide-binding domain. These regions on FtsZ is yet to be reported in the literature and small molecules which bind these regions will potentially inhibit FtsZ from polymerising and therefore inhibit its function. Analysis of the nucleotide-binding domain did not show any differences between FtsZ species and perhaps this is not surprising since this forms part of the active site in FtsZ.

While the analysis identified two subclasses of FtsZ between the analysed structures, there is still the possibility of other FtsZ structural groups existing and are yet to be discovered.

This has implications in terms of using FtsZ as the target in target-based drug discovery. That is, one cannot assume that FtsZ structures which are yet to be solved will fall into either staphylococcal or non-staphylococcal. Instead we will need to obtain the actual X-ray crystal structures of other FtsZ species. As it currently stands, of the organisms listed by WHO in their priority pathogens list, there are only two organisms for which the FtsZ structure is available; *P. aeruginosa* and *S. aureus*, which indicates a lack of structural information for targeting FtsZ in other organisms such as *A. baumannii* and *Enterococcus faecium*.

Today, it is possible to undertake target-based drug discovery using a homology model for the target when no actual crystal structure of the target is available. This approach, however, is only feasible to a certain extent because the method itself requires a sufficient amount of crystallographic data of similar proteins to be available for use in constructing the homology model itself. Another parameter which affects the method is amino acid sequence identity between the protein of known structure and the protein to be modelled (234). The method might be suitable for use in the initial target-based drug design approach with FtsZ. However, downstream experimentation with X-ray crystallography will without a doubt need to be conducted to show that the structure of the FtsZ of interest is correct, as well as showing the binding of the created compound to FtsZ. For further information about homology modelling in drug discovery, the reader is directed to reference (317).

As a part of this thesis, fragment-based drug discovery was attempted with *B. subtilis* FtsZ to firstly identify other possible binding pockets on FtsZ that were suggested in Chapter 5 and at the same time identify lead fragments which are able to be used for creating new antibacterials with a novel mechanism of action. Thus far, the research identified three lead

fragments with two of these fragments (fragment **1** and **3**) favouring the interdomain cleft while the other (fragment **14**) binding both the nucleotide-binding domain and interdomain cleft. However, taking the nature of the TROSY-HSQC NMR competition experiment and also analysis of the obtained data, it was indicated that fragment **14** is not actually binding in the nucleotide-binding domain per se, but is actually binding in a newly identified pocket that is adjacent to the nucleotide-binding domain and is located towards the front of the pocket. This said pocket was one of the pockets suggested in Chapter 5 to be a potential binding pocket which can be utilised for creating broad-spectrum FtsZ inhibitors. This pocket is yet to be reported in the literature and the implication of this finding could potentially address antibiotic resistance, especially with compounds that work against a single target and in this case FtsZ. Any compound which binds this newly identified pocket will potentially inhibit the ability of FtsZ to polymerize since it is located near the nucleotide-binding domain. At the same time, any mutation obtained by the protein to combat any compound binding this region, will need to be accommodated with a mutation at the T7-loop because the catalytic site of FtsZ is made complete through the insertion of the T7-loop of one monomer unit into the nucleotide-binding domain of another subunit. Therefore, since mutations on two regions of the protein is needed for resistance, it will likely decrease the rate of resistance appearing in comparison to the resistance rate of mutation in just one region of the protein, as seen with **PC190723**.

Attempts to solve how the fragments bind these regions on the protein and hence understand the possible mechanism of interaction between the fragments with the protein was attempted using crystallography. Crystal screening and optimizations conducted in Chapter 6 managed to obtain FtsZ crystals that were approximated to be resolvable up to

$R = 3.5 \text{ \AA}$. This, however, is not a high enough resolution for undertaking structural determination of the fragment with the protein. In the future, further optimization of the crystals will need to be conducted to obtain better resolution crystals which can be resolved to approximately $R = 2 \text{ \AA}$ or less. Another reason for needing high resolution crystals is that the subsequent handling of the crystals such as soaking with fragments and cryoprotecting the crystals will certainly decrease the crystal resolution. Other experiments to conduct in the future will involve identifying the appropriate cryoprotectant since in Chapter 6 it was shown that use of the cryoprotectant reported in the literature, used to solve the 1.7 \AA *B. subtilis* FtsZ structure, was not the appropriate cryoprotectant in this study because it reduced the resolution of the crystal in this study dramatically.

To conclude, antibiotic resistance is a complex issue that needs addressing immediately and amongst other efforts, it will require the development of novel classes of antibiotics to which resistance is slow to attain. This thesis is only a small part in the continuous battle against antibiotic resistance. As part of addressing this global issue, the work presented in this thesis has been performed in order to gain new insights for creating novel antibacterials which target the essential bacterial cell division protein, FtsZ. This is a step forward for humankind in the fight against antibiotic resistance.

Chapter 8 - References

1. Singh SB, Barrett JF. Empirical antibacterial drug discovery--foundation in natural products. *Biochemical Pharmacology*. 2006;71(7):1006 - 15.
2. Carlet J, Jarlier V, Harbarth S, Voss A, Goossens H, Pittet D. Ready for a world without antibiotics? The Pensières antibiotic resistance call to action. *Antimicrobial Resistance and Infection Control*. 2012;1(1):11.
3. Laxminarayan R, Matsoso P, Pant S, Brower C, Røttingen J-A, Klugman K, et al. Access to effective antimicrobials: a worldwide challenge. *The Lancet*. 2016;387:168 - 75.
4. WHO. Antibacterial Resistance Global Report on surveillance. Geneva; 2014.
5. Brown ED, Wright GD. Antibacterial drug discovery in the resistance era. *Nature*. 2016;529:336 - 43.
6. Singh SB, Young K, Silver LL. What is an “ideal” antibiotic? Discovery challenges and path forward. *Biochemical Pharmacology*. 2017;133:63-73.
7. Walsh C. Antibiotics: actions, origins, resistance. Washington, USA: American Society for Microbiology (ASM); 2003.
8. Sharma P, Tomar SK, Goswami P, Sangwan V, Singh R. Antibiotic resistance among commercially available probiotics. *Biochimica et Biophysica Acta*. 2014:176-95.
9. Walsh C. Where will new antibiotics come from? *Nature Reviews Microbiology*. 2003;1:65 - 70.
10. Hagberg K. Antimicrobial resistance learning site University of Minnesota 2018 [Available from: <https://amrls.cvm.msu.edu/pharmacology/historical-perspectives/the-golden-age-of-antibacterials>].

11. Vollmer W, Blanot D, Pedro MAD. Peptidoglycan structure and architecture. FEMS Microbiology Reviews. 2008;32(2):149 - 67.
12. Egan AJF, Biboy J, Veer Ivt, Breukink E, Vollmer W. Activities and regulation of peptidoglycan synthases. Philosophical Transactions B. 2015;370:20150031.
13. King DT, Sobhanifar S, Strynadka NCJ. The Mechanisms of Resistance to β -Lactam Antibiotics. In: Berghuis A, Matlashewski G, Wainberg MA, Sheppard D, editors. Handbook of Antimicrobial Resistance. New York, NY: Springer New York; 2017. p. 177-201.
14. Lovering AL, Safadi SS, Strynadka NCJ. Structural perspective of peptidoglycan biosynthesis and assembly. Annual Review of Biochemistry. 2012;81:451 - 78.
15. Schneider T, Sahl HG. An oldie but a goodie - cell wall biosynthesis as antibiotic target pathway. International Journal of Medical Microbiology. 2010;300(2):161 - 9.
16. Berti AD, Theisen E, Sauer J-D, Nonejuie P, Olson J, Pogliano J, et al. Penicillin Binding Protein 1 Is Important in the Compensatory Response of *Staphylococcus aureus* to Daptomycin-Induced Membrane Damage and Is a Potential Target for β -Lactam–Daptomycin Synergy. Antimicrobial Agents and Chemotherapy. 2016;60(1):451 - 8.
17. Silver LL. Does the cell wall of bacteria remain a viable source of targets for novel antibiotics? biochemical pharmacology. 2006;996-1005.
18. Kumarasamy KK, Toleman MA, Walsh TR, Bagaria J, Butt F, Balakrishnan R, et al. Emergence of a new antibiotic resistance mechanism in India, Pakistan, and the UK: a molecular, biological, and epidemiological study. The Lancet Infectious Diseases. 10(9):597-602.

19. Katz L, Mankin AS. Macrolides. In: Schaechter M, editor. Encyclopedia of Microbiology (Third Edition). Oxford: Academic Press; 2009. p. 529-58.
20. Kirst HA, Allen NE. 7.21 - Aminoglycosides Antibiotics. In: Taylor JB, Triggie DJ, editors. Comprehensive Medicinal Chemistry II. Oxford: Elsevier; 2007. p. 629-52.
21. Gill SK, Garcia GA. Rifamycin inhibition of WT and Rif-resistant *Mycobacterium tuberculosis* and *Escherichia coli* RNA polymerases in vitro. Tuberculosis. 2011;91(5):361-9.
22. Hearnshaw SJ, Edwards MJ, Stevenson CE, Lawson DM, Maxwell A. A New Crystal Structure of the Bifunctional Antibiotic Simocyclinone D8 Bound to DNA Gyrase Gives Fresh Insight into the Mechanism of Inhibition. Journal of Molecular Biology. 2014.
23. Fasugba O, Gardner A, Mitchell BG, Mnatzaganian G. Ciprofloxacin resistance in community- and hospital-acquired *Escherichia coli* urinary tract infections: a systematic review and meta-analysis of observational studies. BMC Infectious Diseases. 2015;15:545.
24. Peterson SW, Martin I, Demczuk W, Bharat A, Hoang L, Wylie J, et al. Molecular Assay for Detection of Ciprofloxacin Resistance in *Neisseria gonorrhoeae* Isolates from Cultures and Clinical Nucleic Acid Amplification Test Specimens. Journal of Clinical Microbiology. 2015;53(1):3606 - 8.
25. Valderas MW, Andi B, Barrow WW, Cook PF. Examination of intrinsic sulfonamide resistance in *Bacillus anthracis*: A novel assay for dihydropteroate synthase. Biochimica et Biophysica Acta (BBA) - General Subjects. 2008;1780(5):848-53.

26. Chen CQ, Zheng L, Zhou JL, Zhao H. Persistence and risk of antibiotic residues and antibiotic resistance genes in major mariculture sites in Southeast China. *Science of The Total Environment*. 2017;580:1175 - 84.
27. Muziasari WI, Managaki S, Pärnänen K, Karkman A, Lyra C, Tamminen M, et al. Sulphonamide and Trimethoprim Resistance Genes Persist in Sediments at Baltic Sea Aquaculture Farms but Are Not Detected in the Surrounding Environment. *PLOS One*. 2014;9(3):e92702.
28. Su JQ, Wei B, Xu CY, Qiao M, Zhu YG. Functional metagenomic characterization of antibiotic resistance genes in agricultural soils from China. *Environment International*. 2014;9-15.
29. von Wintersdorff CJH, Penders J, van Niekerk JM, Mills ND, Majumder S, van Alphen LB, et al. Dissemination of Antimicrobial Resistance in Microbial Ecosystems through Horizontal Gene Transfer. *Frontiers in Microbiology*. 2016;7(173).
30. Vranakis I, Goniotakis I, Psaroulaki A, Sandalakis V, Tselentis Y, Gevaert K, et al. Proteome studies of bacterial antibiotic resistance mechanisms. *Journal of Proteomics*. 2014;97(0):88-99.
31. McDermott PF, Walker RD, White DG. Antimicrobials: modes of action and mechanisms of resistance. *International Journal Of Toxicology*. 2003;22(2):135-43.
32. Riley M, Abe T, Arnaud MB, Berlyn MKB, Blattner FR, Chaudhuri RR, et al. *Escherichia coli* K-12: a cooperatively developed annotation snapshot—2005. *Nucleic Acids Research*. 2006;34(1):1-9.

33. Quinn RK, Cianci AL, Beaudoin JA, Sculimbrene BR. Synthesis of a d-Ala-d-Ala peptide isostere via olefin cross-metathesis and evaluation of vancomycin binding. *Bioorganic & Medicinal Chemistry Letters*. 2010;20(15):4382-5.
34. Blair JMA, Webber MA, Baylay AJ, Ogbolu DO, Piddock LJV. Molecular mechanisms of antibiotic resistance. *Nature Reviews Microbiology*. 2015;13:42 - 51.
35. Katayama Y, Ito T, Hiramatsu K. A new class of genetic element, staphylococcus cassette chromosome *mec*, encodes methicillin resistance in *Staphylococcus aureus*. *Antimicrobial Agents and Chemotherapy*. 2000;44(6):1549 - 55.
36. Shaw WV. Chloramphenicol Acetyltransferase: Enzymology and Molecular Biology. *Critical Reviews in Biochemistry*. 1983;14(1):1 - 46.
37. Yang B, Wang Q, Cui S, Wang Y, Shi C, Xia X, et al. Characterization of extended-spectrum beta-lactamases-producing *Salmonella* strains isolated from retail foods in Shaanxi and Henan Province, China. *Food Microbiology*. 2014;42(0):14-8.
38. Marrero A, Mallorquí-Fernández G, Guevara T, García-Castellanos R, Gomis-Rüth FX. Unbound and Acylated Structures of the MecR1 Extracellular Antibiotic-sensor Domain Provide Insights into the Signal-transduction System that Triggers Methicillin Resistance. *Journal of Molecular Biology*. 2006;361(3):506-21.
39. Zgurskaya HI. Molecular analysis of efflux pump-based antibiotic resistance. *International Journal of Medical Microbiology*. 2002:95-105.
40. Berglund B, Khan GA, Weisner SEB, Ehde PM, Fick J, Lindgren P-E. Efficient removal of antibiotics in surface-flow constructed wetlands, with no observed impact on antibiotic resistance genes. *Science of the Total Environment*. 2014:29-37.

41. Schindler BD, Kaatz GW. Multidrug efflux pumps of Gram-positive bacteria. Drug Resistance Updates. 2016;27:1 - 13.
42. Kojima S, Nikaido H. Permeation rates of penicillins indicate that *Escherichia coli* porins function principally as nonspecific channels. PNAS. 2013;110:E2629 - E34.
43. Vargiu AV, Nikaido H. Multidrug binding properties of the AcrB efflux pump characterized by molecular dynamics simulations. PNAS. 2012;109:20637 - 42.
44. Tamber S, Hancock RE. On the mechanism of solute uptake in *Pseudomonas*. Frontiers in Bioscience. 2003;8:s472 - s83.
45. Baroud M, Dandache I, Araj GF, Wakim R, Kanj S, Kanafani Z, et al. Underlying mechanisms of carbapenem resistance in extended-spectrum β -lactamase-producing *Klebsiella pneumoniae* and *Escherichia coli* isolates at a tertiary care centre in Lebanon: role of OXA-48 and NDM-1 carbapenemases. International Journal of Antimicrobial Agents. 2013;41(1):75 - 9.
46. Lavigne J-P, Sotto A, Marie-Hélène, Nicolas-Chanoine, Bouziges N, Jean-Marie Pagès, et al. An adaptive response of *Enterobacter aerogenes* to imipenem: regulation of porin balance in clinical isolates. International Journal of Antimicrobial Agents. 2013;41:130 - 6.
47. Pouloua A, Voulgari E, Vrioni G, Koumaki V, Xidopoulos G, Chatzipantazi V, et al. Outbreak caused by an ertapenem-resistant, CTX-M-15-producing *Klebsiella pneumoniae* sequence type 101 clone carrying an OmpK36 porin variant. Journal of Clinical Microbiology. 2013;51:3176 - 82.

48. Wozniak RA, Waldor MK. Integrative and conjugative elements: mosaic mobile genetic elements enabling dynamic lateral gene flow. *Nature Reviews Microbiology*. 2010;8:552 - 63.
49. Brooks BD, Brooks AE. Therapeutic strategies to combat antibiotic resistance. *Advanced Drug Delivery Reviews*. 2014;78:14 - 27.
50. Transatlantic Taskforce on Antimicrobial Resistance: Recommendations for future collaboration between the U.S. and EU 2011 [Available from: <https://www.cdc.gov/drugresistance/pdf/tatfar-report.pdf>].
51. Ludvigsson JF, Hadjipanayis A, Del Torso S, Mercier JC, Valiulis A, Stiris T. Appropriate use of antibiotics is vital for public health. *Acta Paediatrica*. 2017;106(5):691.
52. WHO. World Health Organization: Antibiotic Resistance: Multi-country public awareness survey: World Health Organization; 2015 [Available from: http://apps.who.int/iris/bitstream/10665/194460/1/9789241509817_eng.pdf?ua=1].
53. Cross ELA, Tolfree R, Kipping R. Systematic review of public-targeted communication interventions to improve antibiotic use *Journal of Antimicrobial Chemotherapy*. 2017;72(4):975 - 87.
54. Chattopadhyay MK. Use of antibiotics as feed additives: a burning question. *Frontiers in Microbiology*. 2014;5:334.
55. Zhang Q-Q, Ying G-G, Pan C-G, Liu Y-S, Zhao J-L. Comprehensive Evaluation of Antibiotics Emission and Fate in the River Basins of China: Source Analysis, Multimedia Modeling, and Linkage to Bacterial Resistance. *Environmental Science & Technology*. 2015;49(11):6772 - 82.

56. Liu Y-Y, Wang Y, Walsh TR, Yi L-X, Zhang R, Spencer J, et al. Emergence of plasmid-mediated colistin resistance mechanism MCR-1 in animals and human beings in China: a microbiological and molecular biological study. *The Lancet Infectious Diseases*. 2016;16(2):161-8.
57. McEachran AD, Blackwell BR, Hanson JD, Wooten KJ, Mayer GD, Cox SB, et al. Antibiotics, Bacteria, and Antibiotic Resistance Genes: Aerial Transport from Cattle Feed Yards via Particulate Matter. *Environmental Health Perspective*. 2015;123(4):337 - 43.
58. Economou V, Gousia P. Agriculture and food animals as a source of antimicrobial-resistant bacteria. *Infection and Drug Resistance*. 2015;8:49 - 61.
59. Aarestrup FM. The livestock reservoir for antimicrobial resistance: a personal view on changing patterns of risks, effects of interventions and the way forward. *Philosophical Transactions B*. 2015;370(1670):20140085.
60. Levy S. Reduced Antibiotic Use in Livestock: How Denmark Tackled Resistance. *Environmental Health Perspectives*. 2014;122(6):A 160 - A 5.
61. Larson E. Skin hygiene and infection prevention: more of the same or different approaches? *Clinical Infectious Diseases*. 1999;29:1287 - 94.
62. Luangasanatip N, Hongsuwan M, Limmathurotsakul D, Lubell Y, Lee AS, Harbarth S, et al. Comparative efficacy of interventions to promote hand hygiene in hospital: systematic review and network meta-analysis. *The BMJ*. 2015;351:h3728.
63. WHO. WHO Guidelines on Hand Hygiene in Health Care: First Global Patient Safety Challenge Clean Care is Safer Care: World Health Organization; 2009 [Available from: http://apps.who.int/iris/bitstream/10665/44102/1/9789241597906_eng.pdf.

64. Doronina O, Jones D, Martello M, Biron A, Lavoie-Tremblay M. A Systematic Review on the Effectiveness of Interventions to Improve Hand Hygiene Compliance of Nurses in the Hospital Setting. *Journal of Nursing Scholarship*. 2016;49(2):143 - 52.
65. Blaauwen Td, Andreu JM, Monasterio O. Bacterial cell division proteins as antibiotic targets. *Bioorganic Chemistry*. 2014.
66. Li X, Ma S. Advances in the discovery of novel antimicrobials targeting the assembly of bacterial cell division protein FtsZ. *European Journal of Medicinal Chemistry*. 2015;95:1-15.
67. de-Boer PA. Advances in understanding *E. coli* cell fission. *Current Opinion in Microbiology*. 2010;13:730-7.
68. Lock RL, Harry EJ. Cell-division inhibitors: new insights for future antibiotics. *Nature Reviews Drug Discovery*. 2008;7:324-38.
69. Robinson A, Causer RJ, Dixon NE. Architecture and Conservation of the Bacterial DNA Replication Machinery, an Underexploited Drug Target *Current Drug Targets*. 2012;13:352-72.
70. Blaauwen Td, Hamoen LW, Levin PA. The divisome at 25: the road ahead. *Current Opinion in Microbiology*. 2017;36:85-94.
71. Errington J, Daniel RA, Scheffers DJ. Cytokinesis in bacteria. *Microbiology and Molecular Biology Reviews*. 2003;67(1):52-65.
72. Goehring NW, Beckwith J. Diverse Paths to Midcell: Assembly of the Bacterial Cell Division Machinery. *Current Biology*. 2005;15(13):R514-R26.
73. Harry E, Monahan L, Thompson L. Bacterial cell division: the mechanism and its precision. *International Review of Cytology*. 2006;253:27-94.

74. Weiss DS. Bacterial cell division and the septal ring. *Molecular Microbiology*. 2004;54:588-97.
75. Vicente M, Rico AI, Martinez-Arteaga R, Mingorance J. Septum enlightenment: assembly of bacterial division proteins. *Journal of Bacteriology*. 2006;188:19-27.
76. Adams DW, Errington J. Bacterial cell division: assembly, maintenance and disassembly of the Z ring. *Nature Reviews Microbiology*. 2009;7(9):642-53.
77. Lutkenhaus J, Pichoff S, Du S. Bacterial Cytokinesis: From Z Ring to Divisome. *Cytoskeleton*. 2012;69(10):778-90.
78. Rothfield L, Justice S, García-Lara J. Bacterial Cell Division. *Annual Review of Genetics*. 1999;33:423 - 48.
79. Robinson A, Brzoska AJ, Turner KM, Withers R, Harry EJ, Lewis PJ, et al. Essential Biological Processes of an Emerging Pathogen: DNA Replication, Transcription, and Cell Division in *Acinetobacter* spp. *Microbiology and Molecular Biology Reviews*. 2010;74(2):273-97.
80. Lowe J, Amos LA. Crystal structure of the bacterial cell-division protein FtsZ. *Nature*. 1998;391:203-6.
81. Nogales E, Downing KH, Amos LA, Löwe J. Tubulin and FtsZ form a distinct family of GTPases. *Nature Structural Biology*. 1998;5(6):451-8.
82. Matsui T, Yamane J, Mogi N, Yamaguchi H, Takemoto H, Yao M, et al. Structural reorganization of the bacterial cell-division protein FtsZ from *Staphylococcus aureus*. *Biological Crystallography*. 2012;D68:1175-88.
83. Margolin W. FtsZ and the Division of Prokaryotic Cells and Organelles. *Nature Reviews Molecular Cell Biology*. 2005;6:862-71.

84. Gardner KAJA, Moore DA, Erickson HP. The C-terminal linker of *Escherichia coli* FtsZ functions as an intrinsically disordered peptide. *Molecular Microbiology*. 2013;89(2):264-75.
85. Buske PJ, Levin PA. A flexible C-terminal linker is required for proper FtsZ assembly *in vitro* and cytokinetic ring formation *in vivo*. *Molecular Microbiology*. 2013;89(2):249-63.
86. Sundararajan K, Miguel A, Desmarais SM, Meier EL, Casey Huang K, Goley ED. The bacterial tubulin FtsZ requires its intrinsically disordered linker to direct robust cell wall construction. *Nature Communications*. 2015;6(7281).
87. Sundararajan K, Goley ED. The intrinsically disordered C-terminal linker of FtsZ regulates protofilament dynamics and superstructure *in vitro*. *The Journal of Biological Chemistry*. 2017;292:20509 - 27.
88. Adams DW, Errington J. Bacterial cell division: assembly, maintenance and disassembly of the Z ring. *Nature Reviews Microbiology*. 2009;7:642-53.
89. Meier EL, Goley ED. Form and function of the bacterial cytokinetic ring. *Current Opinion in Cell Biology*. 2014;26:19-27.
90. Haeusser DP, Margolin W. Structural and functional insights into the dynamic bacterial Z ring. *Nature Reviews Microbiology*. 2016;14(5):305-19.
91. Scheffers DJ, de Wit JG, den Blaauwen T, Driessen AJ. GTP hydrolysis of cell division protein FtsZ: evidence that the active site is formed by the association of monomers. *Biochemistry*. 2002;41(2):521-9.
92. Oliva MA, Cordell SC, Löwe J. Structural insights into FtsZ protofilament formation. *Nature Structural & Molecular Biology*. 2004;11(12):1243-50.

93. Matsui T, Yamane J, Mogi N, Yamaguchi H, Takemoto H, Yao M, et al. Structural reorganization of the bacterial cell-division protein FtsZ from *Staphylococcus aureus*. *Acta Crystallographica Section D*. 2012;68(9):1175-88.
94. Sass P, Brötz-Oesterhelt H. Bacterial cell division as a target for new antibiotics. *Current Opinion in Microbiology*. 2013;16(5):522-30.
95. Shanmugam Hemaiswarya RS, Mohana Lakshmi Narasumani and Mukesh Doble. Phenylpropanoids inhibit protofilament formation of *Escherichia coli* cell division protein FtsZ. *Journal of Medical Microbiology*. 2011:1317–25.
96. Lowe J, Amos LA. Tubulin-like protofilaments in Ca^{2+} -induced FtsZ sheets. *EMBO journal*. 1999;18:2364-71.
97. Mukherjee A, Lutkenhaus J. Dynamic assembly of FtsZ regulated by GTP hydrolysis. *EMBO journal*. 1998;17:462-9.
98. Bisson-Filho AW, Hsu Y-P, Squyres GR, Kuru E, Wu F, Jukes C, et al. Treadmilling by FtsZ filaments drives peptidoglycan synthesis and bacterial cell division. *Science*. 2017;355:739-43.
99. Yang X, Lyu Z, Miguel A, McQuillen R, Huang KC, Xiao J. GTPase activity – coupled treadmilling of the bacterial tubulin FtsZ organizes septal cell wall synthesis. *Science*. 2017;355(6326):744 - 7.
100. Szwedziak P, Wang Q, Bharat TAM, Tsim M, Löwe J. Architecture of the ring formed by the tubulin homologue FtsZ in bacterial cell division. *eLIFE*. 2014;3:e04601.
101. Osawa M, Erickson HP. Liposome division by a simple bacterial division machinery. *PNAS*. 2013;110(27):11000-4.

102. Coltharp C, Buss J, Plumer TM, Xiao J. Defining the rate-limiting processes of bacterial cytokinesis. PNAS. 2016;113(8):E1044-E53.
103. Egan AJF, Vollmer W. The stoichiometric divisome: a hypothesis. Frontiers in Microbiology. 2015;6.
104. Pichoff S, Lutkenhaus J. Unique and overlapping roles for ZipA and FtsA in septal ring assembly in *Escherichia coli*. EMBO journal. 2002;21:685-93.
105. Hale CA, de-Boer PA. ZipA is required for recruitment of FtsK, FtsQ, FtsL, and FtsN to the septal ring in *Escherichia coli*. Journal of Bacteriology. 2002;184:2552-6.
106. Bork P, Sander C, Valencia A. An ATPase domain common to prokaryotic cell cycle proteins, sugar kinases, actin, and hsp70 heat shock proteins. PNAS. 1992;89:7290-4.
107. van-den-Ent F, Lowe J. Crystal structure of the cell division protein FtsA from *Thermotoga maritima*. EMBO journal. 2000;19(22):5300-7.
108. Fujita J, Maeda Y, Nagao C, Tsuchiya Y, Miyazaki Y, Hirose M, et al. Crystal structure of FtsA from *Staphylococcus aureus*. FEBS letters. 2014;588:1879-85.
109. Corbin BD, Geissler B, Sadasivam M, Margolin W. Z-ring-independent interaction between a subdomain of FtsA and late septation proteins as revealed by a polar recruitment assay. Journal of Bacteriology. 2004;186:7736-44.
110. Szwedziak P, Wang Q, Freund SM, Lowe J. FtsA forms actin-like protofilaments. EMBO journal. 2012;31:2249-60.
111. Pichoff S, Lutkenhaus J. Tethering the Z ring to the membrane through a conserved membrane targeting sequence in FtsA. Molecular Microbiology. 2005;55:1722-34.

112. Errington J. Bacterial morphogenesis and the enigmatic MreB helix. *Nature Reviews Microbiology*. 2015;13:241 - 8.
113. Chen X, Ni, F., Tian, X., Kondrashkina, E., Wang, Q., Ma, J. Structural basis of actin filament nucleation by tandem w domains. *Cell Reports*. 2013;3:1910 - 20.
114. Ma X, Margolin. W. Genetic and functional analyses of the conserved C-terminal core domain of *Escherichia coli* FtsZ. *Journal of Bacteriology*. 1999;181:7531-44.
115. Wang X, Huang J, Mukherjee A, Cao C, Lutkenhaus J. Analysis of the Interaction of FtsZ with Itself, GTP, and FtsA. *Journal of Bacteriology*. 1997;179(17):5551-9.
116. Yan K, Pearce KH, Payne DJ. A Conserved Residue at the Extreme C-Terminus of FtsZ Is Critical for the FtsA-FtsZ Interaction in *Staphylococcus aureus*. *Biochemical and Biophysical Research Communications*. 2000;270(2):387–92.
117. Din N, Quardokus EM, Sackett MJ, Brun YV. Dominant C-terminal deletions of FtsZ that affect its ability to localize in *Caulobacter* and its interaction with FtsA. *Molecular Microbiology*. 1998;27(5):1051-63.
118. Guidelines for the prevention and control of carbapenem-resistant Enterobacteriaceae, *Acinetobacter baumannii* and *Pseudomonas aeruginosa* in health care facilities. In: Organisation WH, editor. Geneva: World Health Organisation 2017.
119. TAXIS Pharmaceuticals I. Our Pipeline [Available from: <http://taxispharma.com/research-development/our-pipeline/>].
120. Payne DJ, Gwynn MN, Holmes DJ, Pompliano DL. Drugs for bad bugs: confronting the challenges of antibacterial discovery. *Nature Reviews Drug Discovery*. 2007;6:29 - 40.

121. Silver L. Antibiotics: Current Innovations and Future Trends, Edited by Sergio Sánchez and Arnold L. Demain: Caister Academic Press; 2015.
122. Dai K, Lutkenhaus J. *ftsZ* is an essential cell division gene in *Escherichia coli*. Journal of Bacteriology. 1991;173(11):3500-6.
123. Cushnie TPT, O'Driscoll NIH, Lamb AJ. Morphological and ultrastructural changes in bacterial cells as an indicator of antibacterial mechanism of action. Cellular and Molecular Life Sciences. 2016.
124. Pinho MG, Errington J. Dispersed mode of *Staphylococcus aureus* cell wall synthesis in the absence of the division machinery. Molecular Microbiology. 2003;50(3):871-81.
125. Vaughan S, Wickstead B, Gull K, Addinall SG. Molecular Evolution of FtsZ Protein Sequences Encoded Within the Genomes of Archaea, Bacteria, and Eukaryota. Journal of Molecular Evolution. 2004;58(1):19-29.
126. de Boer P, Crossley R, Rothfield L. The essential bacterial cell-division protein FtsZ is a GTPase. Nature. 1992;359(6392):254-6.
127. Schwedock J, McCormick JR, Angert ER, Nodwell JR, Losick R. Assembly of the cell division protein FtsZ into ladder-like structures in the aerial hyphae of *Streptomyces coelicolor*. Molecular Microbiology. 1997;25(5):847-58.
128. McCormick JR, Su EP, Driks A, Losick R. Growth and viability of *Streptomyces coelicolor* mutant for the cell division gene *ftsZ*. Molecular Microbiology. 1994;14(2):243-54.

129. Jakimowicz D, van Wezel GP. Cell division and DNA segregation in *Streptomyces*: how to build a septum in the middle of nowhere? *Molecular Microbiology*. 2012;85(3):393-404.
130. Lock RL, Harry EJ. Cell-division inhibitors: new insights for future antibiotics. *Nature Reviews Drug Discovery*. 2008;7(4):324-38.
131. Lappchen T, Pinas VA, Hartog AF, Koomen GJ, Schaffner-Barbero C, Andreu JM, et al. Probing FtsZ and tubulin with C8-substituted GTP analogs reveals differences in their nucleotide binding sites. *Chemical Biology*. 2008;15(2):189-99.
132. Domadia P, Swarup S, Bhunia A, Sivaraman J, Dasgupta D. Inhibition of bacterial cell division protein FtsZ by cinnamaldehyde. *Biochemical Pharmacology*. 2007;74(6):831-40.
133. Haydon DJ, Stokes NR, Ure R, Galbraith G, Bennett JM, Brown DR, et al. An inhibitor of FtsZ with potent and selective anti-staphylococcal activity. *Science*. 2008;321:1673-5.
134. Kaul M, Zhang Y, Parhi AK, LaVoie EJ, Tuske S, Arnold E, et al. Enterococcal and streptococcal resistance to PC190723 and related compounds: Molecular insights from a FtsZ mutational analysis. *Biochimie*. 2013;95(10):1880-7.
135. Miguel A, Hsin J, Liu T, Tang G, Altman RB, Huang KC. Variations in the Binding Pocket of an Inhibitor of the Bacterial Division Protein FtsZ across Genotypes and Species. *PLOS Computational Biology*. 2015;11(3):e1004117.
136. Sharma A, Aher, A., Dynes, N.J., Frey, D., Katrukha, E.A., Jaussi, R., Grigoriev, I., Croisier, M., Kammerer, R.A., Akhmanova, A., Gonczy, P., Steinmetz, M.O. Centriolar

CPAP/SAS-4 Imparts Slow Processive Microtubule Growth. *Developmental Cell*. 2016;37:362 - 76.

137. Varma A, Young KD. In *Escherichia coli*, MreB and FtsZ direct the synthesis of lateral cell wall via independent pathways that require PBP 2. *Journal of Bacteriology*. 2009;191(11):3526-33.

138. Margalit DN, Romberg L, Mets RB, Hebert AM, Mitchison TJ, Kirschner MW, et al. Targeting cell division: small-molecule inhibitors of FtsZ GTPase perturb cytokinetic ring assembly and induce bacterial lethality. *PNAS*. 2004;101(32):11821-6.

139. Chan F-Y, Sun N, Leung Y-C, Wong K-Y. Antimicrobial activity of a quinuclidine-based FtsZ inhibitor and its synergistic potential with β -lactam antibiotics. *Journal of Antibiotics*. 2015;68(4):253-8.

140. Beveridge TJ. Structures of Gram-negative cell walls and their derived membrane vesicles. *Journal of Bacteriology*. 1999;181(16):4725-33.

141. Kaul M, Zhang Y, Parhi AK, LaVoie EJ, Pilch DS. Inhibition of RND-type efflux pumps confers the FtsZ-directed prodrug TXY436 with activity against Gram-negative bacteria. *Biochemical Pharmacology*. 2014;89(3):321-8.

142. Poulsen SM, Kofoed C, Vester B. Inhibition of the ribosomal peptidyl transferase reaction by the mycarose moiety of the antibiotics carbomycin, spiramycin and tylosin. *Journal of Molecular Biology*. 2000;304(3):471-81.

143. Haydon DJ, Stokes NR, Ure R, Galbraith G, Bennett JM, Brown DR, et al. An inhibitor of FtsZ with potent and selective anti-staphylococcal activity. *Science*. 2008;321(5896):1673-5.

144. Stokes NR, Baker N, Bennett JM, Berry J, Collins I, Czaplewski LG, et al. An improved small-molecule inhibitor of FtsZ with superior *in vitro* potency, drug-like properties, and *in vivo* efficacy. *Antimicrobial Agents and Chemotherapy*. 2013;57(1):317-25.
145. Kaul M, Mark L, Parhi AK, LaVoie EJ, Pilch DS. Combining the FtsZ-Targeting Prodrug TXA709 and the Cephalosporin Cefdinir Confers Synergy and Reduces the Frequency of Resistance in Methicillin-Resistant *Staphylococcus aureus*. *Antimicrobial Agents and Chemotherapy*. 2016;60(7):4290-6.
146. Ohashi Y, Chijiwa Y, Suzuki K, Takahashi K, Nanamiya H, Sato T, et al. The Lethal Effect of a Benzamide Derivative, 3-Methoxybenzamide, Can Be Suppressed by Mutations within a Cell Division Gene, *ftsZ*, in *Bacillus subtilis*. *Journal of Bacteriology*. 1999;181(4):1348-51.
147. Haydon DJ, Bennett JM, Brown D, Collins I, Galbraith G, Lancett P, et al. Creating an antibacterial with *in vivo* efficacy: synthesis and characterization of potent inhibitors of the bacterial cell division protein FtsZ with improved pharmaceutical properties. *Journal of Medicinal Chemistry*. 2010;53(10):3927-36.
148. Stokes NR, Baker N, Bennett JM, Chauhan PK, Collins I, Davies DT, et al. Design, synthesis and structure–activity relationships of substituted oxazole–benzamide antibacterial inhibitors of FtsZ. *Bioorganic & Medicinal Chemistry Letters*. 2014;24(1):353-9.
149. Stokes NR, Baker N, Bennett JM, Berry J, Collins I, Czaplewski LG, et al. An Improved Small-Molecule Inhibitor of FtsZ with Superior *In Vitro* Potency, Drug-Like

Properties, and In Vivo Efficacy. *Antimicrobial Agents and Chemotherapy*. 2013;57(1):317-25.

150. Kaul M, Mark L, Zhang Y, Parhi AK, Lavoie EJ, Pilch DS. An FtsZ-targeting prodrug with oral antistaphylococcal efficacy *in vivo*. *Antimicrobial Agents and Chemotherapy*. 2013;57(12):5860-9.

151. Kaul M, Mark L, Zhang Y, Parhi AK, Lyu YL, Pawlak J, et al. TXA709: A FtsZ-Targeting Benzamide Prodrug with Improved Pharmacokinetics and Enhanced *In Vivo* Efficacy against Methicillin-Resistant *Staphylococcus aureus*. *Antimicrobial Agents and Chemotherapy*. 2015.

152. Fujita J, Maeda Y, Mizohata E, Inoue T, Kaul M, Parhi AK, et al. Structural Flexibility of an Inhibitor Overcomes Drug Resistance Mutations in *Staphylococcus aureus* FtsZ. *ACS Chemical Biology*. 2017;12(7):1947 - 55.

153. Chan F-Y, Sun N, Neves MAC, Lam PC-H, Chung W-H, Wong L-K, et al. Identification of a New Class of FtsZ Inhibitors by Structure-Based Design and *In Vitro* Screening. *Journal of Chemical Information and Modeling*. 2013;53(8):2131-40.

154. Hurley KA, Santos TMA, Nepomuceno GM, Huynh V, Shaw JT, Weibel DB. Targeting the Bacterial Division Protein FtsZ. *Journal of Medicinal Chemistry*. 2016.

155. Lian Z-M, Sun J, Zhu H-L. Design, synthesis and antibacterial activity of isatin derivatives as FtsZ inhibitors. *Journal of Molecular Structure*. 2016;1117:8-16.

156. Elsen NL, Lu J, Parthasarathy G, Reid JC, Sharma S, Soisson SM, et al. Mechanism of action of the cell-division inhibitor PC190723: modulation of FtsZ assembly cooperativity. *Journal of the American Chemical Society*. 2012;134(30):12342-5.

157. Andreu JM, Schaffner-Barbero C, Huecas S, Alonso D, Lopez-Rodriguez ML, Ruiz-Avila LB, et al. The antibacterial cell division inhibitor PC190723 is an FtsZ polymer-stabilizing agent that induces filament assembly and condensation. *Journal Biological Chemistry*. 2010;285(19):14239-46.
158. Ma S, Cong C, Meng X, Cao S, Yang H, Guo Y, et al. Synthesis and on-target antibacterial activity of novel 3-elongated arylalkoxybenzamide derivatives as inhibitors of the bacterial cell division protein FtsZ. *Bioorganic & Medicinal Chemistry Letters*. 2013;23(14):4076-9.
159. Chiodini G, Pallavicini M, Zanotto C, Bissa M, Radaelli A, Straniero V, et al. Benzodioxane-benzamides as new bacterial cell division inhibitors. *European Journal of Medicinal Chemistry*. 2015;89:252-65.
160. Sun N, Chan FY, Lu YJ, Neves MA, Lui HK, Wang Y, et al. Rational design of berberine-based FtsZ inhibitors with broad-spectrum antibacterial activity. *PLoS One*. 2014;9(5):e97514.
161. Hamoud R, Reichling J, Wink M. Synergistic antibacterial activity of the combination of the alkaloid sanguinarine with EDTA and the antibiotic streptomycin against multidrug resistant bacteria. *Journal of Pharmacy and Pharmacology*. 2015;67(2):264-73.
162. Kelley C, Zhang Y, Parhi A, Kaul M, Pilch DS, Lavoie EJ. 3-Phenyl substituted 6,7-dimethoxyisoquinoline derivatives as FtsZ-targeting antibacterial agents. *Bioorganic and Medicinal Chemistry*. 2012;20(24):7012-29.
163. Rai D, Singh JK, Roy N, Panda D. Curcumin inhibits FtsZ assembly: an attractive mechanism for its antibacterial activity. *Biochemical Journal*. 2008;410(1):147-55.

164. Li X, Sheng J, Huang G, Ma R, Yin F, Song D, et al. Design, synthesis and antibacterial activity of cinnamaldehyde derivatives as inhibitors of the bacterial cell division protein FtsZ. *European Journal of Medicinal Chemistry*. 2015;97:32-41.
165. Jaiswal R, Beuria TK, Mohan R, Mahajan SK, Panda D. Totarol inhibits bacterial cytokinesis by perturbing the assembly dynamics of FtsZ. *Biochemistry*. 2007;46(14):4211-20.
166. Wang J, Galgoci A, Kodali S, Herath KB, Jayasuriya H, Dorso K, et al. Discovery of a small molecule that inhibits cell division by blocking FtsZ, a novel therapeutic target of antibiotics. *Journal of Biological Chemistry*. 2003;278(45):44424-8.
167. Keffer JL, Huecas S, Hammill JT, Wipf P, Andreu JM, Bewley CA. Chrysophaentins are competitive inhibitors of FtsZ and inhibit Z-ring formation in live bacteria. *Bioorganic & Medicinal Chemistry*. 2013;21(18):5673-8.
168. Keffer JL, Hammill JT, Lloyd JR, Plaza A, Wipf P, Bewley CA. Geographic Variability and Anti-Staphylococcal Activity of the Chrysophaentins and Their Synthetic Fragments. *Marine Drugs*. 2012;10(5):1103-25.
169. Plaza A, Keffer JL, Bifulco G, Lloyd JR, Bewley CA. Chrysophaentins A-H, antibacterial bisdiarylbutene macrocycles that inhibit the bacterial cell division protein FtsZ. *Journal of American Chemical Society*. 2010;132(26):9069-77.
170. Duggirala S, Nankar RP, Rajendran S, Doble M. Phytochemicals as inhibitors of bacterial cell division protein FtsZ: coumarins are promising candidates. *Applied Biochemistry and Biotechnology*. 2014;174(1):283-96.

171. Bhattacharya A, Jindal B, Singh P, Datta A, Panda D. Plumbagin inhibits cytokinesis in *Bacillus subtilis* by inhibiting FtsZ assembly-a mechanistic study of its antibacterial activity. FEBS Journal. 2013;280(18):4585-99.
172. Parhi AK, Zhang Y, Saionz KW, Pradhan P, Kaul M, Trivedi K, et al. Antibacterial activity of quinoxalines, quinazolines, and 1,5-naphthyridines. Bioorganic & Medicinal Chemistry Letters. 2013;23(17):4968-74.
173. Zhang Y, Giurleo D, Parhi A, Kaul M, Pilch DS, LaVoie EJ. Substituted 1,6-diphenylnaphthalenes as FtsZ-targeting antibacterial agents. Bioorganic & Medicinal Chemistry Letters. 2013;23(7):2001-6.
174. Wang Y, Yan M, Ma R, Ma S. Synthesis and antibacterial activity of novel 4-bromo-1H-indazole derivatives as FtsZ inhibitors. Archiv der Pharmazie (Weinheim). 2015;348(4):266-74.
175. Kumar K, Awasthi D, Lee SY, Zanardi I, Ruzsicska B, Knudson S, et al. Novel trisubstituted benzimidazoles, targeting Mtb FtsZ, as a new class of antitubercular agents. Journal of Medicinal Chemistry. 2011;54(1):374-81.
176. Park B, Awasthi D, Chowdhury SR, Melief EH, Kumar K, Knudson SE, et al. Design, synthesis and evaluation of novel 2,5,6-trisubstituted benzimidazoles targeting FtsZ as antitubercular agents. Bioorganic & Medicinal Chemistry. 2014;22(9):2602-12.
177. Singh P, Jindal B, Surolia A, Panda D. A rhodanine derivative CCR-11 inhibits bacterial proliferation by inhibiting the assembly and GTPase activity of FtsZ. Biochemistry. 2012;51(27):5434-42.

178. Nepomuceno GM, Chan KM, Huynh V, Martin KS, Moore JT, O'Brien TE, et al. Synthesis and Evaluation of Quinazolines as Inhibitors of the Bacterial Cell Division Protein FtsZ. *ACS Medicinal Chemistry Letters*. 2015;6(3):308-12.
179. Ruiz-Avila LB, Huecas S, Artola M, Vergoños A, Ramírez-Aportela E, Cercenado E, et al. Synthetic Inhibitors of Bacterial Cell Division Targeting the GTP-Binding Site of FtsZ. *ACS Chemical Biology*. 2013;8(9):2072-83.
180. Neylon C, Brown SE, Kralicek AV, Miles CS, Love CA, Dixon NE. Interaction of the *Escherichia coli* Replication Terminator Protein (Tus) with DNA: A Model Derived from DNA-Binding Studies of Mutant Proteins by Surface Plasmon Resonance. *Biochemistry*. 2000;39:11989-99.
181. Expedeon. High Throughput Colorimetric GTPase assay kit: Expedeon; 2018 [Available from: https://www.expedeon.com/wp-content/uploads/2017/08/Expedeon_HTC-GTPase-assay-kit.pdf.
182. Bruker. TopSpin: Bruker; 2018 [updated 2018. Available from: <https://www.bruker.com/products/mr/nmr/nmr-software/nmr-software/topspin/overview.html>.
183. Lee W, Tonelli M, Markley JL. NMRFAM-SPARKY: enhanced software for biomolecular NMR spectroscopy. *Bioinformatics*. 2015;31(8):1325 - 7.
184. Chen R, Weng Z. A novel shape complementarity scoring function for protein-protein docking. *Proteins*. 2003;51:397 - 408.
185. Chen R, Li L, Weng ZP. ZDOCK: An initial-stage protein-docking algorithm. *Proteins*. 2003;52(1):80 - 7.

186. Li L, Chen R, Weng ZP. RDOCK: Refinement of rigid-body protein docking predictions. *Proteins*. 2003;53:693-707.
187. 1.43 Angstrom resolution crystal structure of cell division protein FtsZ (ftsZ) from *Staphylococcus epidermidis* RP62A in complex with GDP [Internet]. RCSB Protein Data Bank. 2015 [cited 1 November 2018]. Available from: <https://www.rcsb.org/structure/4M8I>.
188. Leung AKW, Lucile White E, Ross LJ, Reynolds RC, DeVito JA, Borhani DW. Structure of Mycobacterium tuberculosis FtsZ Reveals Unexpected, G Protein-like Conformational Switches. *Journal of Molecular Biology*. 2004;342(3):953-70.
189. Li Y, Hsin J, Zhao L, Cheng Y, Shang W, Huang KC, et al. FtsZ protofilaments use a hinge-opening mechanism for constrictive force generation. *Science*. 2013;341(392-395).
190. Raymond A, Lovell S, Lorimer D, Walchli J, Mixon M, Wallace E, et al. Combined protein construct and synthetic gene engineering for heterologous protein expression and crystallization using Gene Composer. *BMC Biotechnology*. 2009;9:37.
191. Oliva MA, Trambaiolo D, Lowe J. Structural Insights Into the Conformational Variability of Ftsz. *Journal of Molecular Biology*. 2007;373:1229.
192. Berman HM, Westbrook J, Feng Z, Gilliland G, Bhat TN, Weissig H, et al. The Protein Data Bank. *Nucleic Acids Research*. 2000;28(1):235-42.
193. J. D. Thompson, D. G. Higgins, T. J. Gibson. CLUSTAL W: improving the sensitivity of progressive multiple sequence alignment through sequence weighting, position-specific gap penalties and weight matrix choice. *Nucleic Acids Research*. 1994;22(22):4673–80.

194. C. M. Venkatachalam, X. Jiang, T. Oldfield, M. Waldman. LigandFit: a novel method for the shape-directed rapid docking of ligands to protein active sites. *Journal of Molecular Graphics and Modelling*. 2003;21(4):289-307.
195. Brooks BR, Bruccoleri RE, Olafson BD, States DJ, Swaminathan S, Karplus M. CHARMM: A program for macromolecular energy, minimization, and dynamics calculations. *Journal of Computational Chemistry*. 1983;4(2):187-217.
196. Brooks BR, Brooks CL, Mackerell AD, Nilsson L, Petrella RJ, Roux B, et al. CHARMM: The biomolecular simulation program. *Journal of Computational Chemistry*. 2009;30(10):1545-614.
197. Allen M, Tildesley D. Periodic Boundary Conditions and Potential Truncation. *Computer Simulation of Liquids*. 1987.
198. Klamt A, Schüürmann G. COSMO: a new approach to dielectric screening in solvents with explicit expressions for the screening energy and its gradient. *Journal of the Chemical Society, Perkin Transactions 2*. 1993(5):799-805.
199. Cohen ML. Epidemiology of drug resistance: implications for a post-antimicrobial era. *Science*. 1992;257:1050-5.
200. Gaynes R, Edwards JR. Overview of nosocomial infections caused by Gram-negative bacilli. *Clinical Infectious Diseases*. 2005;41:848-54.
201. Levy SB. Multidrug resistance - a sign of the times. *The New England Journal of Medicine*. 1998;338:1376-8.
202. Levy SB, Marshall B. Antibacterial resistance worldwide: causes, challenges and responses. *Nature Medicine*. 2004;10:S122-S9.

203. Quinn JP. Clinical problems posed by multiresistant nonfermenting Gram-negative pathogens. *Clinical Infectious Diseases*. 1998;27 (Suppl 1):S117-S24.
204. Tacconelli E, Cataldo MA, Dancer SJ, Angelis GD, Falcone M, Frank U, et al. ESCMID guidelines for the management of the infection control measures to reduce transmission of multidrug-resistant Gram-negative bacteria in hospitalized patients. *Clinical Microbiology and Infection*. 2014;20(1):1-55.
205. Nikaido H, Vaara M. Molecular basis of bacterial outer membrane permeability. *Microbiological reviews*. 1985;49:1-32.
206. Ple'siat P, Nikaido H. Outer membranes of Gram-negative bacteria are permeable to steroid probes. *Molecular Microbiology*. 1992;6:1323-33.
207. Peleg AY, Seifert H, Paterson DL. *Acinetobacter baumannii*: emergence of a successful pathogen. *Clinical microbiology reviews*. 2008;21:538-82.
208. Towner KJ. *Acinetobacter*: an old friend, but a new enemy. *Journal of Hospital Infection*. 2009;73(4):355-63.
209. Chen TL, Siu LK, Lee YT, Chen CP, Huang LY, Wu RCC, et al. *Acinetobacter baylyi* as a pathogen for opportunistic infection. *Journal of Clinical Microbiology*. 2008;46:2938-44.
210. Murray CK, Hospenthal DR. *Acinetobacter* infection in the ICU. *Critical Care Clinics*. 2008;24:237-48.
211. Rathinavelu S, Zavros Y, Merchant JL. *Acinetobacter lwoffii* infection and gastritis. *Microbes and Infection*. 2003;5:651-7.
212. Dijkshoorn L, Nemec A, Seifert H. An increasing threat in hospitals: multidrug-resistant *Acinetobacter baumannii*. *Nature Reviews Microbiology*. 2007;5:939-51.

213. WHO. WHO publishes list of bacteria for which new antibiotics are urgently needed Geneva: World Health Organisation: World Health Organisation; 2017 [Available from: <http://www.who.int/mediacentre/news/releases/2017/bacteria-antibiotics-needed/en/>].
214. Beall B, Lutkenhaus J. Impaired cell division and sporulation of a *Bacillus subtilis* strain with the *ftsA* gene deleted. *Journal of Bacteriology*. 1992;174:2398 - 403.
215. Jensen SO, Thompson LS, Harry EJ. Cell division in *Bacillus subtilis*: FtsZ and FtsA association is Z-ring independent, and FtsA is required for efficient midcell Z-ring assembly. *Journal of Bacteriology*. 2005;187:6536 - 44.
216. Ishikawa S, Kawai Y, Hiramatsu K, Kuwano M, Ogasawara N. A new FtsZ-interacting protein, YlmF, complements the activity of FtsA during progression of cell division in *Bacillus subtilis*. *Molecular Microbiology*. 2006;60:1364 - 80.
217. Berardinis Vrd, Vallenet D, Castelli V, Besnard M, Pinet As, Cruaud C, et al. A complete collection of single-gene deletion mutants of *Acinetobacter baylyi* ADP1. *Molecular Systems Biology*. 2008;4(1).
218. Haney SA, Glasfeld E, Hale C, Keeney D, He Z, de-Boer P. Genetic analysis of the *Escherichia coli* FtsZ/ZipA interaction in the yeast two-hybrid system. Characterization of FtsZ residues essential for the interactions with ZipA and with FtsA. *Journal of Biological Chemistry*. 2001;276:11980-7.
219. Inc AS. Discovery Studio Modeling Environment. 3.5 ed. San Diego: Accelrys Software Inc; 2012.

220. Mosyak L, Zhang Y, Glasfeld E, Haney S, Stahl M, Seehra J, et al. The bacterial cell-division protein ZipA and its interaction with an FtsZ fragment revealed by X-ray crystallography. *EMBO journal*. 2000;19:3179-91.
221. Goujon M, McWilliam H, Li W, Valentin F, Squizzato S, Paern J, et al. A new bioinformatics analysis tools framework at EMBL–EBI. *Nucleic Acids Research*. 2010;38(suppl_2):W695-W9.
222. Sievers F, Wilm A, Dineen D, Gibson TJ, Karplus K, Li W, et al. Fast, scalable generation of high-quality protein multiple sequence alignments using Clustal Omega. *Molecular Systems Biology*. 2011;7(1).
223. Pierce B, Weng Z. ZRANK: Reranking Protein Docking Predictions with an Optimized Energy Function. *Proteins*. 2007;67(4):1078 - 86.
224. Ascough S, Ingram RJ, Altmann DM. Anthrax Lethal Toxin and the Induction of CD4 T Cell Immunity. *Toxins*. 2012;4(10):878-99.
225. Roy KK, Singh S, Saxena AK. Integration-mediated prediction enrichment of quantitative model for Hsp90 inhibitors as anti-cancer agents: 3D-QSAR study. *Molecular Diversity*. 2011;15(2):477-89.
226. Hossaina MU, Oanya AR, Ahmada SAI, Hasanb A, Khana A, Siddikey AA. Identification of potential inhibitor and enzyme-inhibitor complex on trypanothione reductase to control Chagas disease. *Computational Biology and Chemistry*. 2016;65:29-36.
227. Bao Q-C, Wang L, Wang L, Xu X-L, Jiang F, Liu F, et al. Betulinic acid acetate, an antiproliferative natural product, suppresses client proteins of heat shock protein pathways through a CDC37-binding mechanism. *RSC Advances*. 2016;6:42537-44.

228. Shen M-y, Sali A. Statistical potential for assessment and prediction of protein structures. *Protein Science*. 2006;15(11):2507-24.
229. Discovery Studio 4.5. 17.1.0.16143 ed. San Diego: Dassault Systèmes: Dassault Systèmes BIOVIA; 2017.
230. Huang Y-F. Study of Mining Protein Structural Properties and its Application. National Taiwan University 2007.
231. Blow D. Outline of Crystallography for Biologists. New York: Oxford University Press; 2002. p. 196.
232. Gardner KAJA, Moore DA, Erickson HP. The C-terminal linker of *Escherichia coli* FtsZ functions as an intrinsically disordered peptide. *Molecular Microbiology*. 2013;89(2):264-75.
233. Buske PJ, Levin PA. A flexible C-terminal linker is required for proper FtsZ assembly in vitro and cytokinetic ring formation *in vivo*. *Molecular Microbiology*. 2013;89(2):249-63.
234. Chothial C, M.Lesk A. The relation between the divergence of sequence and structure in proteins. *EMBO Journal*. 1986;5(4):823-6.
235. Kinch LN, Wrabl JO, Krishna SS, Majumdar I, Sadreyev RI, Qi Y, et al. CASP5 assessment of fold recognition target predictions. *Proteins: Structure, Function, and Bioinformatics*. 2003;53:395-409.
236. Dueñas M, Vázquez J, Ayala M, Söderlind E, Ohlin M, Pérez L, et al. Intra- and extracellular expression of an scFv antibody fragment in *E. coli*: effect of bacterial strains and pathway engineering using GroES/L chaperonins. *Biotechniques*. 1994;16(3):476-7, 80-83.

237. Baneyx F. Recombinant protein expression in *Escherichia coli*. Current Opinion in Biotechnology. 1999;10(5):411–21.
238. Schein CH. Production of Soluble Recombinant Proteins in Bacteria. Nature Biotechnology. 1989;7:1141-9.
239. Cordell SC, Robinson EJH, Löwe J. Crystal structure of the SOS cell division inhibitor SulA and in complex with FtsZ. PNAS. 2003;100:7889-94.
240. White EL, Ross LJ, Reynolds RC, Seitz LE, Moore GD, Borhani DW. Slow Polymerization of *Mycobacterium tuberculosis* FtsZ. Journal of Bacteriology. 2000;182(14):4028 - 34.
241. You DL, Jen CJ, Chiu FW, Sui CW, Shu TC. Removal of N-terminal methionine from recombinant proteins by engineered *E. coli* methionine aminopeptidase. Protein Science. 2004;13:1802-10.
242. Hirel PH, Schmitter MJ, Dessen P, Fayat G, Blanquet S. Extent of N-terminal methionine excision from *Escherichia coli* proteins is governed by the side-chain length of the penultimate amino acid. PNAS. 1989;86:8247-51.
243. Asherie N. Protein crystallization and phase diagrams. Methods. 2004;34:266-72.
244. van den Ent F, Löwe J. Crystal structure of the cell division protein FtsA from *Thermotoga maritima*. The EMBO journal. 2000;19(20):5300-7.
245. Fujita J, Miyazaki Y, Hirose M, Nagao C, Mizohata E, Matsumoto Y, et al. Expression, purification, crystallization and preliminary crystallographic study of FtsA from methicillin-resistant *Staphylococcus aureus*. Acta Crystallographica Section F. 2013;69(8):895-8.

246. Vagenende V, Yap MG, Trout BL. Mechanisms of protein stabilization and prevention of protein aggregation by glycerol. *Biochemistry*. 2009;48(46):11084-96.
247. Pichoff S, Lutkenhaus J. Tethering the Z ring to the membrane through a conserved membrane targeting sequence in FtsA. *Molecular Microbiology*. 2005;55(6):1722-34.
248. Tan S, Hunziker Y, Pellegrini L, Richmond TJ. Crystallization of the yeast MATalpha2/MCM1/DNA ternary complex: general methods and principles for protein/DNA cocrystallization. *Journal of Molecular Biology*. 2000;297(4):947-59.
249. Predictor of Natural Disordered Regions Indianapolis: Molecular Kinetics, Inc.; 2007 [Available from: <http://www.pondr.com/>].
250. Krauss IR, Merlino A, Vergara A, Sica F. An Overview of Biological Macromolecule Crystallization. *International Journal of Molecular Sciences*. 2013;14(6):11643-91.
251. Hwang PM, Pan JS, Sykes BD. Targeted expression, purification, and cleavage of fusion proteins from inclusion bodies in *Escherichia coli*. *FEBS Letters*. 2013;588:247-52.
252. Costa S, Almeida A, Castro A, Domingues L. Fusion tags for protein solubility, purification, and immunogenicity in *Escherichia coli*: the novel Fh8 system. *Frontiers in Microbiology*. 2014;5:24-44.
253. Ramón A, Señorale-Pose M, Marín M. Inclusion bodies: not that bad.... *Frontiers in Microbiology*. 2014;5(56).
254. Burgess RR. Refolding solubilized inclusion body proteins. *Methods in Enzymology*. 2009;463:259-82.
255. Loose M, Mitchison TJ. The bacterial cell division proteins FtsA and FtsZ self-organize into dynamic cytoskeletal patterns. *Nature Cell Biology*. 2014;16(1):38-46.

256. Conti J, Viola MG, Camberg JL. FtsA reshapes membrane architecture and remodels the Z-ring in *Escherichia coli*. *Molecular microbiology*. 2018;107(4):558 - 76.
257. Bakail M, Ochsenbein F. Targeting protein-protein interactions, a wide open field for drug design. *Comptes Rendus Chimie*. 2016;19:19 - 27.
258. Panda D, Bhattacharya D, Gao QH, Oza PM, Lin HY, Hawkins B, et al. Identification of agents targeting FtsZ assembly. *Future medicinal chemistry*. 2016;8(10):1111-32.
259. Ballu S, Itteboina R, Sivan SK, Manga V. Structural insights of *Staphylococcus aureus* FtsZ inhibitors through molecular docking, 3D-QSAR and molecular dynamics simulations. *Journal of receptor and signal transduction research*. 2018;38(1):61-70.
260. Mingorance J, Rivas G, Vélez M, Gómez-Puertas P, Vicente M. Strong FtsZ is with the force: mechanisms to constrict bacteria. *Trends in Microbiology*. 2010;18(8):348-56.
261. Erickson HP. FtsZ, a tubulin homolog, in prokaryote cell division. *Trends Cell Biology*. 1997;7:362-7.
262. Matsui T, Han X, Yu J, Yao M, Tanaka I. Structural change in FtsZ Induced by intermolecular interactions between bound GTP and the T7 loop *Journal of Biological Chemistry*. 2014;289:3501-9.
263. Wlodawer A, Minor W, Dauter Z, Jaskolski M. Protein crystallography for non-crystallographers, or how to get the best (but not more) from published macromolecular structures. *FEBS Journal*. 2008;275(1):1 - 21.
264. Martín-Galiano AJ, Buey RnM, Cabezas M, Andreu JM. Mapping Flexibility and the Assembly Switch of Cell Division Protein FtsZ by Computational and Mutational Approaches. *The Journal of Biological Chemistry*. 2010;285(29):22554-2565.

265. Wagstaff JM, Tsim M, Oliva MA, García-Sánchez A, Kureisaite-Ciziene D, Andreu JM, et al. A Polymerization-Associated Structural Switch in FtsZ That Enables Treadmilling of Model Filaments. *Mbio*. 2017;8(3):e00254-17
266. Chen H, Zhou X, Wang A, Zheng Y, Gao Y, Zhou J. Evolutions in fragment-based drug design: the deconstruction–reconstruction approach. *Drug Discovery Today*. 2015;20(1):105-13.
267. Macarron R, Banks MN, Bojanic D, Burns DJ, Cirovic DA, Garyantes T, et al. Impact of high-throughput screening in biomedical research. *Nature Reviews Drug Discovery*. 2011;10:188-95.
268. Congreve M, Carr R, Murray C, Jhoti H. A ‘Rule of Three’ for fragment-based lead discovery? *Drug Discovery Today*. 2003;8(19):876-7.
269. Barker A, Kettle JG, Nowak T, Pease JE. Expanding medicinal chemistry space. *Drug Discovery Today*. 2013;18:298-304.
270. Bienstock RJ. Overview: Fragment-Based Drug Design. Library Design, Search Methods, and Applications of Fragment-Based Drug Design. 1076: American Chemical Society; 2011. p. 1-26.
271. Irwin JJ, Duan D, Torosyan H, Doak AK, Ziebart KT, Sterling T, et al. An Aggregation Advisor for Ligand Discovery. *Journal of Medicinal Chemistry*. 2015;58(17):7076-87.
272. Bohacek RS, McMartin C, Guida WC. The art and practice of structure-based drug design: A molecular modeling perspective. *Medicinal Research Reviews*. 1996;16(1):3 - 50.

273. Erlanson DA, Fesik SW, Hubbard RE, Jahnke W, Jhoti H. Twenty years on: the impact of fragments on drug discovery. *Nature Reviews Drug Discovery*. 2016;15:605-19.
274. Congreve M, Chessari G, Tisi D, Woodhead AJ. Recent Developments in Fragment-Based Drug Discovery. *Journal of Medicinal Chemistry*. 2008;51(13):3661-80.
275. Lipinski CA, Lombardo F, Dominy BW, Feeney PJ. Experimental and computational approaches to estimate solubility and permeability in drug discovery and development settings. *Advanced Drug Delivery Reviews*. 1997;23:3-25.
276. Murray CW, Rees DC. Opportunity Knocks: Organic Chemistry for Fragment-Based Drug Discovery (FBDD). *Angewandte Chemie International Edition*. 2015;55(2):488-92.
277. Doak B, Morton CJ, Simpson JS, Scanlon MJ. Design and evaluation of the performance of an NMR screening fragment library. *Australian Journal of Chemistry*. 2013;66:1465-72.
278. Scanlon MJ, Norton RS. Fragment-based drug discovery, an accessible approach to new therapeutics. *Australian Biochemist* 2013;44:9-12.
279. Patel D, Bauman JD, Arnold E. Advantages of crystallographic fragment screening: functional and mechanistic insights from a powerful platform for efficient drug discovery. *Progress in Biophysics & Molecular Biology*. 2014;116:92-100.
280. Oster L, Tapani S, Xue Y, Kack H. Successful generation of structural information for fragment-based drug discovery. *Drug Discovery Today*. 2015;20:1104-11.
281. Bollag G, Tsai J, Zhang J, Zhang C, Ibrahim P, Nolop K, et al. Vemurafenib: The first drug approved for BRAF-mutant cancer. *Nature Reviews Drug Discovery*. 2012;11:873-86.

282. Souers AJ, Levenson JD, Boghaert ER, Ackler SL, Catron ND, Chen J, et al. ABT-199, a potent and selective BCL-2 inhibitor, achieves antitumor activity while sparing platelets. *Nature Medicine*. 2013;19:202-8.
283. Petros AM, Dinges J, Augeri DJ, Baumeister SA, Betebenner DA, Bures MG, et al. Discovery of a Potent Inhibitor of the Antiapoptotic Protein Bcl-xL from NMR and Parallel Synthesis. *Journal of Medicinal Chemistry*. 2006;49(2):656-63.
284. Fabbretti A, Gualerzi CO, Brandi L. How to cope with the quest for new antibiotics. *FEBS Letters*. 2011;585(11):1673-81.
285. Mochalkin I, Miller JR, Narasimhan L, Thanabal V, Erdman P, Cox PB, et al. Discovery of antibacterial biotin carboxylase inhibitors by virtual screening and fragment-based approaches. *ACS Chemical Biology*. 2009;4:473-83.
286. Rawls KA, Lang PT, Takeuchi J, Imamura S, Baguley TD, Grundner C, et al. Fragment-based discovery of selective inhibitors of the *Mycobacterium tuberculosis* protein tyrosine phosphatase PtpA. *Bioorganic & Medicinal Chemistry Letters*. 2009;19:6851-4.
287. Scheich C, Puetter V, Schade M. Novel small molecule inhibitors of MDR *Mycobacterium tuberculosis* by NMR fragment screening of antigen 85C. *Journal of Medicinal Chemistry*. 2010;53:8362-7.
288. Abell C, Dagostin C. Different Flavours of Fragments, in *Fragment-Based Drug Discovery*. In: Howard S, Abell C, editors. *Fragment-Based Drug Discovery*: Royal Society of Chemistry; 2015. p. 1 - 18.

289. Dalvit C, Pevarello P, Tatò M, Veronesi M, Vulpetti A, Sundström M. Identification of compounds with binding affinity to proteins via magnetization transfer from bulk water. *Journal of Biomolecular NMR*. 2000;18(1):65 - 8.
290. Begley DW, Moen SO, Pierce PG, Zartler ER. Saturation transfer difference NMR for fragment screening. *Current Protocols in Chemical Biology*. 2013;5(4):251 - 68.
291. Meiboom S, Gill D. Modified Spin-Echo Method for Measuring Nuclear Relaxation Times. *Review of Scientific Instruments*. 1958;29:688.
292. Rees DC, Congreve M, Murray CW, Carr R. Fragment-based lead discovery. *Nature Reviews Drug Discovery*. 2004;3:660-72.
293. de Boer P, Crossley R, Rothfield L. The essential bacterial cell-division protein FtsZ is a GTPase. *Nature*. 1992;359:254.
294. Wang X, Lutkenhaus J. The FtsZ protein of *Bacillus subtilis* is localized at the division site and has GTPase activity that is dependent upon FtsZ concentration. *Molecular Microbiology*. 1993;9(3):435 - 42.
295. Ahijado-Guzmán R, Alfonso C, Reija B, Salvarelli E, Mingorance J, Zorrilla S, et al. Control by Potassium of the Size Distribution of *Escherichia coli* FtsZ Polymers Is Independent of GTPase Activity. *The Journal of Biological Chemistry*. 2013;288(38):27358-65.
296. Król E, Scheffers D-J. FtsZ Polymerization Assays: Simple Protocols and Considerations. *Journal of Visualized Experiments*. 2013;81:e50844.
297. McPherson A, Gavira JA. Introduction to protein crystallization. *Acta Crystallographica Section F Structural Biology Communications*. 2014;70:2 - 20.

298. Battye TGG, Kontogiannis L, Johnson O, Powella HR, Leslie AGW. iMOSFLM: a new graphical interface for diffraction-image processing with MOSFLM. *Acta Crystallographica Section D*. 2011;67:271 - 81.
299. Henderson R. Cryo-protection of protein crystals against radiation damage in electron and X-ray diffraction. *Proceedings of the Royal Society B*. 1990;241(1300):6 - 8.
300. Wells JA, McClendon CL. Reaching for high-hanging fruit in drug discovery at protein-protein interfaces. *Nature*. 2007;450(7172):1001 - 9.
301. Keserü GM, Erlanson DA, Ferenczy GG, Hann MM, Murray CW, Pickett SD. Design Principles for Fragment Libraries: Maximizing the Value of Learnings from Pharma Fragment-Based Drug Discovery (FBDD) Programs for Use in Academia. *Journal of Medicinal Chemistry*. 2016;59(18):8189-206.
302. Schuffenhauer A, Ruedisser S, Marzinzik AL, Jahnke W, Blommers M, Selzer P, et al. Library design for fragment based screening. *Current topics in medicinal chemistry*. 2005;5(8):751-62.
303. Lau WF, Withka JM, Hepworth D, Magee TV, Du YJ, Bakken GA, et al. Design of a multi-purpose fragment screening library using molecular complexity and orthogonal diversity metrics. *Journal of Computer-Aided Molecular Design*. 2011;25(7):621-36.
304. Leach AR, Hann MM, Burrows JN, Griffen EJ. Fragment screening: an introduction. *Molecular BioSystems*. 2006;2(9):430-46.
305. Eswaran M, Gallini N. Rescuing the Golden Age of Antibiotics: Can Economics Help Avert the Looming Crisis? ; 2016.

306. Laxminarayan R, Duse A, Wattal C, Zaidi AKM, Wertheim HFL, Sumpradit N, et al. Antibiotic resistance—the need for global solutions. The Lancet Infectious Diseases Commission. 2014;13:1057-98.
307. Perez F, Hujer AM, Hujer KM, Decker BK, Rather PN, Bonomo RA. Global Challenge of Multidrug-Resistant *Acinetobacter baumannii*. Antimicrobial Agents and Chemotherapy. 2007;51(10):3471-84.
308. Rowlett VW, Margolin W. The bacterial divisome: ready for its close-up. Philosophical Transactions of the Royal Society B: Biological Sciences. 2015;370(1679):20150028.
309. Yeh PJ, Hegreness MJ, Aiden AP, Kishony R. Drug interactions and the evolution of antibiotic resistance. Nature Reviews Microbiology. 2009;7:460.
310. Silver LL. Challenges of Antibacterial Discovery. Clinical Microbiology Reviews. 2011;24(1):71-109.
311. Silver LL, Bostian KA. Discovery and development of new antibiotics: the problem of antibiotic resistance. Antimicrobial Agents and Chemotherapy. 1993;37(3):377-83.
312. Silver LL. Multi-targeting by monotherapeutic antibacterials. Nature Reviews Drug Discovery. 2007;6:168.
313. Silver LL. The Antibiotic Future. In: Fisher JF, Mobashery S, Miller MJ, editors. Antibacterials: Volume I. Cham: Springer International Publishing; 2018. p. 31-67.
314. Silver LL. Fosfomycin: Mechanism and Resistance. Cold Spring Harbor Perspectives in Medicine. 2017.
315. Scott LJ. Fidaxomicin: A Review of Its Use in Patients with *Clostridium difficile* Infection. Drugs. 2013;73(15):1733-47.

316. Kaul M, Mark L, Parhi AK, LaVoie EJ, Pilch DS. Combining the FtsZ-Targeting Prodrug TXA709 and the Cephalosporin Cefdinir Confers Synergy and Reduces the Frequency of Resistance in Methicillin-Resistant *Staphylococcus aureus*. *Antimicrobial Agents and Chemotherapy*. 2016;60(7):4290-6.
317. Hillisch A, Pineda LF, Hilgenfeld R. Utility of homology models in the drug discovery process. *Drug Discovery Today*. 2004;9(15):659-69.